

Université Mohamed Khider – Biskra
Faculté des Sciences et de la technologie
Département de Génie Electrique
Ref :.....



جامعة محمد خيضر بسكرة
كلية العلوم و التكنولوجيا
قسم الهندسة الكهربائية
المرجع:.....

Thèse présentée en vue de l'obtention
Du diplôme de

Doctorat en : Génie Electrique

Option : Commande des systèmes énergétiques

Thèse préparée au Laboratoire de Génie Electrique de Biskra LGEB

Amélioration des Performances de la Commande Directe de Couple (DTC) de La Machine Asynchrone par des Techniques Non-Linéaires

Présentée par :

Abdelkarim AMMAR

Soutenue publiquement le : 29 Juin 2017

Devant le jury composé de :

Dr. GOLEA Amar	Professeur	Président	Université de Biskra
Dr. BOUREK Amor	Maitre de Conférences 'A'	Rapporteur	Université de Biskra
Dr. BENAKCHA Abdelhamid	Professeur	Co- Rapporteur	Université de Biskra
Dr. NAIT-SAID Mohamed Said	Professeur	Examineur	Université de Batna 2
Dr. NACERI Farid	Professeur	Examineur	Université de Batna 2
Dr. BETKA Achour	Professeur	Examineur	Université de Biskra

University Mohamed Khider – Biskra

Faculty of Science and Technology

Department of Electrical Engineering

Ref :.....



جامعة محمد خيضر بسكرة
كلية العلوم و التكنولوجيا
قسم الهندسة الكهربائية
المرجع:.....

A thesis submitted for the fulfillment of
the degree of
Doctorate in Electrical Engineering

Thesis has been prepared in the Electrical Engineering Laboratory of Biskra LGEB
Option: Control of energetic systems

**Improvement of Direct Torque Control Performances
for Asynchronous Machine Using Non-Linear
Techniques**

Presented by:

Abdelkarim AMMAR

The public thesis defense on: 29 June 2017

Board of Examiners:

Dr. GOLEA Amar	Professor	Chairman	University of Biskra
Dr. BOUREK Amor	Lecturer 'A'	Supervisor	University of Biskra
Dr. BENAKCHA Abdelhamid	Professor	Co-supervisor	University of Biskra
Dr. NAIT-SAID Mohamed Said	Professor	Examiner	University of Batna 2
Dr. NACERI Farid	Professor	Examiner	University of Batna 2
Dr. BETKA Achour	Professor	Examiner	University of Biskra

Dedication

I dedicate this thesis to the memory of my dear father "AMMAR Said", who passed away this year. He would be very happy to see my Ph.D. graduation. May Allah bless him with mercy and forgiveness and grant him Jannah "Ameen".

I also dedicate it to my mother "Baouia Fatiha" who has taken the biggest part of sacrificing for our education. May Allah protect her.

To my brothers: Hadj, Mohammed Elamin, Elhachemi, Zakaria and Abdelfattah.

To my sisters: Hayat, Mouna and Chafia.

To all my friends, in my social and academic life.

Abdelkarim AMMAR

إهداء

أهدي هذا العمل إلى والدي الغالي "عمار السعيد" الذي وافته المنية مطلع هذه السنة، أسأل الله أن يتغمده برحمته ومغفرته ويسكنه فسيح جنانه "آمين"

أهدي هذا العمل أيضا إلى والدتي "باوية فتيحة" التي كان لها النصيب الأكبر من التضحيات من أجل تربيتنا وتعليمنا، أسأل الله أن يحفظها.

إلى إخوتي: الحاج ، محمد الأمين، الهاشمي، زكرياء و عبد الفتاح.

إلى أخواتي: حياة، منى وشافية.

إلى جميع أصدقائي في حياتي الإجتماعية والأكاديمية.

عبد الكريم عمار

Acknowledgments

First of all, I would like to thank God “Allah” the Most Gracious and the Most Merciful, for blessing me with knowledge and giving me strength, courage, patience and serenity during all these years of study.

I would like to express my thanks to everyone that makes the achievement of this work. My great gratitude goes to my supervisors: **Dr. Amor Bourek** and **Pr. Abdelhamid Benakcha** members of the electrical engineering laboratory of Biskra LGEB for their continuous support, guidance, encouragement throughout my project, their extensive knowledge and diligent working.

I want to express my special appreciation to **Pr. Zouzou Salaheddine** the Head of electrical engineering laboratory of Biskra (LGEB) for providing the appropriate environment for research and experimental work in the laboratory. Without his help, this work would not have been in this form.

I also wish to thank President of jury **Mr. Golea Amar** Professor at the university of Biskra and member of the electrical engineering laboratory LGEB, and the members of the jury: **Mr. Betka Achour** Professor at the university of Biskra and member of the electrical engineering laboratory LGEB and **Mr. Nait-Said Mohamed Said, Mr. Nacéri Farid** Professors at the university of Batna 2, Algeria for serving as my committee members and taking the time to revise my thesis. I am thankful that in the midst of all their activities, they accepted to be members of the reading committee.

Further, I thank the members of LGEB, my colleagues Ph.D. students with a special mention to **Madam Saadi Meriem** the engineer of the laboratory for her precious advices and moral support. It was great to share the laboratory with all of you during last four years.

Last but not the least, I am grateful to my parents for their prayers, guidance and support throughout my education. Their inspiration and encouragement has been invaluable.

Abdelkarim AMMAR.

Abstract

Improvement of Direct Torque Control Performances for Asynchronous Machine Using Non-Linear Techniques

The direct torque control (DTC) was proposed as an alternative to the vector control in the middle of 1980s for AC machines control. This strategy bases on the direct determination of inverter switching states and offers a simpler scheme and less sensitivity to machine parameters. However, the variable switching frequency of DTC causes high flux and torque ripples which lead to an acoustical noise and degrade the performance of the control technique, especially at low-speed regions.

In the objective of improving the performance of DTC for the induction motor, this thesis addresses the most important points concerning this issue. The reduction of high ripples, which are the major drawbacks, by applying a constant switching frequency using the space vector modulation (SVM) has been done firstly. Then, we have presented a nonlinear control design based on input-output feedback linearization and sliding mode control to ensure a robust control against different uncertainties and external disturbances. Moreover, the sensorless control can increase the reliability and decrease the cost of the control system. Therefore, we have presented several observers structures to improve speed and flux estimation in high and low speed operations. Finally, we have discussed the insertion of losses minimization strategy for efficiency optimization based on the online adjusting of the produced flux according to the load value. The results of all the discussed aspects of this thesis have been obtained by numerical simulation using Matlab/Simulink software. Furthermore, a real-time implementation in the electrical engineering laboratory of Biskra (LGEB) equipped with dSpace 1104 is conducted. The experimental results have been depicted in order to validate the simulation results.

Keywords: Induction motor, Direct torque control, Space vector modulation, Nonlinear control, Sliding mode control, Observer, Low speed, Efficiency optimization

Résumé

Amélioration des Performances de la Commande Directe de Couple (DTC) de La Machine Asynchrone par des Techniques Non-Linéaires

La commande directe de couple (DTC) a été proposée en tant qu'alternative de la commande vectorielle au milieu des années 1980 pour les machines à courant alternatif. Cette stratégie repose sur la détermination directe des états de commutation de l'onduleur et offre un schéma plus simple et moins sensible aux paramètres de la machine. Cependant, la fréquence de commutation variable de la DTC provoque des ondulations élevées au niveau du flux et du couple qui conduisent à un bruit acoustique dégradent les performances de la commande, en particulier aux faibles vitesses.

Dans le but d'améliorer les performances de la DTC pour le moteur asynchrone, cette thèse a abordé les points les plus importants concernant cette problématique : la réduction des ondulations, qui sont les principaux inconvénients, par l'application d'une fréquence de commutation constante en utilisant la modulation vectorielle (SVM). Ensuite, nous avons présenté la conception d'une commande non linéaire basée sur la linéarisation entrée-sortie et la commande par mode glissant pour assurer un contrôle robuste contre les différentes incertitudes et les perturbations externes. De plus, la commande sans capteur peut augmenter la fiabilité et diminuer le coût du système. Pour cela, nous avons présenté des structures d'observateurs pour améliorer l'estimation de la vitesse et du flux dans le fonctionnement à basses et hautes vitesses. Enfin, nous avons discuté de l'insertion de la stratégie de minimisation des pertes pour l'optimisation du rendement, cette stratégie basée sur l'ajustement online du flux produit en fonction de la charge. Les résultats de tous les aspects discutés dans cette thèse ont été obtenus par simulation numérique en utilisant le logiciel Matlab/Simulink. En outre, une mise en œuvre en temps réel dans le laboratoire de génie électrique de Biskra (LGEB), équipé de la carte dSpace 1104 a été réalisée. Des résultats expérimentaux ont été présentés afin de valider les résultats de simulation.

Mots-clés : Moteur asynchrone, commande directe de couple, Modulation vectorielle, Commande non linéaire, Commande par mode glissant, Observateur, Basse vitesse, Optimisation du rendement.

ملخص

تحسين أداء التحكم المباشر للعزم للآلة الغير المتزامنة باستعمال تقنيات غير خطية

تم تقديم تقنية التحكم المباشر في العزم (DTC) كبديل للتحكم الشعاعي في منتصف الثاينيات للتحكم في آلات التيار المتناوب. تعتمد هذه التقنية على التحديد المباشر لوضعيات تبديل الموج وتميز بمخطط تحكم أبسط وحساسية أقل تجاه وسائط الماكنة. لكن تواتر التبديل المتغير للتقنية يسبب ظهور تموجات على مستوى التدفق المغناطيسي والعزم مما يحدث ضجيج ويقود الى ضعف أداء التقنية خصوصا عند السرعات المنخفضة. يهدف تحسين أداء استراتيجية التحكم المباشر في العزم للمحرك الغير المتزامن، تتطرق هذه الأطروحة لأهم النقاط المتعلقة بهذه الإشكالية. أولا تم القيام بتخفيض التموجات العالية للتدفق المغناطيسي والعزم والتي تمثل أهم العيوب بتطبيق تواتر تبديل ثابت باستعمال تقنية تعديل طول النبضة الشعاعي (SVM). ثم قمنا بعرض تصميم تحكم غير خطي يعتمد على خطية المداخل والمخارج والتحكم ذو النمط إنزلاقي لضمان تحكم متين ضد مختلف الاضطرابات الخارجية.

علاوة على هذا، يستطيع التحكم بدون لاقط الزيادة من وثوقية نظام التحكم وتخفيض تكلفته، لهذا قمنا بتقديم ملاحظات مختلفة لتحسين تقدير السرعة والتدفق المغناطيسي في السرعات المرتفعة والمنخفضة. وفي الأخير تطرقنا إلى استراتيجية تقليل عموم الضياعات للحصول على المردود الأمثل بالتعديل الآني للتدفق المنتج وفق قيمة المحولة. جميع النتائج المتعلقة بالجوانب المتطرق إليها في الأطروحة تم عرضها بالمحاكاة الرقمية باستعمال برنامج ماتلاب، بالإضافة الى تطبيق تجريبي في مختبر الهندسة الكهربائية بسكرة (LGEB) المجهز بالبطاقة الرقمية dSpace 1104 ولقد تم عرض النتائج التجريبية للتحقق من صحة نتائج المحاكاة.

الكلمات المفتاحية: محرك غير متزامن، التحكم المباشر في العزم، تعديل طول النبضة الشعاعي، تحكم غير خطي، تحكم ذو نمط إنزلاقي، ملاحظ، سرعة منخفضة، المردود الأمثل.

List of Publications Related to Thesis

Journal Publications

1. **Abdelkarim Ammar**, Amor Bourek, Abdelhamid Benakcha "Nonlinear SVM-DTC for induction motor drive using input-output feedback linearization and high order sliding mode control" ISA Transactions. Vol.67, pp. 428–442, 2017.
2. **Abdelkarim Ammar**, Abdelhamid Benakcha, Amor Bourek, "Adaptive MRAC-based direct torque control with SVM for sensorless induction motor using adaptive observer", The International Journal of Advanced Manufacturing Technology. Vol.91(5), pp. 1631–1641, 2017.
3. **Abdelkarim Ammar**, Amor Bourek, Abdelhamid Benakcha, "Sensorless SVM-direct torque control for induction motor drive using sliding mode observers", Journal of Control, Automation and Electrical Systems. Vol.28(2), pp.189–202, 2017.
4. **Abdelkarim Ammar**, Abdelhamid Benakcha, Amor Bourek, "Closed loop torque SVM-DTC based on robust super twisting speed controller for induction motor drive with efficiency optimization". International Journal of Hydrogen Energy, 2017.
5. **Abdelkarim Ammar**, Amor Bourek and Abdelhamid Benakcha "Robust SVM-direct torque control of induction motor based on sliding mode controller and sliding mode observer" Frontiers in Energy, 2017.
6. **Abdelkarim Ammar**, Amor Bourek, Abdelhamid Benakcha "Robust load angle direct torque control with SVM for sensorless induction motor using sliding mode controller and observer" "Accepted in" International Journal of Computer Aided Engineering and Technology, 2016

Conference Proceedings

1. **Abdelkarim Ammar**, Amor Bourek, Abdelhamid Benakcha, Ameid Tarek "Sensorless stator field oriented-direct torque control with SVM for induction motor based on MRAS and fuzzy logic regulation" 6th IEEE International Conference on Systems and Control (ICSC2017), May 7-9, 2017, University of Batna 2, Batna, Algeria.
2. Tarek Ameid, Arezki Menacer, Hichem Talhaoui, Imad Harzelli, **Abdelkarim Ammar** "Backstepping control for induction motor drive using reduced model in healthy state: simulation and experimental study" 6th IEEE International Conference on Systems and Control (ICSC2017), May 7-9, 2017, University of Batna 2, Batna, Algeria.
3. **Abdelkarim Ammar**, Amor Bourek, Abdelhamid Benakcha "Efficiency optimization for sensorless induction motor controlled by MRAS based hybrid FOC-DTC strategy" The International Conference on Control, Automation and Diagnosis (ICCAD'17) January 19-21, 2017. Hammamet - Tunisia
4. **Abdelkarim Ammar**, Amor Bourek, Abdelhamid Benakcha "Implementation of robust SVM-DTC for induction motor drive using second order sliding mode control" IEEE The 8th International Conference on Modelling, Identification and Control (ICMIC'2016) 15-17 November 2016, Algiers, Algeria.
5. Tarek Ameid, Arezki Menacer, Hichem Talhaoui, Imad Harzelli, **Abdelkarim Ammar** "Simulation and real-time implementation of sensorless field oriented control of induction motor at healthy state using rotor cage model and EKF" IEEE The 8th International

Conference on Modelling, Identification and Control (ICMIC'2016) 15-17 November 2016, Algiers, Algeria.

6. Abdelkarim Ammar, Abdelhamid Benakcha, Amor Bourek *"Real time implementation of speed sensorless SVM-DTC for induction motor drive based on adaptive flux observer"* The 9th International Conference on Electrical Engineering and First Workshop on Robotics and Controls CEE 2016, October 2-4, 2016 Batna. Algeria.

7. Abdelkarim Ammar and Abderrahim Zemmit *"Design of combined vector control and direct torque control for induction motor drive with speed MRAS observer"* The 9th International Conference on Electrical Engineering and First Workshop on Robotics and Controls CEE 2016, October 2-4, 2016 Batna. Algeria.

8. Abdelkarim Ammar, Abdelhamid Benakcha, Amor Bourek *"Closed loop torque SVM-DTC of induction motor drive with efficiency optimization"* VI European Conference on Renewable Energy Systems ECRES 2016, 28-31 August 2016, Istanbul, Turkey.

9. Abdelkarim Ammar, Amor Bourek, Abdelhamid Benakcha *"Modified load angle direct torque control for sensorless induction motor using sliding mode flux observer"* IEEE 4th International Conference on Electrical Engineering ICEE'201513-15 December 2015, Boumerdes, Algeria

10. Abdelkarim Ammar, Amor Bourek, Abdelhamid Benakcha *"Implementation of sensorless direct torque control of induction motor using sliding mode observer"* International Conference on Automatic control, Telecommunications and Signals (ICATS15) November 16-18, 2015 University BADJI Mokhtar - Annaba - Algeria

11. Abdelkarim Ammar, Amor Bourek, Abdelhamid Benakcha *"High performance direct torque control of induction motor based on space vector modulation and fuzzy logic controller for speed regulation"* First International Conference on Electrical Engineering, ICEEB'14, December 07-08, 2014 Biskra, Algeria.

12. Abdelkarim Ammar, Amor Bourek, Abdelhamid Benakcha *"Improved direct torque control of induction motor using space vector modulation"* The International Conference on Information Processing and Electrical Engineering, ICIPEE'14, November 24-25, 2014 in Tébessa, Algeria.

List of Figures

Fig.1.1	Classification of variable frequency control strategies for IM drive	08
Fig.1.2	Closed loop scalar control for variable frequency induction motor drive.	08
Fig.1.3	Basic indirect field oriented control (IFOC) of induction motor.	09
Fig.1.4	Direct torque control strategy based on lookup switching table.	10
Fig.1.5	Block diagram of direct self-control (DSC).	11
Fig.1.6	General block diagram of SVM Direct torque control method.	12
Fig.1.7	Multi-input multi-output feedback linearizing structure	14
Fig.1.8	Function $sign(s)$.	16
Fig.1.9	Saturation and sigmoid functions.	16
Fig.1.10	Classification of different Sensorless estimation techniques for AC motor drives	19
Fig.1.11	Block diagram of the model reference adaptive system observer.	21
Fig.1.12	Block diagram of model based adaptive observer.	22
Fig.1.13	General structure of the Kalman filter estimator.	23
Fig.1.14	General structure of adaptive sliding mode observer.	24
Fig 2.1	Three-phase VSI fed star-connected induction machine.	28
Fig 2.2	VSI Voltage vectors in the complex plane.	29
Fig 2.3	Evolution of stator flux vector in the complex plan.	30
Fig.2.4	Tow-level hysteresis comparator for stator flux control.	31
Fig.2.5	Three level hysteresis comparator for electromagnetic torque control	32
Fig.2.6	Voltage vector selection when the stator flux vector is located in sector i	34
Fig.2.7	Voltage space vector in 12 sectors case	35
Fig.2.8	Speed anti-windup PI controller	36
Fig.2.9	Global control scheme of basic direct torque control	37
Fig.2.10	Diagram of voltage space vector	38
Fig.2.11	Reference vector as a combination of adjacent vectors at sector 1	38
Fig.2.12	Switching times of sector 1	39
Fig.2.13	Global control scheme of stator flux oriented SVM- direct torque control	41

Fig.2.14	Rotor speed response at the starting up and steady states followed by load application.	42
Fig.2.15	Electromagnetic torque followed by load application of 5 N.m at $t=0.5s$.	42
Fig.2.16	Stator phase current i_{sa}	42
Fig.2.17	ZOOM of stator phase current i_{sa}	42
Fig.2.18	FFT analysis and spectrum of THD for stator phase current i_{sa} .	43
Fig.2.19	Stator flux magnitude [Wb]	43
Fig.2.20	ZOOM of Stator flux	43
Fig.2.21	ZOOM of stator phase flux	43
Fig.2.22	Flux circular trajectory (α,β) [Wb]	44
Fig.2.23	Position of stator flux vector	44
Fig.2.24	Inverter switching state S_a	44
Fig.2.25	Rotation sense reversing: rotor speed ($1000rpm;-1000rpm$)	46
Fig.2.26	Rotation sense reversing : Electromagnetic torque [N.m]	46
Fig.2.27	Rotation sense reversing: Stator phase current [A]	46
Fig.2.28	Rotation sense reversing: ZOOM of Stator phase current [A]	46
Fig.2.29	Rotation sense reversing: Stator flux components $[\alpha,\beta]$	47
Fig.2.30	Rotation sense reversing: Position of stator flux vector [rad]	47
Fig.2.31	Low speed operation: Rotor speed [rpm]	48
Fig.2.32	Low speed operation: Stator flux position [rad]	48
Fig.2.33	Low speed operation: Stator phase current [A]	48
Fig.2.34	Low speed operation: Stator flux magnitude [Wb]	48
Fig.2.35	Low speed operation: Electromagnetic torque [N.m]	49
Fig.2.36	Presentation of the experimental setup.	50
Fig.2.37	Starting up: Rotor speed and torque responses with load application of 5 N.m.	50
Fig.2.38	Rotor speed and electromagnetic torque with load application of 5 N.m	51
Fig.2.39	Stator phase current with load application	51
Fig.2.40	Stator phase THD using power analyzer	51
Fig.2.41	Stator flux magnitude	52
Fig.2.42	Stator flux axes components $(\psi_{sa}, \psi_{s\beta})$	52

Fig.2.43	Stator flux circular trajectory	52
Fig.2.44	Inverter switching state S_a	53
Fig.2.45	Rotation sense reversing: Rotor speed, electromagnetic torque	54
Fig.2.46	Rotation sense reversing: Rotor speed, electromagnetic torque (ZOOM)	54
Fig.2.47	Rotation sense reversing: Flux components, current and flux position	54
Fig.2.48	Low speed operation test :(200 rpm–600 rpm): Speed, current and flux position	55
Fig.2.49	Low speed operation test (200 rpm–600 rpm): Flux magnitude, torque	55
Fig.3.1	Block diagram of the linearization by the state feedback.	60
Fig.3.2	Sliding mode principle of state trajectory.	64
Fig.3.3	Equivalent control structure.	66
Fig.3.4	Phase trajectory of twisting algorithm.	68
Fig.3.5	Diagram of global sliding mode IFOL-DTC strategy with super twisting speed controller	73
Fig.3.6	Startup and steady states of speed response followed by load application at $t=0.5s$.	73
Fig.3.7	Electromagnetic torque response with load application of 5 N.m at $t=0.5s$	74
Fig.3.8	Stator phase current i_{sa} [A].	74
Fig.3.9	Stator flux magnitude [Wb].	74
Fig.3.10	Stator flux axes components [Wb].	74
Fig.3.11	Stator flux circular trajectory [Wb].	75
Fig.3.12	Stator Resistance variation profile [Ω].	76
Fig.3.13	Speed's response in low region (50 rpm) with variation of stator resistance $R_s +50\%$.	76
Fig.3.14	Torque's response with load of 5 N.m in low speed and variation of stator resistance.	76
Fig 3.15	Stator flux magnitude with variation of stator resistance $R_s +50\%$.	76
Fig.3.16	Rotor speed (1000 rpm; –1000 rpm) response for PI and STSC speed controllers.	77
Fig.3.17	Torque response (Load applied at $t=0.5s$) for PI and STSC speed controllers	77
Fig.3.18	Rotor speed response for PI and STSC at low-medium region (200-600 rpm).	78

Fig.3.19	Rotor speed response for PI and STSC at low region (50-25 rpm).	78
Fig.3.20	Speed response following benchmark trajectory in different regions (PI and STSC).	78
Fig.3.21	Speed and torque responses during the starting up then load application.	80
Fig.3.22	Stator phase current i_{sa} [A].	80
Fig.3.23	Stator flux magnitude [Wb].	80
Fig.3.24	Stator flux components and position.	81
Fig.3.25	Stator flux circular trajectory ($\psi_{sa}, \psi_{s\beta}$) ($I_{div}=0.5Wb$).	81
Fig.3.26	Speed response with disturbance introduction (PI and STSC).	82
Fig.3.27	Speed response while direction reverse with trapezoidal reference (PI and STSC).	82
Fig.3.28	Benchmark speed trajectory: Reference and measured speed in different regions (PI and super twisting controllers).	82
Fig.3.29	Low speed operation: speed variation ($a:200\text{ rpm}-600\text{ rpm}$, $b:50\text{ rpm}-25\text{ rpm}$).	83
Fig.4.1	Modified flux estimator	87
Fig.4.2	Three-phase stator currents waveforms in medium speed region (400 rpm).	88
Fig.4.3	Stator flux magnitude and components using modified flux estimator at very low speed	88
Fig.4.4	Block diagram of speed adaptive flux observer.	94
Fig.4.5	Proposed sliding mode stator flux observer	95
Fig.4.6	Industrial benchmark trajectory	97
Fig.4.7	Global diagram of sensorless nonlinear SVM-DTC based on speed and flux observer	97
Fig.4.8	Starting up and steady states: Real and estimated speed [rpm].	98
Fig.4.9	Rotor speed estimation errors [rpm].	98
Fig.4.10	Estimated stator flux magnitude [Wb].	99
Fig.4.11	Estimated stator flux components [Wb].	99
Fig.4.12	Real and estimated speed at low speed operation (200rpm, 400rpm).	100
Fig.4.13	Real and estimated speed at low speed operation (50 rpm; 25 rpm)	100
Fig.4.14	Rotor speed estimation errors in different speed regions [rpm].	100
Fig.4.15	Estimated Stator flux magnitude in different speed regions [Wb].	100
Fig.4.16	Real and estimated speed at 1000 rpm then zero speed region.	101

Fig. 4.17	Estimated stator flux magnitude at <i>1000 rpm</i> then zero speed region	101
Fig.4.18	Speed estimation under industrial benchmark trajectory in different speed regions.	102
Fig.4.19	Speed estimation errors under industrial benchmark trajectory in different speeds	102
Fig.4.20	Robustness test: Low speed operation with parametre variation $((R_s, R_r)+50\%)$.	103
Fig.4.21	Robustness test: flux magnitude with parametres variation $((R_s, R_r)+50\%)$.	103
Fig.4.22	Applied and estimated load torque [N.m].	104
Fig.4.23	Load torque estimation error [N.m].	104
Fig.4.24	Starting up and steady states: Estimated and real speed with estimation error	105
Fig.4.25	Starting up and steady states: Estimated flux magnitude, and components.	105
Fig.4.26	Low speed operation (<i>200;400 rpm</i>): Estimated and real speed and estimation error.	106
Fig.4.27	Low speed operation (<i>200;400 rpm</i>): Estimated flux magnitude and components.	106
Fig.4.28	Low speed operation (<i>50;25 rpm</i>): Estimated and real speed and estimation error.	106
Fig.4.29	Zero speed operation: Estimated and real speed and estimation error.	107
Fig.4.30	Zero speed operation: Estimated flux magnitude and components.	107
Fig.4.31	Benchmark trajectory: Estimated and real speed and estimation error.	108
Fig.4.32	Applied and estimated load torque with estimation error.	108
Fig.4.33	Association of Stator Flux model-MRAS speed observer with SMO.	110
Fig.4.34	a: Starting up and steady state (<i>1000 rpm</i>), b: low speed operation (<i>50 rpm;25 rpm</i>).	110
Fig.4.35	a: Speed estimation errors at <i>1000 rpm</i> , b: Speed estimation errors at low speeds (<i>50 rpm;25 rpm</i>).	110
Fig.4.36	a: Zero-speed operation, b: variable profile (benchmark) tests.	111
Fig.4.37	a: Speed estimation errors at zero-speed, b: at variable profile (benchmark) tests.	111
Fig.4.38	a: Starting up and steady state (<i>1000 rpm</i>), b: low speed operation (<i>50 rpm;25 rpm</i>) with estimation errors.	112
Fig.4.39	a: Zero-speed operation, b: variable profile tests with estimation errors.	112
Fig.5.1	Per-phase steady state equivalent circuit of IM.	115

Fig.5.2	Induction motor steady-state equivalent circuit in (d, q) frame..	119
Fig.5.3	Block Diagram of SVM-DTC with efficiency optimization strategy.	122
Fig.5.4	Stator flux magnitude [Wb].	122
Fig.5.5	Stator flux axes components (α, β) [Wb].	123
Fig.5.6	Stator flux trajectory [Wb].	123
Fig.5.7	3D presentation of stator flux trajectory [Wb].	123
Fig.5.8	Electromagnetic torque with load application of (5N.m)	123
Fig.5.9	Stator phase current i_{sa} [A].	124
Fig.5.10	Total losses [W] and efficiency.	124
Fig.5.11	Stator flux magnitude [Wb]	125
Fig.5.12	Stator flux components with zoom [Wb].	125
Fig.5.13	Stator flux trajectory [Wb].	125
Fig.5.14	Stator phase current [A].	126
Fig.5.15	Flux and torque according to the applied load value $(0-2 N.m)$.	127
Fig.5.16	Load variation and Efficiency.	127
Fig.5.17	Curve of efficiency evolution according to different load values.	128
Fig.A.1	Cross section of the squirrel cage induction motor (Copyright granted, 2012, ABB)	132
Fig.A.2	Induction motor equivalent structure.	133
Fig.A.3	The passage of three-phase to two-phase system using Park transformation.	137
Fig.A.4	Speed control loop.	140
Fig.A.5	Block diagram of the stator flux control loop.	142
Fig.A.6	Block diagram of the torque control loop.	142
Fig.A.7	Presentation of the experimental setup.	143
Fig.A.8	Induction machine's nameplate	144
Fig.A.9	dSpace DS1104 Controller.	145
Fig.A.10	Architecture of DS1104	145
Fig.A.11	dSpace 1104 interface board.	146
Fig.A.12	Descriptive block diagram of the dSpace based experimental setup.	146
Fig.A.13	Layout of the dSpace instrumentation panel Controldesk.	147

List of Tables

Table.2.1	Look-up table for basic direct torque control.	34
Table.2.2	Look up switching table with twelve sectors.	35
Table.2.3	Switching times for each sector	39
Table.2.4	The Advantages of DTC–SVM compared to the classical DTC	56
Table.3.1	Comparative analysis of SFOC SVM-DTC and SMFL-DTC with various speed controllers	79
Table.3.2	Comparative assessment of both of the presented control algorithms.	84
Table.4.1	Comparative analysis between different observer structures.	111
Table.5.1	Induction motor efficiency analysis under different load values.	127
Table.A.1	Parameters of the induction machine.	144

List of Abbreviations

AC	Alternative Current.
DC	Direct Current.
DFOC	Direct-Field Oriented Control.
DSC	Direct Self Control.
DSP	Digital Signal Processor.
DTC	Direct Torque Control.
EKF	Extended Kalman Filter.
EMF	Electro-Motive Force.
FOC	Field Oriented Control.
FPGA	Field Programable Gate Array.
HPF	High-Pass Filter.
ILOC	Indirect-Field Oriented Control.
IM	Induction Machine/Motor.
IOFL	Input-Output Feedback Linearization.
LPF	Low Pass Filter.
LMC	Loss Model Control.
MIMO	Multi-Input-Multi-Output.
MRAS	Model Reference Adaptive System.
PF	Power factor
PI	Proportional-Integral.
PMSM	Permanent Magnet Synchronous Motor/Machine.
PWM	Pulse Width Modulation.
RTI	Real Time Interface.
SC	Search Controller.
SFOC	Stator Filed Oriented Control.
SISO	Single-Input-Single-Output.
SMC	Sliding Mode Control.
SMFL	Sliding Mode Feedback Linearization.
SMO	Sliding Mode Observer.
ST	Super Twisting.
STSC	Super Twisting Speed Controller.
SVM	Space Vector Modulation.
THD	Total Harmonics Distortion.
VFD	Variable Frequency Drives.
VSC	Variable Structure Control.
VSI	Voltage Source Inverter.

List of Symbols

$i_{s\alpha}$ $i_{s\beta}$	α and β components of stator currents.
$V_{s\alpha}$ $V_{s\beta}$	α and β components of stator voltage.
$ \psi_s $	Stator flux magnitude.
ψ_r	Rotor flux.
$\psi_{s\alpha}, \psi_{s\beta}$	α and β components of stator flux.
R_s R_r	Stator and rotor resistances respectively.
L_s L_r	Stator and rotor inductances respectively.
T_e	Electromagnetic torque
T_s T_r	Stator and rotor time constants.
σ	Blondel's coefficient.
M_{sr}	Stator-rotor mutual inductance
T_e	Electromagnetic torque
p	Number of poles pairs.
ω_r	Rotor speed
ω_s	Synchronous speed
ω_{sl}	Slip speed.
J	Inertia moment.
f	Coefficient of friction.
V_{dc}	Dc-bus voltage.
$cflx$	Flux logic output.
$ctrq$	Torque logic output.
h_{ψ_s}	Hysteresis band of stator flux.
h_{T_e}	Hysteresis band of stator torque.
θ_s	Flux angle.
δ	Load angle between the stator and rotor flux vectors.
T_z	Sampling time.
T_1 T_2	Reference voltages vectors corresponding durations
K_p K_i	Proportional and integral gains.

$V_{sd} V_{sq}$	Direct and quadratic stator voltage components.
$V_{rd} V_{rq}$	Direct and quadratic rotor voltage components.
$y_1 y_2$	IOFL control objectives
e_1, e_2	IOFL torque and flux tracking errors.
$V_1 V_2$	Auxiliary inputs of the IOFL control technique.
$k_1 k_2$	Positive constants of the IOFL control technique
V	Lyapunov candidate function.
s	Slip value
S	Sliding surface
u	Control law
u_{eq}	Equivalent control
u_n	Discontinues control
u_{ST}	Super twisting control law.
λ, K	Positives gains of super twisting control law.
T_L	Load torque.
K	Sliding mode controller gain.
G	Adaptive observer gain matrix.
$P_{sc} P_{rc}$	Stator and rotor copper losses respectively.
P_{fs}	Stator core losses.
$P_{hs} P_{es}$	Stator hysteresis and eddy-current losses respectively.
K_h, K_e	Hysteresis and eddy-current coefficients
f_s	Stator frequency.
$\psi_{s_opt}^*$	Optimal reference value of rotor flux.
$\psi_{s_opt}^*$	Optimal reference value of stator flux.
η	Efficiency

Table of Contents

<i>Dedication</i>	
<i>Acknowledgments</i>	
<i>Abstract</i>	
<i>List of Publications</i>	
<i>List of figures</i>	
<i>List of tables</i>	
<i>Nomenclature</i>	
<i>Table of Contents</i>	
<i>General Introduction</i>	1

Chapter 01

State of The Art in Different Control Strategies for Induction machine

1.1 Introduction.....	6
1.2. Background on Variable Speed Drives.....	7
1.2.1 Scalar control.....	8
1.2.2 Field oriented control	9
1.2.3 Direct torque control	10
1.2.3.1 Basic direct torque control and direct self-control	10
1.2.3.2 Direct torque control with constant switching frequency.....	11
1.3 Nonlinear Control Techniques.....	12
1.3.1 Feedback linearization.....	13
1.3.1.1 Input-output feedback linearization.....	13
1.3.1.2 Other linearization methods.....	14
1.3.1.3 Summary.....	14
1.3.2 Sliding Mode Control.....	15
1.3.2.1 Brief Historical on sliding mode theory	15
1.3.2.2 Basic concepts of SMC.....	15
1.3.2.3 Chattering phenomenon.....	16
1.3.2.4 High order sliding mode control.....	17
1.3.3. Survey on the application of nonlinear techniques for electrical machines control....	18
1.4 Sensorless Control Techniques for Induction Motor	19
1.4.1 Open loop estimation methods (Estimators without feedback)	20

1.4.1.1. Voltage model flux estimator	20
1.4.1.2. Current model flux estimator.....	20
1.4.1.3. Rotor speed estimation	20
1.4.2 Model reference adaptive system (MRAS).....	21
1.4.3 Closed Loop Observers based on Machine State Reconstruction.....	21
1.4.3.1 Adaptive observers	21
1.4.3.2 Extended Kalman filter.....	22
1.4.3.3 Sliding mode observers	23
1.5 Efficiency Optimization Based Control.....	24
1.6 Conclusion	26

Chapter 02

Basic Direct Torque Control Methods for the Induction Motor Drive

2.1 Introduction.....	27
2.2 Model of Induction Motor Dedicated for Direct Torque Control.....	27
2.3 Tow-Level Voltage Source Inverter (VSI) Model.....	28
2.4 Principles of Direct Torque Control	29
2.4.1 Control of stator flux and electromagnetic torque	30
2.4.1.1 Control of stator flux	30
2.4.1.2 Control of electromagnetic torque.....	31
2.4.2 Estimation of stator flux and electromagnetic torque	32
2.4.2.1 Stator flux estimation.....	32
2.4.2.2 Electromagnetic torque estimation	33
2.5 Switching Table Construction and Control Algorithm Design.....	33
2.5.1 Six sectors Switching table	33
2.5.2 DTC improvement using twelve sector switching table	34
2.5.3 Speed regulation in DTC strategy	36
2.5.4 Global scheme of basic direct torque control.....	36
2.6 Constant Switching Frequency Direct Torque Control Using SVM	37
2.6.1 Space vector modulation algorithm.....	38
2.6.2 Stator flux oriented (SFO) SVM-DTC strategy	40
2.7 Simulation Results	41
2.7.1 Starting up and steady states with load application	41
2.7.2. Rotation sense reversing.....	45

2.7.3. Low speed operation	47
2.8. Real-Time Control of Induction Motor.....	49
2.9. Experimental Results:	50
2.9.1. Starting up and steady states with load application.....	50
2.9.2. Speed sense reversing:	54
2.10.3. Low speed operation	55
2.10 Comparative evaluation of direct torque control techniques	56
2.11. Conclusion	57

Chapter 03

Nonlinear SVM-DTC Using Feedback Linearization and Sliding Mode Control

3.1 Introduction:.....	58
3.2 Nonlinear Control Strategies.....	59
3.2.1 Input-output feedback linearization (IOFL) approach	59
3.2.1.1 Relative degree and lie derivatives:.....	59
3.2.1.2 Control design.....	60
3.2.2 Application of IOFL on direct torque control for IM drive (IOFL-DTC)	61
3.2.2.1 Model presentation	61
3.2.2.2 IOFL-DTC control design	61
3.2.2.3 Feedback linearization improvement.....	64
3.2.3 Sliding mode control	64
3.2.3.1 Sliding surface choice.....	64
3.2.3.2 Existence conditions of sliding mode	65
3.2.3.3 Control design.....	65
3.2.4 Second order sliding mode control.....	67
3.2.4.1 Twisting control.....	67
3.2.4.2 Sub-optimal control	68
3.2.4.3 Super twisting control.....	68
3.2.5 Application of first order sliding mode control on direct torque control	69
3.2.6 Improved direct torque control using second order sliding mode control	71
3.2.6.1 First order SM-speed controller design	71
3.2.6.2 Second order SM-speed controller design.....	72
3.3. Simulation Results	73

3.3.1. SFOC SVM-DTC and nonlinear SMFL-DTC starting up and steady states	73
3.3.2 Robustness test of parameters variation in low speed region.....	75
3.3.3. PI and super twisting speed (STSC) controllers comparative analysis	77
3.4. Experimental Results	79
3.4.1 SFOC SVM-DTC and nonlinear SMFL-DTC starting up and steady states	79
3.4.2 PI and super twisting speed controller (STSC) comparative analysis	82
3.4.3 Low speed operation	83
3.5 Summarized comparative evaluation of control techniques	84
3.6. Conclusion	84

Chapter 04

Estimation and Sensorless Control for DTC Controlled Induction Motor

4.1 Introduction.....	86
4.2. Open-Loop Flux Estimation	86
4.2.1 Conventional stator flux estimation	87
4.2.2 Solution 1: Modified flux estimator.....	87
4.2.3 Solution 2: Current-model based flux estimator	88
4.3 Closed-Loop Estimation of The Induction Motor (<i>Sensorless control</i>)	89
4.3.1 Definition: observability and observers	89
4.3.2 Observers based on machine state reconstruction.....	89
4.3.3 Model reference adaptive system MRAS.....	90
4.4. Limits of Sensorless Control in Low-Speed Operation Condition	90
4.4.1 Signal acquisition errors.....	90
4.4.2 Inverter non-linearity.....	91
4.4.3 Distortions in the flux angle.....	91
4.4.4 Incorrect speed estimation.....	91
4.4.5 Delay due to filtering.....	91
4.5 Sensorless Control Design for Nonlinear SVM-DTC Strategy	91
4.5.1 Full order adaptive observer for DTC controlled IM.....	92
4.5.2 Sliding mode flux observer for DTC controlled IM	94
4.5.2.1 Sliding mode flux observer design	94
4.5.2.2 Gain selection	95
4.5.2.3 Speed estimation.....	95
4.5.3 Second order sliding mode load torque observer	96

4.6. Operating Conditions and Benchmarks	97
4.7 Simulation and Experimental Comparative Study.....	98
4.7.1 Simulation results.....	98
4.7.1.1 Starting up and steady state	98
4.7.1.2 Low speed operations	99
4.7.1.3 Zero speed operation and industrial benchmark test	101
4.7.1.4 Parameters variation test.....	103
4.7.1.6 Load torque estimation	104
4.7.2 Experimental results.....	104
4.7.2.1 Starting up and steady state	105
4.7.2.2 Low speed operation.....	106
4.7.2.3 Zero speed operation and industrial benchmark test	107
4.7.2.4 Load torque estimation	108
4.8 Association of MRAS with stator flux SMO for speed estimation	109
4.8.1 Simulation results.....	110
4.8.2 Experimental results.....	112
4.9 Conclusion	113

Chapter 05

Efficiency Optimization of The IM Controlled by Nonlinear SVM-DTC Strategy

5.1. Introduction.....	114
5.2. Steady State Performance, Power Losses and Efficiency of The IM	115
5.2.1 Per phase equivalent circuit of IM	115
5.2.2 Power Losses of IM.....	115
5.2.2.1 Stator and rotor copper losses.....	115
5.2.2.2 Core losses	116
5.2.2.3 Mechanical losses	116
5.2.2.4 Stray load losses	116
5.2.2.5 Converters losses	117
5.2.3 Induction motor efficiency and power factor.....	117
5.3. Efficiency Optimization Methods of IM.....	118
5.3.1 Search control (SC)	118

5.3.2. Loss model based controller (LMC)	118
5.4 Application of Losses Minimization with Nonlinear DTC Control Scheme.....	119
5.4.1 Induction motor loss model in (d, q) reference frame.....	119
5.4.2 Loss minimization algorithm	120
5.4.3 The optimal choice of flux level	121
5.5 Simulation Results	122
5.6 Experimental Results	125
5.6.1 Starting up, steady state and load application	125
5.6.2 Application of different load values in steady state	126
5.7. Conclusion	128
<i>General Conclusion</i>	130
<i>Appendix</i>	
<i>References</i>	



General Introduction

General Introduction

Overview:

Nowadays, the AC machines have replaced the DC machines in industry applications because of their advantages, such as, the reliability and the lack of commutator and brushes which make them able to work under unfriendly conditions. The most popular AC machines are the induction motors (IMs) and the permanent magnet synchronous motors (PMSMs). They are used in various industrial applications, electric vehicles (EV), tools and drives etc. The squirrel cage induction motor in particular, is widely used due to its reduced cost and lower maintenance requirement.

In the early decades, the induction motors have been operated directly from the grid under a fixed frequency/speed. Later, with the development of modern semiconductor devices and power electronic converters, these machines had become able to operate with adjustable frequency/speed by supplying them through a power converter like the voltage source inverter (VSI). The employment of the variable speed motor drive in open loop may offer a satisfied performance at steady state without need of speed regulation for simple applications [Li05]. But, in cases where the drive requires fast dynamic response and accurate speed, the open loop control becomes unsatisfactory. Therefore, it is necessary to operate the motor in a closed loop mode. Several techniques have been proposed for this purpose. They are classified mainly into scalar and vector controls [Buj04].

The scalar control, that called also volts/hertz, is a simple strategy which is applied to control the speed of IMs based on the constant ratio of voltage magnitude and frequency using the steady-state equivalent circuit model of the machine. However, this method does not dedicate for high performance applications due to its slow response and the existence of coupling between torque and flux. The vector control, which is known also by the field oriented control (FOC), was developed to overcome the limitation of the scalar control. It was presented in the 1970s by Hasse [Has69] and Blaschke [Bla72] to provide an independent control of torque and flux in similar way to the separate excitation DC machine. The vector representation of the motor quantities makes it valid to work in both steady and dynamic conditions, this achieves a good transient response. In the control algorithm of FOC based on the transformation to the synchronous frame, all quantities will appear as DC quantities. Nevertheless, the main disadvantages of FOC are the coordinates transformation which needs the flux angle that cannot be directly measured, in addition, the sensitivity to the variation of the machine parameters, like the stator and the rotor resistances.

Another method guarantees a separated flux and torque control is called Direct Torque Control (DTC). It was introduced by Takahashi and Nagochi in the middle of 1980s in Japan [Tak86], and also in Germany by Depenbrock under the name of Direct Self-Control (DSC) [Dep88]. In contrast to FOC, this control is completely done in stationary frame (stator fixed coordinates). Furthermore, DTC generates the inverter gating signals directly through a look up switching table and the use of modulator is not necessary. It offers an excellent torque response using less model's parameters than FOC. Due to its simplicity and very fast response it can be so applicable for high performance drive applications [Wan14].

However, the standard DTC method suffers from high flux and torque ripples owing to the use of hysteresis controllers. Many modified DTC schemes have been proposed in order to reduce ripples. The insertion of the space vector modulation (SVM) was a very useful solution [Hab92]. This method, known by SVM-DTC, reduces the high ripples level in spite of its complexity. Several SVM-DTC control schemes have been mentioned in the literature [Las00; Rod04], one of the developed methods is stator flux orientated (SFO). This method combines the advantages of both of FOC and DTC methods and eliminate their drawbacks. SVM-DTC algorithm uses linear PI torque and flux controllers instead of hysteresis comparators to generate the reference control voltages.

The linear proportional integral differential (PID) controllers have encountered a wide interest in the industrial applications. However, extra extensions should be made to fulfill an acceptable behavior like the output limitation and anti-windup. Nevertheless, another important issue is proposed for stability reasons in the control loop [Sto13]. The industrial control processes usually deal with complex systems with multiple variable and multiple parameters which may have nonlinear coupling (i.e. the induction machine in particular) [Pan13]. The initial mathematical model based on conventional analytic methods usually contains approximate hypothesis and unmodeled dynamics. Moreover, it may be affected also by the variation in parameters due to environment conditions and the external disturbance during operating. Consequently, the use of linear methods cannot achieve high promising performance.

The development of robust control methods to solve this problem has made a big achievement recently. The nonlinear controllers can offer several advantages compared to linear control schemes. Among the interest researches in the field of nonlinear control techniques are the feedback linearization and the sliding mode control (SMC) [Isi84; Utk93]. Feedback linearization is a nonlinear control approach used to transform a nonlinear system into an equivalent linear one, then to apply a conventional controller design. This algorithm

provides a good behavior in steady and dynamical states. In addition, it offers also an exact decoupling between system variables. Due to some limits, such as the sensitive to modeling errors and disturbances, it has been rarely applied to IM drives [Kaz95]. Contrariwise, the sliding mode control is featured by high robust behavior while the presence of uncertainties. SMC forces the system trajectory to slide along the switching surface by determined control law. The most powerful advantages of the SMC are the high robustness against the different system uncertainties, the rapid dynamic response and the simple implementation. The application of aforementioned nonlinear techniques (i.e. feedback linearization and SMC) for the improvement of basic electrical drive control strategies like the vector and the direct torque control has been presented in several works. In [Ben99a] a feedback linearization with PI controllers is used in vector control regulation. The combining of SMC and DTC with space vector modulation has been done by Lascu in [Las04] for high performance robust SVM-DTC. The combining of both feedback linearization and SMC has been proposed also in some recent works, where the feedback linearization is applied firstly, after that the SMC will be used to control linearized induction motor. In [Yaz08; Haj09; Las17] similar modified strategies are applied to SVM-DTC controlled drive. In our research paper [Amr17a], a higher order sliding mode controller has been incorporated to a nonlinear DTC control with SVM based on feedback linearization in order to get high robustness control and reduce the effect of chattering problem.

Moreover, the sensorless control is another major issue in control domain. The developed control schemes using advanced strategies such as the SVM and nonlinear techniques require an accurate speed and flux measurement or estimation for closed loop control design. The use of sensors has several downsides like high cost, fragility and low reliability. Furthermore, the physical environment sometimes, does not allow to use sensors. When the sensor is eliminated, it is called then a sensorless control. Due to the multiple variables and nonlinearity of induction motor dynamics, the estimation of the rotor speed and flux without the measurement is still very challenging subject. Various sensorless approaches have been proposed in the literature. They are classified as open loop estimators and closed loop estimators which are called observers. We mentioned among of them, the determinist adaptive observers [Kub93], stochastic extended Kalman filter (EKF) [Kim94] and model reference adaptive system (MRAS) [Sch92]. Aside from the control design, the sliding mode theory proves its worth in estimation also in diverse structures of sliding mode observers [Reh02; Las06].

Another problem has been arisen also which is the improvement of machine energy efficiency. It has been reported that 56% of the electric energy is consumed by electric motors [Abr98]. Induction motors have a high efficiency at rated speed and load, but at light loads, iron losses increase causing a considerable reducing in the efficiency. The efficiency optimization techniques treat this drawback by controlling the level of generated flux level like the search control (SC) and loss model control algorithms (LMC) [Udd08; Stu13].

Aims of the thesis

The main objective of this thesis is the improvement of the performance of an induction motor drive controlled by DTC (Direct Torque Control) using nonlinear and robust techniques. This research work is addressing four principal points: firstly, the minimization of high torque and flux ripples which are the major drawbacks of the conventional DTC method by inserting the space vector modulation. SVM provides a constant switching frequency which reduces considerably the flux and torque ripples.

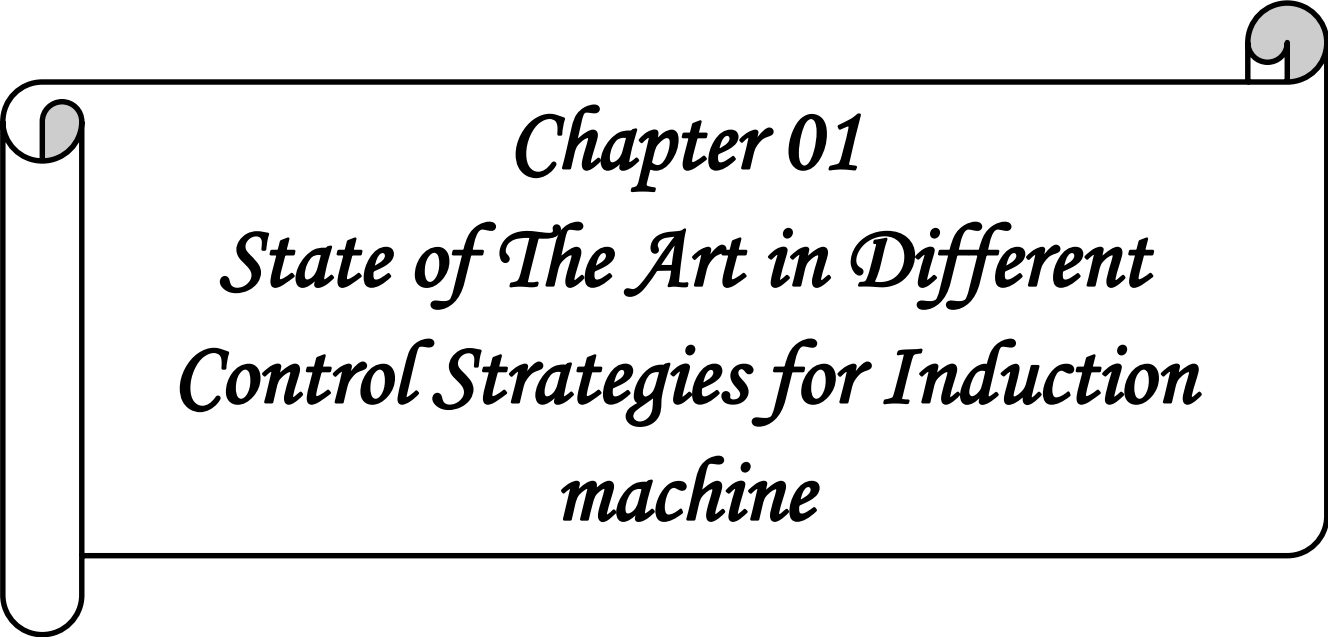
By solving this problem, the thesis aims then to enhance the robustness and the stability of control algorithm by replacing the linear PI controllers by nonlinear control law using the feedback linearization, first and second order sliding mode control. The combination of these techniques can achieve fast-dynamic decoupled control with low chattering and robust response against external disturbance and system uncertainties in wide speed rang. After that, the inserting of some improved sensorless strategies for the purpose of dispensing with the use of high cost sensors comes next. The last objective of the thesis is the efficiency optimization based on loss minimization of the induction motor. The effectiveness of different control techniques will be examined by simulation using Matlab/Simulink software. Moreover, an experimental implementation is conducted in LGEB laboratory of Biskra to validate the simulation results based on real-time interface using dSpace 1104 board.

Organization of the thesis

After the general introduction, which gives an overview about the main points which will be treated in this thesis concerning the control of the induction motor, the main body of the thesis is structured as follows:

The first chapter summarizes a background about different control strategies of the induction motor, like the classical methods (the scalar and the vector control) and DTC which take the most of our interest. Then, nonlinear techniques, sensorless control approaches and efficiency optimization strategies will be presented.

The second chapter presents a comparative study between the classical and the constant switching frequency DTC methods. Simulation and experimental results are presented. The third chapter presents the nonlinear DTC control design using the feedback linearization and the sliding mode control in order to improve the performance of SVM-DTC method and get more robust control scheme. After that, the fourth chapter deals with elimination of speed sensor and the association of the control scheme with sensorless observer approach for speed and flux estimation. Finally, the fifth which is the last chapter presents another association of the control algorithm to an efficiency optimization technique for losses minimization.



Chapter 01
State of The Art in Different
Control Strategies for Induction
machine

1.1 Introduction

Generally, the control and estimation of induction machines in variable speed operation is more complicate than DC machines. The main reasons are that they have more complex dynamic and they more request of complicated calculations. The vector control and direct torque control (DTC) are the most known control algorithms in literature for variable-speed AC motors. DTC strategy was introduced in the middle of the 80s as an alternative of field oriented control (FOC) because of many advantages, such as simpler structure, faster dynamic response and less dependence to machine parameters [Cas02]. However, the basic DTC strategy has a variable switching frequency due to the use of hysteresis controllers, consequently, they cause non-desired ripples in flux and torque. The insertion of space vector modulation strategy (SVM) in DTC scheme is among the proposed solution to overcome this drawback, where SVM can reduce the ripples by providing a constant switching.

This modified control schemes which so-called SVM-DTC use a linear proportional-integral (PI) controllers which make its dynamic and stability so sensitive to different uncertainties, parameters variation and external disturbance. All of this can lead to waste the robustness of the whole control system. To solve this kind of problems and ensure a decoupled control of the machine, robust and nonlinear control techniques were presented widely in for this context in control field. We mention in particular the sliding mode control (SMC) and the input-output feedback linearization (IOFL) [Las04; Yaz08]. The feedback linearization approach can convert a nonlinear system into an equivalent linear one which makes it simpler for control design [Yaz08]. Furthermore, the sliding mode control can provide an excellent dynamic performance, high robustness and simple implementation. Furthermore, the higher order sliding mode control has the ability to reduce the effect of chattering which is the main problem of the first order SMC while keeping the same desirable properties [Aur07].

Over and above, the sensorless control applications can improve the control system by reducing minimizing the number of the used sensors, reduce the cost of installation and cabling and increases the reliability of the drive. Thus, the observers remain an important area in process engineering. Many considerable researches have been proposed for the estimation of rotor speed and flux of electrical drive's such as model reference adaptive system (MRAS) [Sch92], full order adaptive observers [Kub93] and Kalman filter [Kim94]. Moreover, the design of observers based on sliding mode methodology had an important discussion in many works [Hab02; Las06;].

Although the advantages of the algorithms for induction control and observation, they can get more performance by achieving the maximum of efficiency through losses minimization. These strategies are mainly related to the choice of the proposed flux level according to the desired load value [Had07].

By Summarizing all the mentioned above, this chapter present a state of the art in the different control strategies for AC electrical drive and the induction machine practically, a brief theoretical review on the conventional controllers and the nonlinear control techniques which can be used for the improvement is given firstly. Then, this chapter presents a summary on sensorless control and different observers types used for induction motor estimation. Finally, short a discussion about machine energy efficiency optimization is presented.

1.2. Background on Variable Speed Drives

Traditionally, the induction motor has been operated directly from the grid with fixed speed/frequency (50Hz/60Hz), but since the development of the power electronic converts, it can be used now in variable frequency by inserting a converter between the motor and the electrical grid. This make it possible to obtain an adjustable speed motor [Abr00].

The variable frequency drives (VFDs) are able to provide smoother speed tuning and greater motor control. To control the speed, the torque and the position, various AC drives control strategies have been developed over the years. They can be classified based on their principles into two main categories namely by the scalar and vector control methods. The scalar control is developed by the steady state model of the machine (per phase equivalent circuit model), where only the magnitude and frequency of voltage, current, and flux can be controlled [Mar01]. Thus, it does not operate on the space vector position during the transient state. Contrariwise, the vector control is developed in the dynamic states, more than the magnitudes, the instantaneous positions of voltage, current, and flux can be controlled [Buj04].

The most popular method of vector control is known by the Field-Oriented Control (FOC) which proposed at the beginning of 1970s by Hasse and Blaschke [Has72; Bla72]. In the middle of 1980s, another method is presented by Takahashi and Depenbrock [Tak86; Dep88] which is called the Direct Torque Control. **Fig.1.1** below illustrate the different classification of the variable frequency drives control strategies.

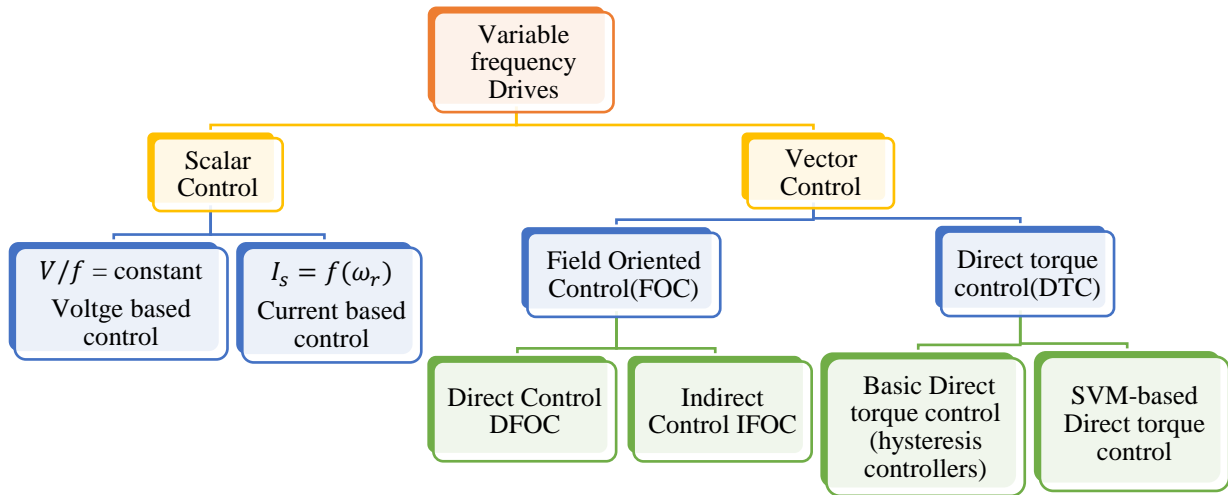


Fig.1.1 Classification of variable frequency control strategies for IM drive.

1.2.1 Scalar control

The Scalar control (V/f) which is known also by Volt/Hertz control is a simple technique used to control the speed the induction Motors. The main concept of V/f method is to keep the ratio of the stator voltage to frequency constant to maintain constant maximum available torque.

To control speed is in a closed loop, a proportional integral controller (PI) is employed to maintain the speed at a desired value and to improve speed accuracy by regulating slip speed of the motor. The controller receives the speed tracking error which is the difference between the desired reference ω_r^* and the actual sensed rotor speed ω_r as described in **Fig.1.2**.

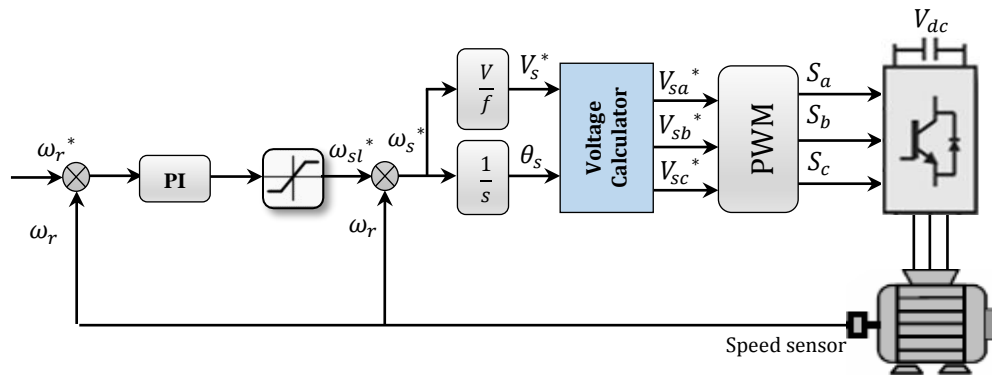


Fig.1.2 Closed loop scalar control for variable frequency induction motor drive.

This technique can operate in open loop also (i.e. without speed feedback), however, it provides poor speed regulation which is become depended on the applied external load [Com05]. The main drawbacks of this technique are the unsatisfied speed accuracy. In addition, the sluggish dynamic response which produce slow torque response. Since the control design is maintained in the steady state, the magnitude of the stator flux is not controlled during the transient and the machine's torque cannot respond quickly [Asf13].

1.2.2 Field oriented control

The modern approach for induction machine control is based on vector or field oriented control. On the contrary to the scalar control, the development of FOC control scheme is based on the dynamic model of the IM (Appendix A1) which make it valid for the both of steady and transient states. In spite of the coupled and nonlinear nature of the induction machine, FOC can control it as a separate excitation DC machine which featured by a nature decoupling. FOC achieves a similar behavior by transforming of all quantities to a rotating synchronous frame (d,q) where all quantities will appear as DC quantities.

The rotor flux orientation principle maintains the amplitude of the rotor flux at a fixed value by aligning the flux vector to d -axis of the synchronous frame [Li05]. Since all the variables are DC quantities, the electromagnetic torque can be controlled via the quadratic component of the stator current i_{sq} and the rotor flux magnitude is controlled by its direct component i_{sd} . The traditional PI controllers are the common solution for control design, other types of controllers can be used also. The rotor field orientation control is mainly classified to a direct field orientation control (DFOC) or an indirect field orientation control (IFOC) depending on the required information about the flux and the its position. The general block diagram of the indirect field orientation control for an induction motor is shown in **Fig.1.3**.

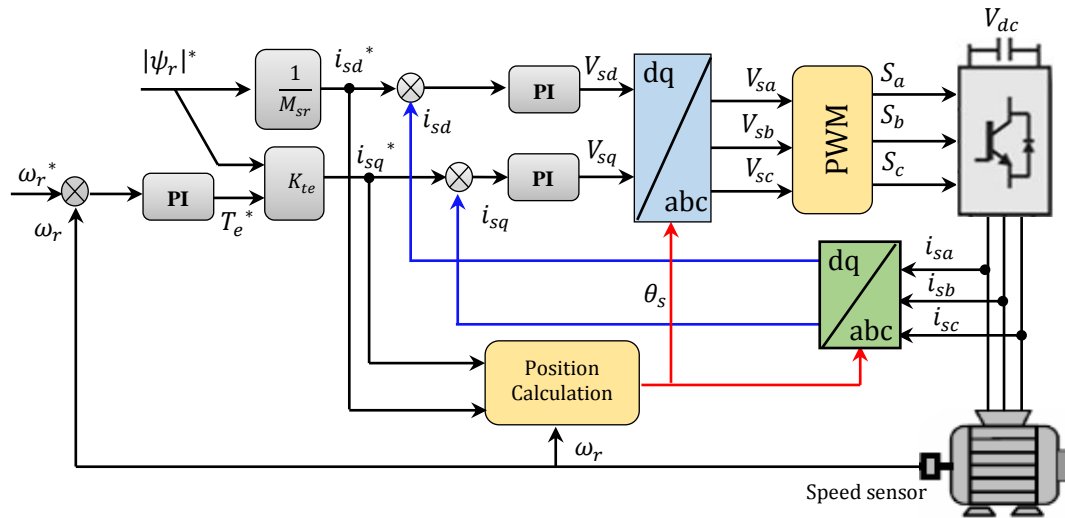


Fig.1.3 Basic indirect field oriented control (IFOC) of induction motor.

The rotor position is a necessary condition need to be acquired accurately in order to perform the frame transformation and to guarantee that the flux is aligned along d -axis. In IFOC the angle can be then calculated by adding the rotor angle to the slip angle. In the other side, DFOC computes the rotor flux angle based on the flux components in the stationary reference

frame, therefore, the knowledge of the flux components is needed. Several estimation and observation methods can be used to obtain them.

1.2.3 Direct torque control

1.2.3.1 Basic direct torque control and direct self-control

The direct torque control (DTC) has been proposed by Takahashi for induction motor drives in the middle of 1980s. It bases on the direct selection of voltage vector (switching state) for the voltage inverter which fed the motor according to the instantaneous errors of the stator flux and the electromagnetic torque. DTC uses separated hysteresis controllers to ensure a decoupled control of flux and torque without requiring a complex field orientation or current regulation loop [Cas02]. The outputs of the hysteresis comparators choose the appropriate voltage vector through a look-up switching table along the estimated position of the flux vector. Usually, the mathematical model of IM is used to estimate the stator flux and the electromagnetic torque. **Fig.1.4** shows a simple structure of the switching table based DTC which proposed by Takahashi [Tak86].

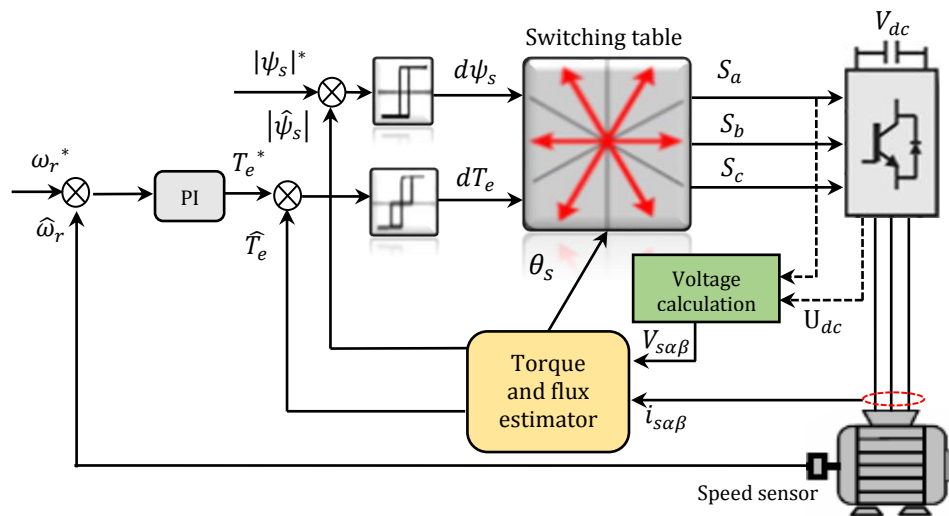


Fig.1.4 Direct torque control strategy based on lookup switching table.

This control scheme is very often used in the industry in low and medium power applications. The main advantages of DTC are summarized in its fast dynamic of the drive, the absence of coordinate transformations and current control loops and its universal structure, where the switching table DTC can be used for all AC machines. In the other hand, the main disadvantages of DTC are the variable switching frequency, high torque ripples and high switching losses.

Another similar method which is dedicated for high power applications, it was presented in the middle of 1980 also by Depenbrock [Dep88], it is so-called direct self-control (DSC). It can be characterized as a simplified version of DTC.

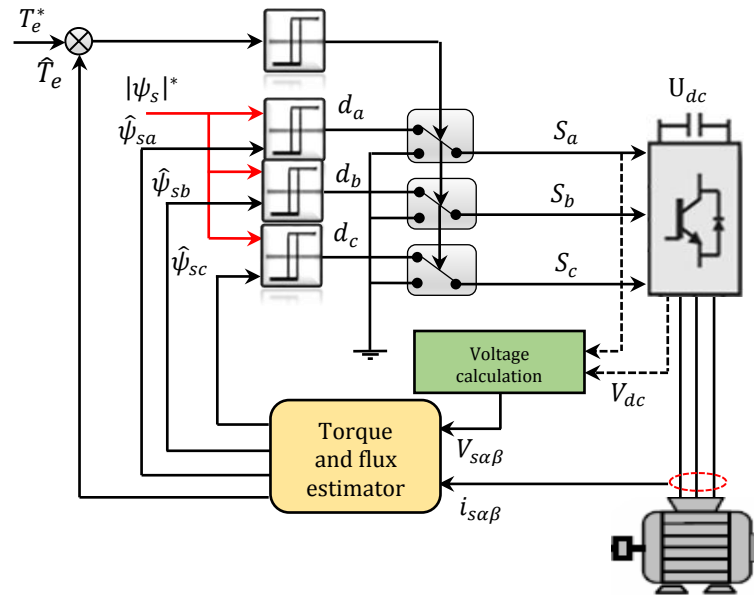


Fig.1.5 Block diagram of direct self-control (DSC)

This technique uses the reference torque and the three phase components of flux to generate the switching states which correspond to active voltage vectors through three hysteresis flux comparators. The hysteresis torque comparator generates the signal which corresponds to the zero states.

The common applications of DSC scheme are the high-power drives and traction systems, DSC is mainly featured by low inverter switching frequency (hexagon stator flux trajectory), the absence of switching table or PWM modulator, good torque and flux dynamics. In the other side, it has non-sinusoidal current and high ripples.

1.2.3.2 Direct torque control with constant switching frequency

In this DTC strategy, the lookup switching table and the hysteresis comparators are replaced by the space voltage modulation (SVM) unit and PI controllers for the purpose of voltage vector selection. This control scheme can preserve a constant switching frequency, consequently it reduces the high torque and flux ripples which is the main drawback of the conventional switching table DTC. SVM was first presented in the second half of the 1980s as an alternative strategy to the basic Pulse Width Modulator (PWM). Since then, a lot of work has been done on its theory and implementation.

SVM bases on the space vector representation of the voltage inverter output. It has several advantages such as minimizing ripple and Total Harmonic Distortion (THD) and switching losses [Opk08]. The incorporation of SVM with DTC schemes has been presented at the first time by Habetler in 1992 [Hab92], then several SVM-DTC schemes have been proposed [Buj04; Zng05; Ksn08].

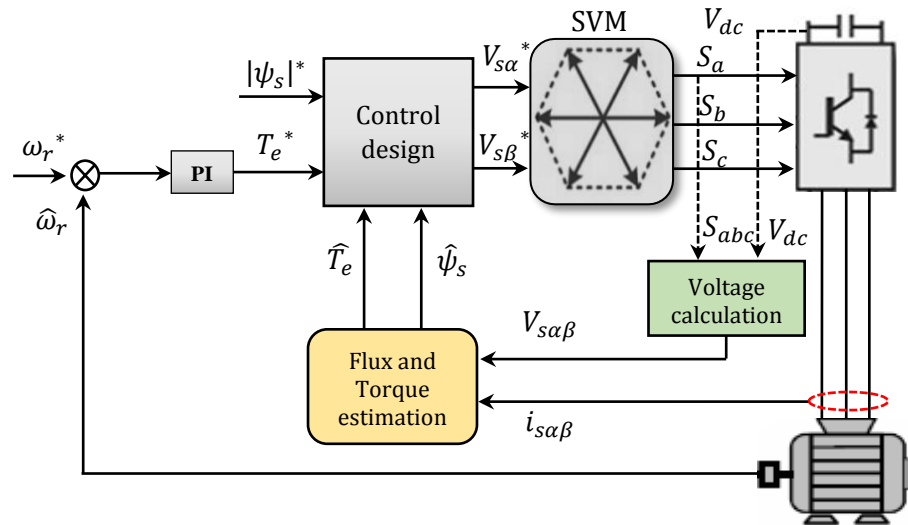


Fig.1.6 General block diagram of SVM Direct torque control method

The common target of these various structures is providing the reference voltages to modulate them by the SVM unit in order to generate the inverter switching state. **Fig.1.6** above illustrates a general diagram of SVM-DTC control algorithm. The SVM-DTC keeps a number of classical DTC features and offer more advantages, such as the constant switching frequency and low flux and torque ripples. The generalized SVM-DTC scheme offer a high fertility for performance improvement, whereas it can be designed in different ways. This strategy will take the majority of our interest in this thesis.

1.3 Nonlinear Control Techniques

Most physical systems are nonlinear and multivariable, by nature, they have inherent interconnected nonlinearities in their internal dynamics[Gar03]. We take in particular the induction motor. It has control problems in speed adjustable drives contrary to the DC motor due to some reasons [Kow14b]:

- The high order of internal coupled nonlinearity.
- Some state variables are not directly measurable (i.e. rotor currents and fluxes).
- Parameters variation because of environment effects.
- External load perturbations during its operation.

The use of conventional approaches such as the proportional-integral-differential (PID) controllers to understand the behavior of those systems by analytical techniques can be inadequate. Even at the initial stages of establishing the mathematical model, the existence of discrepancies between the real and the developed model for control design is so potential. This has led to an intense interest in the development of so-called nonlinear control theory which seeks to solve this problem [Pan13].

The successful application of modern mathematical tools played an important role in the development of the nonlinear control. Since the 1970s, a breakthrough advancement has been achieved [Gen10]. Among the most important developed nonlinear control strategies in the last few decades are the feedback linearization and the sliding mode control.

1.3.1 Feedback linearization

Feedback linearization has attracted a big number of research in nonlinear control filed. Unlike the Jacobian linearization which consist of the approximating of a nonlinear system by a linear one in the vicinity of a reference equilibrium point, the feedback linearization approach use an algebraic transformation to transform the nonlinear system dynamics into linear. By cancelling system nonlinearities, a linear control law can be applied [Isi95].

Furthermore, the feedback linearization can be used to cancel the coupling and the interactions between variables in case of multi-input-multi-output (MIMO) systems. A state feedback linearizing law is designed to compensate these interconnections and decompose the multivariable system into a number of single-input-single-output (SISO) linear systems [Gar03].

1.3.1.1 Input-output feedback linearization

The objective of input-output feedback linearization (IOFL) is to achieve decoupling and generate the original input u for MIMO systems by a nonlinear transformation based on state feedback and introducing a new input variable v . Considering a system of n states and m inputs/outputs as demonstrated in Eq (1.1).

$$\begin{cases} \dot{x} = f(x) + g(x)u \\ y = h(x) \end{cases} \quad (1.1)$$

where:

$x \in \mathfrak{R}^n$ is the state vector, $u \in \mathfrak{R}^m$ is the control input, y is the output state vector, f and g are smooth vector fields on \mathfrak{R}^n and h is a smooth nonlinear function.

A MIMO nonlinear system can be called input-output linearizable if there exists a static state feedback of the form:

$$u = F(x) + C(x)v \quad (1.2)$$

With $F(x) \in \mathfrak{R}^m$, $C(x) \in \mathfrak{R}^{m \times m}$ nonsingular and $v \in \mathfrak{R}^m$ an external input vector [Kra90]

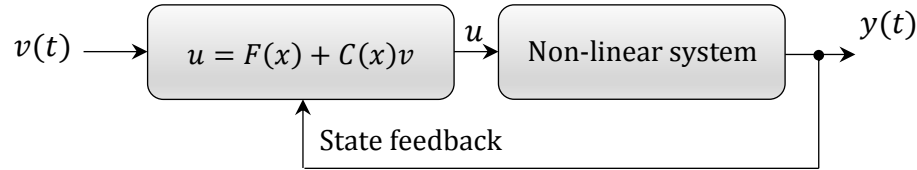


Fig.1.7. Multi-input multi-output feedback linearizing structure

1.3.1.2 Other linearization methods

In theoretical literature, linearization techniques similar to the input-output feedback linearization were developed [Kra90]. Which they, the linearization by immersion [Cla83], and then the Volterra linearization [Isi84]. Both method have been presented in order to mathematically define the situation where a state system as the form of Eq (1.1) has linear input/output behavior. Another technique became a popular for designing stabilizing control laws for nonlinear systems in strict feedback form. It is known by the backstepping [Bai99]. It is a feedback linearization based on Lyapunov theory, it can cancel the nonlinearities in the derivative of Lyapunov candidature function. The advantage of backstepping over feedback linearization is that one does not need to cancel benign nonlinearities.

1.3.1.3 Summary

The feedback linearization is a transformation of nonlinear dynamics into a linear form by using state feedback. When a MIMO system is input-output linearized and decoupled, a standard linear control can be applied to simplifies control design and stabilization. However, this method has some limitations. For example, it is not applicable to all nonlinear systems, it only applies to the system with precise mathematical model. While the presence of parameters uncertainty the system robustness cannot be guaranteed.

In order to overcome this shortcoming and increase the robustness of the system while the presence of uncertainties a robust control should be injected to feedback linearization system. The next section will introduce a robust control strategy based on variable structure system which is the sliding mode control.

1.3.2 Sliding Mode Control

1.3.2.1 Historical brief on sliding mode theory

The sliding mode control (SMC) is a particular type of variable structure control (VSC). The first concepts of SMC appeared in Russian literature (The former Soviet Union) in 1950s and developed by Emelyanov in 1960s [Eme67]. Later, Utkin has written an English summary of papers on the sliding mode control [Utk77]. Due to the implementation difficulties of high speed switching this approach didn't receive the attention it deserved until the 1970s. Then, the sliding mode control theory was widely disseminated to the different areas at the beginning of 1980s.

In the first works, SMC was planted for linear second order system. Then, it has been developed into a general design method being examined for a wide use, including nonlinear systems, MIMO systems, discrete time models and stochastic systems [Pan13]. From the most considerable application of SMC methods in over recent decades can be founded in:

- Robots control [Slo83]
- Control in planes [Sin89].
- Observers design [Slo91]
- Control of electric motors [Sab81; Utk93].

1.3.2.2 Basic concepts of SMC

The sliding mode variable structure control is designed to drive and then constrain the system state to lie within a neighborhood of the switching surface. The main features to this approach are the dynamics behavior of the system which may be tailored by a particular choice of switching function. Furthermore, the structure is independent of the object parameters which make the closed loop response becomes totally insensitive to a particular class of uncertainty in the system, this provides a very strong and inherent robustness to the resulting controllers [Utk93].

The main issue of SMC is to choose a control law which meet the next conditions, the reaching to the sliding surface and the existence of sliding mode in all points of the surface. The used discontinuous switching function in conventional sliding mode is the function $sign(x)$, it is defined in Eq (1.3).

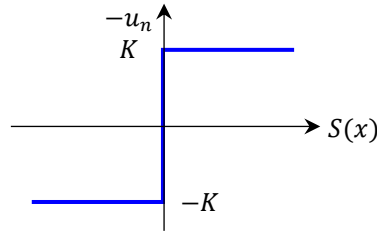


Fig.1.8 Function $sign(S)$.

$$sign(x) = \begin{cases} +1 & \text{if } x \geq 0 \\ -1 & \text{if } x < 0 \end{cases} \quad (1.3)$$

Then the control law in case of SISO system is given by:

$$u = Ksign(S) \quad (1.4)$$

where:

u is the control law, S is the sliding surface and K is the sliding mode gain.

In general, the strengths of SMC can be concluded:

- Low sensitivity to plant parameter uncertainty.
- Greatly reduced-order modeling of plant dynamics.
- Finite-time convergence (due to discontinuous control law).

1.3.2.3 Chattering phenomenon

The main drawback of the SMC is the chattering phenomenon which is caused by an infinite commutation due to the depending on the switching function relay ($sign(x)$) (**Fig.1.8**) in the control design. The disagreeable chattering phenomenon can excite high frequency harmonics and can also lead to damage of moving mechanical parts and heat losses in the electrical parts.

The common solution of this problem, is to replace the classical $sign(x)$ function by smoother switching functions, such as *saturation* function ($sat(x)$) [Ben99a] and *sigmoid* ($sigm(x)$) function [Lee13] as shown in **Fig.1.9**.

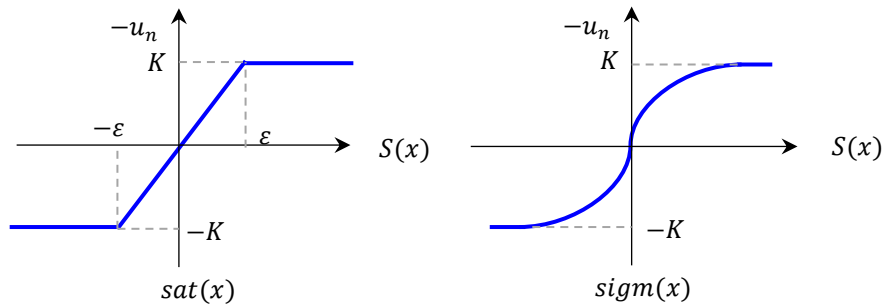


Fig.1.9 Saturation and sigmoid functions.

The shown functions are defined by:

$$sat(x) = \begin{cases} 1 & \text{if } x > \varepsilon \\ \frac{x}{\varepsilon} & \text{if } |x| \leq \varepsilon \\ -1 & \text{if } x < -\varepsilon \end{cases} \quad (1.5)$$

$$sigm(x) = \left(\frac{2}{1 + e^{\alpha x}} \right) - 1 \quad (1.6)$$

Where:

ε is a small positive constant representing the width of boundary layer.

α is a small positive constant which adjusts the sigmoid function slope.

Some other alternative methods are presneted in literature for eliminating this phenomenon such as:

- Combining the sliding mode control with fuzzy logic technique in [Sag15].
- Using the integral sliding mode control [Che10].
- Using the higher order sliding mode control [Las14].

1.3.2.4 High order Sliding Mode Control

The higher order sliding mode control is another method used to eliminate the problem of chattering. It is a generalized idea of the first order which based on higher order derivatives of the sliding surface. Besides keeping the same robustness and performance of the conventional sliding mode control (i.e., fast response and high robustness) it can reduce considerably the effect of chattering [Gen14].

The n^{th} sliding mode order can be determined by:

$$s = \dot{s} = \ddot{s} = \dots = s^{(n-1)} = 0 \quad (1.7)$$

When we talk about the higher order sliding mode control, we mean in particular the second order sliding mode. It called sometimes SMC without chattering, because this phenomenon of is strongly limited. The design of second order sliding mode control shows a variety of algorithms in the liturature. The most applicable algorithms proposed in literature are:

- Twisting control [Lew85; Lev93].
- Sub-optimal control [Bar97].
- Super twisting control [Lev93; Lev03].

1.3.3. Survey on the application of nonlinear techniques for electrical machines control

The first application of SMC on IM for controlling torque, speed and position was presented by Sabanovic and Izosimov [Sab81]. This work consists of enforcing the input of control using SMC in the form of the three phase voltages so they can be implemented directly by the inverter. Then, in [Sab89], the sliding mode control inputs have been replaced by two voltages components in the synchronous rotating frame. Thereafter, Utkin presented some general guidelines of SMC design for DC and AC electrical drives [Utk93]. Benchaib in [Ben99a; Ben99b] has done a comparative study between SMC and FOC with input output linearization through DSP real-time implementation of the control algorithm. Then Lascu in [Las04] presented the first combination of the principles of sliding mode control with DTC, where the variable structure controllers replaced the conventional PI controllers in stator flux oriented SVM-DTC to achieve flux and torque robust control. Then, several incorporated sliding mode direct torque control (SM-DTC) strategies have been presented in order to benefit the advantages of both control schemes [Haj09].

In the other hand, the feedback linearization is used on linearized IM model for FOC scheme in direct and quadratic (d-q) reference frame for current control [Kaz95; Chi98]. In [Bou04] an error sensitivity analysis presented to check the robustness against perturbations and measurement errors for feedback linearization field oriented control. After that, some works proposes an improved DTC controller which is integrated with SVM and feedback linearization [Zar10; Cho16].

The combination of the feedback linearization and sliding mode control is mentioned in [Cas05]. This incorporation consists of applying the sliding mode strategy on the resulting linearized system which obtained by feedback linearization. The robustness and the discontinuous nature of variable structure control can overcome the drawbacks of feedback linearization technique. In [Liu08], an application of combined SMC and feedback linearization to control a cascade of rectifier/inverter feeding an induction motor. In [Las17; Amr17a; Amr17c] a sliding mode direct torque via feedback linearization technique is suggested to improve the performance of the DTC-SVM technique for induction motor drive. The combination of these techniques preserves fast and robust response of DTC while eliminating the torque and flux ripple using SVM.

1.4 Sensorless Control Techniques for Induction Motor

Regardless of the used control strategies, the measurement of speed and flux is an essential step for control design in electrical drives. In another cases the implementation of control algorithms requires the knowledge of all the components of the state vector. However, the use of sensors is associated with several disadvantages, like high cost, fragility and reduced reliability. In addition, sensors require a regular maintenance, and in some applications, it is inappropriate to install sensors due to the physical and environmental constraints. A similar situation arises when a sensor breaks down [Hol06; Asf13].

The main proposed solution in literature is to avoid these difficulties of utilizing sensors by limit their use and replacing them with software sensors. This strategy is known by sensorless control theory in the automatic field, it takes a grand part in this domain. The software sensors are called estimators or observers [Glu15]. The objective of sensorless control for electrical machines is to estimate mechanical speed and torque or flux vector and its position. The speed sensorless control for AC drives has taken a big attention in industry application in the past decade, since it can reduce the cost and avoid the difficulty of installing mechanical sensors. Different techniques have been mentioned extensively in the past two decades for the estimation of flux and rotor speed an of electrical machines [Li05; Abu12]. Generally, they can be classified into two main categories [Bed14]:

- Mathematical model based techniques.
- Estimator without mathematical machine model (non-model techniques).

The shown diagram in **Fig.1.10** describe the essential classification of sensorless techniques.

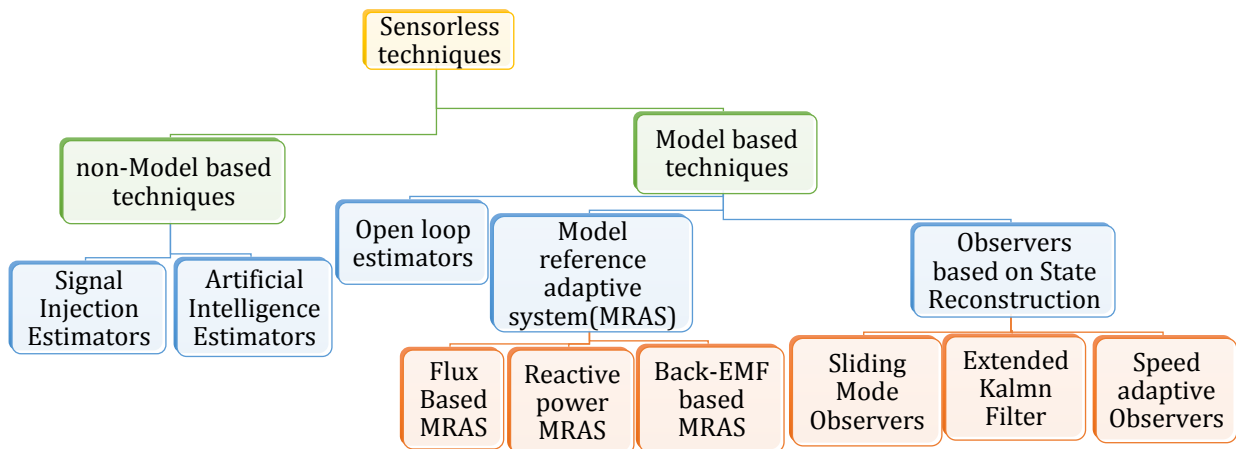


Fig.1.10 Classification of different Sensorless estimation techniques for AC motor drives.

1.4.1 Open loop estimation methods (Estimators without feedback)

Generally, the open loop estimation is a re-arrangement operation using the known machine model (appendix A.1) with the measured quantities (i.e. stator voltages and currents) to estimate the flux and as well the rotor speed of the machine. Most of these techniques use somehow the integrations in order to obtain the desired quantities of estimation.

1.4.1.1. Voltage model flux estimator

The stator flux of the induction motor can be obtained from the voltage model utilizes the measured stator voltages and currents, the stator flux can be estimated by the integration as follow:

$$\hat{\psi}_{s\alpha\beta} = \int_0^t (V_{s\alpha\beta} - R_s i_{s\alpha\beta}) dt \quad (1.8)$$

The rotor flux can be estimate from the stator flux and the measured current, as:

$$\hat{\psi}_{r\alpha\beta} = \frac{L_r \hat{\psi}_s - L_s L_r \sigma i_{s\alpha\beta}}{M_{sr}} \quad (1.9)$$

1.4.1.2. Current model flux estimator

For rotor flux estimation, the measured stator current and rotor speed are counted, the derivative of the estimated rotor flux can be computed using machine parameters as:

$$\hat{\psi}_{r\alpha\beta} = R_r \frac{M_{sr}}{L_r} i_{s\alpha\beta} - \omega_r \hat{\psi}_{r\beta\alpha} \quad (1.10)$$

1.4.1.3. Rotor speed estimation

The rotor speed can be computed from a difference between the synchronous speed and the slip speed using the following known equation:

$$\hat{\omega}_r = \hat{\omega}_s - \hat{\omega}_{sl} \quad (1.11)$$

The synchronous speed ω_s can be calculated by the stator or rotor flux from the model of IM as:

$$\hat{\omega}_s = \frac{\hat{\psi}_{s\beta} \hat{\psi}_{s\alpha} - \hat{\psi}_{s\alpha} \hat{\psi}_{s\beta}}{\sqrt{\hat{\psi}_{s\alpha}^2 + \hat{\psi}_{s\beta}^2}} = \frac{\hat{\psi}_{r\beta} \hat{\psi}_{r\alpha} - \hat{\psi}_{r\alpha} \hat{\psi}_{r\beta}}{\sqrt{\hat{\psi}_{r\alpha}^2 + \hat{\psi}_{r\beta}^2}} \quad (1.12)$$

And the slip speed can be calculated by:

$$\hat{\omega}_{sl} = \frac{R_s \hat{T}_e}{p \psi_r^2} \quad (1.13)$$

where \hat{T}_e is the estimated electromagnetic torque.

The estimation accuracy depends on machine model and its parameter exactness [Bed14].

1.4.2 Model reference adaptive system (MRAS)

The model reference adaptive systems (MRAS) is one of the most successful techniques for parameter estimation. It has been widely used due to its simplicity. The structure of MRAS observer consist of three parts, a reference model, an adaptive model, and an adaptation mechanism. The estimation using MRAS is based on the comparison of the outputs of the two models. Then, the calculated error used to drive an adaptation mechanism (Mostly PI controller) that generates the desired estimated quantity (Rotor speed in general cases) [Com05].

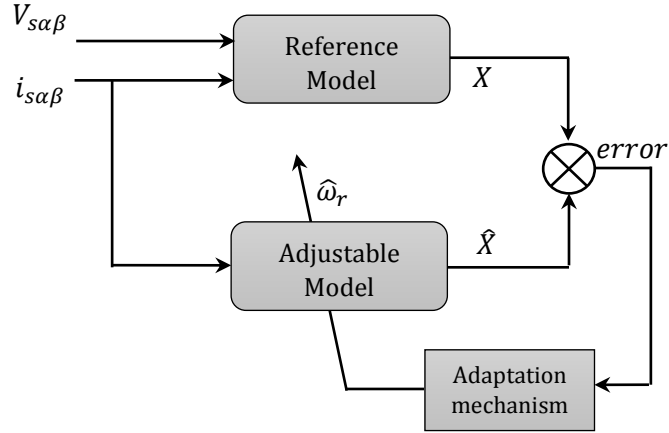


Fig.1.11 Block diagram of the model reference adaptive system observer.

Various MRAS structures have been presented in literature, the most used MRAS structure is the rotor flux MRAS which proposed by Schauder [Sch92]. Back-EMF and reactive power based MRAS have been presented also [Pen94; Kum15]. Another MRAS structures based on advanced techniques are presented in [Gad09; Ben15; Smi16].

1.4.3 Closed Loop Observers based on Machine State Reconstruction.

1.4.3.1 Adaptive observes

The basic adaptive observer design was proposed in [Kub93; Mae00]. It contains basically two parts, an open loop estimator based on the mathematical model and a closed correction loop with gain matrix G to correct the estimation errors. For the induction motor drive, the adaptive full-order observer model is defined by:

$$\frac{d\hat{x}}{dt} = \hat{A}\hat{x} + Bu_s + G(\hat{i}_s - i_s) \quad (1.14)$$

The hat '^' indicate to the estimated value.

The state variables of the observer (i.e. stator current and flux) are represented by the vector x . The Matrix A defines the parameters of the machine. The rotor speed which is the estimation objective is considered as an adaptive quantity and feedback signal to the matrix A .

The general adaptive observer diagram which proposed by [Kub93] is illustrated in the **Fig.1.12**.

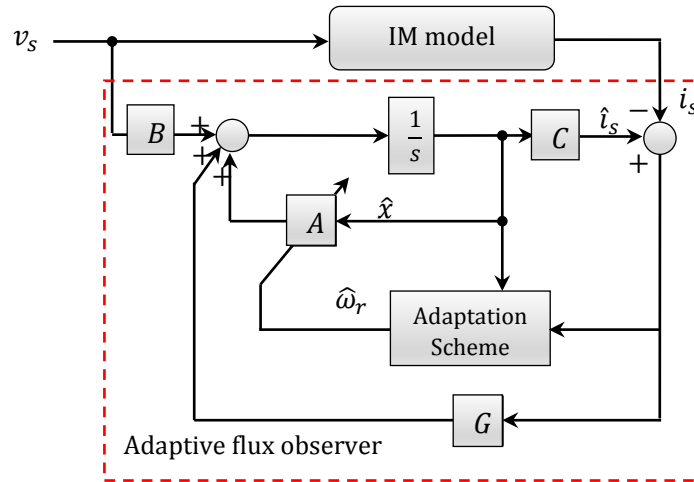


Fig.1.12 Block diagram of model based adaptive observer.

The adaptation scheme of the rotor speed consists of PI controller with cross product of the estimated flux and the current error as an input.

1.4.3.2 Extended Kalman filter

All the aforementioned closed-loop observers are classified as deterministic observers, they can be easily polluted by measuring noise and require parameter adaptation algorithms especially at very low speed. As an alternative, there are also stochastic approaches using Extended Kalman Filter (EKF). The Kalman filter observer has high convergence rate and good disturbance rejection, which can take into account the model uncertainties, random disturbances, computational inaccuracies and measurement errors [Kim94]. These properties are the advantages of EKF over other estimation methods. For these reasons, it had wide application in sensorless control in spite of its computational complexity.

For nonlinear problems Kalman can overcome this difficulty by using a linearized approximation, where, the stochastic continuous time system must be expressed in the discrete form in order to fit with the structure of extended Kalman filter. The process of observation of the extended Kalman filter is given in two stages, prediction and filtering. The prediction stage is aimed to obtain the next predicted states and predicted state-error covariance, while in the filtering stage, the next estimated states is obtained as the sum of the next predicted states and a correction term [Bar07; Asf13].

The EKF algorithm diagram is presented below in **Fig.1.13**.

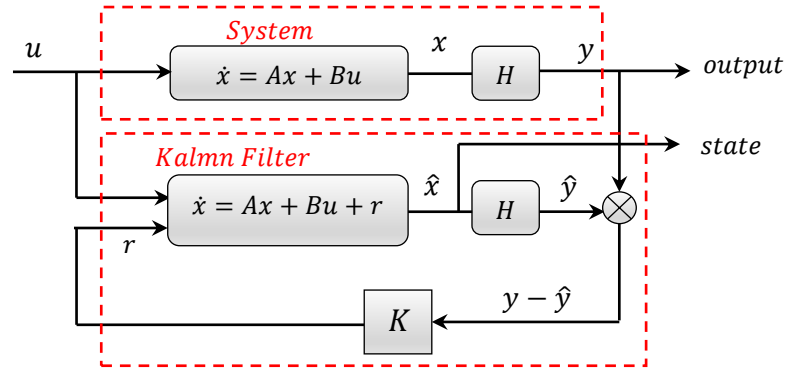


Fig.1.13 General structure of the Kalman filter estimator.

However, the high degree of complexity of EKF structure and the high system orders causes higher computational requirement (i.e. the sampling time). Thus, additional challenges and problems are introduced, such as the reduction of dynamic performance and the increase of harmonics [Asf16]. Nevertheless, the development of new processors technology (DSPs and FPGA) solves this problem due to the powerful calculations processing [Hab15].

Recently, different works have been conducted to improve the effectiveness and performance of the sensorless EKF for IM drive control. A bi-input EKF estimator, which deals with the estimation of the whole state of the IM together with stator and rotor resistances is presented in [Bar10]. Another multi model EKFs are proposed in [Zho14] in order to improve EKF performance under different noise conditions. Then, in [Asf16] Kalman filter estimator has been designed for DTC controlled induction motor drives.

1.4.3.3 Sliding mode observers

As we have mentioned before, the sliding mode approach is well known by its simplicity and high robustness. Besides the control design, it proves its effectiveness as an observation techniques also. The sliding mode observers (SMOs) commonly, have a similar structure as the full order observer adaptive observers. The difference is in feedback signal manipulation, where the adaptive signal is not multiplied by gain matrix G , but this matrix was replaced by a nonlinear sliding mode switching function [Bed14].

The SMOs can provide high effectiveness due to a number of advantages such as, the easy implementation and the high robustness to parameter variations, In addition, no extensive computations [Amr16a]. For induction motor observation, the stator phase current error, which is the difference between the actual and the estimated currents, is used to define sliding surface. The block diagram of the sliding mode observer for IM is shown in **Fig. 1.14**.

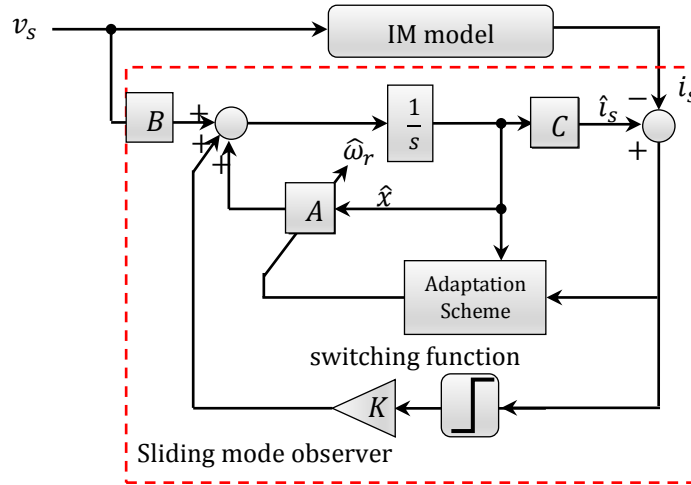


Fig.1.14 The general structure of adaptive sliding mode observer.

Several works have been addressed in the literature presenting modifications related to the SMO for the sensorless IM. A current model flux observer without requiring speed adaptation scheme is presented in [Reh02]. In this observer, all the terms that contain the rotor time constant and the rotor speed have been replaced by the sliding mode functions to make the estimation completely insensitive to the rotor time constant variation and any error in the estimated speed. Another sliding mode stator flux observer do not employ the speed adaptation has been associated with DTC control scheme is presented in [Las06; Las09]. These observers are referred as inherently observers, such the speed estimator is separated from the observer in order to increase accuracy in a wide-speed-range operation and to have reduced complexity.

Since the chattering is the common problem of the sliding mode control, new observers based on super twisting second order approach are presented recently in [Aur07; Rao10]. In [Zha14], super twisting observer has been associated with MRAS estimator for speed estimation where it takes the place of the reference voltage model of the MRAS. This combination has been successfully eliminated the chattering behavior and it is insensitive to variations machine parameters.

1.5 Efficiency Optimization Based Control

Today, the Induction machines are responsible for about 56% of the total industrial electric power consumption [Abr98]. However, the power efficiency of an induction machine is lower than some other AC machine types, such as the permanent-magnet synchronous machine (PMSM), especially in the small power area. The main reasons of this is the required current from the induction motor for field and torque generating and the low-cost of stator design which cause higher power losses [Stu13]. It can be deduced that a small minimization in

induction motors losses will have a major impact on the total energy consumption. Induction motors generally operate at rated flux in a variable frequency. However, many of the times, the system operates with light loads. In this case the core losses become excessive causing poor efficiency.

To improve the motor efficiency, the generated magnetic flux should be reduced to an optimal level. Then, the torque will be obtained with lower stator current and magnetic flux, resulting lower ohmic and iron losses [Li05]. Several efficiency improvement methods have been reported concerning the flux level control. In general, they can be divided into two categories. The first category is termed as the power measure-based approach, known also as search controller (SC). This controller searches iteratively for the flux level until the electrical input power set to the lowest value for a given torque and speed [Kir85]. The second category is the so-called the loss-model controller (LMC), this approach consists of computing the losses by using the induction motor model and selecting the flux level that minimizes these losses [Gar94; Abr01].

To make a comparison, we can conclude that the SC is always slow comparing to LMC and the LMC works on the model and not on the actual drives which means it is not effective for non-stationary states. In LMC, the optimum flux is calculated analytically. The main advantage is the simplicity of the method and not requiring extra hardware. However, it is sensitive to motor parameters which change considerably with temperature and load condition. On the other hand, SC method measures input power to searches the flux where the motor runs at maximum efficiency. This approach is insensitive to motor parameters and operating condition. However, it requires extra hardware to measure DC bus current and does not be used in the classical vector control system where additional sensor is not available.

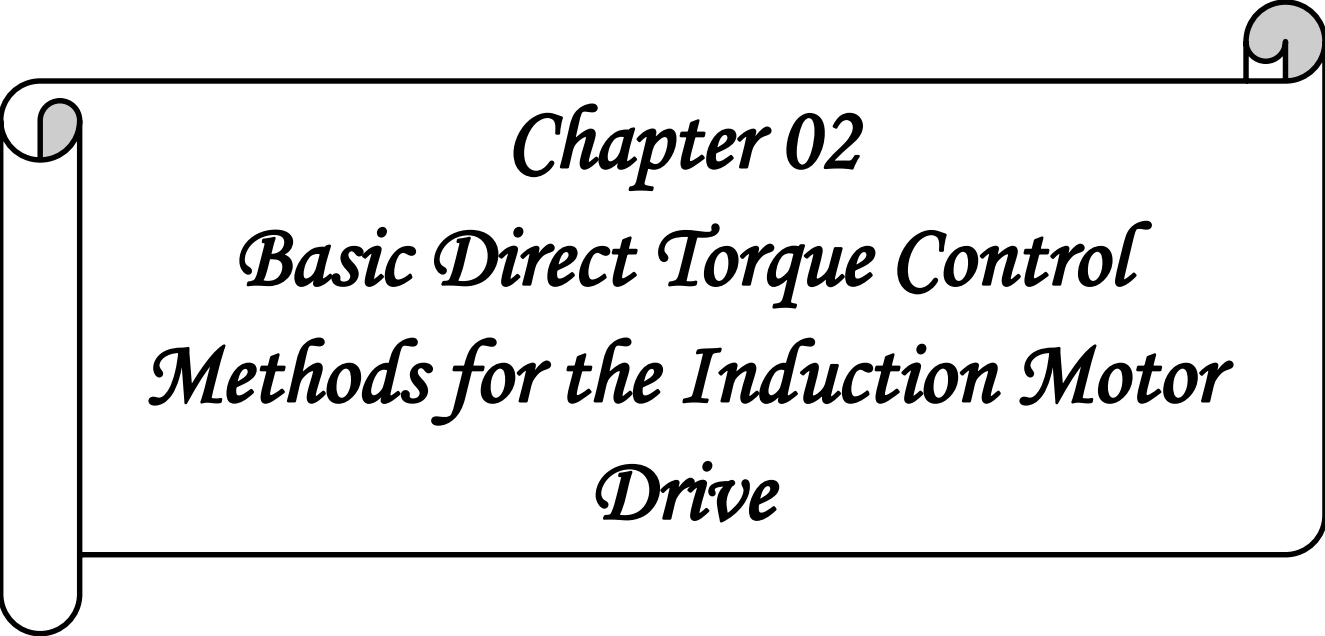
Some other recent works have combined the features of both LMCs and SCs in order to benefit from their advantages, in [Sou95] a fuzzy logic based efficiency optimization does not require extra hardware and insensitive to motor parameters is presented. Generally, the association of efficiency optimization strategy with a speed adjustable control and observation algorithm can be a good addition and get more high performance of the electrical drive.

1.6 Conclusion

In this first chapter, the conventional variable speed drive techniques systems have been presented and compared. The direct torque control has taken the majority of our interest, where we have highlighted its advantages and drawbacks. Then, an overview is devoted for the nonlinear control techniques (i.e. the feedback linearization and the sliding mode control). They are commonly inserted to enhance the basic control schemes, especially their dynamic, stability and robustness.

We have presented also as a second objective of this chapter, a survey on the different estimators and observers which used as sensorless algorithm to limit the use sensors of that can increase the reliability and decrease the cost of the control system. Finally, this chapter has discussed the association of an efficiency optimization strategy based on the minimization of machine losses for the developed sensorless control algorithm to get more features.

The next chapter will present a comparative study between the conventional DTC and the constant switching frequency DTC based on SVM. A comprehensive theory will be given firstly, then performance analysis for both strategies will be investigated using numerical simulation based on Matlab/Simulink. Moreover, an experimental implementation will be employed in order to validate the simulation results.



Chapter 02
Basic Direct Torque Control
Methods for the Induction Motor
Drive

2.1 Introduction

The Direct Torque Control (DTC) was proposed by Takahashi [Tak86] and Depenbrock [Dep88] in the middle of the 80s. This strategy was an alternative to the field oriented control (FOC). It bases on the direct selecting of the switching states to control the voltage source inverter (VSI) through a switching look-up table. Due to the limits of the conventional DTC strategy, especially the high torque and flux ripples problem, various control structures are presented to improve the performances of control. The twelve sectors DTC based on an extended switching table and the constant switching frequency DTC using the space vector modulation (SVM-DTC) are well discussed solutions. This chapter will concern on a comprehensive descriptive study on the basic and the improved DTC strategies, including the used IM model, the control design of the classical DTC using switching table and the control design of the constant switching frequency DTC based on SVM. Subsequently, the presented DTC control methods will be investigated as a comparative study using a numerical simulation by MATLAB/Simulink software.

Over and above, the real-time control will represent another objective of this chapter. In many works, the control of electrical drives is executed using a Digital Signal Processor (DSP) with C language code or a graphical programming approach [Sut13]. Our control system is implemented by dSpace DS1104 signal card. This board operates with MATLAB/Simulink platform basing on TMS320F240 DSP processor. Therefore, DTC control strategies will be investigated also by an experimental implementation in order to validate the simulation results using real time interface (RTI).

2.2 Model of Induction Motor Dedicated for Direct Torque Control

The dynamic equation's model of the induction motor which is dedicated for direct torque control is expressed below in Eq (2.1) and Eq (2.2). It can be written in the stator fixed reference frame (α, β) (stationary frame) by assuming the stator current and the stator flux as state variables.

$$\begin{cases} \frac{di_{s\alpha}}{dt} = -\left(\frac{R_s}{\sigma L_s} + \frac{R_r}{\sigma L_r}\right)i_{s\alpha} - \omega_r i_{s\beta} + \frac{R_s}{\sigma L_s L_r} \psi_{s\alpha} + \frac{\omega_r}{\sigma L_r} \psi_{s\beta} + \frac{1}{\sigma L_s} u_{s\alpha} \\ \frac{di_{s\beta}}{dt} = -\left(\frac{R_s}{\sigma L_s} + \frac{R_r}{\sigma L_r}\right)i_{s\beta} + \omega_r i_{s\alpha} + \frac{R_s}{\sigma L_s L_r} \psi_{s\beta} - \frac{\omega_r}{\sigma L_r} \psi_{s\alpha} + \frac{1}{\sigma L_s} u_{s\beta} \end{cases} \quad (2.1)$$

$$\begin{cases} \frac{d\psi_{s\alpha}}{dt} = u_{s\alpha} - R_s i_{s\alpha} \\ \frac{d\psi_{s\beta}}{dt} = u_{s\beta} - R_s i_{s\beta} \end{cases} \quad (2.2)$$

where:

$i_{s\alpha}, i_{s\beta}$ are stator current components.

$\psi_{s\alpha}, \psi_{s\beta}$ are stator flux components.

R_s, R_r are stator and rotor resistance.

L_s, L_r are stator and rotor inductance.

$\sigma = 1 - \frac{M_{sr}}{L_s L_r}$ is the Blondel's coefficient.

M_{sr} is the mutual stator-rotor inductance.

The dynamic model of the IM is detailed and demonstrated in the Appendix (A.1).

2.3 Two-Level Voltage Source Inverter (VSI) Model

Before moving to the algorithm of basic DTC, we should represent the model of two-level voltage inverter. The **Fig.2.1** below shows a simplified scheme of the two-level bridge topology of the voltage source inverter. The induction motor is supposed as a star-connected three phase balanced load [Taz16].

The Type of the used switches depends on the power of the inverter and switching frequency. In the most applications, IGBT transistors with anti-parallel diodes are so helpful. The output phase voltages are produced by a plus or minus DC link voltage V_{dc} which is provided by a rectifier or another DC source [Wjk09; Bnz14].

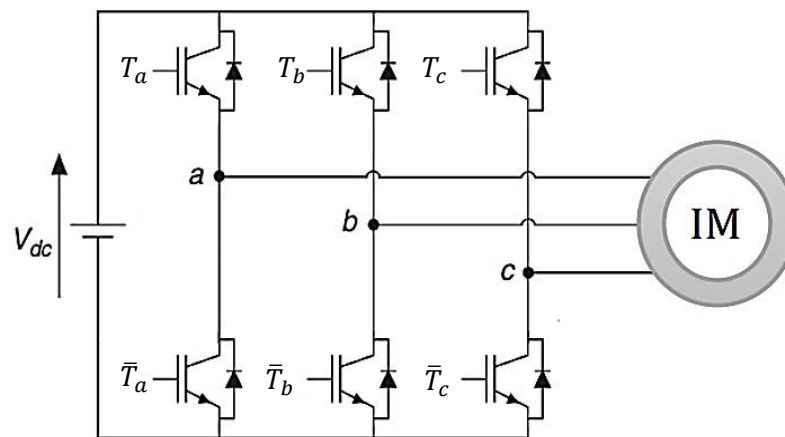


Fig 2.1 Three-phase VSI fed star-connected induction machine.

The inverter's control bases on the logic values S_i , where:

$S_i=1, T_i$ is ON and \bar{T}_i is OFF.

$S_i=0, T_i$ is OFF and \bar{T}_i is ON.

with: $i = a, b, c$.

The voltage vector is generated by the following equation [Taz16]:

$$V_s = \sqrt{\frac{2}{3}} V_{dc} \left[S_a + S_b e^{j\frac{2\pi}{3}} + S_c e^{j\frac{4\pi}{3}} \right] \quad (2.3)$$

V_{dc} : is the DC link voltage

There are eight possible positions from the combinations of switching states. Six are active vectors ($V_1, V_2 \dots V_6$) and two are zero vectors (V_0, V_7) [Zlk05]. These eight switching states are shown as space vectors in **Fig.2.2**:

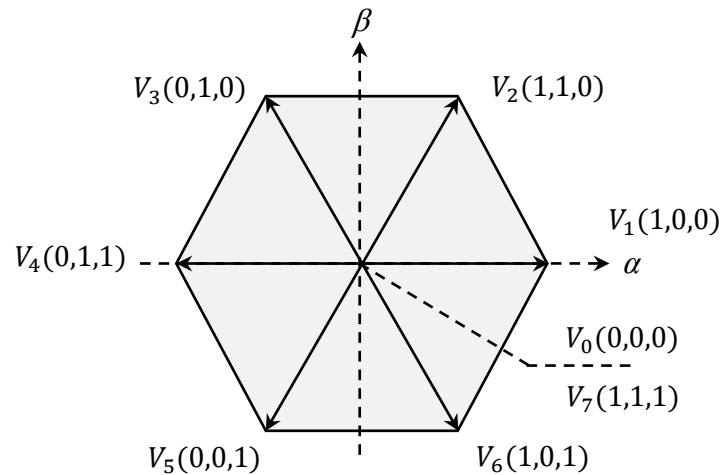


Fig 2.2 VSI Voltage vectors in the complex plane.

2.4 Principles of Direct Torque Control

Direct torque control achieves a decoupled control of the stator flux and the electromagnetic torque in the stationary frame (α, β). It uses a switching table for the selection of an appropriate voltage vector. The selection of the switching states is related directly to the variation of the stator flux and the torque of the machine. Hence, the selection is made by restricting the flux and torque magnitudes within two hysteresis bands. Those controllers ensure a separated regulation of both of these quantities. The inputs of hysteresis controllers are the flux and the torque errors as well as their outputs determine the appropriate voltage vector for each commutation period [Rum04].

2.4.1 Control of stator flux and electromagnetic torque

2.4.1.1 Control of stator flux

Basing on the IM model in stationary frame, the stator flux equation can be expressed as follows:

$$\frac{d\psi_s}{dt} = V_s - R_s i_s \tag{2.4}$$

and:

$$\psi_s(t) = \int_0^{T_z} (V_s - R_s i_s) dt + \psi_s(0) \tag{2.5}$$

ψ_{s0} : is the flux vector at the instant $t=0s$.

By applying a non-zero vector in T_z sampling period, we can neglect the stator resistance voltage drop $R_s i_s$ compared to V_s for high speed regions. Then Eq (2.5) can be written as:

$$\psi_s(t) \approx V_s T_z + \psi_s(0) \tag{2.6}$$

The relation between the stator voltage and the stator flux change can be established as:

$$\Delta\psi_s = \psi_s(t) - \psi_s(0) = V_s T_z \tag{2.7}$$

The Eq (2.7) means that the stator flux can be changed by the application of stator voltage during a time T_z . The stator flux vector's extremity moves in direction given by the voltage vector and making a circular trajectory (**Fig.2.3**) [Rod12].

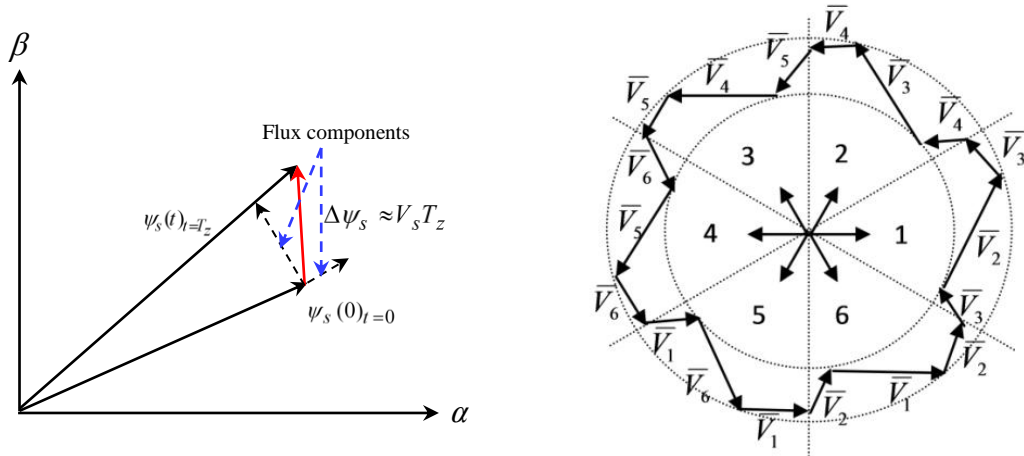


Fig 2.3 Evolution of stator flux vector in the complex plan.

A two-level hysteresis comparator is used for flux regulation. It allows to drop easily the flux vector extremity within the limits of the two concentric circles with close radius, as shown in **Fig.2.4**. The choice of the hysteresis bandwidth h_{ψ_s} depends on the switching frequency of the inverter [Tou08; Seb11].

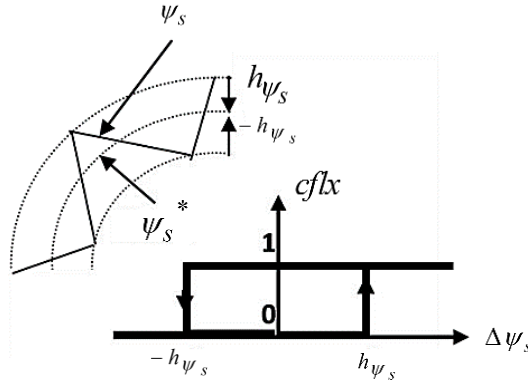


Fig.2.4 Two-level hysteresis comparator for stator flux control.

The logical outputs of the flux controller are defined as:

$$\begin{cases} cflx = 1 & \text{if } \Delta\psi_s > h_{\psi_s} \\ cflx = 0 & \text{if } \Delta\psi_s \leq -h_{\psi_s} \end{cases} \quad (2.8)$$

h_{ψ_s} is hysteresis band of stator flux

The stator flux error is defined by the difference between the references value of flux and the actual estimated value:

$$\Delta\psi_s = |\psi_s^*| - |\psi_s| \quad (2.9)$$

2.4.1.2 Control of electromagnetic torque

During one sampling period, the rotor flux vector is supposed invariant. The torque of induction motor can be expressed in terms of stator and rotor flux vectors as follows:

$$T_e = p \frac{M_{sr}}{\sigma L_s L_r} \psi_s \times \psi_r \quad (2.10)$$

$$|T_e| = p \frac{M_{sr}}{\sigma L_s L_r} |\psi_s| |\psi_r| \sin(\delta) \quad (2.11)$$

where:

p is the number of poles pairs.

ψ_s, ψ_r are stator and rotor flux vectors.

δ angle between the stator and rotor flux vectors

From expression (2.11), it is clear that the electromagnetic torque is controlled by the stator and rotor flux amplitudes. If those quantities are maintaining constant, the torque can be controlled by adjusting the load angle δ .

The torque regulation can be realized using three-level hysteresis comparator (**Fig.2.5**). It allows to control the motor in both rotation senses. The two-level comparator can be used for one rotation sense.

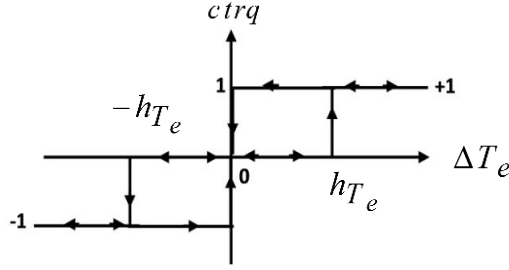


Fig.2.5 Three level hysteresis comparator for electromagnetic torque control.

The logical outputs of the torque controller are defined as:

$$\begin{cases} ctrq = 1 & \text{if } \Delta T_e > h_{T_e} \\ ctrq = 0 & \text{if } -h_{T_e} \leq \Delta T_e \leq h_{T_e} \\ ctrq = -1 & \text{if } \Delta T_e < -h_{T_e} \end{cases} \quad (2.12)$$

h_{T_e} is hysteresis band of torque.

The torque error is defined by the difference between the references values of the torque and the actual estimated values:

$$\Delta T_e = T_e^* - T_e \quad (2.13)$$

2.4.2 Estimation of stator flux and electromagnetic torque

2.4.2.1 Stator flux estimation

The estimation of the stator flux is usually done by the integration of the back-emf (Electromotive force). The stator flux components can be expressed using stator voltages and currents in the stationary reference frame (α, β) by:

$$\begin{cases} \psi_{s\alpha} = \int_0^t (V_{s\alpha} - R_s i_{s\alpha}) dt \\ \psi_{s\beta} = \int_0^t (V_{s\beta} - R_s i_{s\beta}) dt \end{cases} \quad (2.14)$$

The stator flux magnitude and flux angle can be computed as:

$$|\psi_s| = \sqrt{\psi_{s\alpha}^2 + \psi_{s\beta}^2} \quad (2.15)$$

$$\theta_s = \tan^{-1}(\psi_{s\beta}/\psi_{s\alpha}) \quad (2.16)$$

The stator voltage components ($V_{s\alpha}, V_{s\beta}$) are obtained by applying Concordia transformation on the output voltage of the three-phase VSI [Haf14].

$$\begin{bmatrix} V_{s\alpha} \\ V_{s\beta} \end{bmatrix} = \begin{bmatrix} 1 & -1/2 & -1/2 \\ 0 & \sqrt{3}/2 & -\sqrt{3}/2 \end{bmatrix} \begin{bmatrix} V_{sa} \\ V_{sb} \\ V_{sc} \end{bmatrix} \quad (2.17)$$

The output voltages of VSI which are the input stator voltages of the IM are given by:

$$\begin{cases} V_{sa} = \frac{V_{dc}}{3}(2S_a - S_b - S_c) \\ V_{sb} = \frac{V_{dc}}{3}(2S_b - S_c - S_a) \\ V_{sc} = \frac{V_{dc}}{3}(2S_c - S_a - S_b) \end{cases} \quad (2.18)$$

The stator currents components $(i_{s\alpha}, i_{s\beta})$ can be obtained also by applying Concordia transformation on the measured currents:

$$\begin{cases} i_{s\alpha} = \sqrt{\frac{2}{3}}i_{sa} \\ i_{s\beta} = \frac{1}{\sqrt{2}}(i_{sb} - i_{sc}) \end{cases} \quad (2.19)$$

2.4.2.2 Electromagnetic torque estimation

The produced electromagnetic torque of the induction motor can be determined using the cross product of the stator quantities (i.e., stator flux and stator currents). The torque formula is expressed as following:

$$T_e = p(\psi_{sa}i_{s\beta} - \psi_{s\beta}i_{sa}) \quad (2.20)$$

2.5 Switching Table Construction and Control Algorithm Design

2.5.1 Six sectors Switching table

To maintain a decoupled control, pair of hysteresis comparators receives the stator flux and torque errors as inputs. Then, the comparators outputs determine the appropriate voltage vector selection [Cas02; Swi05]. However, the choice of voltage vector is not only depending on the output of hysteresis controllers, but on the position of stator flux vector also. Thus, the circular stator flux vector trajectory will be divided into six symmetrical sectors [Ben10; Otk08].

where:

Sector 1: $11\pi/6 \leq \theta_s < \pi/6$, sector 2: $\pi/6 \leq \theta_s < \pi/2$, ..., sector 6: $3\pi/2 \leq \theta_s < 11\pi/6$.

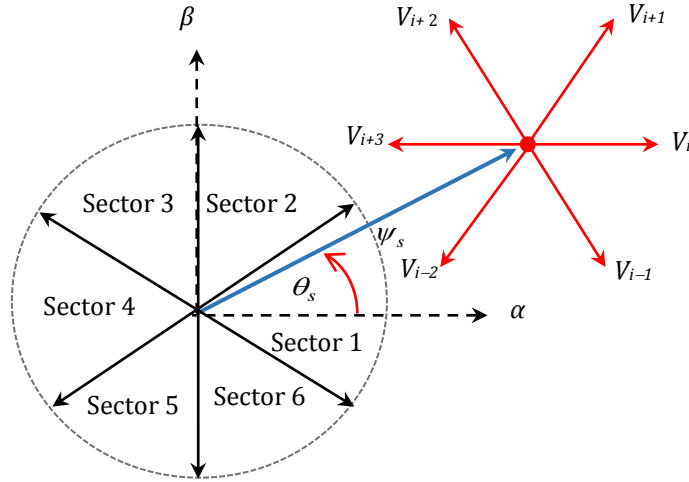


Fig.2.6 Voltage vector selection when the stator flux vector is located in sector i .

While the stator flux vector is located in the sector i we have [Otk08]:

- If V_{i+1} is selected, ψ_s increases and T_e increases.
- If V_{i-1} is selected, ψ_s increases and T_e decreases.
- If V_{i+2} is selected, ψ_s decreases and T_e increases.
- If V_{i-2} is selected, ψ_s decreases and T_e decreases.

For each sector, the vectors (V_i and V_{i+3}) are not considered because both of them can increase or decrease the torque in the same sector according to the position of flux vector on the first or the second sector [Puj00]. If the zero vectors V_0 and V_7 are selected, the stator flux will stop moving and its magnitude will not change, the electromagnetic torque will decrease, but not as much as when the active voltage vectors are selected [Zha16]. The resulting look-up table for DTC which was proposed by Takahashi is presented in **Table 2.1**:

Error	Sectors	I	II	III	IV	V	VI
$cflx = 1$	$ctrq = 1$	V_2	V_3	V_4	V_5	V_6	V_1
	$ctrq = 0$	V_7	V_0	V_7	V_0	V_7	V_0
	$ctrq = -1$	V_6	V_1	V_2	V_3	V_4	V_5
$cflx = 0$	$ctrq = 1$	V_3	V_4	V_5	V_6	V_1	V_2
	$ctrq = 0$	V_0	V_7	V_0	V_7	V_0	V_7
	$ctrq = -1$	V_5	V_6	V_1	V_2	V_3	V_4

Table 2.1 Look-up table for basic direct torque control.

2.5.2 DTC improvement using twelve sectors switching table

In the conventional six sectors DTC, two switching states per sector are not considered. This presents an ambiguity in torque control. A sector shifting takes the first sector from $(0$ to $\pi/3)$ instead of $(11\pi/6$ to $\pi/6)$. This provides a new switching table. However, in a similar way, it has two unused vectors per sector also (i.e. V_{i+2} and V_{i-1})

which present an ambiguity in flux instead of torque. Another strategy divides the circular flux locus into 12 sectors instead of 6 as shown in Fig.2.7 [Puj00]. This makes all the six states used per sector.

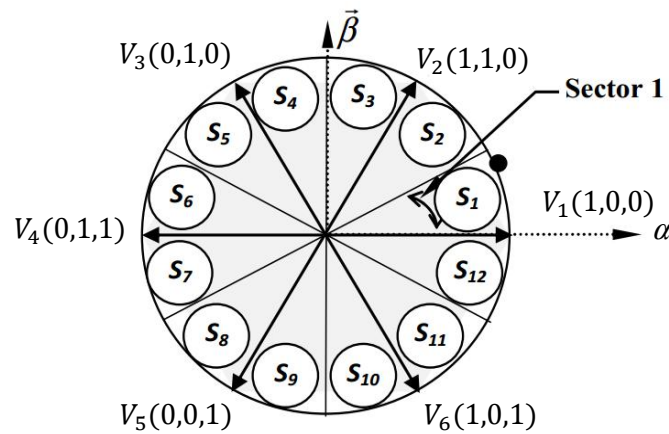


Fig.2.7 Voltage space vector in 12 sectors case.

In twelve sectors DTC, the vector V_1 produces a large increase in flux and a small increase in torque for the sector 12. On the contrary, V_2 produces a large increase in torque and small in flux. We can deduce that it is necessary to define now small and large torque variations. This requires to divide the hysteresis band of the torque into four parts. Then, a twelve-sectors look-up table is provided as shown in Table 2.2:

Error	Sector	I	II	III	IV	V	VI	VII	VIII	IX	X	XI	XII
$cflx=1$	$ctrq = 2$	V_2	V_3	V_3	V_4	V_4	V_5	V_5	V_6	V_6	V_1	V_1	V_2
	$ctrq = 1$	V_2	V_2	V_3	V_3	V_4	V_4	V_5	V_5	V_6	V_6	V_1	V_1
	$ctrq = -1$	V_1	V_1	V_2	V_2	V_3	V_3	V_4	V_4	V_5	V_5	V_6	V_6
	$ctrq = -2$	V_6	V_1	V_1	V_2	V_2	V_3	V_3	V_4	V_4	V_5	V_5	V_6
$cflx=0$	$ctrq = 2$	V_3	V_4	V_4	V_5	V_5	V_6	V_6	V_1	V_1	V_2	V_2	V_3
	$ctrq = 1$	V_4	V_4	V_5	V_5	V_6	V_6	V_1	V_1	V_2	V_2	V_3	V_3
	$ctrq = -1$	V_5	V_5	V_6	V_6	V_1	V_1	V_2	V_2	V_3	V_3	V_4	V_4
	$ctrq = -2$	V_5	V_6	V_6	V_1	V_1	V_2	V_2	V_3	V_3	V_4	V_4	V_5

Table 2.2 Look up switching table with twelve sectors.

Considerable studies in literature mentioned that the increasing of the number of the sectors have a slight effect on reducing the high ripples and current harmonics. In addition, the twelve sectors DTC provides good dynamic in high and low speed regions [Tou07].

Therefore, the 12 sectors DTC will be chosen instead of the 6 sectors DTC for simulation and real-time implementation in this chapter.

2.5.3 Speed regulation in DTC strategy

DTC strategy has the ability to operate even without a speed regulation loop, so it doesn't require any information about rotor speed. This can classify DTC as a speed sensorless strategy for many industrial applications. Otherwise, to achieve an adjustable speed control, a speed controller is necessary to have a speed regulation and to generate the reference of electromagnetic torque.

Commonly, the proportional-integral (PI) controllers are used for the regulation. It is performed by comparing the speed reference signal to the actual measured speed value. Then the comparison error becomes the input of the PI controller. The poles placement method is used to determine the controller gains (Appendix A.2).

The tuning of PI controllers is usually disregarding the physical limitation of the system such as the maximum current and voltage. The used PI controller in our work in the outer speed loop is the anti-windup controller. It allows to enhance speed control performance by cancelling the windup phenomenon which is caused by the saturation of the pure integrator [Yan15]. **Fig.2.8** shows the speed anti-windup PI controller diagram block.

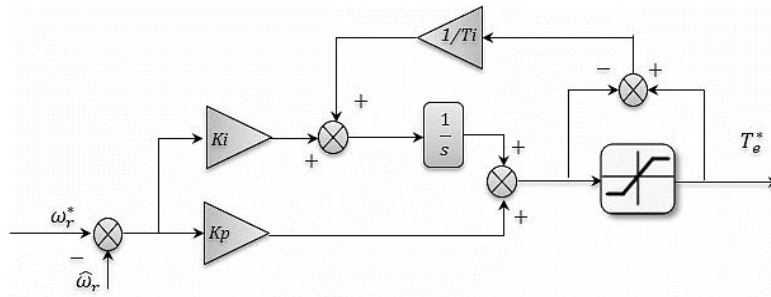


Fig.2.8 Speed anti-windup PI controller.

This strategy consists on the correction of the integral action based on the difference between the control signal and the saturation limit. The difference value is passed through a gain block (tracking time constant T_i) before arriving as feedback to the integrator.

2.5.4 Global scheme of basic direct torque control

The global control scheme of basic direct torque control strategy is shown in **Fig.2.9**. It is composed of: speed regulation loop using PI controller, decoupled flux and torque hysteresis controllers, look-up switching table, an association of VSI-Induction motor, voltage and current calculation blocks with 3/2 (Concordia) transformation and flux/torque estimators with position/sector determination.

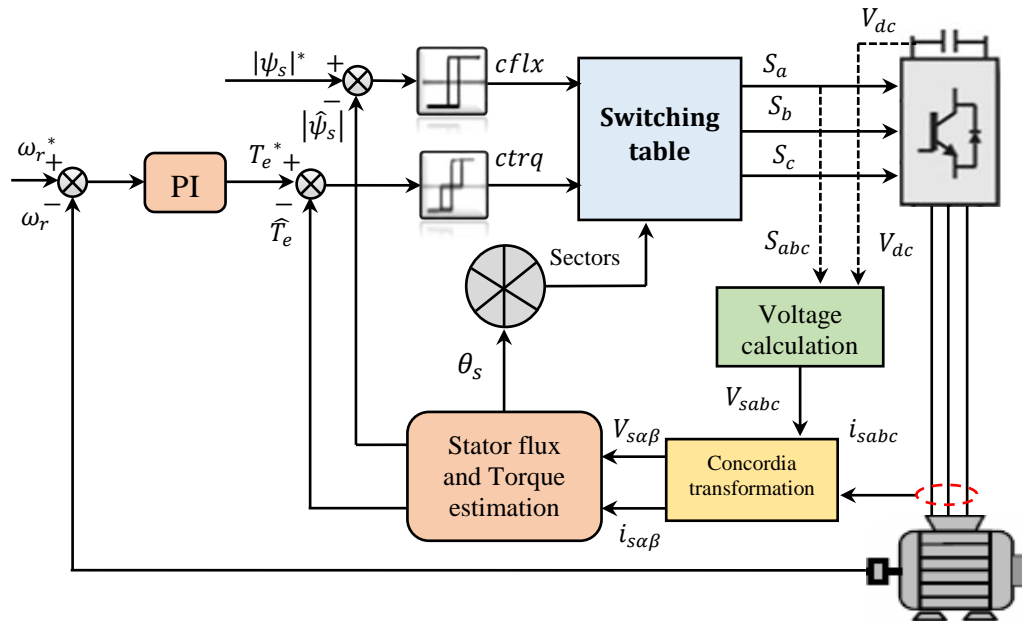


Fig.2.9 Global control scheme of basic direct torque control.

2.6 Constant Switching Frequency Direct Torque Control Using SVM

The main drawbacks of the conventional direct torque control are the variable switching frequency and the high level of ripples. Consequently, they lead to high currents harmonics, an acoustical noise and they degrade the control performance especially at low-speed values [Asf16]. The ripples are affected proportionally by the width of the hysteresis band. However, even with choosing a reduced bandwidth values, the ripples still important due to the discrete nature of the hysteresis controllers. Moreover, the very small values of bandwidths increase inverter switching frequency [Udd12].

The insertion of the space vector modulation (SVM) in DTC control scheme has been discussed also in literature. SVM preserves a constant switching frequency which can reduce high torque/flux ripples and minimize current harmonic distortion. Consequently, an effective control of the stator flux and torque is achieved. Several SVM-DTC methods have been proposed according to their structures, such as, the closed loop torque control and the closed loop torque and flux control.

This section presents a constant switching frequency DTC strategies based on the closed loop torque and flux control in order to improve the classical DTC strategy. This technique uses two (PI) controllers instead of hysteresis controllers to achieve a decoupled control and replaces the switching table by SVM unit for the switching signals calculation [Las00; Zik05]. It is known also by the stator field oriented control (SFOC) direct torque control.

2.6.1 Space vector modulation algorithm

SVM is different from the conventional pulse width modulation (PWM). It relies on the space vector representation of the inverter output. There are no separate modulators for each phase. The reference voltages are given by space voltage vector (i.e. voltage vector components in the complex plan) [Zlk05]. The principle of SVM is the prediction of inverter voltage vector by the projection of the reference vector V_s^* between adjacent vectors corresponding to two non-zero switching states. [Hab92; Amr15]. For two-levels inverter, the switching vectors diagram forms a hexagon divided into six sectors, each one is expanded by 60° as shown in **Fig.2.10**.

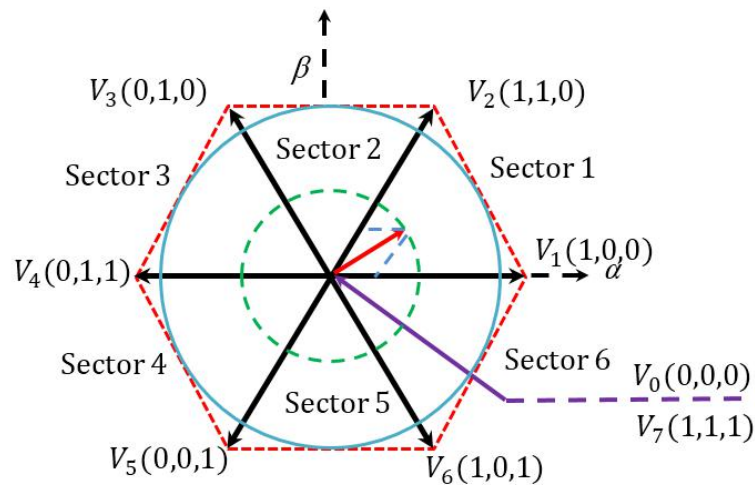


Fig.2.10 Diagram of voltage space vector.

The application time for each vector can be obtained by vector calculations and the rest of the time period will be spent by applying the null vector.

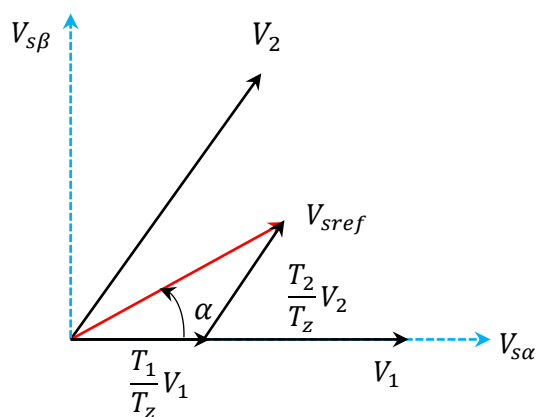


Fig.2.11 Reference vector as a combination of adjacent vectors at sector 1.

When the reference voltage is in sector 1 (**Fig.2.11**), the reference voltage can be synthesized by using the vectors V_1 , V_2 , and V_0 (zero vector) [Abr12].

The volt-second principle for sector 1 can be expressed by:

$$V_s^* T_z = V_1 T_1 + V_2 T_2 + V_0 T_0 \tag{2.23}$$

$$T_z = T_1 + T_2 + T_0 \tag{2.24}$$

T_1 , T_2 and T_0 are the corresponding application times of the voltage vectors respectively.

T_z is the sampling time.

The determination of times T_1 and T_2 corresponding to voltage vectors are obtained by simple projections:

$$T_1 = \frac{T_z}{2V_{dc}} (\sqrt{6}V_{s\beta}^* - \sqrt{2}V_{s\alpha}^*) \tag{2.25}$$

$$T_2 = \sqrt{2} \frac{T_z}{V_{dc}} V_{s\alpha}^* \tag{2.26}$$

V_{dc} : DC bus voltage.

The calculation of switching times (duty cycles) is expressed as follows:

$$T_{aon} = \frac{T_z - T_1 - T_2}{2} \tag{2.27}$$

$$T_{bon} = T_{aon} + T_1 \tag{2.28}$$

$$T_{con} = T_{bon} + T_2 \tag{2.29}$$

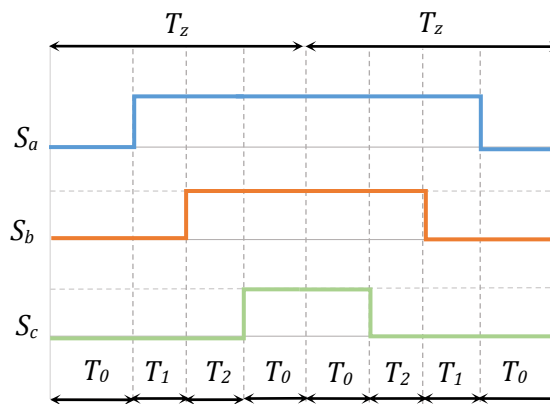


Fig.2.12 Switching times of sector 1.

Table 2.3 summarizes switching times (output) for each sector as:

Sector	1	2	3	4	5	6
S_a	T_{bon}	T_{aon}	T_{aon}	T_{con}	T_{bon}	T_{con}
S_b	T_{aon}	T_{con}	T_{bon}	T_{bon}	T_{con}	T_{aon}
S_c	T_{con}	T_{bon}	T_{con}	T_{aon}	T_{aon}	T_{bon}

Table 2.3 Switching times for each sector.

2.6.2 Stator flux oriented (SFO) SVM-DTC strategy

The SFO-SVM direct torque control strategy consists on controlling both of stator flux and torque directly without any current regulation. This can help to achieve a good tracking and fast response. The control strategy is expressed in stator-flux-oriented coordinates (SFOC). The orientation makes a decoupling between flux and electromagnetic torque, where the stator flux vector becomes aligned with the d -axis and torque with the q -axis. It's well known that the d -axis is the magnetizing axis and q -axis is the torque axis [Sab14]. This strategy combines the advantages of both of direct torque control and field oriented control [Wjk09].

SVM-DTC uses the dynamic model of the induction machine in the synchronous reference frame (d, q) [Bou09 ;Seb11]. The voltages model of the IM can be expressed as:

$$\begin{cases} v_{sd} = R_s i_{sd} + \frac{d\psi_{sd}}{dt} - \omega_s \psi_{sq} \\ v_{sq} = R_s i_{sq} + \frac{d\psi_{sq}}{dt} + \omega_s \psi_{sd} \\ 0 = v_{rd} = R_r i_{rd} + \frac{d\psi_{rd}}{dt} - (\omega_s - \omega_r) \psi_{rq} \\ 0 = v_{rq} = R_r i_{rq} + \frac{d\psi_{rq}}{dt} + (\omega_s - \omega_r) \psi_{rd} \end{cases} \quad (2.30)$$

The stator field-orientation method is based on the alignment of stator flux vector with the d -axis and the maintaining of quadratic components of stator flux equal to zero:

$$\begin{cases} \psi_{sd} = \psi_s \\ \psi_{sq} = 0 \end{cases} \quad (2.31)$$

Consequently, the voltage model can be written as:

$$\begin{cases} v_{sd} = R_s i_{sd} + \frac{d\psi_s}{dt} \\ v_{sq} = R_s i_{sq} + \omega_s \psi_s \end{cases} \quad (2.32)$$

The electromagnetic torque is given by:

$$T_e = p \psi_s i_{sq} \quad (2.33)$$

This algorithm achieves stator flux and torque closed-loop control with SVM to produce the inverter's command signals. Mostly, decoupled PI controllers are used to receive the stator flux and torque errors as inputs and generate the (d, q) voltage components (V_{sd}, V_{sq}) in a synchronous reference frame [Las00; Sab14].

Fig.2.13 shows the global block diagram of the stator field oriented DTC with SVM.

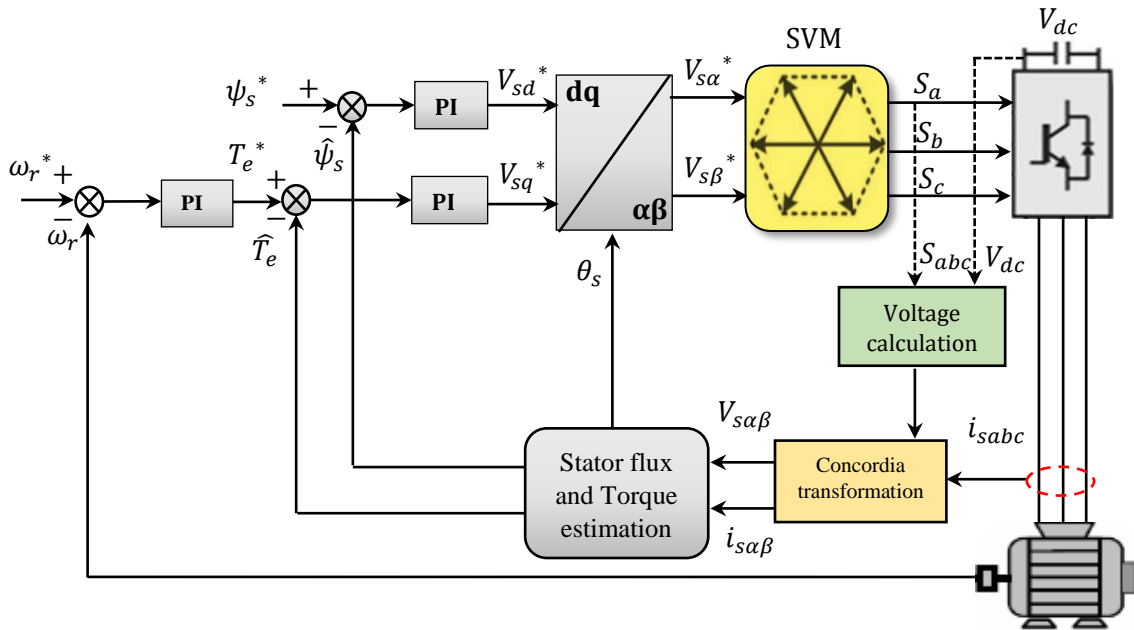


Fig.2.13 Global control scheme of stator flux oriented SVM- direct torque control.

2.7 Simulation Results

The DTC control algorithms have been simulated by MATLAB/Simulink software. A comparative study between the switching table classical DTC and the SFOC direct torque control with SVM (SVM-DTC) is presented. The simulation has been conducted for a three phases 1.1 kW squirrel-cage induction motor with characteristics given in the appendix (A.II). Different operation conditions are employed for both control methods. The starting up and the steady states of the controlled motor with load introduction are presented firstly. Then the rotation sense reversing test and low speed operation are presented. For the classical DTC, the chosen bandwidths of the hysteresis controllers are $\pm 0.005Wb$ for flux and $\pm 0.05N.m$ for torque.

2.7.1 Starting up and steady states with load application

This section presents the starting up state of the induction motor according to speed step reference of 1000 rpm. Then, a load of 5N.m at $t=0.5s$ is introduced. Figs.2.14-2.24 show respectively rotor speed, torque, stator phase current i_{sa} with THD analysis, stator flux components, flux magnitude and the circular trajectory. The figures are specified: ((a) for conventional DTC, and (b) for SVM-DTC).

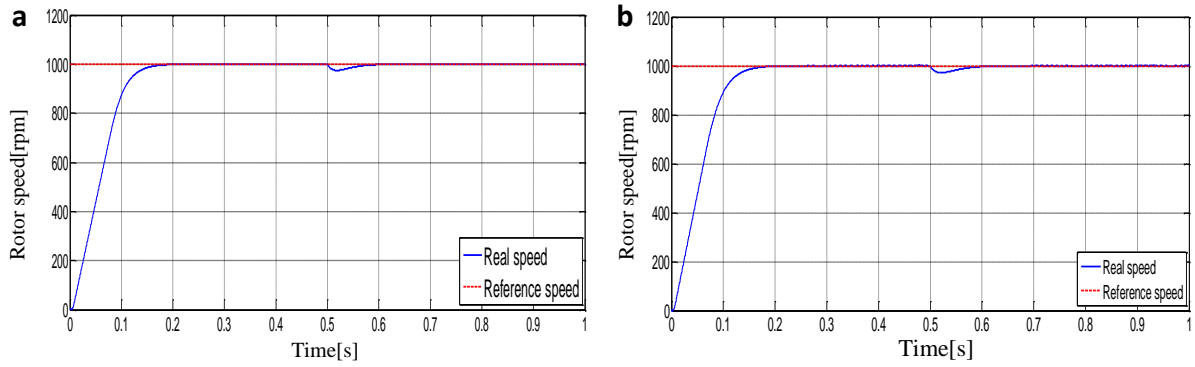


Fig.2.14 Rotor speed response at the starting up and steady states followed by load application.

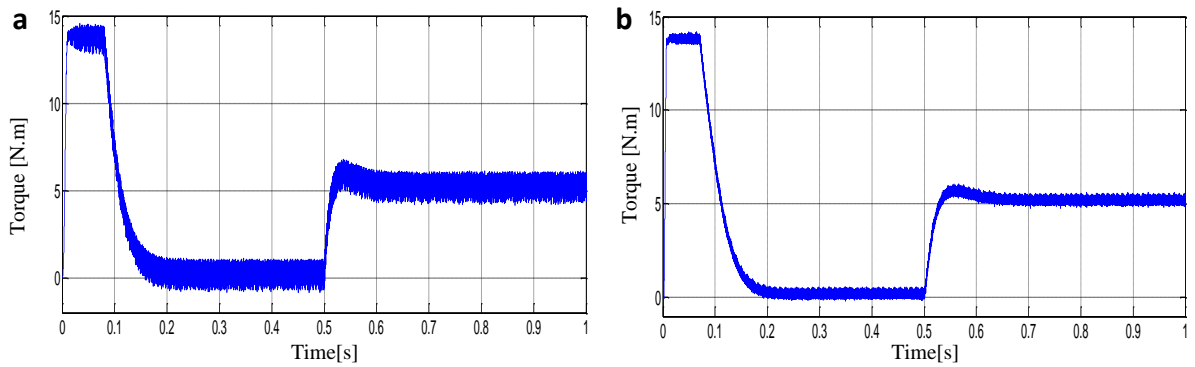


Fig.2.15 Electromagnetic torque with load application of 5 N.m at $t=0.5s$.

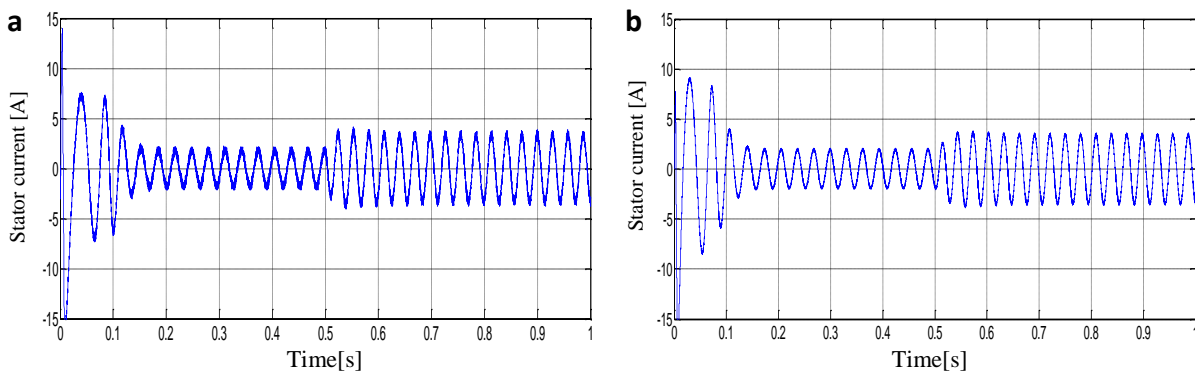


Fig.2.16 Stator phase current i_{sa}

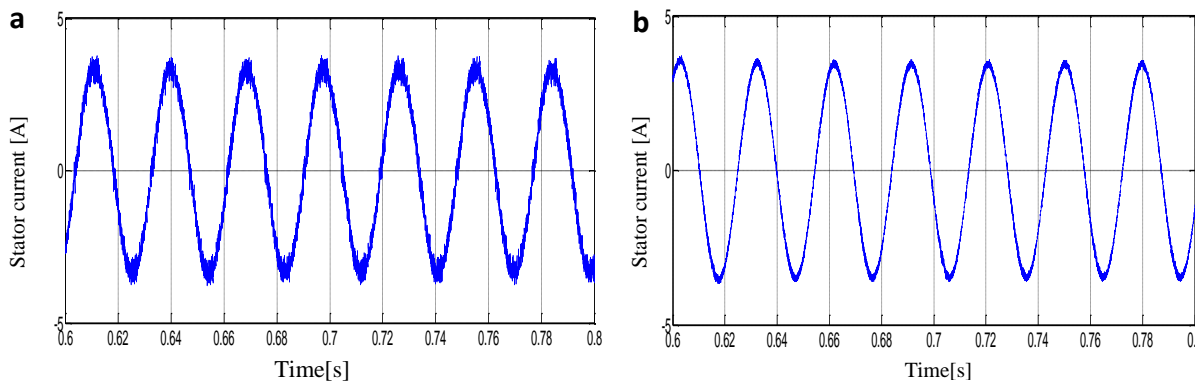


Fig.2.17 ZOOM of stator phase current i_{sa}

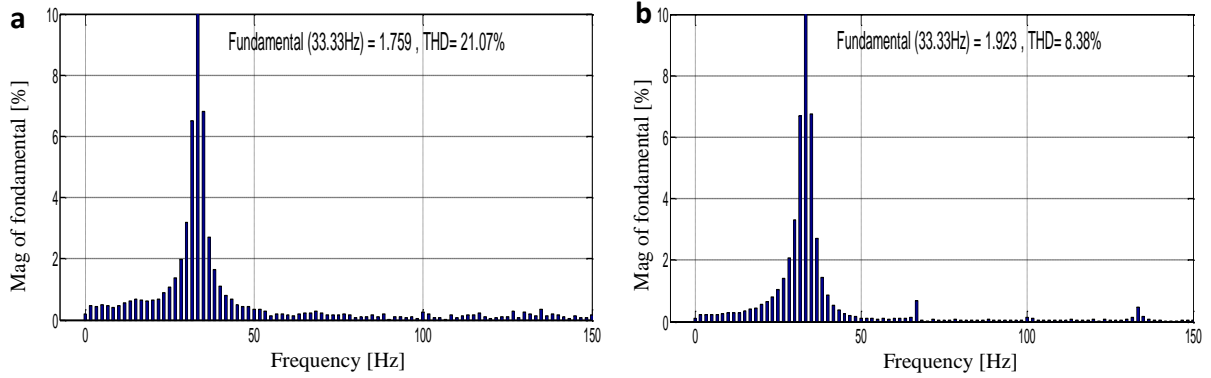


Fig.2.18 FFT analysis and spectrum of THD for stator phase current i_{sa} .

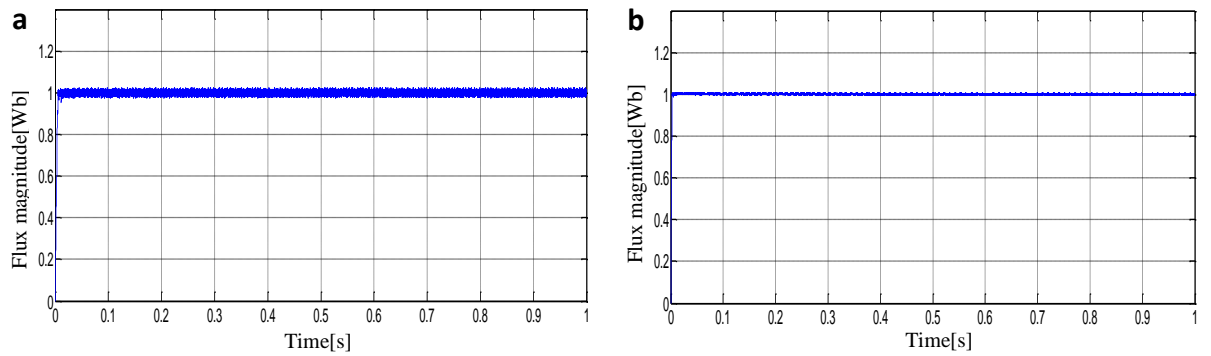


Fig.2.19 Stator flux magnitude [Wb].

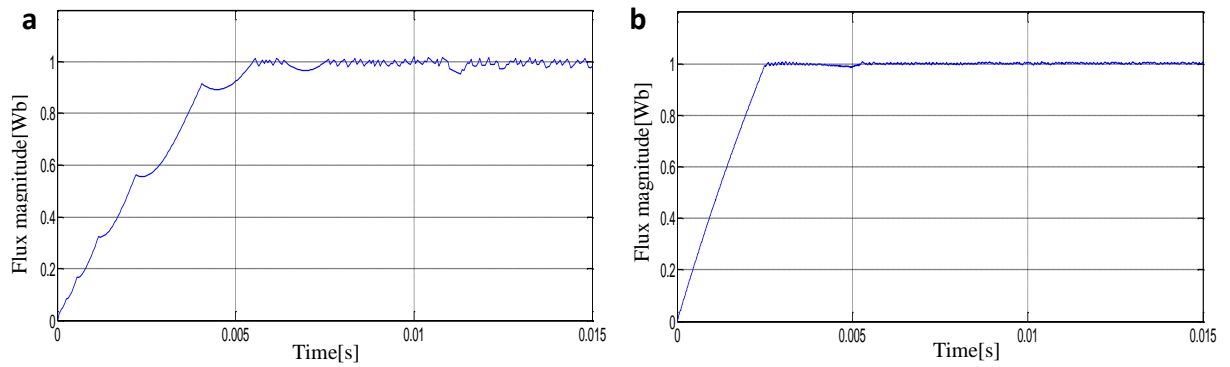


Fig.2.20 ZOOM of Stator flux magnitude.

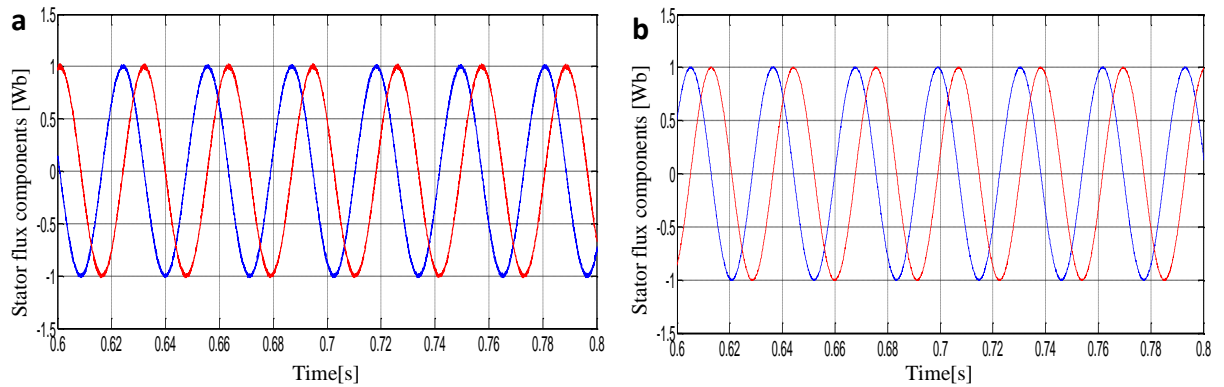


Fig.2.21 ZOOM of stator flux components.

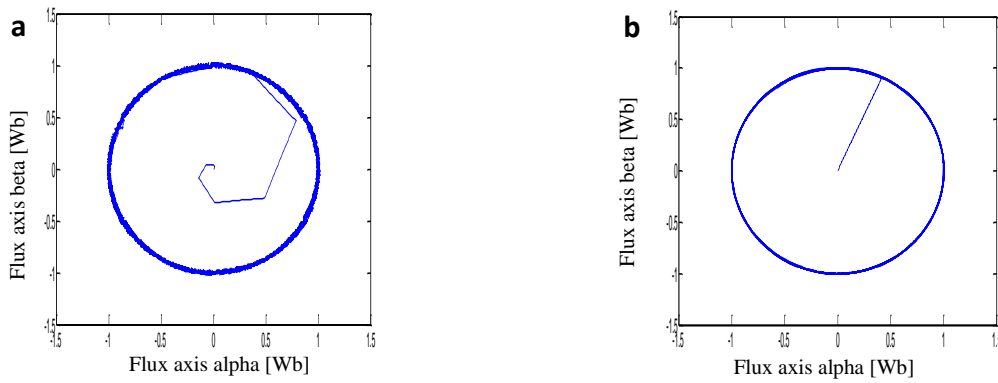


Fig.2.22 Flux circular trajectory (α, β) [Wb].

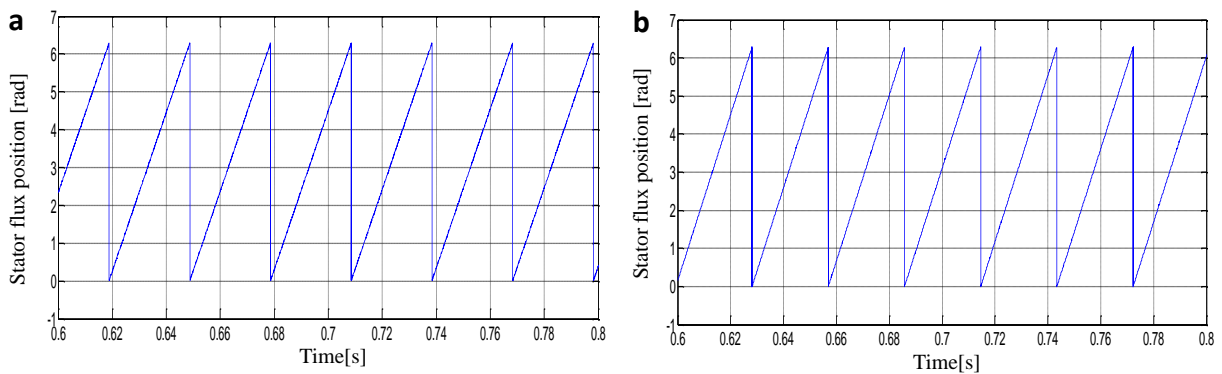


Fig.2.23 Position of stator flux vector.

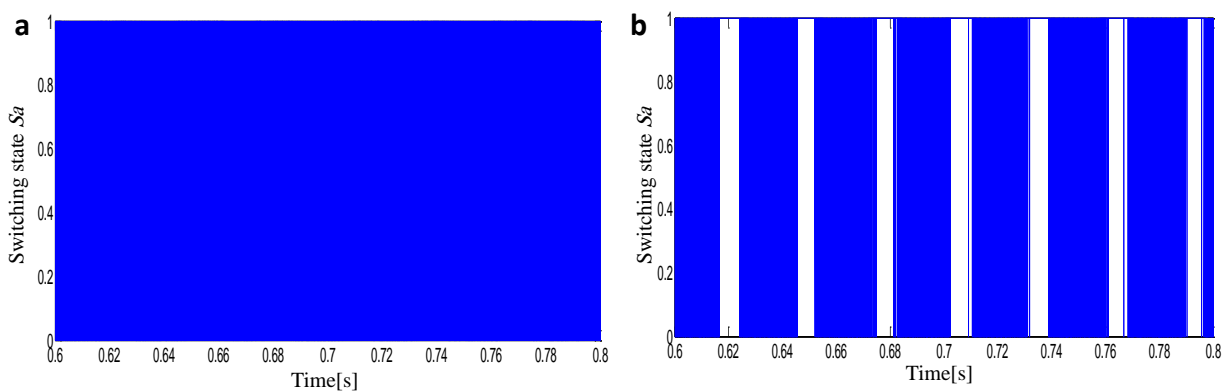


Fig.2.24 Inverter switching state S_a

The displayed simulation results above (**Figs.2.14-2.24**) show the starting up and the steady states with load application for the DTC controlled induction motor. **Fig.2.14** illustrates the comparison between speed responses of conventional DTC and SVM-DTC according to the speed reference step of 1000 rpm . The load disturbance has been introduced at ($t=0.5s$). The figure shows that both techniques show good dynamic at starting up. We can notice that the speed regulation loop rejects the applied load disturbance quickly. The SVM-DTC in **Fig.2.14(b)** kept the same fast speed response of DTC strategy. Since the same PI speed controller is used for both schemes, there is no difference in the transient response.

Then, **Fig.2.15** illustrates the torque responses with by load application. The figure shows that at the beginning the speed controller (PI anti-windup) operates the system at the

physical limit. It can be seen clearly that the constant switching frequency based DTC strategy in **Fig.2.15(b)** has a reducer ripples level owing to the use of SVM compared to the conventional DTC in **Fig.2.15(a)**, where it is observed that the high torque ripples exceed the hysteresis boundary. Next, in **Figs.2.16-2.18**, the stator phase current with ZOOM and its FFT analysis are presented. The conventional DTC in **Fig.2.17(a)** shows a chopped sinusoid waveform of current which indicates to high harmonics level, while SVM-DTC in **Fig.2.17(b)** shows a smoother sinusoid waveform. It can be justified in the next figure where SVM-DTC has lower THD level (total harmonics distortion), 8.38% in **Fig.2.18(b)** compared to 21.07% for the classical DTC in **Fig.2.18(a)**.

After that, **Figs.2.19-2.22** exhibit the stator flux evolution (i.e. stator flux magnitude, components and circular trajectory). In **Fig.2.19(a)**, it is clear that the flux ripples of the conventional DTC have exceeded the hysteresis boundary. The magnitude and the trajectory illustrate that the flux takes a few steps before reaching the reference value ($1Wb$) at the starting stage due to the zone's changing (**Fig.2.20(a)**, **Fig.2.22(a)**). The stator flux components show an acceptable waveform but high ripples level (**Fig.2.21(a)**). The SVM-DTC in **Figs.2.20(b)-2.22(b)** shows a reducer flux ripples, faster magnitude tracking at the starting up and better components waveform than the conventional DTC. **Fig.2.23** presents the position of the stator flux vector. Finally, **Fig.2.24** shows the comparison of inverter switching state of the first voltage phase (S_a) for both techniques. For the classical DTC in **Fig.2.24(a)**, it is observed that the switching frequency is variable, this leads to considerable commutation losses which is a major disadvantage in this strategy. Contrariwise, the presented switching state in **Fig.2.24(b)** shows that the switching frequency of SVM-DTC is constant and each inverter's interrupter has a rest moment (switching off), this can reduce the commutation losses.

2.7.2. Rotation sense's reversing

This section presents the test of rotation sense's reversing of the IM from (1000 rpm to -1000 rpm). The following figures show rotor speed, torque, current and flux components. The figures are specified: ((a) for conventional DTC, and (b) for SVM-DTC).

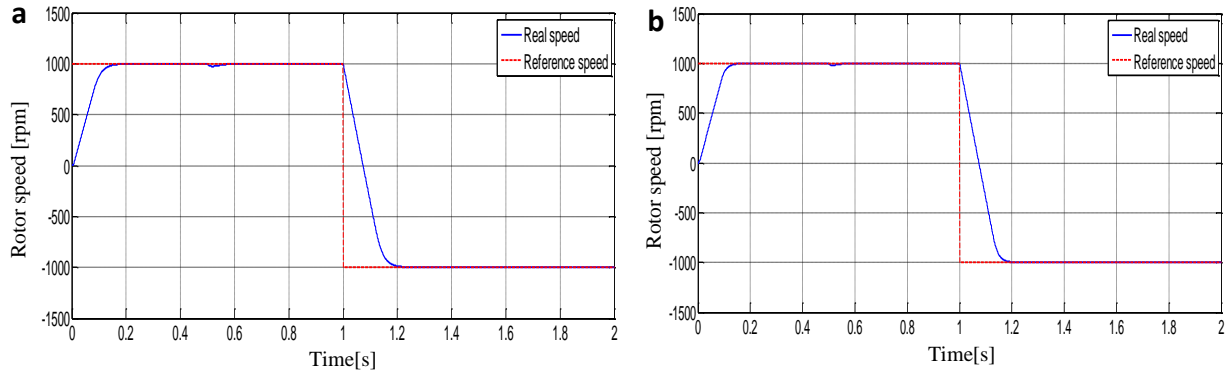


Fig.2.25 Rotation sense's reversing: rotor speed ($1000rpm$; $-1000rpm$).

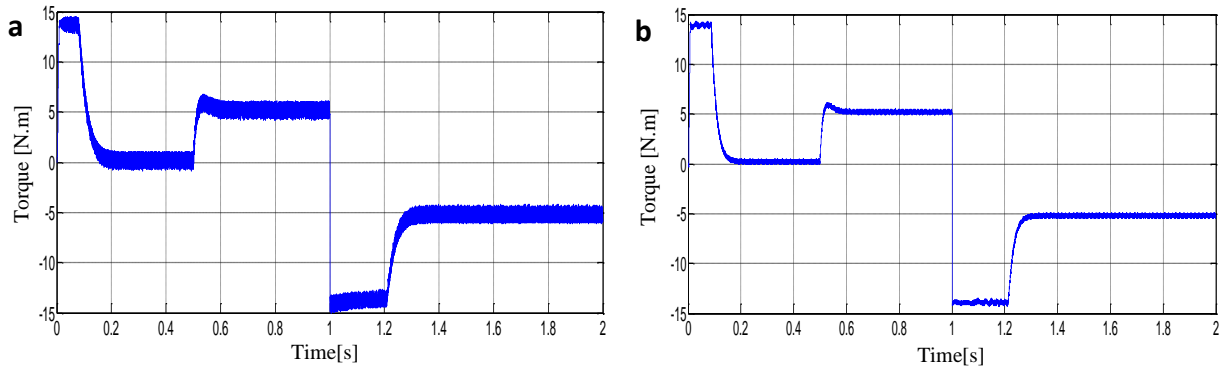


Fig.2.26 Rotation sense reversing : Electromagnetic torque [N.m].

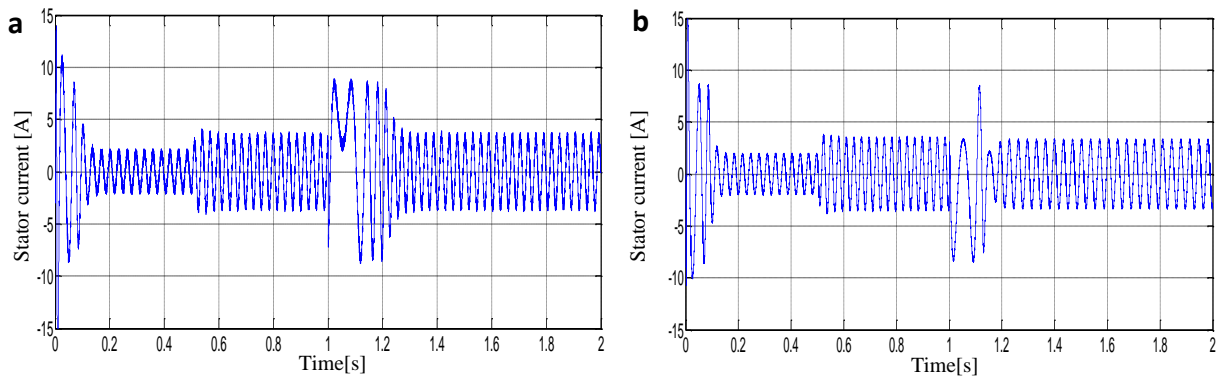


Fig.2.27 Rotation sense reversing: Stator phase current [A].

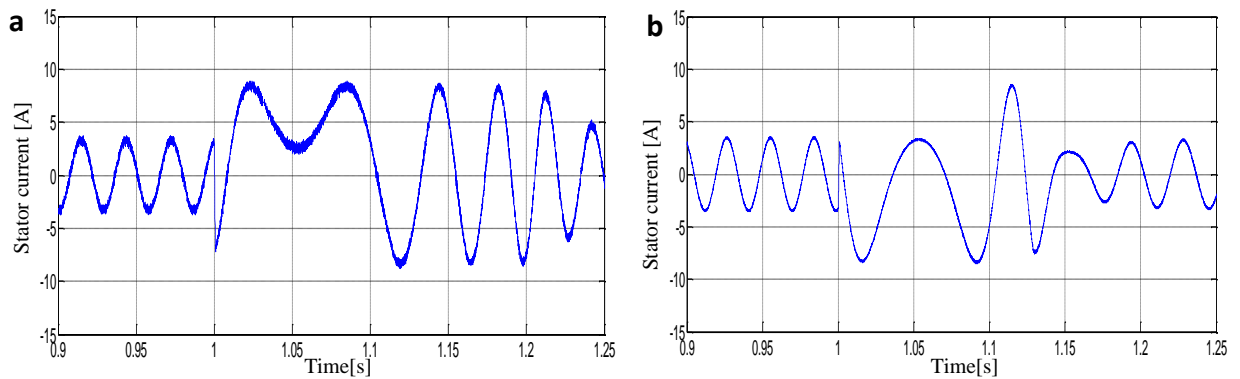


Fig.2.28 Rotation sense reversing: ZOOM of Stator phase current [A].

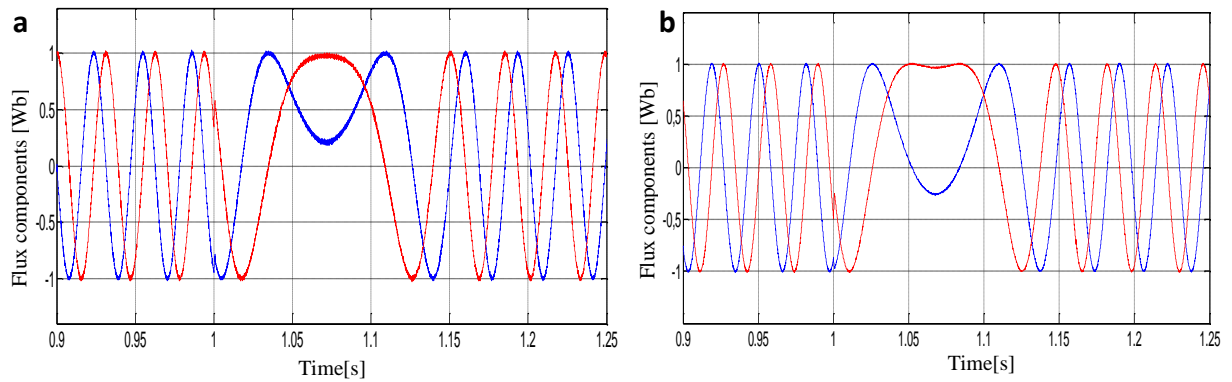


Fig.2.29 Rotation sense reversing: Stator flux components (α, β).

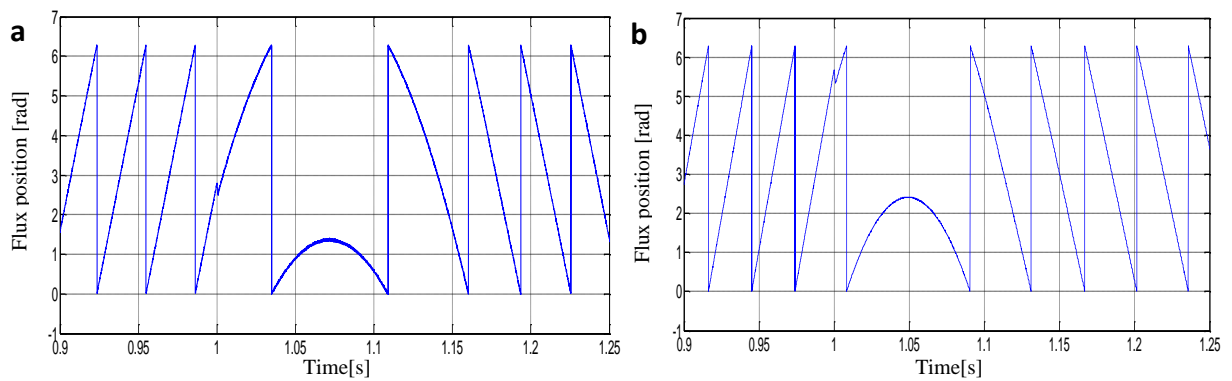


Fig.2.30 Rotation sense reversing: Position of stator flux vector [rad].

A speed reversal from positive to negative value (1000 rpm ; -1000 rpm) is executed in (Figs.2.25-2.30) in order to show that DTC can operate at different speed points. During the reversing stage, the speed controller shows a similar behavior as the starting up state by operating the system at the physical limit. This can be seen clearly in torque response (Fig.2.26). The speed and torque response in (Figs.2.25-2.26) show good dynamic and reference tracking while transient and steady state. The SVM-DTC provides better dynamic with reduced torque ripples in this condition also. In Figs. 2.27-2.29, the sense's reversing of stator current and flux components is presented for both techniques. They show good sinusoid waveform with a reduced level of harmonics for SVM-DTC. The flux angle has been shown in Fig.2.30 in order to indicate the reversing of rotation direction.

2.7.3. Low speed operation

The figures below depict the test of operating at low and medium speeds of the DTC controlled IM. This test has been employed as a speed variation in low region from (200 rpm to $600 \text{ rpm} \approx 20.93 \text{ rad/s}$ to 62.8 rad/s). The figures show rotor speed, flux position, stator phase current, flux magnitude and electromagnetic torque.

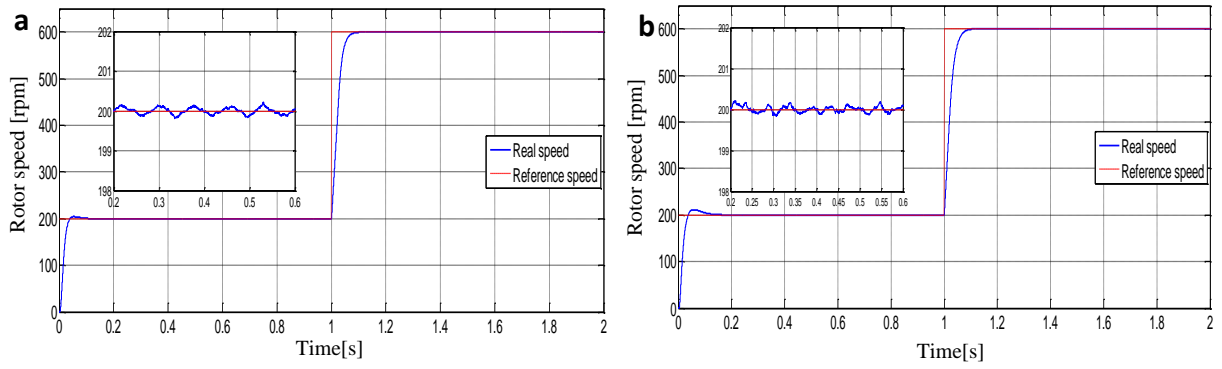


Fig.2.31 Low speed operation: Rotor speed [rpm].

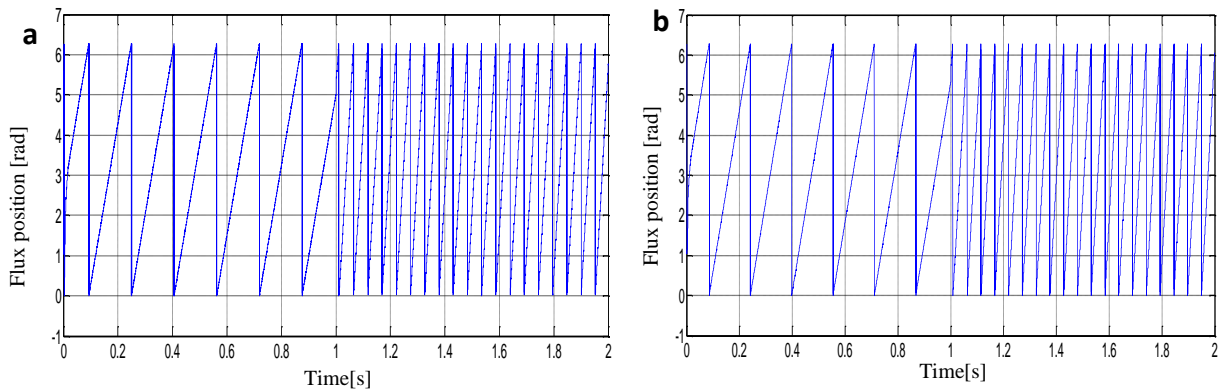


Fig.2.32 Low speed operation: Stator flux position [rad].

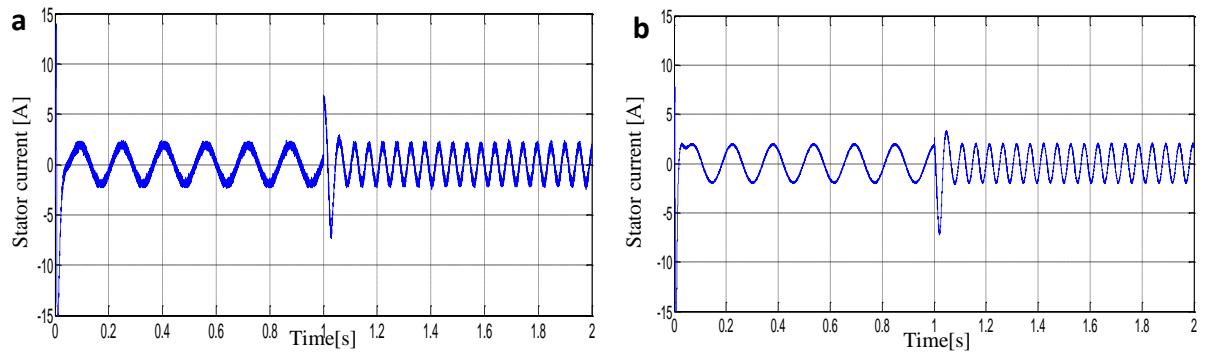


Fig.2.33 Low speed operation: Stator phase current [A]

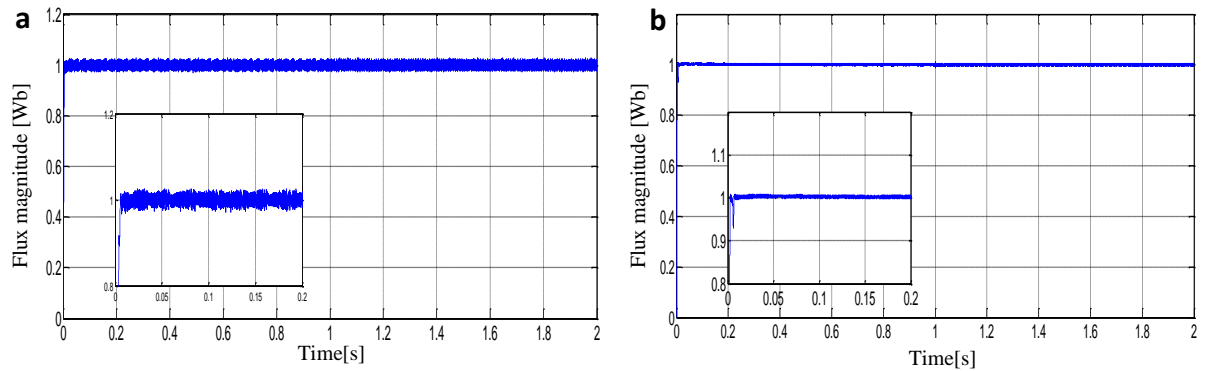


Fig.2.34 Low speed operation: Stator flux magnitude [Wb]

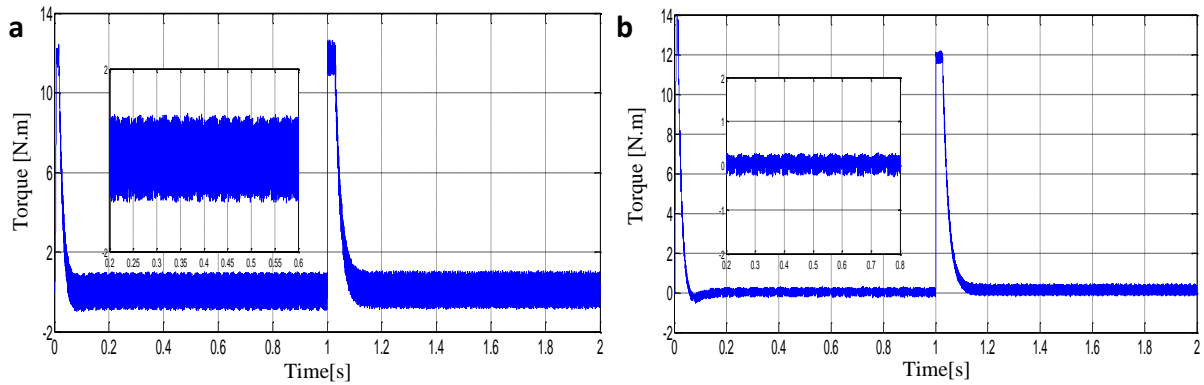


Fig.2.35 Low speed operation: Electromagnetic torque [N.m]

Fig.2.31 shows the speed reference changing of (200 rpm – 600 rpm), the flux angle has been added in **Fig.2.32** to indicate the variation of the rotation frequency. It can be seen that the rotor speed presents an overshoot at the starting up, moreover, it has presented some fluctuations for both control strategies. In addition, the level of current harmonics and flux ripples has been increased for the classical DTC in **Fig.2.33(a)**, while the SVM-DTC kept an acceptable current waveform. Then, in **Figs.2.34-2.35**, the flux magnitude and electromagnetic torque are presented with ZOOM. We can observe that the flux magnitude has been deformed as well as the torque, especially at 200 rpm . Generally, at low speeds, the machine becomes unstable, the torque performance is diminished and speed regulation may be inaccurate.

2.8. Real-Time Control of Induction Motor

The real-time control of the induction motor is employed basing on dSpace 1104 board. dSpace is an input-output (I/O) interface between the power electronics converter and the software part (MATLAB/Simulink/ControlDesk). The experimental setup based on dSpace and induction motor drives has been designed and constructed in order to check and validate the simulation results above. The realized implementation ground of LGEB laboratory of Biskra is shown in **Fig. 2.36(a)**. A simplified real-time control scheme is presented in **Fig.2.36(b)**. All details about the experimental setup components will be presented in the Appendix A.3.

For implementation purpose, the choice of sampling frequency has an apparent influence on quality of signals, especially the phase currents and the produced electromagnetic torque, regardless to the implemented control algorithm. The sampling frequency of dSpace 1104 can reach 20 kHz . However, due to some limits and constraints imposed by real-time implementation and the degree of complexity of the control algorithm we were obliged to choose a reducer value of sampling frequency (10 kHz).

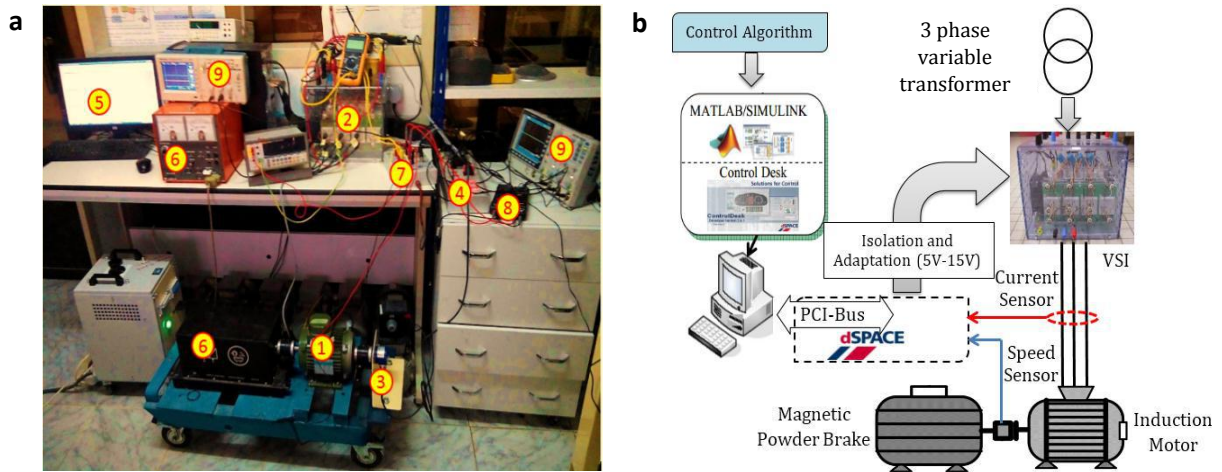


Fig.2.36 Presentation of the experimental setup.

2.9. Experimental Results

The experimental results have been obtained by GW-INSTEK numerical oscilloscope which was linked with the real-time interface. The THD analysis has been obtained by Fluke 3 phase power analyzer. The figures below exhibit the experimental results of the comparative analysis of the SVM-DTC compared with conventional DTC. The conducted tests are the same as the presented in the simulation section (i.e. starting up and steady states, load application, rotation sense's reversing and low-speed region). (The figures are specified :(a) for conventional DTC and (b) for SVM-DTC).

2.9.1. Starting up and steady states with load application

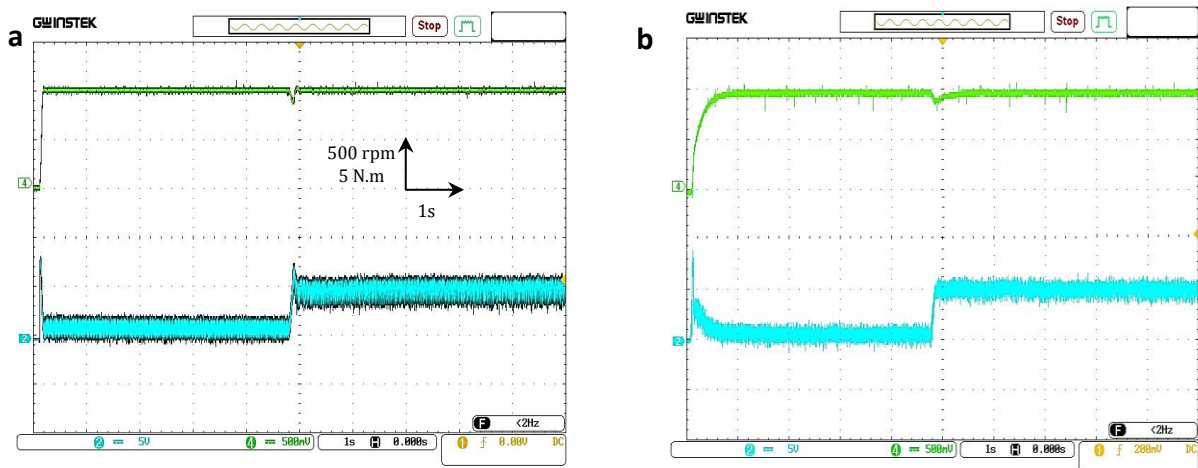


Fig.2.37 Starting up: Rotor speed and torque responses with load application of 5 N.m.

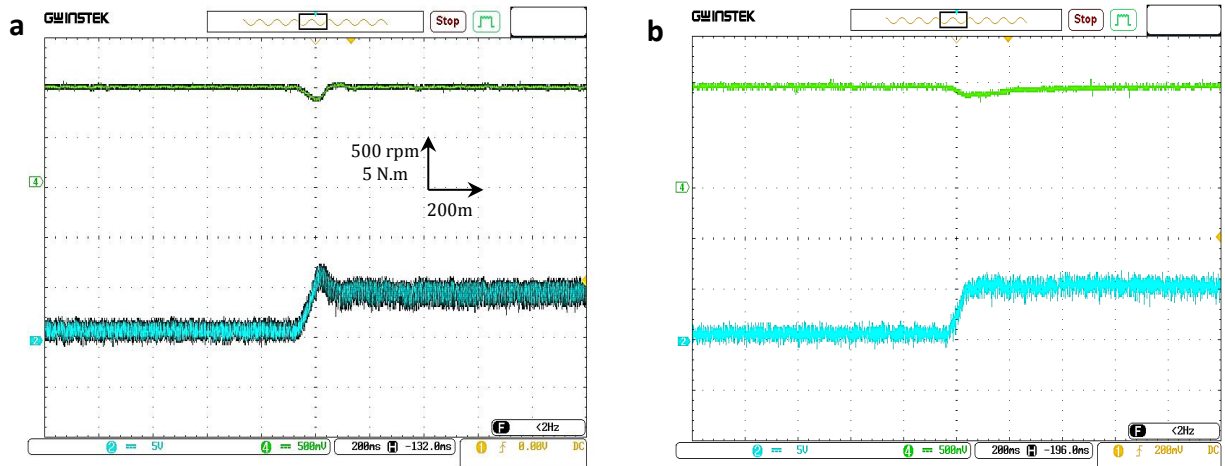


Fig.2.38 Rotor speed and electromagnetic torque with load application of 5 N.m.

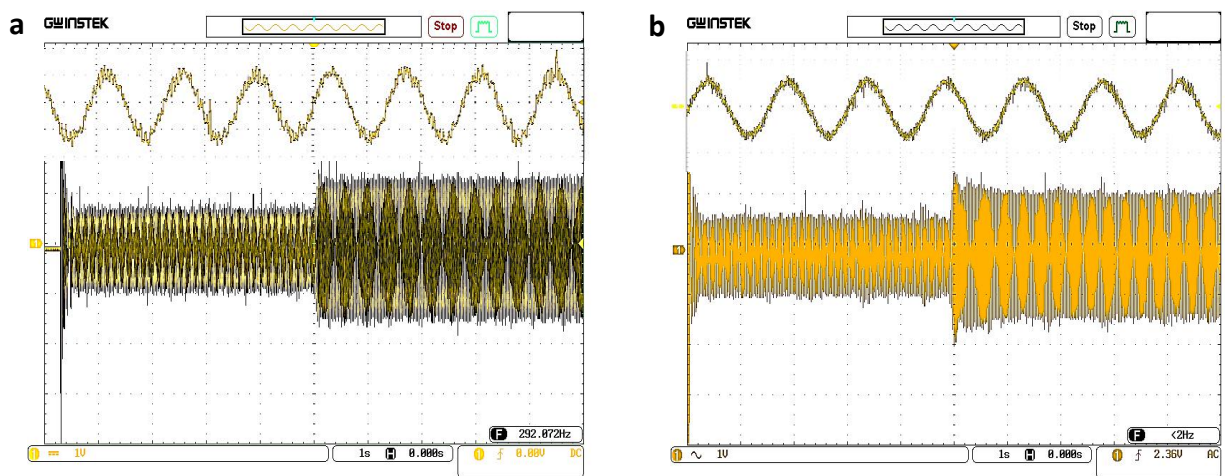


Fig.2.39 Stator phase current with load application.

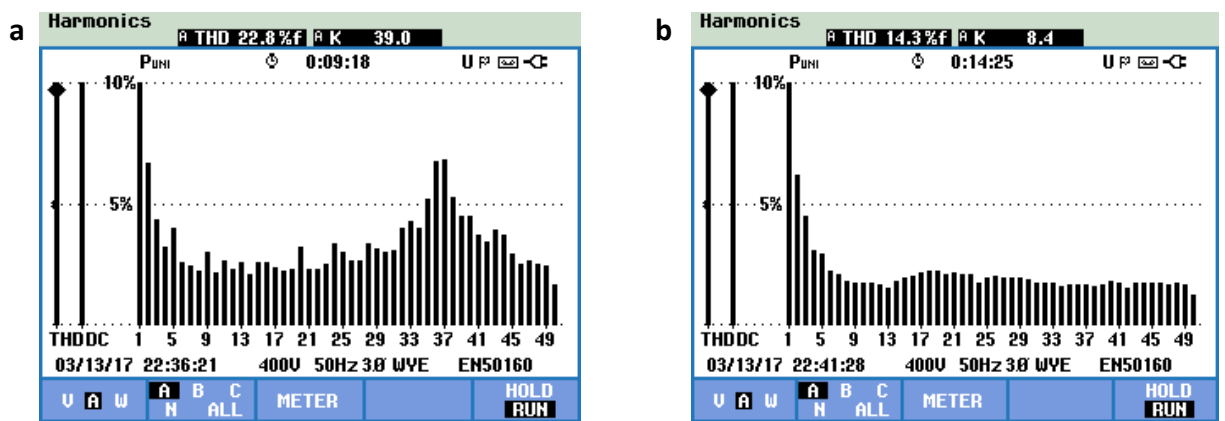


Fig.2.40 Stator phase THD using power analyzer.

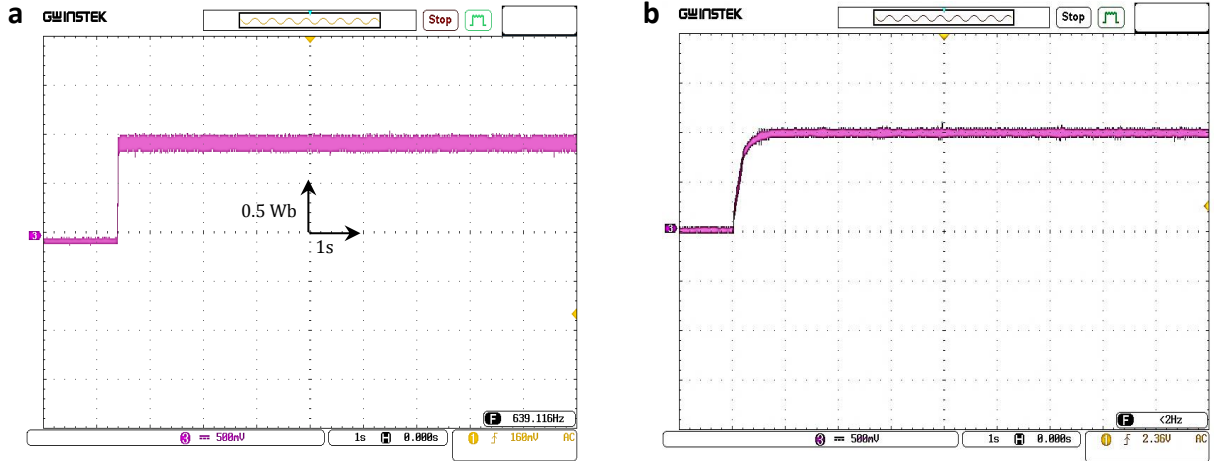


Fig.2.41 Stator flux magnitude.

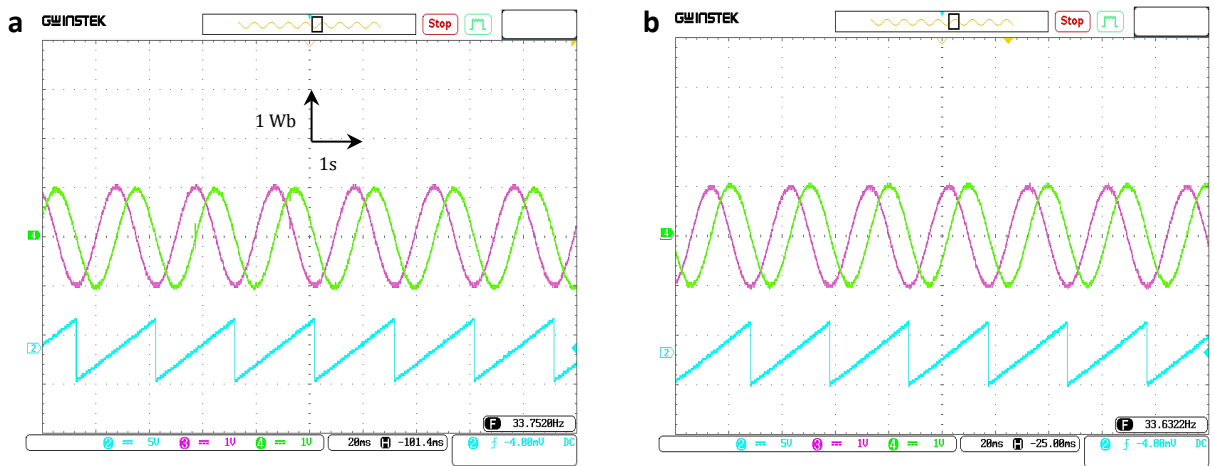


Fig.2.42 Stator flux axes components ($\psi_{s\alpha}$, $\psi_{s\beta}$) and position.

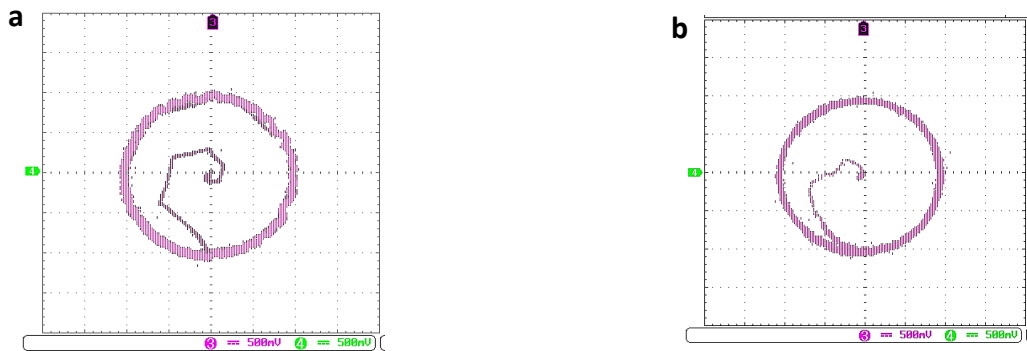


Fig.2.43 Stator flux circular trajectory.

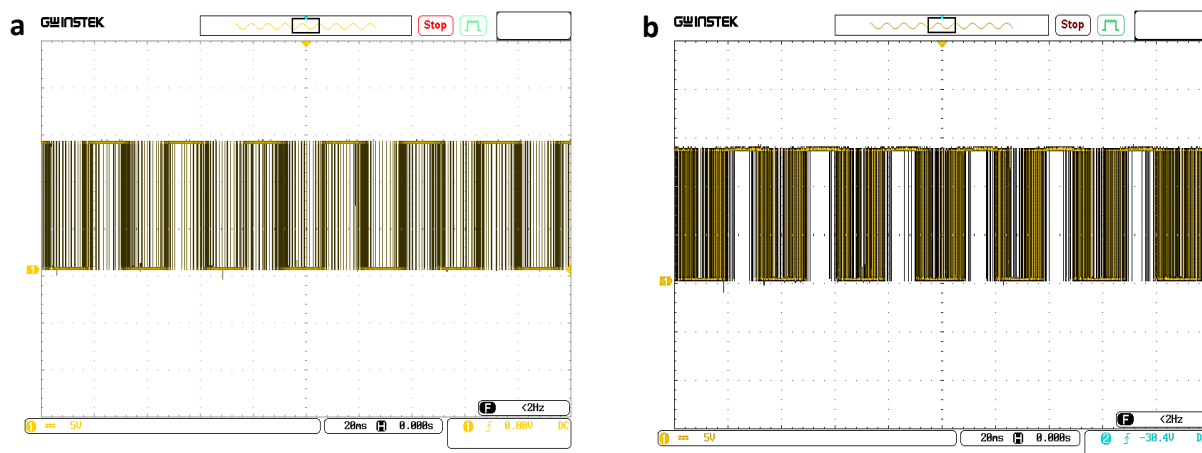


Fig.2.44 Inverter switching state S_a .

Fig.2.37 shows the experimental results of the starting up of the motor, a load application for classical and SVM-DTC. The figure illustrates from the top to bottom rotor speed ($1div=500 rpm$) and electromagnetic torque ($1div=5N.m$). Both of control strategies featured by an identical speed response owing to the use of PI controller for both schemes. **Fig.2.38** is a ZOOM of load application instant. It is clearly observed that SVM-DTC has the reducer torque ripples level. Next, in **Fig.2.39** the stator phase current is presented in the same conditions. It can be seen in **Fig.2.39(b)** that the SVM-DTC shows better sinusoid waveform of current with less harmonics. Furthermore, it has been verified through THD analysis in **Fig.2.40**, that the SVM-DTC has lower harmonic level (14.3%) than the classical DTC (22.8%). We can notice that these values are different with the obtained ones in simulation section due to some constraints in experimental implementation especially the chosen sampling time.

Then, in **Figs.2.41-2.43**, the flux figures are depicted, they show flux magnitude ($1div=0.5Wb$), flux axes components ($1div=1Wb$) and circular trajectory respectively. All the presented results give a similar appearance as the simulation results. The flux magnitude of the conventional DTC in **Fig.2.41(a)** exceeds the hysteresis band, moreover, it shows in its circular trajectory (**Fig.2.43**) that it takes a few steps before reaching the reference value ($1Wb$). By comparing the results of **Figs.2.41-2.43(a)** with **Figs.2.41-2.43(b)** it can be seen that the flux ripples are considerably reduced in SVM-DTC. Finally, **Fig.2.44** shows the comparison of inverter outputs through the adaptation circuit in the range of ($0V-15V$) ($1div=5V$). This represents the amplified image of the inverter switching states of the first inverter leg (S_a). The classical DTC in **Fig.2.44(a)** provides a variable switching frequency compared to the SVM-DTC in **Fig.2.44(b)** which presents a constant switching frequency due to the use of SVM where the inverter had a switching off moment for each interrupter.

2.9.2. Speed sense's reversing

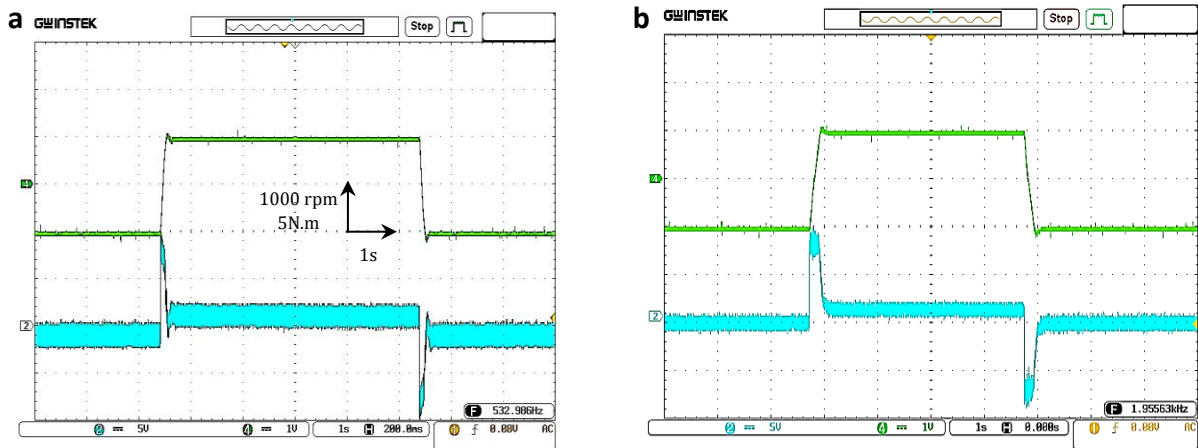


Fig.2.45 Rotation sense's reversing: Rotor speed, electromagnetic torque.

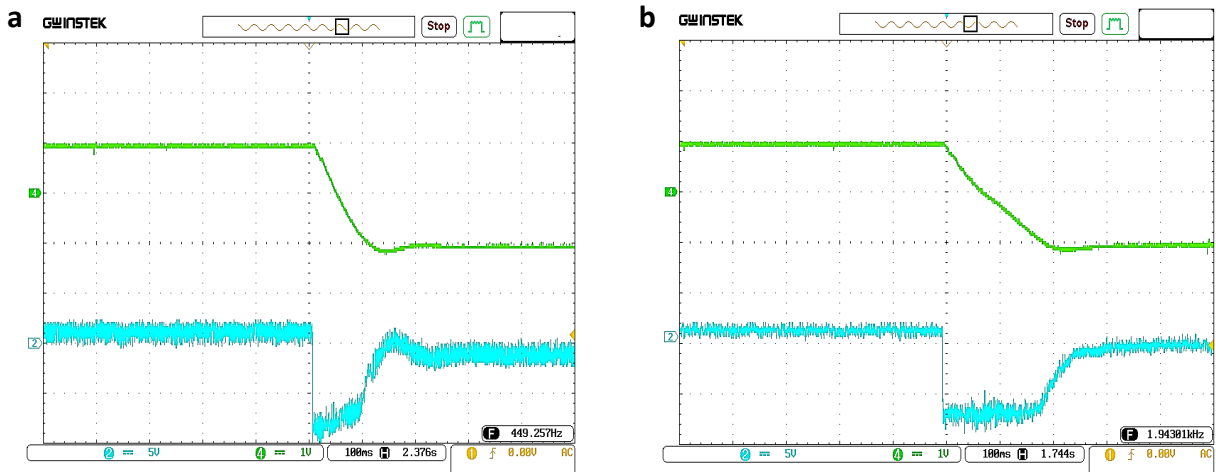


Fig.2.46 Rotation sense's reversing: Rotor speed, electromagnetic torque (ZOOM).

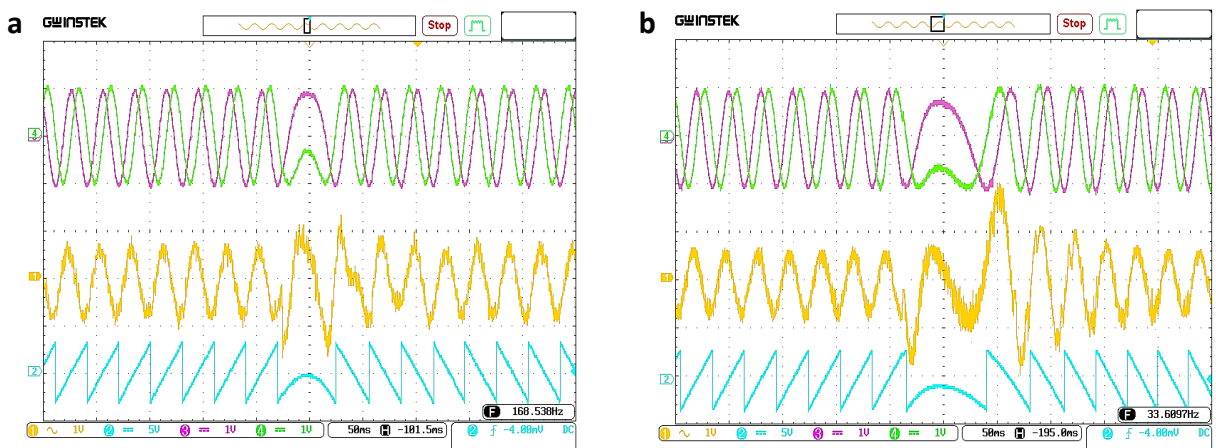


Fig.2.47 Rotation sense's reversing: Flux components, current and flux position.

The test of speed direction reversing has been employed in the figures above (Figs.2.45-2.47). The speed reference is changing from (1000 rpm; -1000 rpm). Fig.2.45 illustrates the rotor speed ($1div=1000\text{ rpm}$) and the electromagnetic torque ($1div=5N.m$), ZOOM is displayed in the next figure (Fig.2.46).

As we have presented in the simulation section, the motor has been operated at the physical limit at the transient state during the sense’s reversing. **Fig.2.47** presents from the top to the bottom flux components, stator phase current and flux position. We can see that SVM-DTC offers low ripples and harmonics in this operation condition (**Fig.2.47(b)**). Both strategies show fast dynamic in this stage, in spite of the important level of ripples for the conventional DTC. The flux position is added to indicate the sense’s changing.

2.10.3. Low speed operation

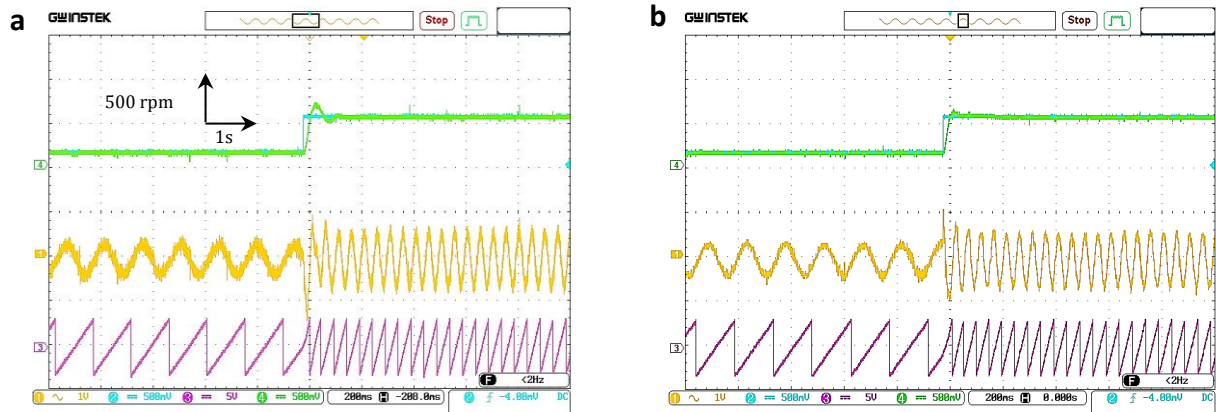


Fig.2.48 Low speed operation test :(200 rpm–600 rpm): Speed, current and flux position.

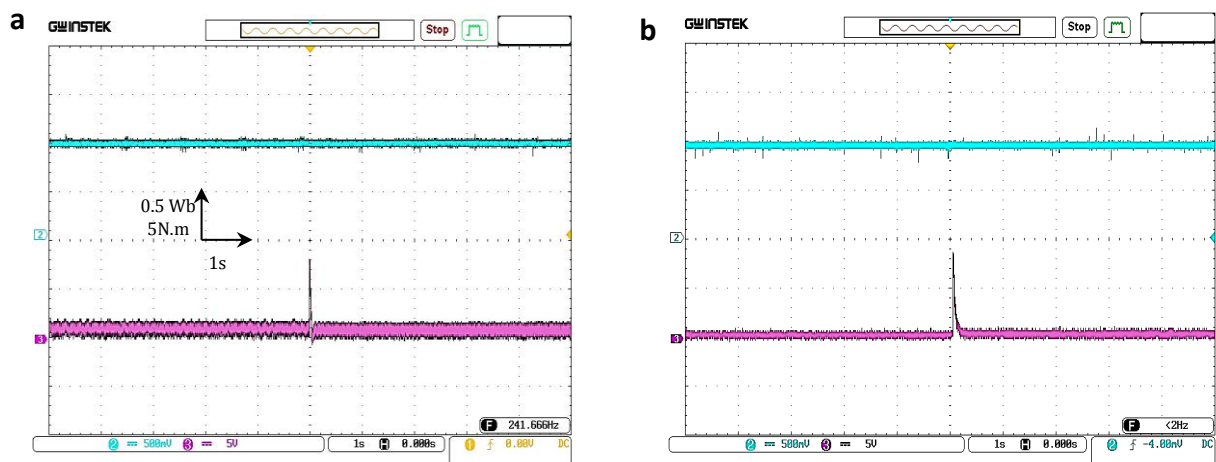


Fig.2.49 Low speed operation test (200 rpm–600 rpm): Flux magnitude, torque.

The low speed operation is the last considered test. It is shown in **Figs.2.48-2.49** where the reference speed changes from low to medium speed regions (200 rpm; 600 rpm). As presented in the simulation section, the rotor speed shows a degraded dynamic and an inaccurate reference tracking (**Fig.2.48**). It can be seen that the rotor speed has shown an overshoot at the starting up and some fluctuations for both control strategies. In addition, the level of current harmonics has been increased specially for the classical DTC at (200 rpm \approx 20.93 rad/s) as illustrated in **Fig.2.48(a)**, while the SVM-DTC kept an acceptable current waveform as presented in **Fig.2.48(b)**. Then, **Fig.2.49** presents the flux magnitude and

electromagnetic torque. It is observed that the flux waveform has been deformed and the torque has been distorted.

When the machine operates with low speed/frequency, the performance of DTC has been diminished comprehensively. In physical explanation, at low speeds, the back EMF decreases as the rotor speed slows and the stator resistance voltage dropping becomes significant compared to the commanded voltage. This dropping voltage cannot be longer neglected. Therefore, the accuracy of stator flux estimation at very low speed range becomes a major issue.

In general, the experimental results have validated the simulation by giving a similar behavior in all tests. However, the existence of small disagreement between the results is noticed. This is owing to many reasons. The most influential factor is the limited sampling time of the processor. In addition, the ideality of the simulation unlike the inaccuracies which exist in the real-time implementation, the dead times of the inverter switching signals and the measurement offset.

2.10 Comparative evaluation of direct torque control techniques

The switching table based DTC is featured by simple decoupled control scheme and fast dynamic torque response, while the direct torque control with space vector modulation combines the advantages of DTC and FOC strategies. According to the mentioned comparative analysis, the following table summarizes the features of the SVM-DTC control scheme compared to the conventional DTC.

Classical DTC with switching table	SVM-DTC Structures
+ Fast dynamic torque response.	+ Fast dynamic torque response.
+ No coordinate transformation.	+ – No coordinate transformation.
+ No current regulation.	+ No current regulation.
+ Independence on machine parameters.	+ Independence on machine parameters.
– High current and torque and flux ripples.	+ Reduced torque and flux ripples.
– Variable switching frequency.	+ Constant switching frequency.
– High noise levels at low speed operation	+ Good dynamic at low speed operation.
– High switching losses.	+ Low switching losses.

+ Advantages; – Disadvantages

Table.2.4 Advantages of DTC–SVM compared to the classical DTC.

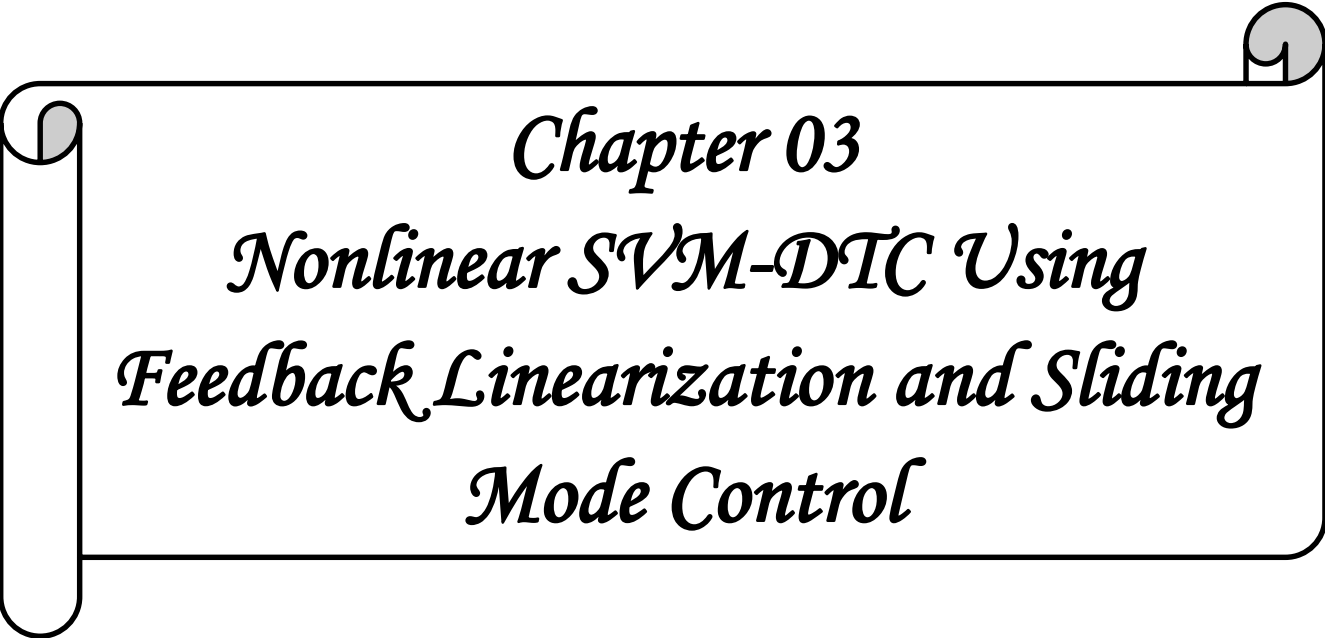
2.11. Conclusion

This chapter presents a general study about the basic direct torque control of induction motor drive. The used model for the control and the main concepts of DTC strategy have been introduced firstly. DTC uses separated hysteresis controllers for stator flux and electromagnetic torque control, and a lookup switching table for voltage vector selection. The speed regulation in the outer control loop has been done using an anti-windup PI controller to solve the problem of using a pure integrator. Moreover, in purpose of improving the conventional DTC, this chapter presents a constant switching frequency DTC control method based on SVM.

The performances of the two DTC methods has been investigated as a comparative study by the numerical simulation using MATLAB/Simulink. Furthermore, an experimental implementation has been employed in order to validate the theory and the simulation results. It has been done using MATLAB/Simulink with real time interface linked to dSpace 1104 board.

The obtained experimental results have been discussed also and resembled to simulation results. Generally, the test results indicate that the torque and the stator flux ripples have been considerably reduced owing to the SVM use. In addition, the stator phase current provides good current waveform with less harmonics. Furthermore, SVM-DTC achieves better dynamic control under different operation conditions, such as load application, speed sense's reversing and low speed operation.

The insertion of SVM in DTC control scheme solves the most common DTC drawbacks (i.e., high flux and torque ripples). However, this modified algorithm has moved a bit from the principles of DTC. It uses a non-stationary frame (synchronous frame) and requests axes coordinate transformation which increase the complexity of control scheme. Furthermore, it becomes more vulnerable to sensitivity against external disturbance and parameters variation due to use of PI controllers. The next chapter will present a proposed DTC algorithm based on a nonlinear approach in order to overcome the aforementioned problems and achieve a robust decoupled machine control in the stationary reference frame.



Chapter 03
Nonlinear SVM-DTC Using
Feedback Linearization and Sliding
Mode Control

3.1 Introduction:

The last chapter proposed a constant switching frequency strategy to cover the main drawbacks of the conventional DTC. It replaces the hysteresis controllers and the switching table by two (PI) controllers and SVM unit to modulate the generated reference voltages and produces the inverter switching states. However, this modification moved a bit away from the principles of DTC. It bases on a non-stationary frame which may increase the complexity of control's algorithm by requesting coordinates transformation. In addition, the robustness and the stability of the system can be affected by parameters variation owing to the use of PI controllers. Since the machine parameters are obtained by classical identification experiments, the measurement errors cannot be avoided. Furthermore, the values of parameters cannot be fixed because of the physical properties which can be influenced by environment conditions, namely, the resistance varies with temperature and the inductance with saturation.

To solve these problems and ensure a perfect decoupling, various control methods are presented for this context, such as the artificial intelligent techniques and the adaptive control [Sab14; Amr16]. The robust nonlinear control techniques were also mentioned widely in power electronics and drives field, like the backstepping, the input-output feedback linearization (IOFL) and the sliding mode control [Haj10; Zha10; Kow14a; Zaa16; Las17]. The feedback linearization is a nonlinear approach which can improve the performance of the system by disappearing the coupling effect. It converts a nonlinear system into an equivalent linear one to make it simpler for control design [Yaz08]. The sliding mode control (SMC) is also a control method which provides an excellent performance for the electrical drives. Moreover, it shows high robustness and simple software and hardware implementation.

This chapter presents a combination of SVM-DTC with input-output feedback linearization and sliding mode control approaches. This incorporation can cover the disadvantages of SFOC SVM-DTC and achieves fast dynamic robust control in stationary frame. The decoupled model of the induction motor is presented by assuming the stator flux and electromagnetic torque as control states. The global control strategy will be investigated by simulation and experimental implementation.

3.2 Nonlinear Control Strategies

3.2.1 Input-output feedback linearization (IOFL) approach

The feedback linearization theory was introduced by Isidori [Isi95]. It has been used for various applications in the area of power electronics and drives. The main idea of IOFL is to transform algebraically a nonlinear system dynamic into linear one by cancelling its nonlinearity. Then, it uses an inverse transformation to obtain the desired control for the original nonlinear system [Zha10]. The input-output feedback linearization has been suggested to improve SVM-DTC in several works [Yaz08; Cho16; Las17]. It can guarantee a good decoupling of the motor torque and stator flux. Thus, this control method gives a possibility to get very good behavior in both dynamic and steady states [Kow14b].

For generalized multi-input-multi-output (MIMO) nonlinear system having n states and m inputs/outputs, the following representation is used:

$$\begin{cases} \dot{x} = f(x) + \sum_{j=1}^m g_j u_j \\ y_i = h_i(x) \end{cases} \quad (3.1)$$

where $1 \leq i \leq m$, $x \in \mathfrak{R}^n$ is the state vector, $u \in \mathfrak{R}^m$ is the control input, y is the output state vector, f and g are smooth vector fields on \mathfrak{R}^n and h is a smooth nonlinear function.

3.2.1.1 Relative degree and lie derivatives

The lie derivative and relative degree of the nonlinear system play an important role for SISO and MIMO systems. The partial relative degrees r_i is equal to the number of times that the output y_i has to be differentiate until at least one input appears in the derivative. The total relative degree of the system is defined by the sum of the relative degrees of each output [Obe10].

$$r = \sum_{j=1}^m r_j \quad (3.2)$$

The Input-output linearization of MIMO systems is obtained by differentiation of each output r times. For each output signal, we define γ_j as the smallest integer such that at least one of the inputs appears in $y_j^{\gamma_j}$:

$$y_j^{\gamma_j} = F_j^{\gamma_j} + \sum_{i=1}^m G_i \left(F_j^{\gamma_j-1} \right) u_i \quad (3.3)$$

and at least one term $G_i \left(F_j^{\gamma_j-1} \right) u_i \neq 0$.

3.2.1.2 Control design

After performing the procedure for each output, we are left with the m equations corresponding to the m outputs.

$$\begin{bmatrix} y_1^{r_1} \\ y_2^{r_2} \\ \vdots \\ y_m^{r_m} \end{bmatrix} = \begin{bmatrix} F_1^{r_1} \\ F_2^{r_2} \\ \vdots \\ F_m^{r_m} \end{bmatrix} + C(x) \begin{bmatrix} u_1 \\ u_2 \\ \vdots \\ u_m \end{bmatrix} \quad (3.4)$$

The matrix $C(x)$ is defined as the decoupling matrix of the system. It is given by:

$$C(x) = \begin{bmatrix} G_1(F_1^{r_1-1}) & \dots & G_m(F_1^{r_1-1}) \\ \vdots & \ddots & \vdots \\ G_1(F_m^{r_m-1}) & \dots & G_m(F_m^{r_m-1}) \end{bmatrix} \quad (3.5)$$

As long as $C(x)$ is non-singular, then the linearizing control law u can be obtained as:

$$\begin{bmatrix} u_1 \\ u_2 \\ \vdots \\ u_m \end{bmatrix} = -C^{-1}(x) \begin{bmatrix} F_1^{r_1} \\ F_2^{r_2} \\ \vdots \\ F_m^{r_m} \end{bmatrix} + C^{-1}(x) \begin{bmatrix} V_1 \\ V_2 \\ \vdots \\ V_m \end{bmatrix} \quad (3.6)$$

where $[V_1 \ V_2 \ \dots \ V_m]^T$ is the auxiliary inputs which imposed by the designer.

To ensure perfect tracking and desired behavior, the auxiliary inputs can be defined as:

$$V_i = y_{iref}^{r_i} - k_0 e - k_1 \dot{e} - \dots - k_{r_i} e^{r_i-1} \quad (3.7)$$

where e is the tracking error given by $e = y - y_{ref}$

k_{r_i} is a positive coefficient should be chosen to guarantee the system convergence.

The shown block diagram in **Fig.3.1** describes the linearization by state feedback, which transforms the original system into a linear decoupled equivalent system under the condition that the decoupling matrix is non-singular.

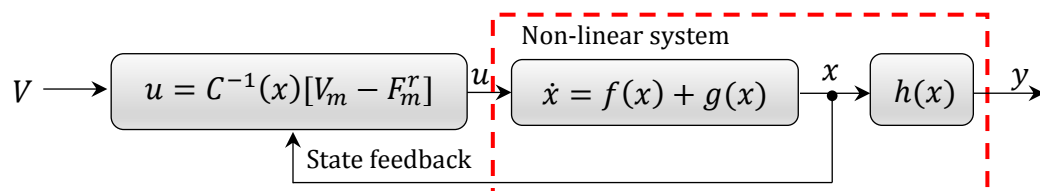


Fig.3.1 Block diagram of the linearization by the state feedback.

3.2.2 Application of IOFL on direct torque control for IM drive (IOFL-DTC)

3.2.2.1 Model presentation

For the proposed nonlinear input-output feedback linearization controller, the induction motor model can be written in stationary frame as follows:

$$\dot{x} = f(x) + gV_{s\alpha\beta} \quad (3.8)$$

$$x = [i_{s\alpha} \quad i_{s\beta} \quad \psi_{s\alpha} \quad \psi_{s\beta}]^T \quad (3.9)$$

$$f(x) = \begin{bmatrix} -\frac{1}{\sigma} \left(\frac{1}{T_r} + \frac{1}{T_s} \right) i_{s\alpha} & -\omega_r i_{s\beta} & \frac{1}{\sigma L_s T_r} \psi_{s\alpha} & \frac{\omega_r}{\sigma L_s} \psi_{s\beta} \\ \omega_r i_{s\alpha} & -\frac{1}{\sigma} \left(\frac{1}{T_r} + \frac{1}{T_s} \right) i_{s\beta} & -\frac{\omega_r}{\sigma L_s} \psi_{s\alpha} & \frac{1}{\sigma L_s T_r} \psi_{s\beta} \\ -R_s i_{s\alpha} & 0 & 0 & 0 \\ 0 & -R_s i_{s\beta} & 0 & 0 \end{bmatrix} \quad (3.10)$$

$$g = \begin{bmatrix} \frac{1}{\sigma L_s} & 0 & 0 & 0 \\ 0 & \frac{1}{\sigma L_s} & 0 & 0 \end{bmatrix}^T \quad (3.11)$$

where:

$f(x)$ is nonlinear function of the state variable x ,

$V_{s\alpha\beta}$: represents the control vector applicable to the system, which is represented in stator voltage components.

3.2.2.2 IOFL-DTC control design

In order to maintain a fast-decoupled torque control of the IM drive, the assumed system outputs are the electromagnetic torque and the square of stator flux magnitude. This latter acts an important role in the motor's performance and it reduces the control design complexity [Yaz08; Kow14a].

The control objectives are defined as:

$$\begin{cases} y_1 = T_e = p(\psi_{s\alpha} i_{s\beta} - \psi_{s\beta} i_{s\alpha}) \\ y_2 = |\psi_s|^2 = \psi_{s\alpha}^2 + \psi_{s\beta}^2 \end{cases} \quad (3.12)$$

$$\begin{cases} e_1 = T_e^* - T_e \\ e_2 = |\psi_s^*|^2 - |\psi_s|^2 \end{cases} \quad (3.13)$$

e_1, e_2 : torque and flux tracking errors.

Basing on the presented model, the relation between the input and the output can be given as:

$$\dot{e} = \begin{bmatrix} \dot{e}_1 \\ \dot{e}_2 \end{bmatrix} = \begin{bmatrix} F_1 \\ F_2 \end{bmatrix} + C(x) \begin{bmatrix} V_{s\alpha} \\ V_{s\beta} \end{bmatrix} \quad (3.14)$$

Where:

$$\begin{cases} F_1 = -p[\mu(\psi_{s\alpha}i_{s\beta} - \psi_{s\beta}i_{s\alpha}) + \omega_r(\psi_{s\alpha}i_{s\alpha} - \psi_{s\beta}i_{s\beta}) - \frac{\omega_r}{\sigma L_s}|\psi_s|^2] \\ F_2 = 2R_s(\psi_{s\alpha}i_{s\alpha} - \psi_{s\beta}i_{s\beta}) \end{cases} \quad (3.15)$$

and where

$$\mu = -\left(\frac{R_s}{\sigma L_s} + \frac{R_r}{\sigma L_r}\right)$$

$$C(x) = \begin{bmatrix} -p\left(i_{s\beta} - \frac{\psi_{s\beta}}{\sigma L_s}\right) & p\left(i_{s\alpha} - \frac{\psi_{s\alpha}}{\sigma L_s}\right) \\ -2\psi_{s\alpha} & 2\psi_{s\beta} \end{bmatrix} \quad (3.16)$$

The determinant of the matrix $C(x)$ is expressed as follows:

$$\det(C(x)) = p \frac{M_{sr}}{\sigma L_s L_r} [\psi_{s\beta}\psi_{r\beta} + \psi_{s\alpha}\psi_{r\alpha}] \quad (3.17)$$

Where:

$\psi_{ra}, \psi_{r\beta}$ are rotor flux components.

The rotor flux can be obtained from the stator flux and stator current as:

$$\psi_r = \frac{L_r\psi_s - L_s L_r \sigma i_s}{M_{sr}} \quad (3.18)$$

The matrix $C(x)$ is a non-singular matrix, it cannot be equal to zero because the product of the stator and the rotor flux cannot be zero [Zha10]. As long as the system is linearizable, we can impose on it the desired dynamics.

The input-output feedback linearization of the system will be given as:

$$U = \begin{bmatrix} V_{s\alpha} \\ V_{s\beta} \end{bmatrix} = C^{-1}(x) \begin{bmatrix} -F_1 + V_1 \\ -F_2 + V_2 \end{bmatrix} \quad (3.19)$$

V_1 and V_2 are presumed auxiliary inputs to ensure more tracking accuracy and desired behavior for the stator flux and the torque.

$$\begin{cases} V_1 = -k_1 e_1 \\ V_2 = -k_2 e_2 \end{cases} \quad (3.20)$$

By Substituting the expression (3.19) and (3.20) in (3.14) we obtain:

$$\dot{e} = \begin{bmatrix} \dot{e}_1 \\ \dot{e}_2 \end{bmatrix} = \begin{bmatrix} -k_1 & 0 \\ 0 & -k_2 \end{bmatrix} \begin{bmatrix} e_1 \\ e_2 \end{bmatrix} \quad (3.21)$$

k_1 and k_2 are constant gains, they have been supposed appropriately positive to have an exponential convergence of the torque and the square of stator flux magnitude errors. The performance of the IOFL-DTC is certainly depending on the suitable choice of these gains. The small gains values can cause a slow convergence and weak robustness of the system, while the very large values can lead to high perturbations and system instability. Consequently, the control gains are seriously effective on the control performance [Cho16]. The feedback linearization control law (3.19) can be written as following:

$$U = C^{-1}(x)(-F + V) \quad (3.22)$$

with:

$$F = \begin{bmatrix} F_1 \\ F_2 \end{bmatrix} \text{ and } V = \begin{bmatrix} V_1 \\ V_2 \end{bmatrix}$$

The control law should be chosen to satisfy Lyapunov stability's condition. The Lyapunov candidate function for MIMO systems is known by:

$$V = \frac{1}{2} e^T e \quad (3.23)$$

The time derivative of Lyapunov function is given by:

$$\dot{V} = e^T \dot{e} \quad (3.24)$$

The stability condition $\dot{V} < 0$ has to be verified. By substituting (3.21) in the derivative of Lyapunov function we can obtain:

$$\dot{V} = e^T \begin{bmatrix} -k_1 & 0 \\ 0 & -k_2 \end{bmatrix} \begin{bmatrix} e_1 \\ e_2 \end{bmatrix} \quad (3.25)$$

and it gives:

$$\dot{V} = -k_1 e_1^2 - k_2 e_2^2 \quad (3.26)$$

For k_1 and k_2 positive, the derivative \dot{V} is negative, which guarantees that the errors asymptotically converge to zero and ensures the stability of the control system.

3.2.2.3 Feedback linearization improvement

The classical feedback linearization has a non-robust dynamic in the presence of uncertainties. In [Far06], the performance of the obtained feedback linearization control law has been associated with a McFarlane and Glover H^∞ controller [Glo92], which called robust feedback linearization. In [Ben99b] FOC control based on IOFL strategy for induction drive has been combined with another robust control technique which is the sliding mode control (SMC). A new DTC controller that integrates IOFL with SMC is presented in [Yaz08; Las17; Amr17a]. The disadvantages of IOFL which are the sensitivity of the linearized model to uncertainties and parameters variation motivate the use of SMC. The next sections present a brief theory about SMC and the insertion of SMC technique in IOFL-DTC control law.

3.2.3 Sliding mode control

The SMC is a variable structure control method which is widely known in the automatic and control field. The strength points of the SMC are the robustness against uncertainties, fast response and simple software and hardware implementation [Utk93; Kow14a]. SMC bases on forcing the system trajectory to slide along a switching surface under determined control law. It consists of two phases, a reaching phase where the state trajectory is driven to the surface $S=0$ and reaches it in a finite time, followed by a sliding phase where it slides on the switching surface to an equilibrium point, as shown in **Fig.3.2** [Gad09].

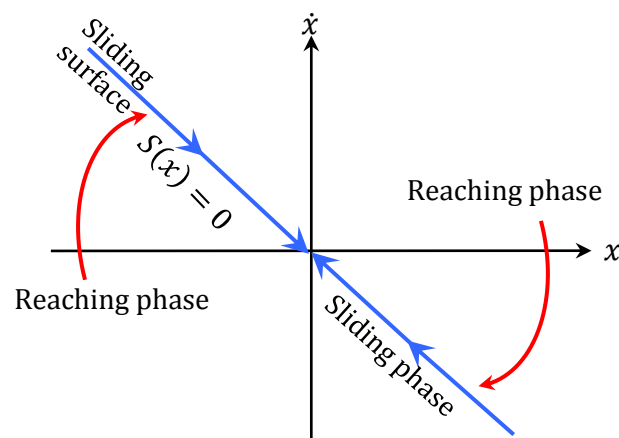


Fig.3.2 Sliding mode principle of state trajectory.

3.2.3.1 Sliding surface choice

The design of SMC can be achieved into two phases. The first phase is determining the switching surface. In engineering applications, the error between control objectives and the reference inputs and its derivative is used to form the sliding surface [Gen10].

The second phase is to design the control law in a way that to steer the system trajectory to the sliding surface [Slo91; Raf12]. The well applied sliding surface was proposed by Slotine as:

$$S = \left(\frac{d}{dt} + \lambda \right)^{n-1} e \quad (3.27)$$

Where S is the sliding surface, λ is positive constant, e is the system error and n is the system relative order.

3.2.3.2 Existence conditions of sliding mode

The sliding mode must exist in all points of the surface $S = 0$. To guarantee that the system state stays in sliding mode after the reaching phase, the existence conditions should be [Utk09; Kow14b]:

$$\begin{cases} \lim_{S \rightarrow 0^-} \dot{S} < 0 \\ \lim_{S \rightarrow 0^+} \dot{S} > 0 \end{cases} \quad (3.28)$$

It means that if S is positive, then its derivative should be negative and if S is negative, then its derivative should be positive. It can be written in a simplified way as:

$$S\dot{S} < 0 \quad (3.29)$$

Since the existence problem looks like a generalized stability problem, it can be summarized in terms of Lyapunov's theory as the follows [Bra09; Ben16]:

$$V = \frac{1}{2} S^2 \quad (3.30)$$

The aim is to determine a control law such that $\dot{V} < 0$ in order to drive the system states to the sliding-mode surface:

$$\dot{V} = S\dot{S} < 0 \quad (3.31)$$

when $S \neq 0$, \dot{V} is negative definite. Therefore, for finite time convergence the condition (3.31) ensures asymptotically convergence towards the sliding surface.

3.2.3.3 Control design

There are various methods in literature for control design. The most common of them are the relay control, the equivalent control scheme and the linear feedback with switched gains. The equivalent control is the most used structure for the control of electrical machines (**Fig.3.3**). It is preferred due to the relay control which is more suitable for the structure of the power electronics converters [Faq03].

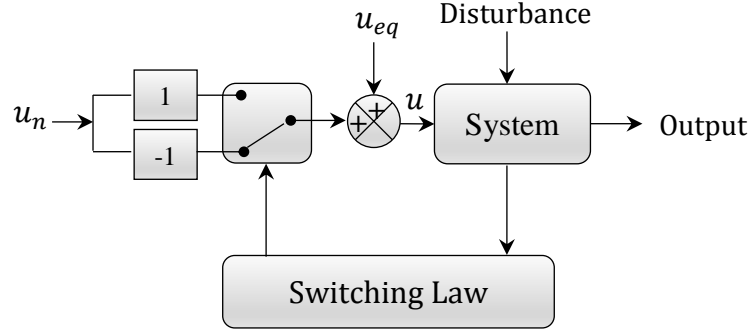


Fig.3.3 Equivalent control structure.

The design of sliding mode control is mostly performed by two parts. The equivalent control u_{eq} is added to another control term called the discontinuous control u_n in order to ensure that the state trajectory reaches and stays on the switching surface.

The control law expression is given by:

$$u = u_{eq} + u_n \quad (3.32)$$

By considering the following state system:

$$\dot{x} = A(x) + B(x)u \quad (3.33)$$

The equivalent control is found by recognizing that $\dot{S} = 0$ is a necessary condition for the state trajectory to stay on the switching surface $S=0$ [Hun93].

The time derivative of the sliding surface is given as:

$$\dot{S} = \frac{\partial S}{\partial t} = \frac{\partial S}{\partial x} \frac{\partial x}{\partial t} \quad (3.34)$$

By substituting (3.32) and (3.34) into Eq (3.33):

$$\dot{S} = \frac{\partial S}{\partial x} A(x) + \frac{\partial S}{\partial x} B(x)u_{eq} + \frac{\partial S}{\partial x} B(x)u_n \quad (3.35)$$

The equivalent control is defined during the sliding phase and the steady state where $S = \dot{S} = 0$ and $u_n=0$ [Ben16].

$$u_{eq} = -\left(\frac{\partial S}{\partial x} B(x)\right)^{-1} \frac{\partial S}{\partial x} A(x) \quad (3.36)$$

The existence of an inverse matrix is a necessary, which means the next condition (3.37):

$$\frac{\partial S}{\partial x} B(x) \neq 0 \quad (3.37)$$

By substituting (3.36) in Eq (3.35), the new sliding surface expression becomes:

$$\dot{S} = \frac{\partial S}{\partial x} B(x)u_n \quad (3.38)$$

The discontinuous control u_n is determined during the convergence state and must guarantee the finite time convergence condition $S\dot{S} < 0$ which is given by:

$$S\dot{S} = S \frac{\partial S}{\partial x} B(x) u_n < 0 \quad (3.39)$$

In order to satisfy this condition, the sign of u_n must be the opposite of the sign of $S \frac{\partial S}{\partial x} B(x)$. The discontinuous control is defined as a switching term formed by relay function $sign(S)$ multiplied by a constant coefficient K .

The relay function is defined by:

$$sign(S) = \begin{cases} +1 & \text{if } S \geq 0 \\ -1 & \text{if } S < 0 \end{cases} \quad (3.40)$$

$$u_n = -K sign(S) \quad (3.41)$$

The coefficient K must be positive to ensure the convergence condition.

In our applications, the “ $sign(S)$ ” will be replaced by sigmoid function “ $sigm(S)$ ” in order to limit the effect of chattering.

$$sigm(S) = \left(\frac{2}{1 + e^{qS}} \right) - 1 \quad (3.42)$$

q is a small positive constant which adjusts the sigmoid function slope.

3.2.4 Second order sliding mode control

The second order sliding mode algorithms require information about S and \dot{S} . They have the ability to stabilize the system having a relative degree 2, except the super twisting which is dedicated for systems having a relative degree 1. The common second order SMC algorithms in control field are presented in the following.

3.2.4.1 Twisting control

The twisting algorithm was introduced by Lewantowski in 1985 and Levant 1993 [Lew85; Lev93]. The control law of the twisting algorithm is defined by:

$$u = \begin{cases} -V_m sign(S) & \text{if } S\dot{S} \leq 0 \\ -V_M sign(S) & \text{if } S\dot{S} > 0 \end{cases} \quad (3.43)$$

To ensure the stabilization in finite time ($S = \dot{S} = 0$) the proper choice of V_m and V_M should be given as:

$$V_M > V_m; V_m > \frac{4\Gamma_M}{s_0}; V_M > \frac{\Phi}{\Gamma_m}; \Gamma_m V_M - \Phi > \Gamma_M V_m + \Phi$$

By assuming uncertain second-order system:

$$\ddot{s} = \phi(t, x) + \gamma(t, x)u \quad (3.44)$$

$\phi(t, x)$ and $\gamma(t, x)$ are uncertain functions and the bound Φ, Γ_m, Γ_M and s_0 are known by:

$$|\phi(t, x)| < \Phi, 0 < \Gamma_m \leq \gamma(t, x) \leq \Gamma_M, s(t, x) < s_0.$$

The system trajectory rotates (“twists”) in the plane (S, \dot{S}) around the origin and converges to the origin after performing infinite number of rotations as presented in **Fig.3.4** [Raf12; Ben13].

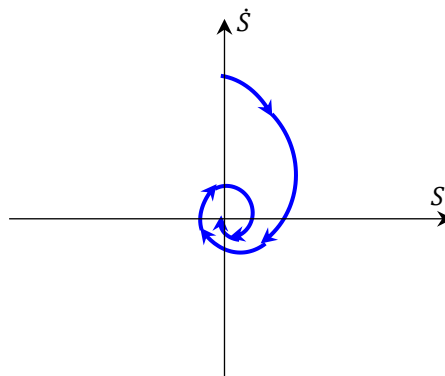


Fig.3.4 Phase trajectory of twisting algorithm.

3.2.4.2 Sub-optimal control

The sub-optimal algorithm was proposed by Bartolini in 1997 [Bar97]. The control law of this algorithm is described by the following expressions:

$$u = \begin{cases} -U \text{sign}(S - \beta s_M) & \text{if } (S - \beta s_M)s_M \geq 0 \\ -\alpha^* U \text{sign}(-\beta s_M) & \text{if } (S - \beta s_M)s_M < 0 \end{cases} \quad (3.45)$$

where: $U > 0$ is the minimum control magnitude, $\alpha^* > 1$ is the modulation factor, β is the anticipation factor, and s_M is the value of S at the last instant where $\dot{S} = 0$.

3.2.4.3 Super twisting control

Super-twisting algorithm was proposed by Levant [Lev93; Lev03]. Since an n^{th} order sliding mode control algorithms require information about $S, \dot{S}, \ddot{S}, \dots, S^{(n-1)}$. This algorithm can provide a continuous control by using only the information on S and the evaluating of the sign of \dot{S} is not necessary. The convergence of this algorithm is also described by the rotation around the origin of the phase diagram (S, \dot{S}) .

The super twisting algorithm has the advantage over the other algorithms that it does not demand the time derivatives of sliding variable. The super twisting (ST) control law u_{ST} is formed by two parts. The first discontinuous term u_1 is defined by its derivative with respect to time \dot{u}_1 while the second is given by the function of the sliding variable u_2 .

The ST control law is defined by:

$$u_{ST} = u_1(t) + u_2(t) \quad (3.46)$$

$$\dot{u}_1 = \begin{cases} -u & \text{if } |u| > 1 \\ -K \text{sign}(S) & \text{if } |u| \leq 1 \end{cases} \quad (3.47)$$

$$u_2 = \begin{cases} -\lambda |S_0|^\rho \text{sign}(S) & \text{if } |S| > S_0 \\ -\lambda |S|^\rho \text{sign}(S) & \text{if } |S| \leq S_0 \end{cases} \quad (3.48)$$

λ and K are positive gains used to adjust the ST controller.

The control law convergence can be reached by an arbitrarily adjusting of these gains [Ras05]. Generally, the gain λ is more effective in system response. The gain K has an effect in steady state accuracy. The sufficient conditions for a finite-time convergence are imposed by Levant [Lev03] as:

$$\begin{cases} K > \frac{\Phi}{\Gamma_M} \\ \lambda \geq \frac{4\Phi\Gamma_M(\beta + \Phi)}{\Gamma_m^3(\beta - \Phi)} \end{cases} \quad (3.49)$$

Φ is defined as the positive bounds of the uncertain function ϕ . Γ_m and Γ_M are the lower and the upper positive bounds of the uncertain function γ at the second derivative of the sliding manifold [Lev03; Ras05],

where:

$$\Phi \geq \phi \text{ and } \Gamma_M \geq \gamma \geq \Gamma_m \quad (3.50)$$

The degree of nonlinearity can be adjusted by the coefficient ρ which is defined in the interval ($0 < \rho \leq 0.5$). It is fixed mostly at “0.5” to realize that the maximum of second order sliding mode control is achieved [Ras05]. The controlled system can be simplified when it is linearly dependent on the control law. Then, Φ , s_0 , Γ_m and Γ_M will be considered as positive constants and the ST control law is given by [Raf12]:

$$\begin{cases} u_{ST} = -\lambda |S|^{\frac{1}{2}} \text{sign}(S) + u_1 \\ \dot{u}_1 = -K \text{sign}(S) \end{cases} \quad (3.51)$$

3.2.5 Application of first order sliding mode control on direct torque control

The control design in this section is presented as reformulation of the IOFL-DTC using the same developed model. This reformulation design called sliding mode feedback linearization direct torque control (SMFL-DTC).

The flux and torque tracking errors represent the sliding surfaces as follows:

$$S_1 = e_1 = T_e^* - T_e \quad (3.52)$$

$$S_2 = e_2 = |\psi_s^*|^2 - |\psi_s|^2 \quad (3.53)$$

To generate the sliding control law, the derivative of sliding surfaces can be written in terms of the feedback linearized model as follows:

$$\dot{S} = \begin{bmatrix} F_1 \\ F_2 \end{bmatrix} + C(x) \begin{bmatrix} V_{s\alpha} \\ V_{s\beta} \end{bmatrix} \quad (3.54)$$

The derivative of sliding surfaces function S will be decoupled with respect the reference stator voltage vectors (control outputs). The switching function should be chosen in manner to keep sliding mode behavior stable.

$$\dot{S} = -k_1 S - k_2 \text{sign}(S) \quad (3.55)$$

When the switching surface $S = 0$ and by equalizing (3.54) and (3.55), we can define the general control law:

$$U = C^{-1}[-k_1 S - k_2 \text{sign}(S)] + C^{-1}F \quad (3.56)$$

The general control law in the sliding mode approach can be written as:

$$U = \begin{bmatrix} V_{s\alpha} \\ V_{s\beta} \end{bmatrix} = \begin{bmatrix} V_{eq\alpha} \\ V_{eq\beta} \end{bmatrix} + \begin{bmatrix} V_{c\alpha} \\ V_{c\beta} \end{bmatrix} \quad (3.57)$$

We can define also the two control parts. The equivalent control can be expressed by:

$$\begin{bmatrix} V_{eq\alpha} \\ V_{eq\beta} \end{bmatrix} = C(x)^{-1} \begin{bmatrix} -F_1 \\ -F_2 \end{bmatrix} \quad (3.58)$$

The discrete (commutation) control is defined as the auxiliary inputs:

$$\begin{bmatrix} V_{c\alpha} \\ V_{c\beta} \end{bmatrix} = C(x)^{-1} \begin{bmatrix} -k_{11}S_1 - k_{12}\text{sign}(S_1) \\ -k_{21}S_2 - k_{22}\text{sign}(S_2) \end{bmatrix} \quad (3.59)$$

where:

$k_{11}, k_{12}, k_{21}, k_{22}$: are positive constants

The global control law U will be expressed as:

$$\begin{bmatrix} V_{s\alpha} \\ V_{s\beta} \end{bmatrix} = -C(x)^{-1} \begin{bmatrix} F_1 + k_{11}S_1 + k_{12}\text{sign}(S_1) \\ F_2 + k_{21}S_2 + k_{22}\text{sign}(S_2) \end{bmatrix} \quad (3.60)$$

The control law should be chosen in such manner to attract the system trajectory to the sliding surface and satisfy the Lyapunov stability's condition which is given as:

$$\dot{V} = S^T \dot{S} \quad (3.61)$$

By substituting the switching function (3.55) in the derivative of Lyapunov function we can obtain:

$$\dot{V} = S^T [-k_1 S - k_2 \text{sign}(S)] \quad (3.62)$$

Then:

$$\dot{V} = -[k_1 S^T S + k_2 S^T \text{sign}(S)] \quad (3.63)$$

and we obtain:

$$\dot{V} = -[k_1 S^T S + k_2 |S|] \quad (3.64)$$

For k_1 and k_2 positive, $\dot{V} < 0$ which ensures the stability of the SMFL-DTC.

3.2.6 Improved direct torque control using second order sliding mode control

In this section, first and second order sliding mode controllers will be designed for speed regulation loop to generate the electromagnetic torque reference and to ensure good dynamic and fast response.

3.2.6.1 First order SM-speed controller design

The sliding surface of the rotor speed is defined by:

$$\begin{cases} S_{\omega_r} = \omega_r^* - \omega_r \\ \dot{S}_{\omega_r} = \dot{\omega}_r^* - \dot{\omega}_r \end{cases} \quad (3.65)$$

The mechanical equation of induction motor is given as:

$$\dot{\omega}_r = \frac{1}{J} (T_e - T_L) - \frac{f}{J} \omega_r \quad (3.66)$$

By substituting the equation (3.66) in the equation of the speed surface derivative, it will be given as follows:

$$\dot{S}_{\omega} = \dot{\omega}_r^* - \frac{1}{J} (T_e - T_L - f \omega_r) \quad (3.67)$$

Basing on sliding mode theory, we can write:

$$T_e = T_{eeq} + T_{en} \quad (3.68)$$

The equivalent control part is defined during the sliding mode state $\dot{S}_{\omega} = 0$, then the equivalent control is:

$$T_{eeq} = f \omega_r + T_L \quad (3.69)$$

The discontinuous part is defined as:

$$T_{en} = K_{\omega_r} \text{sign}(S_{\omega_r}) \quad (3.70)$$

K_{ω_r} is a positive gain.

3.2.6.2 Second order SM-speed controller design

The second order sliding mode speed control law will be designed by the combination of the equivalent control and the super twisting control law. The super twisting speed controller (STSC) design is given as:

$$\begin{cases} u_{ST} = -\lambda_{\omega_r} |S_{\omega_r}|^{\frac{1}{2}} \text{sign}(S_{\omega_r}) + u_1 \\ \dot{u}_1 = -K_{\omega_r} \text{sign}(S_{\omega_r}) \end{cases} \quad (3.71)$$

λ_{ω_r} and K_{ω_r} are the super twisting speed controller gains.

The generated reference torque by the second order sliding mode controller is given by:

$$T_{eref} = T_{eq} + u_{ST} \quad (3.72)$$

The super twisting control law must fulfil Lyapunov stability condition to establish the speed control stability. The derivative of Lyapunov candidature is defined by:

$$\dot{V} = S_{\omega_r} \dot{S}_{\omega_r} < 0 \quad (3.73)$$

By substituting (3.73) in (3.68) we obtain:

$$\dot{S}_{\omega_r} = -\frac{1}{J} (u_{ST}) = -\frac{1}{J} \left(\lambda_{\omega_r} |S_{\omega_r}|^{\frac{1}{2}} \text{sign}(S_{\omega_r}) + \int K_{\omega_r} \text{sign}(S_{\omega_r}) dt \right) \quad (3.74)$$

Then, Lyapunov stability condition is:

$$S_{\omega_r} \dot{S}_{\omega_r} = -\frac{S_{\omega_r}}{J} \left(\lambda_{\omega_r} |S_{\omega_r}|^{\frac{1}{2}} \text{sign}(S_{\omega_r}) + \int K_{\omega_r} \text{sign}(S_{\omega_r}) dt \right) \quad (3.75)$$

And it becomes

$$S_{\omega_r} \dot{S}_{\omega_r} = -\frac{\lambda_{\omega_r}}{J} |S_{\omega_r}|^{\frac{3}{2}} \text{sign}(S_{\omega_r}) - S_{\omega_r} \frac{K_{\omega_r}}{J} \int \text{sign}(S_{\omega_r}) dt \quad (3.76)$$

It can be seen that the both terms of (3.76) are negative as long as λ_{ω_r} and K_{ω_r} are positive. Therefore, the stability condition has been guaranteed.

Finally, the global control scheme includes the SVM-DTC based on input-output feedback linearization with sliding mode control and improved by super twisting speed controller in the outer loop is shown in **Fig.3.5**.

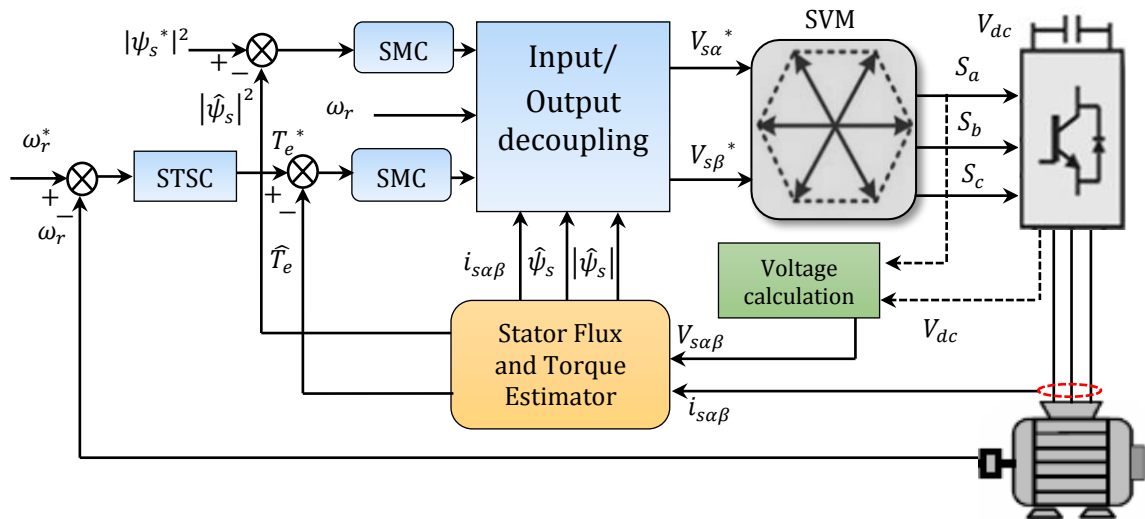


Fig.3.5. Diagram of global sliding mode IOFL-DTC strategy with super twisting speed controller.

3.3. Simulation Results

The simulation results are presented into three phases. A comparative study between the proposed sliding mode feedback linearization DTC and the stator field oriented (SFOC) SVM-DTC using PI controllers is presented firstly. Both of control schemes use the PI in the outer speed loop. Different operation conditions for IM are conducted such as the starting up, the steady state and the load application. In the second phase, machine parameters variations test is employed in low speed region to check the robustness of both control schemes. Finally, we will present the performance analysis of the SMFL-DTC with two speed controllers. The super twisting speed controller is compared with the classical PI controller.

3.3.1. SFOC SVM-DTC and nonlinear SMFL-DTC starting up and steady states

The following figures illustrate the comparative analysis of SVM-DTC and SMFL-DTC associated with PI as a speed controller. The figures are specified ((a) for SVM- DTC, and (b) for SMFL-DTC).

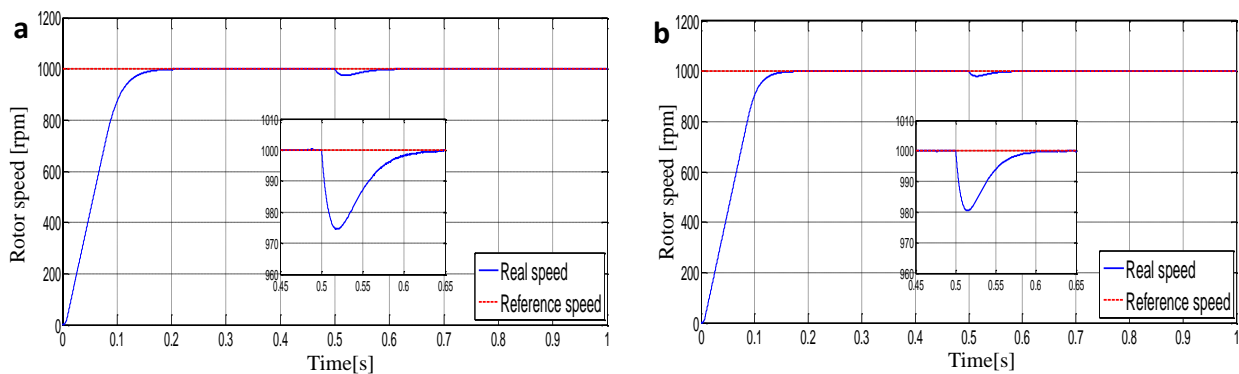


Fig.3.6 Startup and steady states of speed response followed by load application at $t=0.5s$.

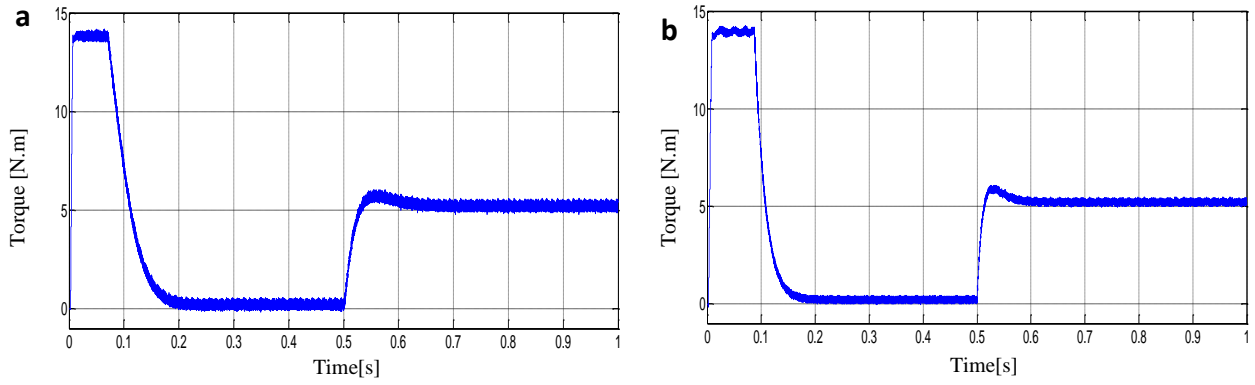


Fig.3.7 Electromagnetic torque response with load application of 5 N.m at $t=0.5$ s

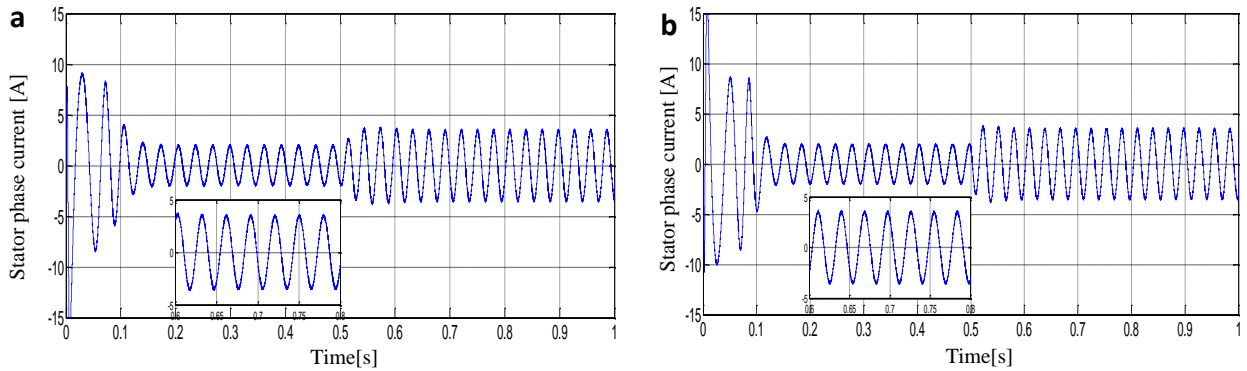


Fig.3.8 Stator phase current i_{sa} [A].

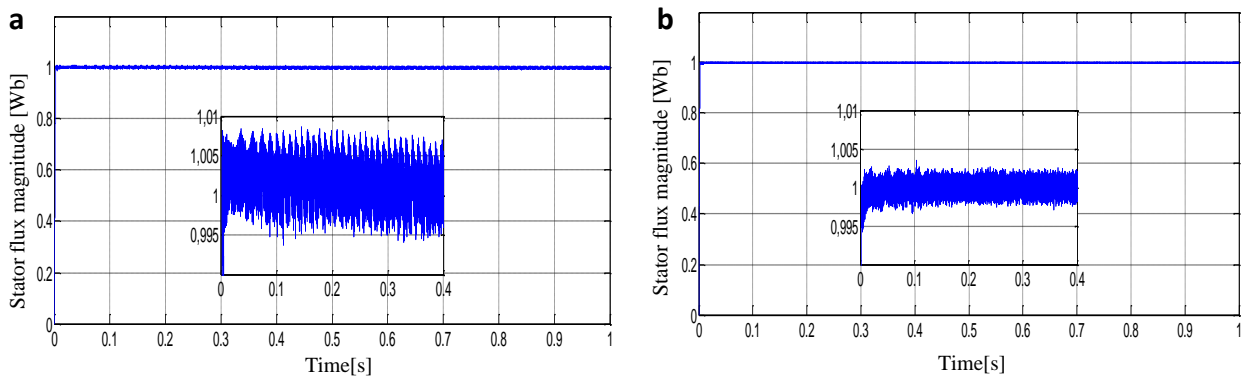


Fig.3.9 Stator flux magnitude [Wb].

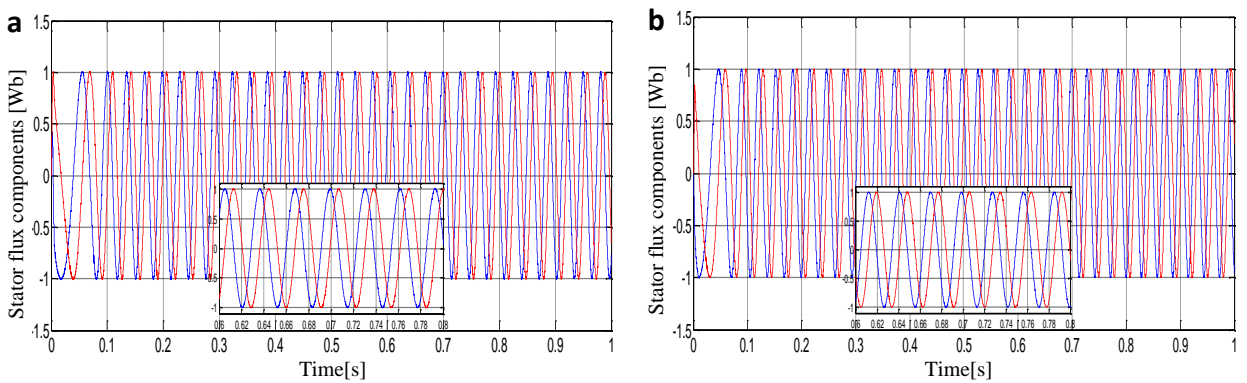


Fig.3.10 Stator flux axes components [Wb].

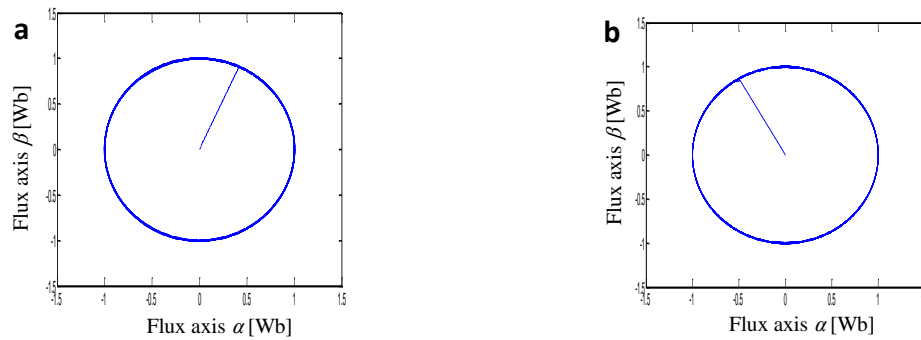


Fig.3.11 Stator flux circular trajectory [Wb].

Firstly, **Fig.3.6** illustrates the comparison between speed responses according to the step of $(0-1000 \text{ rpm})$ as a speed reference. The load disturbance has been introduced at $(t=0.5s)$. The figure shows that both techniques show good dynamic at starting up. It can be noticed that the SMFL-DTC in **Fig.3.6(b)** has the faster speed response and the less dropping from load introduction. Then, **Fig.3.7** presents the response of torque with load application for both of control algorithms, it is clear that the SMFL-DTC provides quick dynamic responding to the load application. Next, **Fig.3.9** illustrates the stator phase current i_{sa} . The current shows a good sinusoid waveform and reduced harmonics due to the application of SVM. SMFL-DTC presents low chattering after the use of the *sigmoid* switching function in the design of SMC. Since both techniques use the space vector modulation, there is no apparent difference in the ripples level or current harmonics. The smoother torque response of SMFL-DTC indicates the accurate control tracking.

Then, the stator flux is presented in **Figs. 3.9 to 3.11**, they show respectively flux magnitude, axes components and the circular trajectory. The two control techniques have a reduced ripples stator flux. The SMFL-DTC flux magnitude has more fast and accurate reference following (1 Wb) . This reflects the good decoupling between the flux and torque axes which achieved by the feedback linearization. Besides, the flux components and trajectory prove that the SMFL-DTC has a smooth flux response without chattering.

3.3.2 Robustness test of parameters variation in low speed region

This robustness test consists of the variation of the stator resistance R_s when the machine operates with low speed and rated load. R_s will be increased by 50% following the profile that presented in **Fig.3.12** starting from $0.5s$. **Figs.3.13-3.15** show rotor speed, torque and flux magnitude under robustness test at low speed value of (50 rpm) . The figures are specified ((a) for SVM- DTC, and (b) for SMFL-DTC).

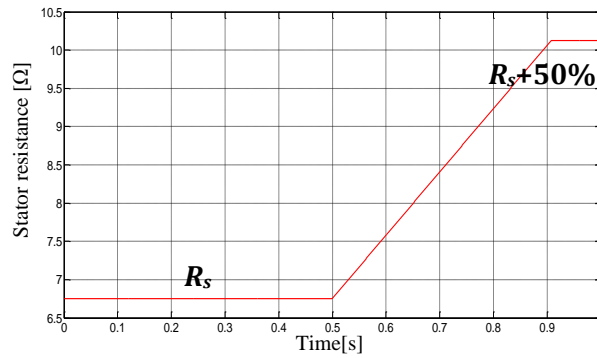


Fig.3.12 Stator resistance variation profile [Ω].

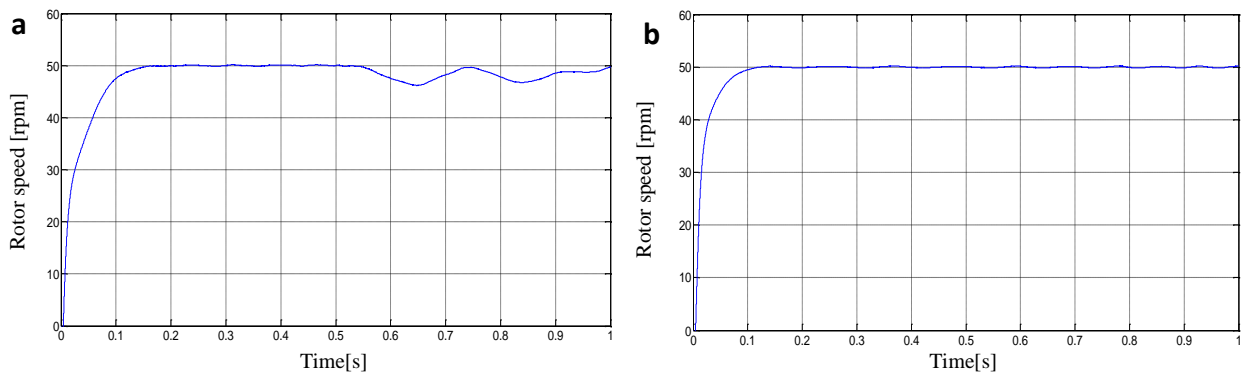


Fig.3.13 Speed's response in low region (50 rpm) with variation of stator resistance R_s +50%.

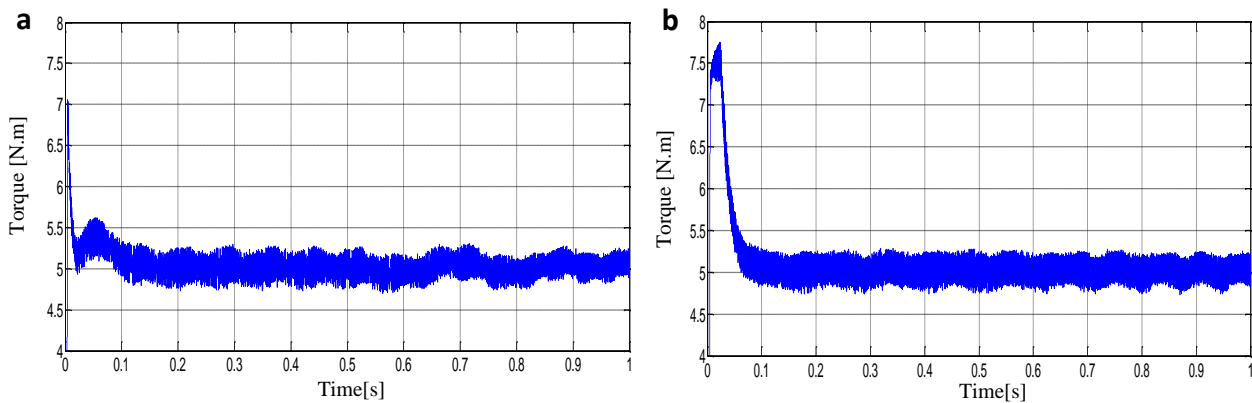


Fig.3.14 Torque's response with load of 5 N.m in low speed and variation of stator resistance.

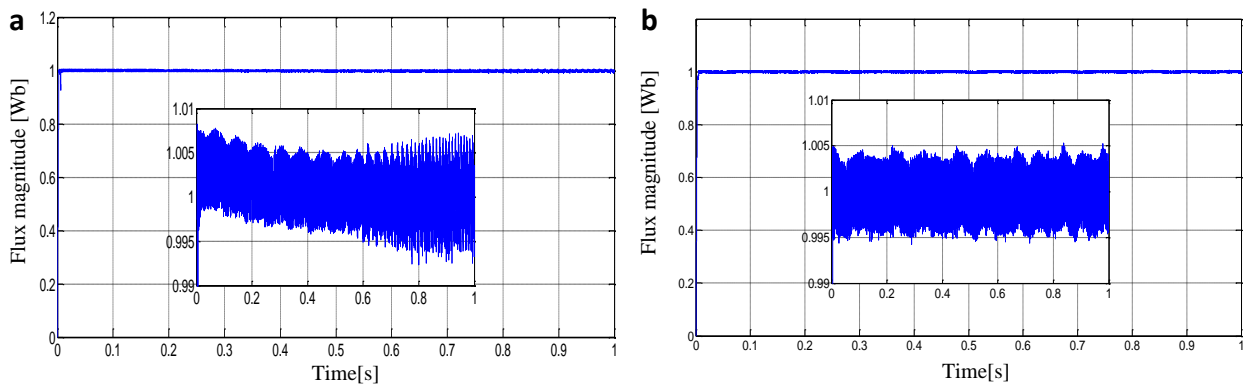


Fig.3.15 Stator flux magnitude with variation of stator resistance R_s +50%.

Figs.3.13-3.15 illustrate the speed, the torque and the flux magnitude with the increase of 50% in R_s starting from $t=0.5s$. It can be seen from **Fig.3.13(a)** that the increase of stator phase resistance has affected the speed's response of SFOC SVM-DTC and made it unstable, unlike the sliding mode feedback DTC strategy which shows no considerable effect on speed response in **Fig.3.13(b)**. Consequently, the torque response is also affected, it can be seen in **Fig.3.14(a)** that torque has been slightly diminished and became unstable. In the other hand, SMFL-DTC preserves an acceptable torque performance under these conditions. Then, **Fig.3.15** shows the comparison of flux magnitudes, it is observed in **Fig.3.15(a)** and its **ZOOM** that the estimation accuracy of SFOC SVM-DTC has been influenced by resistance variation in this low region, this problem has been avoided by SMFL-DTC in **Fig.3.15(b)**.

3.3.3. PI and super twisting speed (STSC) controllers comparative analysis

This section presents a comparative study between different controllers for the outer speed's loop of the SMFL-DTC (i.e., classical PI and second order STSC controllers). The figures are specified ((a) for conventional PI, and (b) for STSC speed controller).

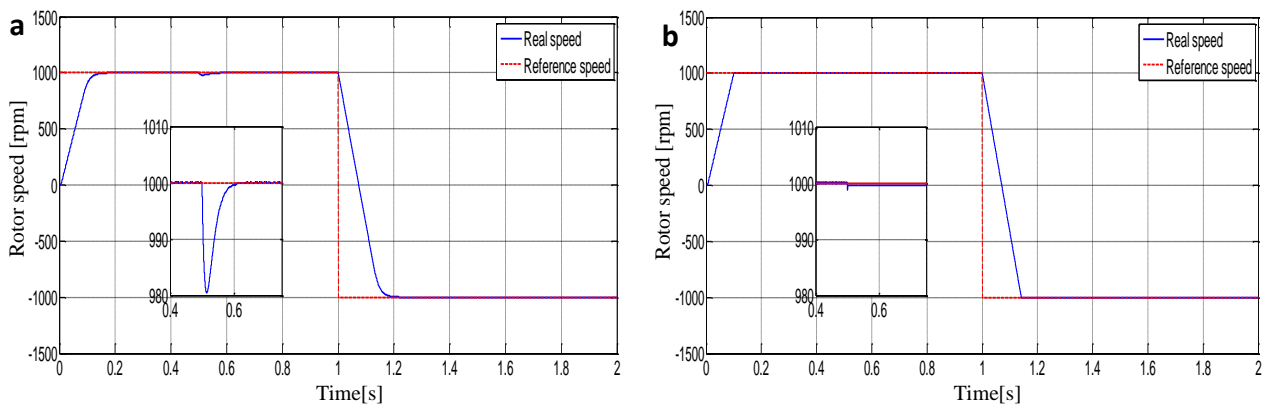


Fig.3.16 Rotor speed (1000 rpm; -1000 rpm) response for PI and STSC speed controllers.

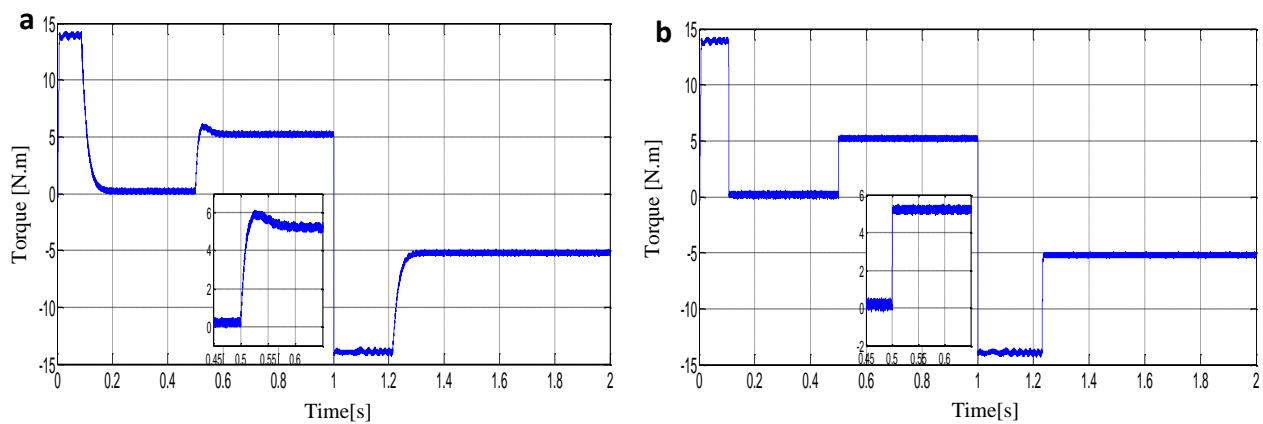


Fig.3.17 Torque response (Load applied at $t=0.5s$) for PI and STSC speed controllers.

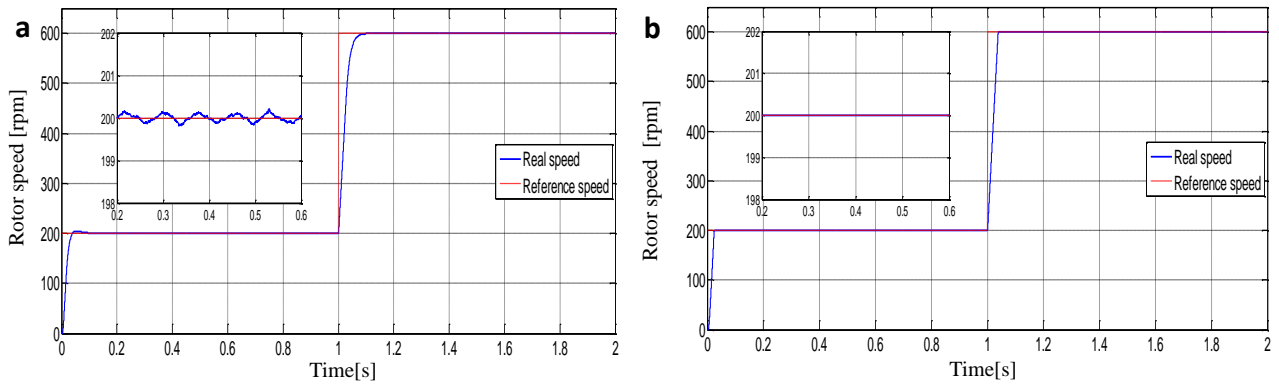


Fig 3.18. Rotor speed response for PI and STSC at low-medium speeds (200-600 rpm).

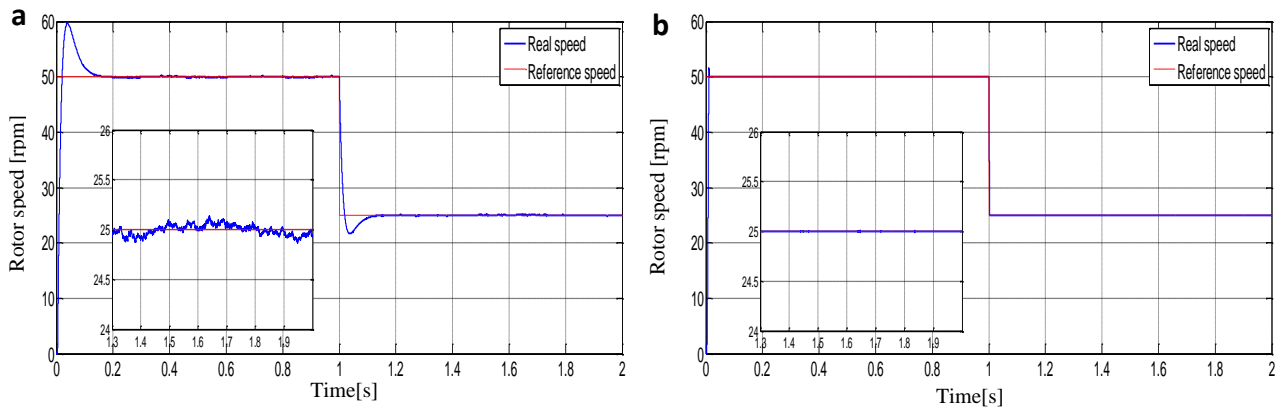


Fig.3.19 Rotor speed response for PI and STSC in low region (50-25 rpm).

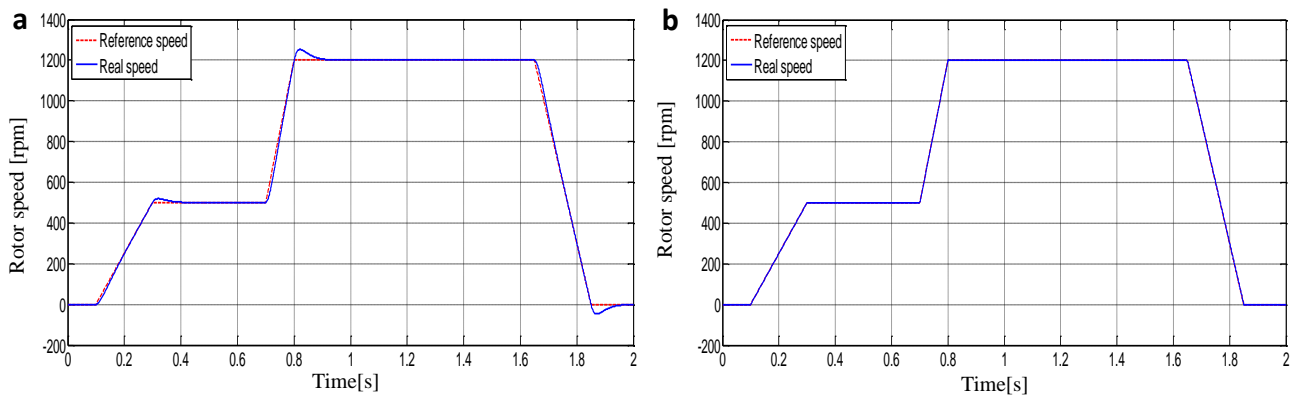


Fig.3.20 Speed response following benchmark trajectory in different regions (PI and STSC).

Figs.3.16-3.17 illustrate the rotor speed and the electromagnetic torque of the control algorithm associated with PI and super twisting controllers during starting up and speed sense reversing (1000; -1000 rpm). The super twisting controller in **Fig.3.16-3.17(b)** presents better speed and torque responses compared with classical PI in **Figs.3.16-3.17(a)**. Moreover, the comparison shows that the influence by the load application of the SMFL with STSC is not considerable and the torque has faster responding as illustrated in **Figs.3.16-3.17(b)** (ZOOM). We can also notice that the super twisting controller is featured by the reduced chattering level, this problem has been eliminated by applying the second order control law.

Figs.3.18-3.19 illustrate the speed responses of the SMFL with PI and STSC controllers in medium and low speed regions. In this test, a speed reference variation has been done in (200 rpm-600 rpm) and at very low-speed (50 rpm-25 rpm). It is clear that the STSC kept the good dynamic in **Figs.3.18 (b)** even at low-speed values contrary to the PI controller which presents some speed fluctuations (**Fig.3.18-3.19(a)**). The last speed test is depicted in **Fig.3.20**. It illustrates a speed reference variation under industrial benchmark trajectory from zero to medium (500 rpm) then high speed values (1200 rpm). This test shows a perfect following and an accurate speed tracking to the variable reference for STSC controller in different speed point without overshoot even at zero and near to zero speed values, contrary to the PI controller which presents certain overshoots and dynamic error due to the instantaneous variation of the speed.

The next table presents a summarized comparative analysis of the both of control schemes performance with different speed controllers.

	SFOC-SVM DTC with PI speed controller	SMLF-DTC with PI speed controller	SMLF-DTC with STSC speed controller
Flux response time [sec]	0.0024 s	0.0022 s	0.0022s
Speed response time [sec]	0.12 s	0.11 s	0.095s
Speed dropping due to load application [rpm, %]	28 rpm 2.8%	19.5 rpm 1.95%	1.2 rpm 0.12%
Torque response time to load application [sec]	0.026 s	0.015 s	0.006 s
Flux bandwidth [Wb]	± 0.006 Wb	± 0.0025 Wb	± 0.0025 Wb
Torque bandwidth [N.m]	± 0.3 N.m	± 0.2 N.m	± 0.3 N.m

Table.3.1 Comparative analysis of SFOC SVM-DTC and SMFL-DTC with various speed controllers.

3.4. Experimental Results

3.4.1 SFOC SVM-DTC and nonlinear SMFL-DTC starting up and steady states

This section presents the experimental results of the same presented tests in the simulation section **3.3.1**.

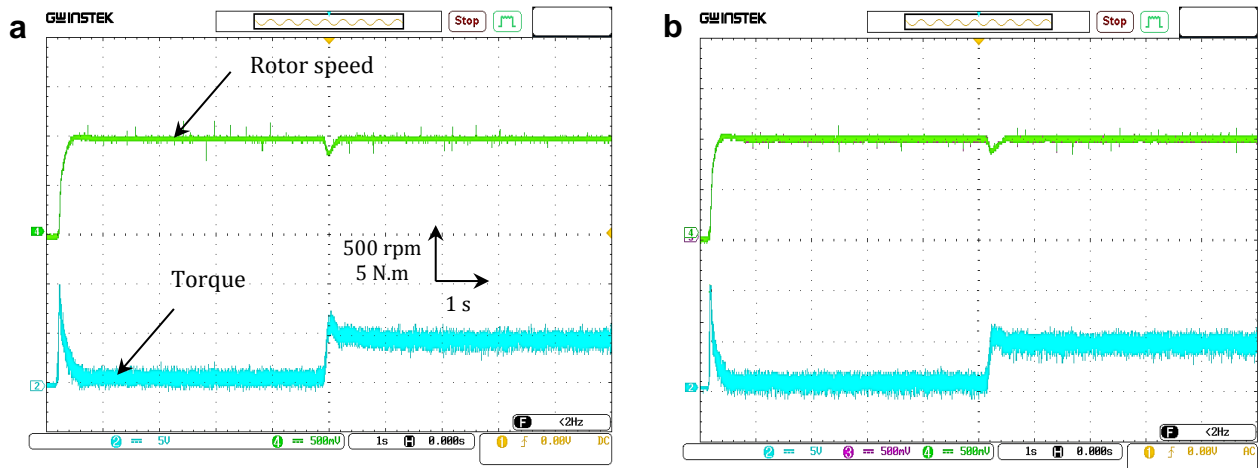


Fig.3.21 Speed and torque responses during the starting up then load application.

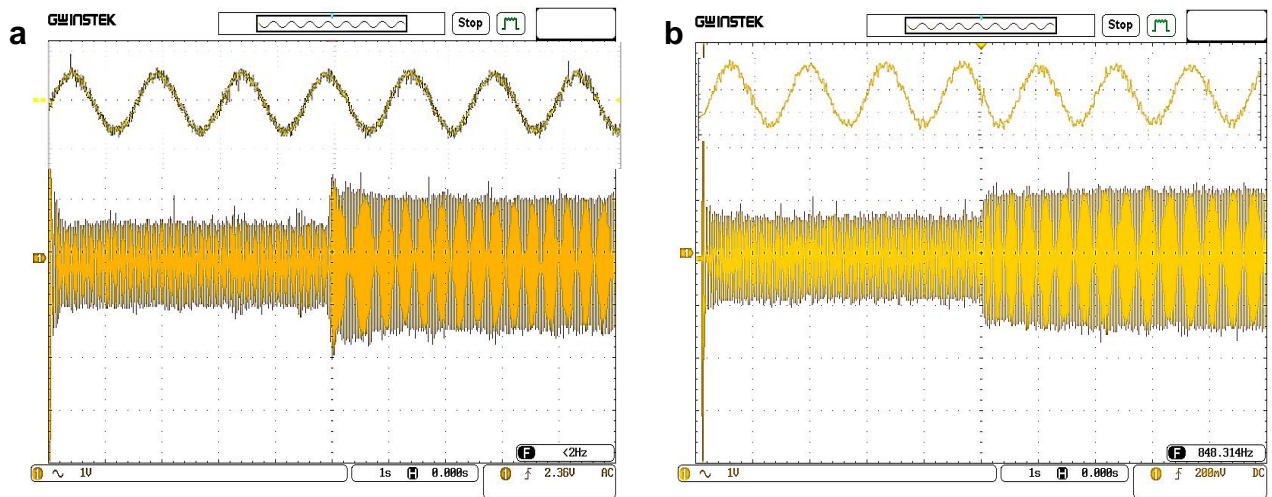


Fig.3.22 Stator phase current i_{sa} [A].

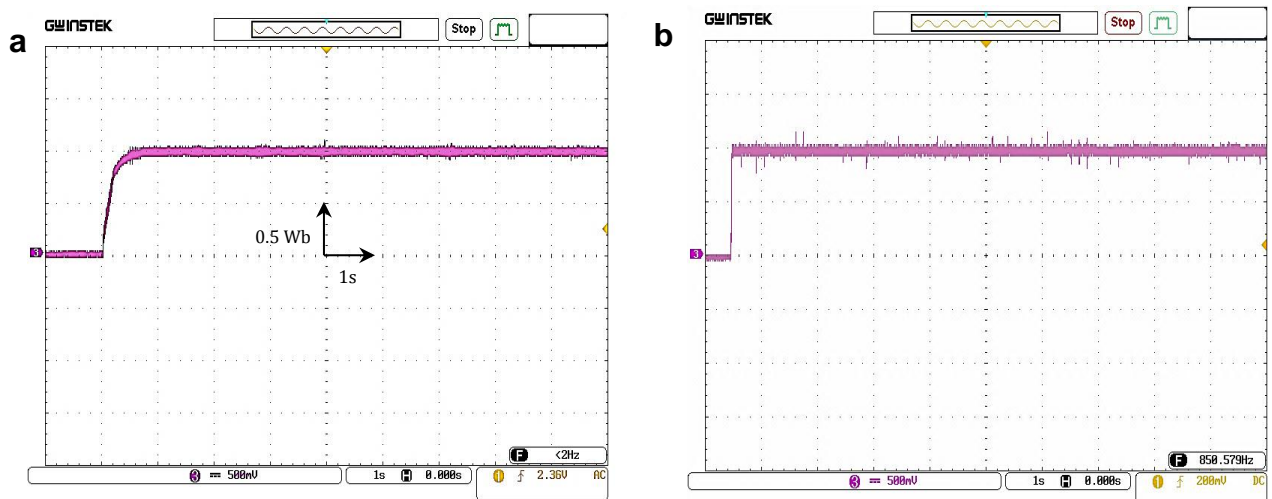


Fig.3.23 Stator flux magnitude [Wb].

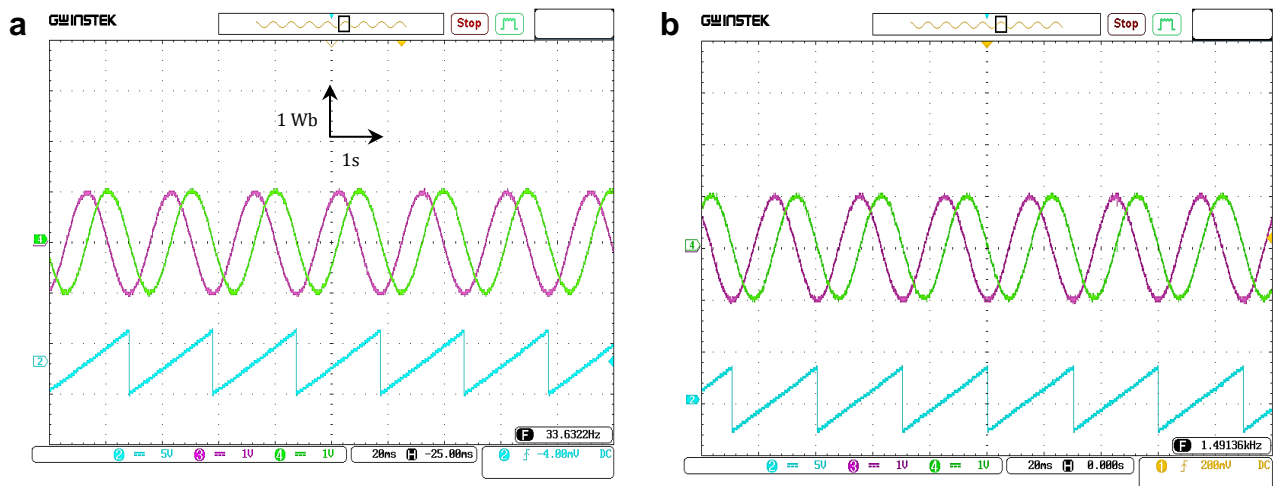


Fig.3.24 Stator flux components and position.

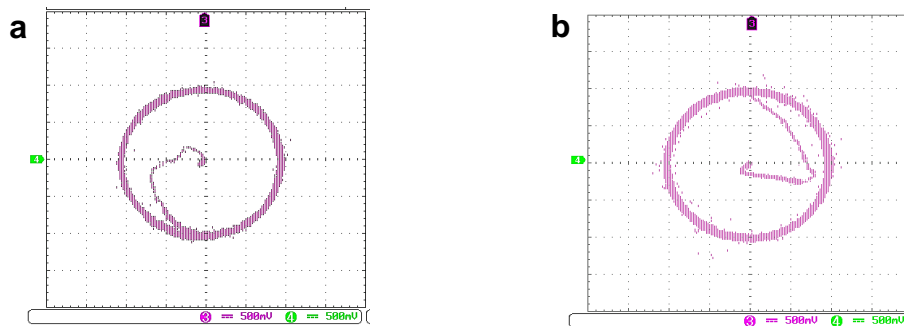
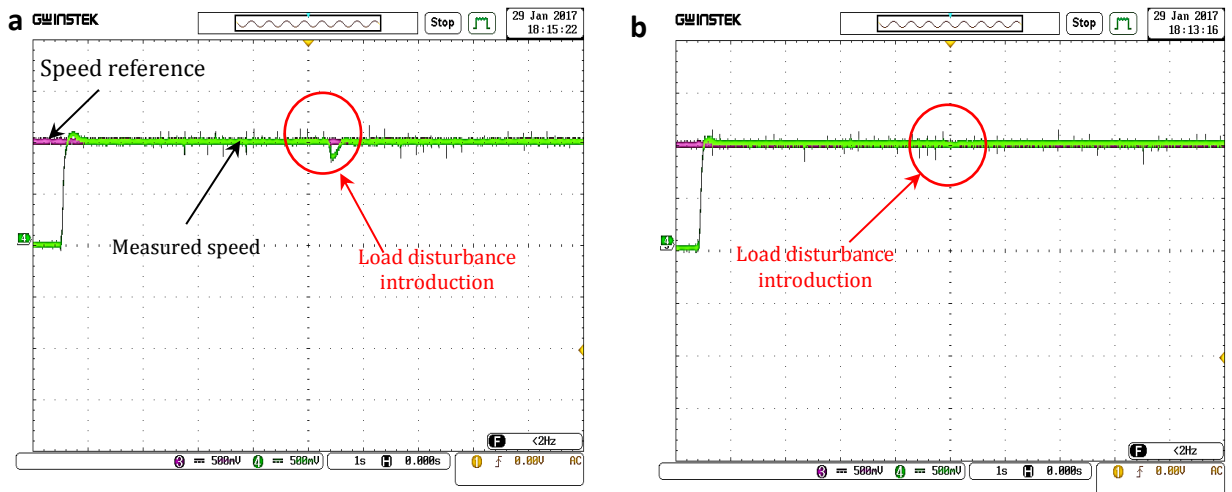


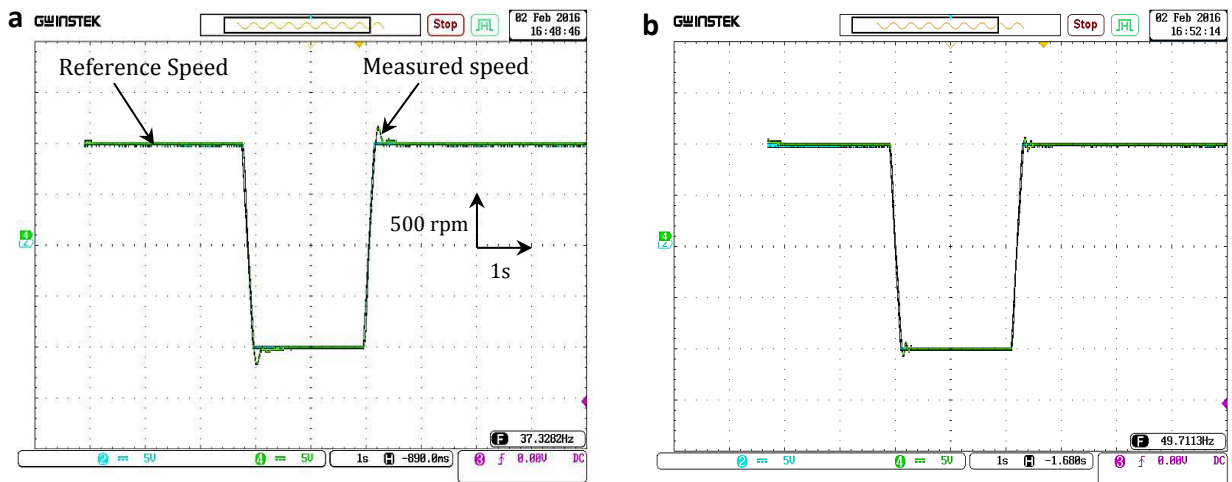
Fig.3.25 Stator flux circular trajectory ($\psi_{s\alpha}$, $\psi_{s\beta}$) ($1div=0.5Wb$).

Firstly, **Fig.3.21-Fig.3.22** show the starting up and the steady state followed by load introduction of the motor controlled by both of SVM-DTC and the proposed SMFL-DTC. **Fig.3.21** illustrates from the top to the bottom: rotor speed ($1div=500rpm$) and the electromagnetic torque ($1div=5N.m$). It is noticed that the both techniques have similar speed/torque response and load rejection since the two of them use the same PI speed controller in outer loop. SMFL-DTC seems better in speed and load responding. **Fig.3.22** presents the stator phase current waveform. We can say that there is no difference in torque ripples level and current harmonics owing to the application of SVM in both cases as it is mentioned before. Next, in **Fig.3.23-3.25**, the stator flux magnitude, axes components, angle and circular trajectory are depicted respectively. In **Fig.3.23(a-b)**, the magnitudes have low ripples and follow the reference's value of $1Wb$ ($1div=0.5Wb$). It is clear in **Fig.3.23(b)** that SMFL-DTC provides faster flux response with instantaneous tracking of reference. Finally, in **Fig.3.24-3.25** the flux components in trajectory show similar good waveform and ripples level.

3.4.2 PI and super twisting speed controller (STSC) comparative analysis



Figs.3.26 Speed response with disturbance introduction (PI and STSC).



Figs.3.27 Speed response while direction reverse with trapezoidal reference (PI and STSC).

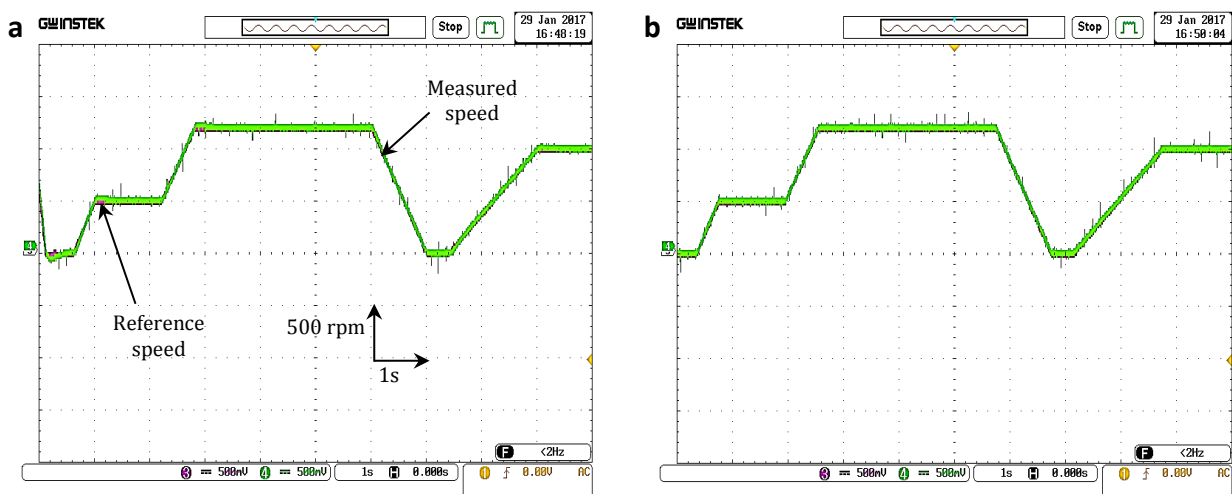


Fig.3.28 Benchmark speed trajectory: Reference and measured speed in different regions (PI and super twisting controllers).

In **Figs.3.26-3.28**, the comparative study of two speed controllers is presented. **Fig.3.26(a)** and **Fig.3.26(b)** show the speed response while startup followed by load disturbance introduction. Both controllers have fast response and good reference following, but we can notice that the STSC is more robust against the external disturbance. The next test in **Fig.3.27(a)** and **Fig.3.27(b)** is rotation's sense reverse following a trapezoidal reference. The superposition between the speed and its reference is noticed. The STSC has better response, it reduces the overshoot compared with the PI controller. Finally, an industrial benchmark speed trajectory for both controllers has been employed. **Fig.3.28**, illustrates speed variation in different regions (0 rpm , 500 rpm , 1200 rpm). The results of this test are similar to the presented ones in simulation section. The STSC controller in **Fig.3.28(b)** gives a better reference tracking in different speed values even at zero and near zero speed (i.e. zero frequency), higher robustness against the instantaneous speed variation. Moreover, it reduces the overshoot which presented by the PI controller.

3.4.3 Low speed operation

This low speed test has been employed only for sliding mode feedback linearization DTC strategy, a speed variation from low to medium speed region (200 rpm to 600 rpm) and very low speed region (50 rpm to 25 rpm)

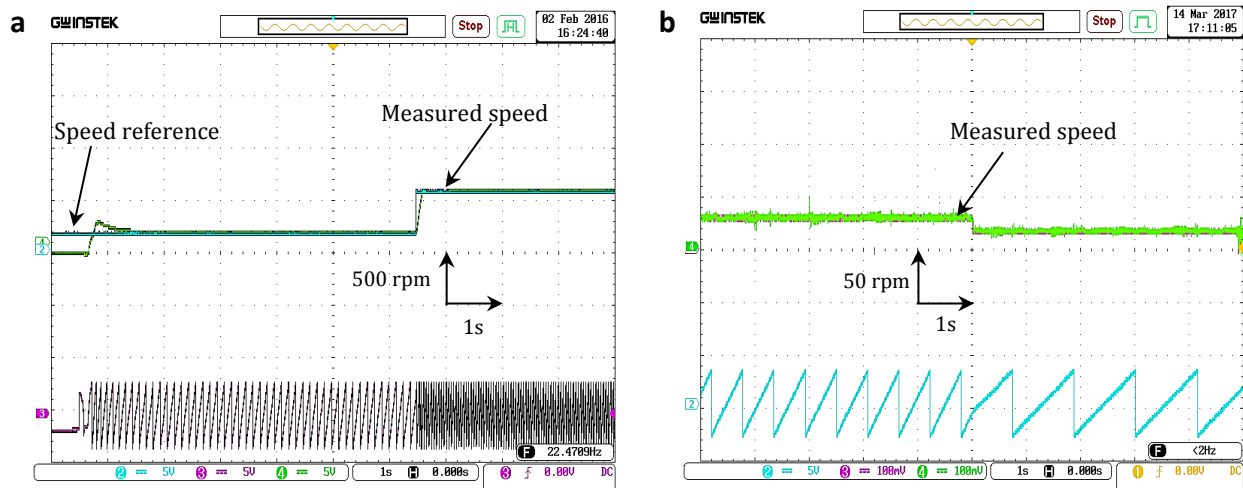


Fig.3.29. Low speed operation: speed variation (*a:200 rpm-600rpm*, *b:50rpm-25rpm*).

Figs.3.29(a-b) display the low-speed operation test with reference variation of (200 rpm - 600 rpm) and (50 rpm - 25 rpm). The speed response and tracking are perfect in different reference values. The control scheme kept good performance even at very low-speed value (25 rpm).

3.5 Summarized comparative evaluation of control techniques

It can be concluded that the robust nonlinear SMFL-DTC provides the same good characteristics of SVM-DTC concerning ripples and harmonics, moreover it offers more advantages. By the combining of different nonlinear techniques (i.e. first and second sliding mode control with feedback linearization) this strategy has provided faster flux response and simple control scheme designed in stationary reference frame and robustness against load disturbance and parameters variation. The parameters variation test has not been done in the experimental section because of some difficulties and risks in the hardware implementation, but we can consider that the stator resistance is varying during the operation by machine's heating due to the load application.

The next table summarized the comparative study by classifying the features of each algorithm.

	SFOC SVM-DTC using PI controllers	SMFL-DTC with Super twisting speed controller
Harmonics and ripples level	Reduced owing to the use of the space vector modulation	Reduced owing to the use of the space vector modulation
Control scheme complexity	Designed in synchronous frame which requires coordinates transformation	Designed in stationary frame, no need of coordinates transformation
Speed and torque responses	Fast	Faster
Robustness against uncertainties	Not robust against load introduction and stator resistance increase	Robust against stator resistance increase, no considerable speed dropping due to load application

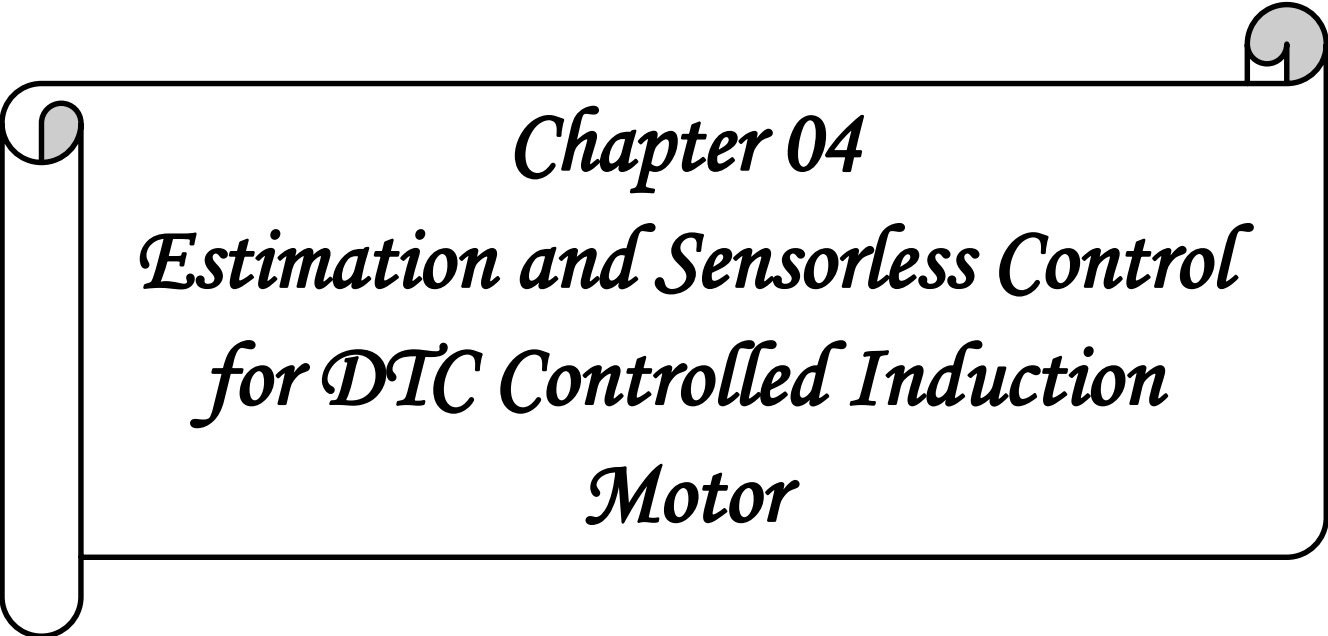
Table 3.2 Comparative assessment of both of the presented control algorithms.

3.6. Conclusion

This chapter presents a performance enhancement on direct torque control with space vector modulation. In order to solve different drawbacks of the classical DTC and SVM-DTC, dual nonlinear control strategies have been presented. The feedback linearization approach has been applied to create a decoupled flux and torque control and to generate the reference voltages in the stationary frame. The coupling of IOFL with first and second order sliding mode control has achieved a robust feedback linearization which is called sliding mode feedback linearization DTC (SMFL-DTC). The second order super twisting speed controller has been inserted in the outer speed loop to generate the torque reference.

The stability of the combined SMFL-DTC with super twisting strategy has been analyzed mathematically using Lyapunov stability theory. The simulation and the experimental results have been presented to investigate the performance of the proposed control algorithm. Generally, SMFL-DTC has provided reduced ripples level due to the use of SVM. The incorporation of nonlinear control strategy instead of conventional PI controllers has given better advantages like the robustness against different uncertainties, fast response, simplicity in control application and good reference tracking in different operation condition. In addition, the design of second order sliding mode speed controller has improved comprehensively the control scheme performance and increased the algorithm robustness against external load and reference variation. Therefore, the coupling of SVM-DTC with robust control is a good solution for induction motor drive control.

Over and above, the use of observers can get more features by minimizing the number of sensors which decrease the cost and increase the reliability of the control system. The next chapter will present a design of a sensorless DTC technique by inserting a number of estimators and observer structures for speed, flux and load torque estimation.



Chapter 04
Estimation and Sensorless Control
for DTC Controlled Induction
Motor

4.1 Introduction

The last chapter has presented a design of robust control strategy based on the combining of two nonlinear approaches with SVM-DTC scheme. However, the development of advanced control algorithm always requires an accurate flux and speed estimation or measurement to ensure proper drive operation and stability. The stator flux estimation is one of the essential tasks for the implementation of DTC motor drive. However, the conventional open-loop flux estimation which is implemented by integrating the back-EMF is prone to several problems. At most, it suffers from the presented DC drift in the pure integrator input, which leads to integrator saturation, and the problem of initial value that causes an undesirable DC offset in the estimated signal of stator flux [Rum02]. This chapter recounts briefly in the first part about the flux estimation issue and some proposed solutions.

Besides, the use of sensors is accompanied by several drawbacks such as the high cost and the fragility. The elimination of the mechanical speed sensor to reduce the cost and the volume of the drive and to increase its reliability is so interest subject. Various model-based approaches are proposed in literature for sensorless control of AC electrical drives. They can estimate effectively in closed loop the motor speed and solve flux estimation problems using the instantaneous measurements of machine voltages and currents. Among them we mention the nonlinear full order observers [Kub93] and sliding-mode observers (SMOs) [Reh02]. It is still a problem to achieve robust sensorless control at very low speed, particularly in a region at and around zero stator frequency.

The main objective of this chapter is to present a comparative study between different observer's structures, a full order adaptive observer based on Lyapunov theory and inherently sliding mode observer which did not take the speed as adaptive quantity. Both of them are linked to the nonlinear DTC strategy which designed in the last chapter. The effectiveness and estimation accuracy will be investigated by simulation and experimental results. Different operation conditions have been conducted in this part, such as the speed reversal, low and zero speed conditions and industrial benchmark tests.

4.2. Open-Loop Flux Estimation

The application of open-loop estimation is quite simple. It consists of using the measured stator voltage and current to estimate machine flux or rotor speed, however, the estimation accuracy depends on machine model and its parameters exactness. The open-loop estimators are not able to correct its estimated signals in comparison with real situation [Bed14].

4.2.1 Conventional stator flux estimation

The conventional voltage-model based estimation of the stator flux is usually done by the integration of the back-emf. The stator flux components can be expressed using stator voltages and currents in the stationary reference frame (α, β) by:

$$\hat{\psi}_{s\alpha\beta} = \int_0^t (V_{s\alpha\beta} - R_s i_{s\alpha\beta}) dt \quad (4.1)$$

Although the simple implementation of a pure integrator, it has significant challenges in providing adequate control performance. They are generally summarized in the drift or DC offset and initial value problems. As a result, the flux estimation will include DC-flux components and the flux vector will not be estimated accurately. This DC component, no matter how small is it, drives the integrator to saturation. Moreover, it leads also to DC-current components and severely affects motor operation. This problem has been discussed in numerous works [Hu98; Rum02; Las06; Rae09; Sto15].

4.2.2 Solution 1: Modified flux estimator

To overcome the drawbacks of the pure integrator, it is well known to replace it by low-pass filter (LPF). We propose a simple method to remove the DC component from the estimated flux as shown in **Fig.4.1**. Firstly, a high-pass filter (HPF) is placed after the pure integrator to extract the flux sinusoid. Since the HPF is not ideal and small DC offset could remain, another filtering is added where the remaining DC offset is extracted using a low pass filter and subtracted from the output of the HPF. This approach was verified experimentally to eliminate the DC offset.

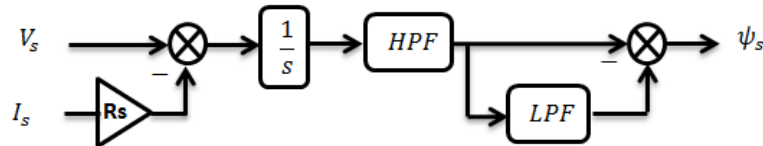


Fig.4.1 Modified flux estimator.

Fig.4.2 shows the effect of flux estimation on the three phase currents for DTC drive in real time implementation at medium speed region (400 rpm). **Fig.4.2(a)** shows the deformation of the currents waveform while the application of the pure integrator. In the other side, **Fig.4.2(b)** depicts the currents waveforms after the use of modified flux estimator.

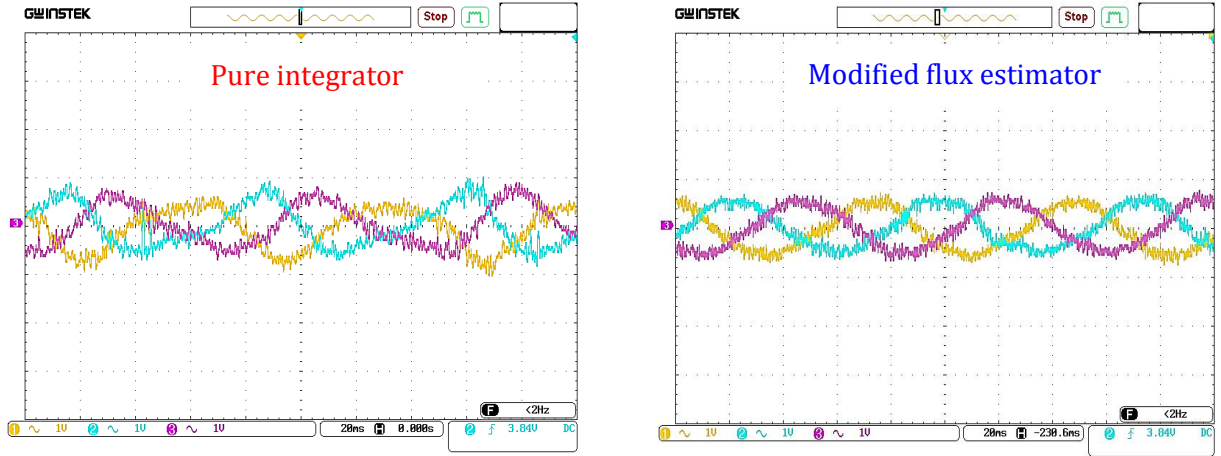


Fig.4.2 Three-phase stator currents waveform in medium speed region (400 rpm).

However, the chosen filter's cutoff frequency should be low enough to avoid filtering the actual sinusoids when the machine operates at low speeds. **Fig.4.3** shows the filtering effect on flux estimation at very low speed region (near to zero frequency).

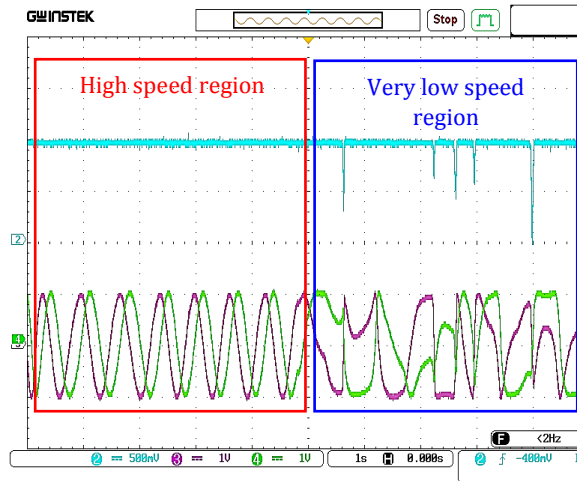


Fig.4.3. Stator flux magnitude and components using modified flux estimator at very low speed.

4.2.3 Solution 2: Current-model based flux estimator

The second proposed solution to avoid the problem of DC component is the application of current model stator flux estimator which is expressed by:

$$\begin{cases} \hat{\psi}_{s\alpha} = \frac{L_r}{R_r + L_r s} \left(\sigma L_s \omega_r i_{s\beta} + \frac{L_s}{L_r} (R_r + \sigma L_r s) i_{s\alpha} - \omega_r \hat{\psi}_{s\beta} \right) \\ \hat{\psi}_{s\beta} = \frac{L_r}{R_r + L_r s} \left(\sigma L_s \hat{\omega} i_{s\alpha} + \frac{L_s}{L_r} (R_r + \sigma L_r s) i_{s\beta} - \omega_r \hat{\psi}_{s\alpha} \right) \end{cases} \quad (4.2)$$

The application of this estimator offers a good current waveform and flux estimation at low speed values. The disadvantage of this open-loop estimator is the requirement of rotor speed and the extensively dependence to machine parameters.

Generally, the estimation based on the current model can be applied at low speeds, whilst the modified voltage model estimator can be considered for a high-speed range. This

later offers an advantage over the current-model-based estimation technique, that it does not require the knowledge of motor parameter excepting the stator resistance.

4.3 Closed-Loop Estimation of the Induction Motor (*Sensorless control*)

The accuracy of the open loop estimation is always depending on how the machine parameters are identified. These parameters have the largest influence on the system operation especially at low speeds. The common estimation problems and the robustness against parameters deviation can be significantly improved by using closed loop estimators, which are called observers [Abu12].

4.3.1 Definition: observability and observers

The observability is the possibility to reconstruct the full trajectory of a state system using the obtained data from the input and output measurements. The developed mean to reconstruct the state of the system is called an observer. It is a mathematical algorithm (can be called soft sensor) which is able to reconstruct the state of the system from the limited information obtained by measurements. The closed loop observers are mainly divided into two categories: observers based on machine state reconstruction and model reference adaptive systems.

4.3.2 Observers based on machine state reconstruction

These observers can be divided also into two main groups: deterministic and stochastic observers, according to the character of the observed system deterministic or stochastic. Kalman filter is representative of a stochastic observer. An example of the deterministic observer is the full order adaptive observer proposed by Kubota [Kub93]. It is composed basically of two parts: an open loop estimator based on the mathematical model and a closed correction loop with gain matrix G to correct the estimation errors. For the induction motor drive, the adaptive full-order observer model is defined by:

$$\frac{d\hat{x}}{dt} = \hat{A}\hat{x} + Bu_s + G(\hat{i}_s - i_s) \quad (4.3)$$

Furthermore, the sliding mode observers (SMOs) also have a similar structure as the full-order observers. The difference is in the use of sliding mode switching function as a feedback signal in state of the gain matrix. The general mode of SMO is expressed as following:

$$\frac{d\hat{x}}{dt} = \hat{A}\hat{x} + Bu_s + K\text{sign}(\hat{i}_s - i_s) \quad (4.4)$$

4.3.3 Model reference adaptive system MRAS

The structure of MRAS observer is consisting of two parts. A reference model which doesn't contain the estimated quantity (rotor speed) and the adaptive model that contains the estimated quantity. In addition, an adaptation mechanism to produce it. The reference model, called mostly the voltage model, is expressed by the reference voltages in the stationary frame and generates the reference flux values. In the other hand, the adaptive model called also the current model, is expressed by stator currents and the rotor speed [Sch92; Gad10].

The error between these two generated signals (mostly rotor flux components) is called the adaptive signal. The adaptation mechanism produces the estimated speed value by a PI controller basing on this error. If the algorithm is designed properly, it goes to zero in steady state.

The estimated speed is expressed by:

$$\hat{\omega}_r = \left(K_p + \frac{K_i}{s} \right) e_{\psi_r} \quad (4.5)$$

K_p and K_i are the PI controller gains [Sch92].

e_{ψ_r} The adaptive error signal.

The MRAS method can be applied for models that yields either to the rotor or stator fluxes, back-EMFs or the reactive powers.

4.4. Limits of Sensorless Control in Low-Speed Operation Condition

Generally, sensorless IM drives work well in the medium and high-speed region. At low speed and particularly at near to zero speed, the drive may become unstable, the torque capability is diminished or lost and speed regulation may be inaccurate. In a sensorless drive system, the field angle and also the mechanical speed, are estimated using the stator current and voltage. The accurate acquisition is a major concern for stable operation at very low speed [Hol03]. There are several issues that contribute to the low-speed instability problem. The main of them are associated as given below.

4.4.1 Signal acquisition errors

In practice, the measured signals mostly contain noise. In addition, the used sensors themselves typically introduce DC offset values that can saturate the integrators employed in the estimations [Asf13].

4.4.2 Inverter non-linearity

The inverter causes nonlinear deadtime effects which require compensation at low speed for good dynamic performance. Another source of nonlinearities is owing to supply voltage drops. They can become significant at low frequency where the magnitude of the voltage is small [Hol06]. Due to these non-linearity characteristics, the calculation of the stator voltage vector from the PWM switching which assumed linear relation becomes inaccurate. Consequently, the stator voltage vector calculation that is used in the speed will introduce speed estimation error.

4.4.3 Distortions in the flux angle

If the estimated fluxes are erroneous, the Park transformation angle is incorrect and field orientation is lost. The quality of flux angle depends on the quality of the flux waveforms. In implementation, DC offsets and distortions can frequently be seen in the flux waveforms. They cause distortions in the transformation angle that can produce instability at low speed. We can notice that this is a resonant chain: non-ideal input signals results in non-ideal flux estimates and distorted rotor position. The result is a control voltage vector that does not rotate smoothly.

4.4.4 Incorrect speed estimation

In the low speed area, it can happen that the estimated speed swings between positive and negative values. The speed controller reacts to this and can produce an oscillatory torque that leads to instability.

4.4.5 Delay due to filtering

Usually, the simulation shows a smooth estimation and no filtering is needed. But experimentally with real signals that contain noise, distortions or offsets, the estimated speed is not smooth and must be filtered. The use of a LPF adds a delay in the feedback portion of the control system. For an excessive filtering, the system has been led to instability, especially at low speeds.

4.5 Sensorless Control Design for Nonlinear SVM-DTC Strategy

This section presents a sensorless DTC strategy. Different observer structures are designed for the elimination of the speed sensor in the nonlinear control scheme which has been developed in the last chapter. An adaptive full order observer for speed, flux and load torque estimation is presented firstly. Then a first order sliding mode observer for speed and flux estimation and a second order sliding mode observer for load torque estimation are presented.

4.5.1 Full order adaptive observer for DTC controlled IM

By considering the stator phase current and the stator flux as state variables, the induction motor model can be formed as:

$$\frac{d}{dt} \begin{bmatrix} i_s \\ \psi_s \end{bmatrix} = \begin{bmatrix} A_{11} & A_{12} \\ A_{21} & A_{22} \end{bmatrix} \begin{bmatrix} i_s \\ \psi_s \end{bmatrix} + \begin{bmatrix} B_1 \\ B_2 \end{bmatrix} [V_s] = Ax + Bu \quad (4.6)$$

$$i_s = Cx \quad (4.7)$$

where:

$$V_s = [V_{s\alpha} \quad V_{s\beta}]^T$$

$$A_{11} = -\left(\frac{1}{\sigma T_s} + \frac{1}{\sigma T_r}\right)I - \omega_r J; \quad I = \begin{bmatrix} 1 & 0 \\ 0 & 1 \end{bmatrix}$$

$$A_{12} = \frac{1}{\sigma L_s T_s} I + \frac{\omega_r}{\sigma T_s} J, \quad J = \begin{bmatrix} 0 & -1 \\ 1 & 0 \end{bmatrix}$$

$$A_{21} = -R_s I; \quad A_{22} = 0$$

$$B_1 = \frac{1}{\sigma L_s} I; \quad B_2 = I \quad C = [I \quad 0]$$

Then, the state observer will be described as follows [Mae00; Sab14]:

$$\frac{d\hat{x}}{dt} = \hat{A}\hat{x} + Bu_s + G(\hat{i}_s - i_s) \quad (4.8)$$

G is the observer gain matrix and the estimated values are marked with the sign of a hat (^).

By subtracting the equation (4.8) from (4.6), the estimation error is defined as:

$$\frac{de_i}{dt} = (A + GC)e_i + \Delta Ax \quad (4.9)$$

where:

$$e_i = x - \hat{x}; \Delta A = A - \hat{A} = \begin{bmatrix} -\Delta\omega_r J & \frac{\Delta\omega_r}{\sigma L_s} J \\ 0 & 0 \end{bmatrix}; \Delta\omega_r = \omega_r - \hat{\omega}_r$$

Lyapunov function V will be defined to ensure the stability:

$$V = e^T e + \frac{(\omega_r - \hat{\omega}_r)^2}{b} \quad (4.10)$$

b is a positive constant.

The time derivative of V is given by:

$$\dot{V} = e^T [(A + GC)^T + (A + GC)]e + \hat{x}^T \Delta A^T e + e^T \Delta A \hat{x} - 2 \frac{\Delta\omega_r}{b} \frac{\Delta\hat{\omega}_r}{dt} \quad (4.11)$$

The derivative of Lyapunov function must be negative to guarantee the stability. The gain matrix G must be chosen as much as the first term of (4.11) is negative semi-definite.

The adaptive scheme for speed estimation can be determined from the second and third term [Mae00].

$$\hat{\omega}_r = K_\omega \int \left[e_{s\alpha} \left(\frac{\hat{\psi}_{s\beta}}{\sigma L_s} - \hat{i}_{s\beta} \right) - e_{s\beta} \left(\frac{\hat{\psi}_{s\alpha}}{\sigma L_s} - \hat{i}_{s\alpha} \right) \right] \quad (4.12)$$

When the load torque is unknown or variable, it is considered as a system uncertainty. An enhanced model will be used to improve the response of the estimated speed and to estimate the applied load torque without need of any torque sensor in order to improve the control performance by reducing the system uncertainty.

$$\begin{cases} \hat{\omega}_r = \frac{1}{J} (T_e - \hat{T}_L) \\ \hat{T}_L = 0 \end{cases} \quad (4.13)$$

\hat{T}_L : Estimated load torque.

The friction coefficient will be neglected and the load torque will be considered as constant.

The speed adaptive scheme becomes

$$\hat{\omega}_r = \frac{1}{J} \int (T_e - \hat{T}_L) + K_\omega \int \left[e_{s\alpha} \left(\frac{\hat{\psi}_{s\beta}}{\sigma L_s} - \hat{i}_{s\beta} \right) - e_{s\beta} \left(\frac{\hat{\psi}_{s\alpha}}{\sigma L_s} - \hat{i}_{s\alpha} \right) \right] \quad (4.14)$$

The load torque can be estimated as follows:

$$\hat{T}_L = -K_T \int \left[e_{s\alpha} \left(\frac{\hat{\psi}_{s\beta}}{\sigma L_s} - \hat{i}_{s\beta} \right) - e_{s\beta} \left(\frac{\hat{\psi}_{s\alpha}}{\sigma L_s} - \hat{i}_{s\alpha} \right) \right] \quad (4.15)$$

K_ω and K_T are arbitrary positive gains.

To ensure stability of the observer, its poles must be selected proportional to the induction machine poles. If we define the machine poles by s_{IM} , the observer poles will be defined by [Mae00; Amr16]:

$$s_{obs} = k_{obs} s_{IM} \quad (4.16)$$

k_{obs} is a factor ($k_{obs} > 1$) which indicates that the observer is dynamically faster than the machine. Then the gain matrix can be obtained by:

$$G = \begin{bmatrix} g_1 I & g_2 J \\ g_3 I & g_4 J \end{bmatrix} \quad (4.17)$$

g_1, g_2, g_3, g_4 are the observer gains, they can be founded from motor parameters and motor speed.

The block diagram of the adaptive flux observer is shown in **Fig.4.4**.

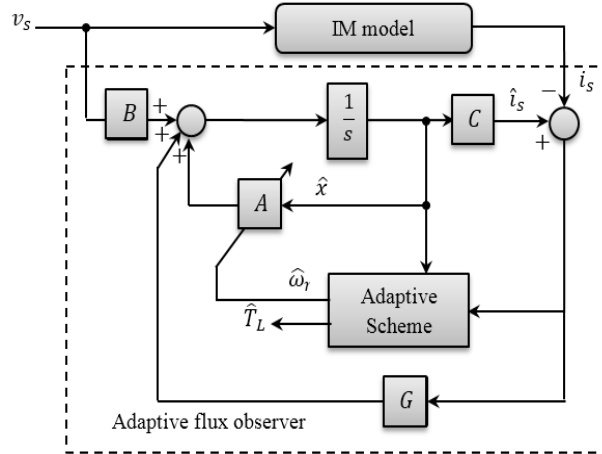


Fig.4.4. Block diagram of speed adaptive flux observer.

4.5.2 Sliding mode flux observer for DTC controlled IM

The Sliding mode observers (SMOs) can provide high effectiveness due to a number of advantages such as, the easy implementation and the high robustness to parameters variation. In addition, no extensive computations are required [Amr17b]. They have commonly similar structure as the full order adaptive observers. The difference is just in feedback signal manipulation.

Other SMO designs do not employ the speed adaptation scheme, which means they do not take the speed as an adaptive quantity like the proposed structures in [Reh02; Las06]. In these observers, the speed estimator is separated completely from the main observer in order to increase the accuracy in a wide-speed-range operation and to reduce the complexity.

4.5.2.1 Sliding mode flux observer design

The goal of the SMO is to construct stator flux components and use them for torque and speed estimation. The SMO is based on the state model of induction motor in rotor reference frame. The stator flux ψ_s and current i_s are considered as state variables [Las09].

$$\begin{cases} \frac{d\bar{\psi}_s}{dt} = R_s \bar{i}_s - j \omega_r \bar{\psi}_s + \bar{V}_s \\ \frac{d\bar{i}_s}{dt} = -\frac{1}{\sigma} \left(\frac{1}{T_r} + \frac{1}{T_s} \right) \bar{i}_s + \frac{1}{\sigma L_s} \left(\frac{1}{T_r} - j \omega_r \right) \bar{\psi}_s + \frac{1}{\sigma L_s} \bar{V}_s, \end{cases} \quad (4.18)$$

In this observer, the back-emf terms ($\omega_r \psi_s$) are considered as disturbances. Then, the model of inherently observer (**Fig.4.5**) can be expressed in (4.19).

$$\begin{cases} \frac{d\hat{\psi}_s}{dt} = R_s \bar{i}_s + V_s - K \text{sign}(S_i) \\ \frac{d\hat{i}_s}{dt} = -\frac{1}{\sigma} \left(\frac{1}{T_r} + \frac{1}{T_s} \right) \bar{i}_s + \frac{1}{\sigma L_s T_r} \hat{\psi}_s + \frac{1}{\sigma L_s} V_s - \frac{1}{\sigma L_s} K \text{sign}(S_i). \end{cases} \quad (4.19)$$

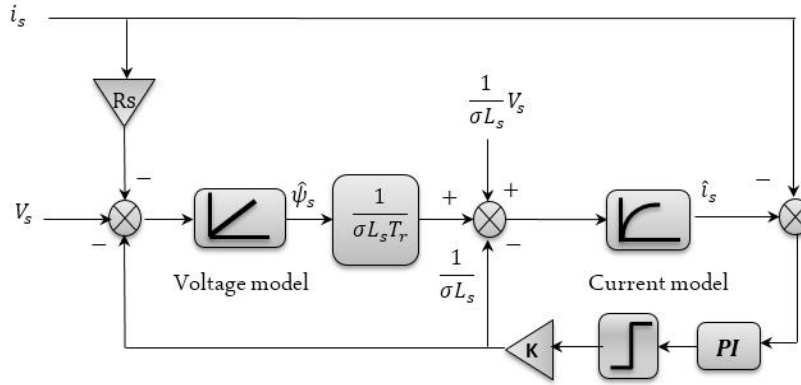


Fig.4.5 Proposed sliding mode stator flux observer

K is the observer switching gain and S_i is the sliding surface of the current error.

The PI controller is added just to impose more desired error convergence.

$$S_i = \left(K_p + \frac{K_i}{s} \right) (\hat{i}_s - i_s). \quad (4.20)$$

4.5.2.2 Gain selection

The observer gain has to be large enough to ensure the stability. By using Lyapunov candidate function which is defined previously with IM and SMO models (4.19) and (4.20), and during sliding mode $S_i=0$ and $\dot{S}_i = 0$, K is given as:

$$K > \max \left(\left\| \frac{e_{\psi_{s\alpha}}}{T_r} - \omega_r \psi_{s\beta} \right\|, \left\| \frac{e_{\psi_{s\beta}}}{T_r} - \omega_r \psi_{s\alpha} \right\| \right) \quad (4.21)$$

where $e_{\psi_{s\alpha\beta}}$ is the flux error.

4.5.2.3 Speed estimation

The advantage of SMO is the unrelated with rotor speed quantity and when it is needed it can be computed easily by the following open loop expression:

$$\hat{\omega}_r = \hat{\omega}_s - \hat{\omega}_{sl} = \frac{1}{\psi_r^2} \left(\frac{d\hat{\psi}_{r\beta}}{dt} \hat{\psi}_{r\alpha} - \frac{d\hat{\psi}_{r\alpha}}{dt} \hat{\psi}_{r\beta} \right) - \frac{R_s T_e}{p \psi_r^2}. \quad (4.22)$$

However, the computation of the rotor flux derivative is sensitive to noise, the estimated speed has to be filtered by using LPF in order to be useable in this control algorithm.

4.5.3 Second order sliding mode load torque observer

In this section, a second order sliding mode observer is proposed in order to estimate the applied load torque to improve the control performance by reducing the system uncertainty.

The IM mechanical model is:

$$\dot{\omega}_r = \frac{1}{J} (T_e - \hat{T}_L) - \frac{f}{J} \omega_r \quad (4.23)$$

where J is the inertia constant and f is the friction coefficient.

By using SFOC model, the electromagnetic torque can be written as:

$$T_e = p\psi_s i_{sq} = K_t i_{sq} \quad (4.24)$$

K_t : Torque coefficient

The load torque can be considered as a quasi-constant if we assume that it only changes at certain instants [Bar14; Amr17b]. The dynamic equations of the IM are:

$$\begin{cases} \dot{\omega}_r = -\frac{f}{J} \omega_r + \frac{K_t}{J} i_{sq} - \frac{1}{J} \hat{T}_L \\ \dot{\hat{T}}_L = 0 \end{cases} \quad (4.25)$$

The proposed sliding mode load torque observer model based on super twisting strategy is:

$$\begin{cases} \dot{\hat{\omega}}_r = -\frac{f}{J} \omega_r + \frac{K_t}{J} i_{sq} - \frac{1}{J} \hat{T}_L \\ \dot{\hat{T}}_L = T_{L1} + \lambda |s|^{1/2} \text{sign}(e_{\omega_r}) \\ \dot{\hat{T}}_L = K \text{sign}(e_{\omega_r}) \end{cases} \quad (4.26)$$

The load torque can be obtained from SMO which is expressed in Eq (4.26).

K_1 , K_2 , λ_1 and λ_2 are positive constants.

The sliding surface is the speed estimation error ($S_\omega = e_\omega$)

The estimation errors are obtained as:

$$\begin{cases} e_{\omega_r} = (\omega_r - \hat{\omega}_r) \\ e_{T_L} = (T_L - \hat{T}_L) \end{cases} \quad (4.27)$$

e_{T_L} : is load torque estimation errors

The estimation error converges to zero if the observer gains are large enough to satisfy the stability condition. They can be demonstrated easily by Lyapunov candidate function.

4.6. Operating Conditions and Benchmarks

The observers and control algorithms are evaluated in the framework by experimental test following a specific trajectories and significant robustness tests noted “Benchmarks”. These benchmarks have been defined, on the one hand, in cooperation with the Electrical Engineering and Automatic Control Laboratories under the support of the French National CNRS Work Group “Control of Electrical Systems,” and on the other hand in cooperation with Electrical Industrial Companies [Glu15]. The trajectories of this benchmarks have been considered taking into account industrial operation conditions, following the nominal values of the torque, the rotor speed and the flux of the machines. An example of speed reference trajectory is shown in **Fig.4.6**. This checks the performance and the robustness of the observer without mechanical sensors at low and high speeds.

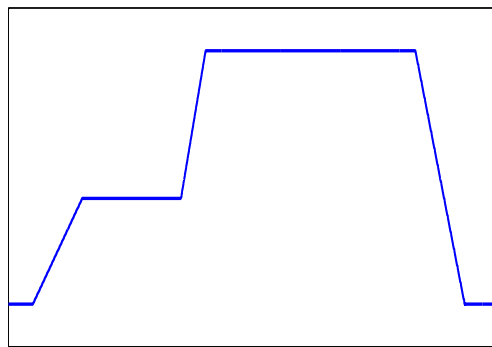


Fig.4.6 Industrial benchmark trajectory.

Fig.4.7 shows the global diagram of the sensorless control scheme of nonlinear SMFL-DTC with SVM associated to flux, speed and load torque observers.

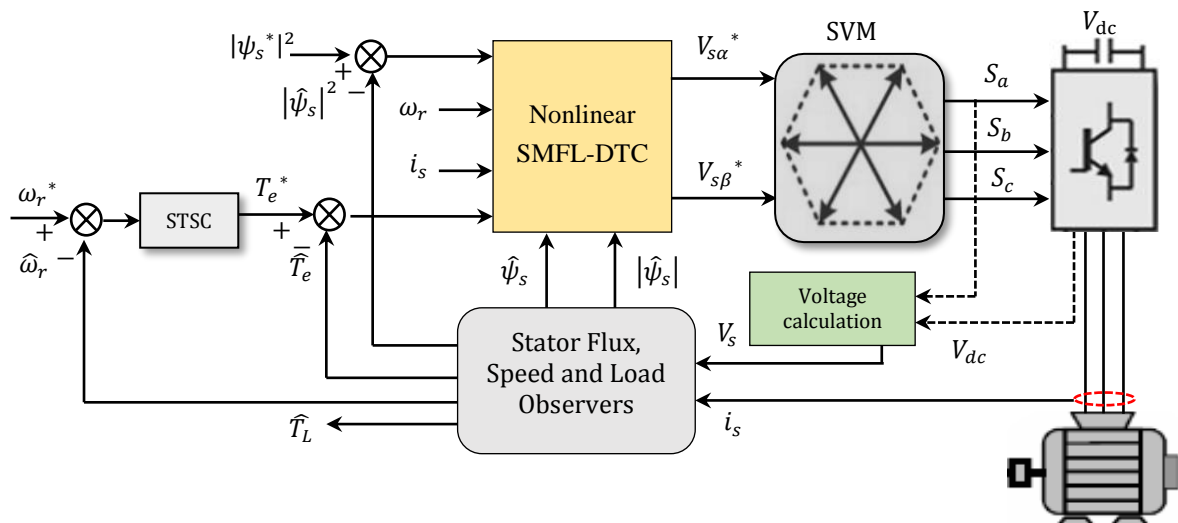


Fig.4.7 Global diagram of sensorless nonlinear SVM-DTC based on speed and flux observers.

4.7 Simulation and Experimental Comparative Study

The simulation and the experimental results are exhibited as a comparative analysis between the two observers. An adaptive observer based on Lyapunov theory compared to dual sliding mode observer structures for speed, stator flux and load torque estimation. In this chapter, we have focused only on the estimation results (i.e. rotor speed, flux and load torque)

4.7.1 Simulation results

The figures below present different operation conditions of the IM such as the starting up, low/zero speed operation tests, industrial benchmark test and parameters variation tests have been done (The figures are specified (a) for the adaptive observer and (b) for the SMO).

4.7.1.1 Starting up and steady state

Fig.4.8 to **Fig.4.11** show respectively the speed with estimation errors and flux estimation at the starting up and the steady states.

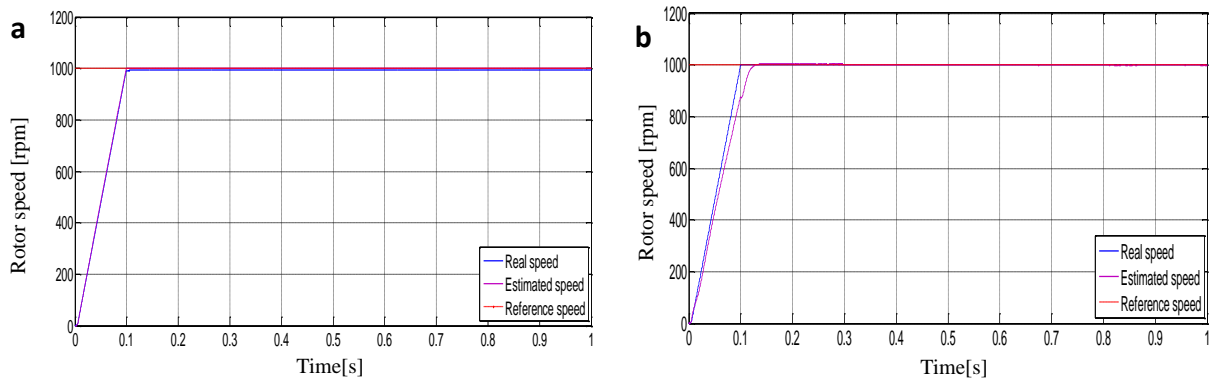


Fig.4.8 Starting up and steady states: Real and estimated speed [rpm].

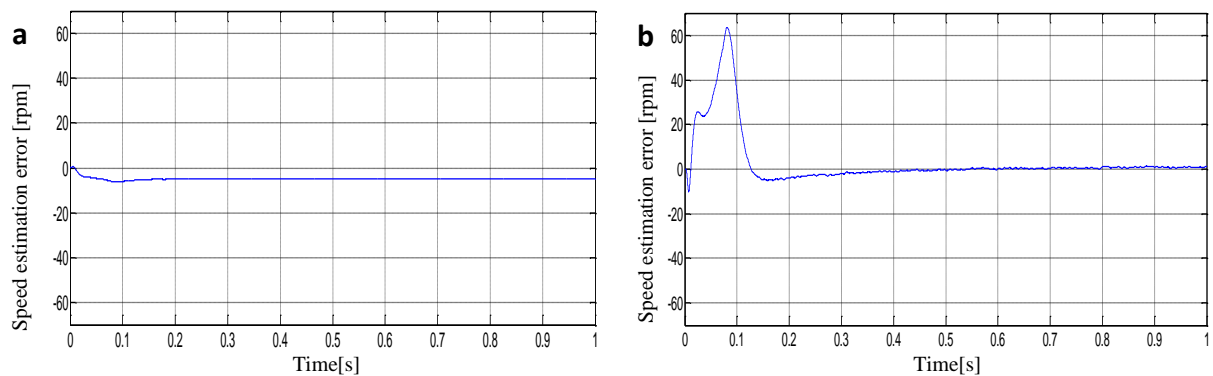


Fig.4.9 Rotor speed estimation errors [rpm].

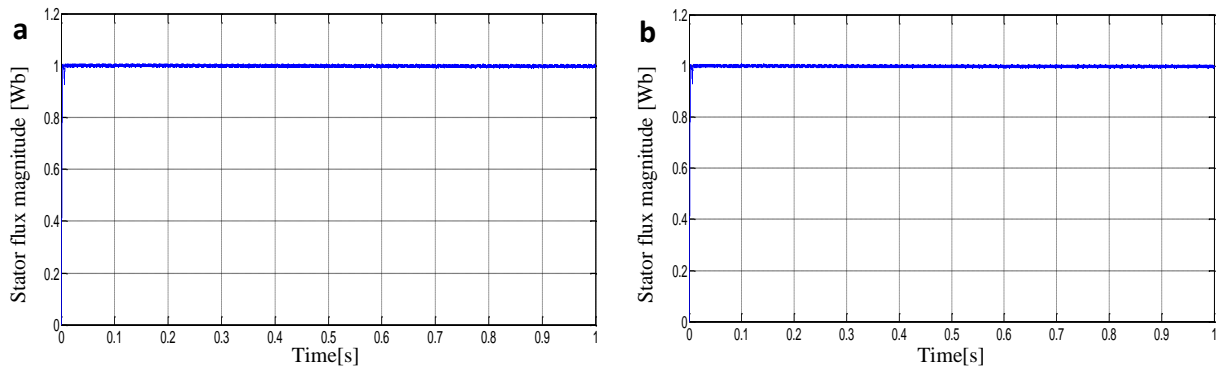


Fig.4.10 Estimated stator flux magnitude [Wb].

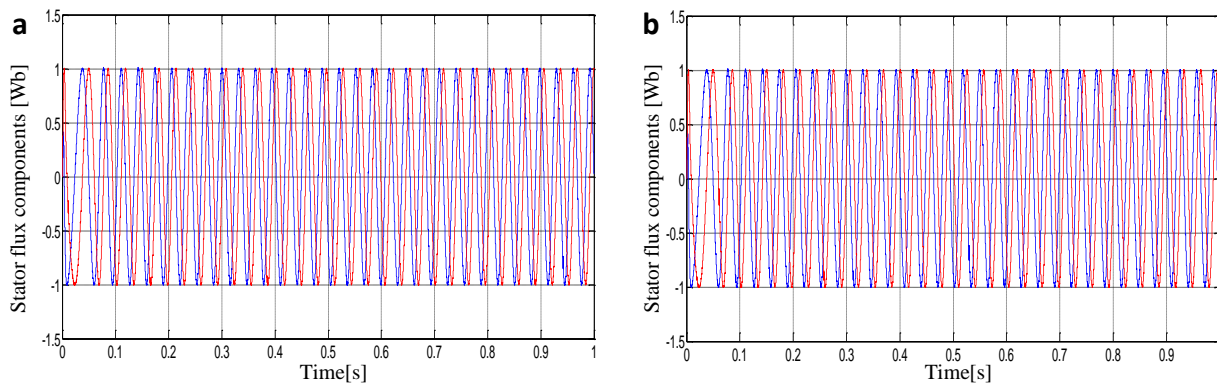


Fig.4.11 Estimated stator flux components [Wb].

Figs.4.8-4.11 illustrate the starting up according to the step of (1000 rpm) and the steady state for both observers. In **Figs.4.8** it is observed that the estimated speed follows the real speed for both observers. The adaptive observer in (**Fig.4.8a**) shows a better superposition between the real and estimated speed quantities in the transient state while the non-adaptive SMO in (**Fig.4.8b**) provides the better superposition and eliminates the static error in steady state. This can be further justified in **Fig.4.9**. It shows the estimation error in both cases. It can be seen that the adaptive observer has a minor error at starting up, but then, this error has not eliminated in steady state ($\pm 5 \text{ rpm}$). Contrariwise, the SMO has eliminated clearly the static error in the steady state in spite of the high augmentation at the beginning. Next, the estimated stator flux is shown in **Figs.4.10-4.11**. We don't have here an estimation error because there is no measured flux to compare with it. Since the stator flux magnitude is forced by the control algorithm, both observers show an accurate estimation and good waveform for stator flux.

4.7.1.2 Low speed operations

The low speed operation test is implemented as speed variation (200 rpm to 400 rpm) and for very low speed values (50 rpm to 25 rpm).

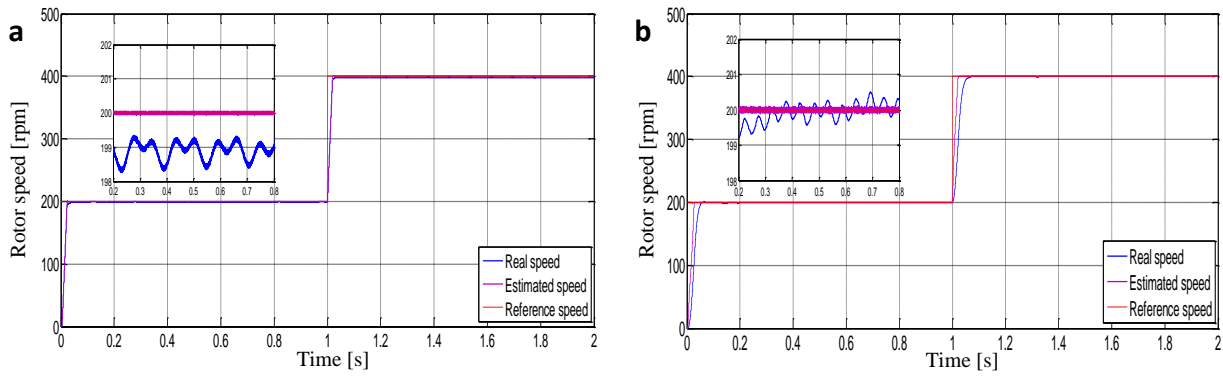


Fig.4.12 Real and estimated speed at low speed operation (200rpm, 400rpm).

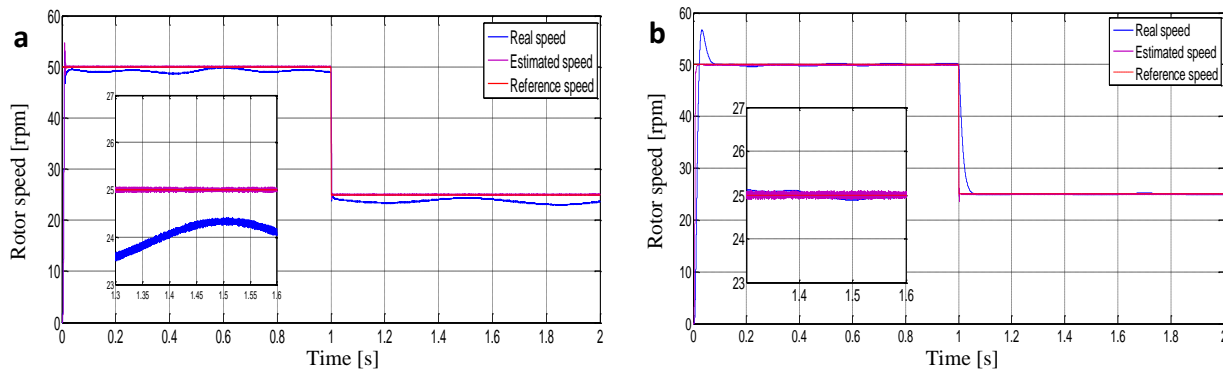


Fig.4.13 Real and estimated speed at low speed operation (50 rpm; 25 rpm)

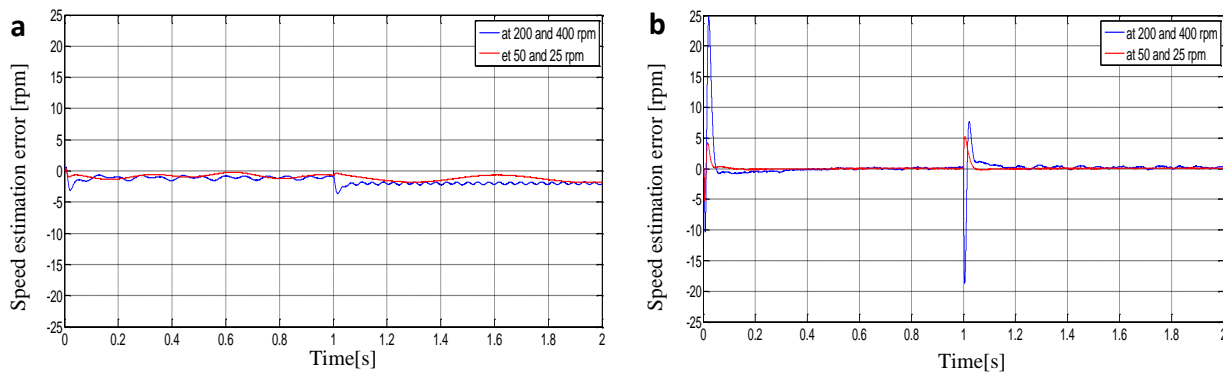


Fig.4.14 Rotor speed estimation errors in different speed regions [rpm].

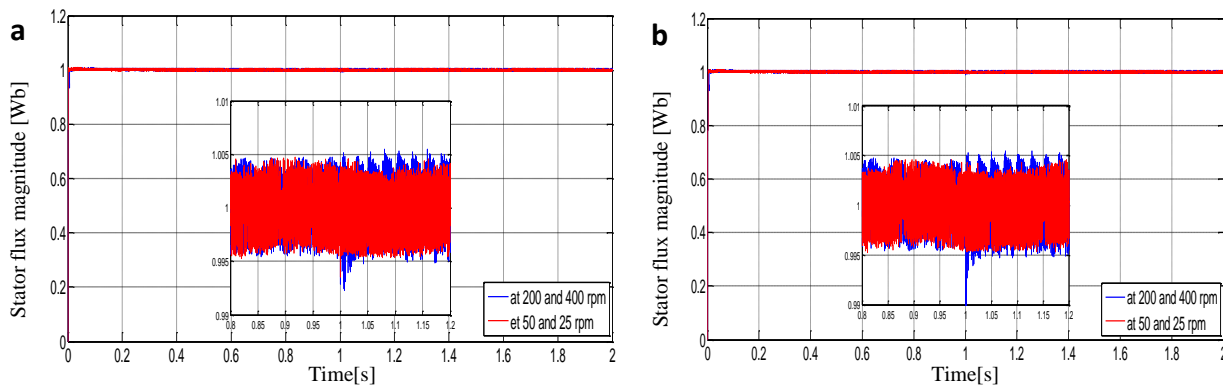


Fig.4.15 Estimated Stator flux magnitude in different speed regions [Wb].

The low-speed operation is obtained in **Figs.4.12-4.15**. A speed variation from 200 rpm to 400 rpm has been conducted in **Fig.4.12**. It is clear from (**Fig.4.12b ZOOM**) that the

SMO has stable estimation and precise superposition between speeds in this operation also, contrary to the adaptive observer which provides an instability with a considerable static error (**Fig.4.12a**). Another speed variation at very low speeds from 50 rpm to 25 rpm has been conducted in **Fig.4.13**. In similar way, the adaptive observer shows inaccurate estimation while the SMO has always good accuracy whatever is the speed value in the steady state.

All these remarks can be confirmed in **Fig.4.14** which illustrates the estimation errors in different speed regions. It can be observed that the estimation errors of the SMO converge to zero in all cases, unlike the adaptive observer, where the static error increases proportionally with the rotor speed. The flux estimation is shown in **Fig.4.15**. Both observers show good estimation and minimized bandwidth in different speed regions.

4.7.1.3 Zero speed operation and industrial benchmark test

Fig.4.16 and **Fig.4.17** show respectively the speed and stator flux magnitude starting with 1000 rpm and a speed variation to zero rpm at $t=1\text{ s}$. The benchmark test is presented in **Fig.4.18** and **Fig.4.19**

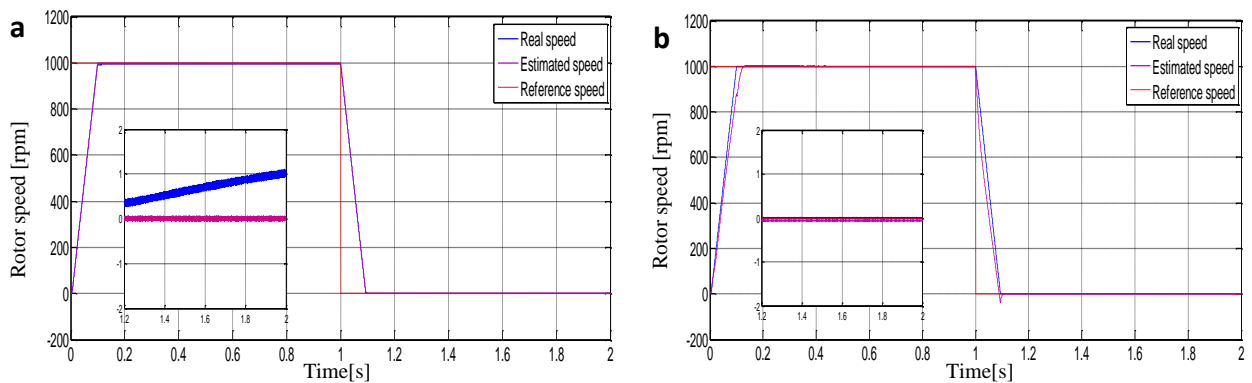


Fig.4.16 Real and estimated speed at 1000 rpm and zero speed region.

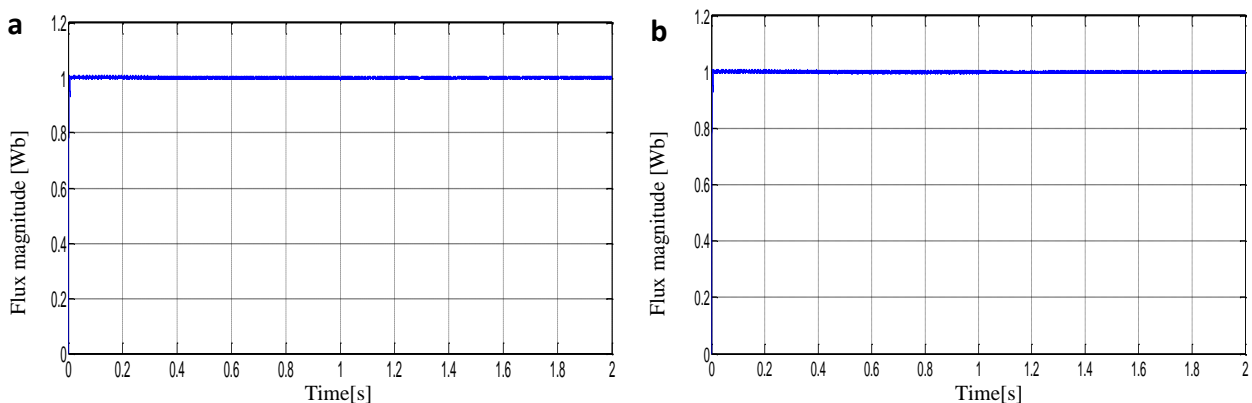


Fig.4.17 Estimated stator flux magnitude at 1000 rpm and zero speed region.

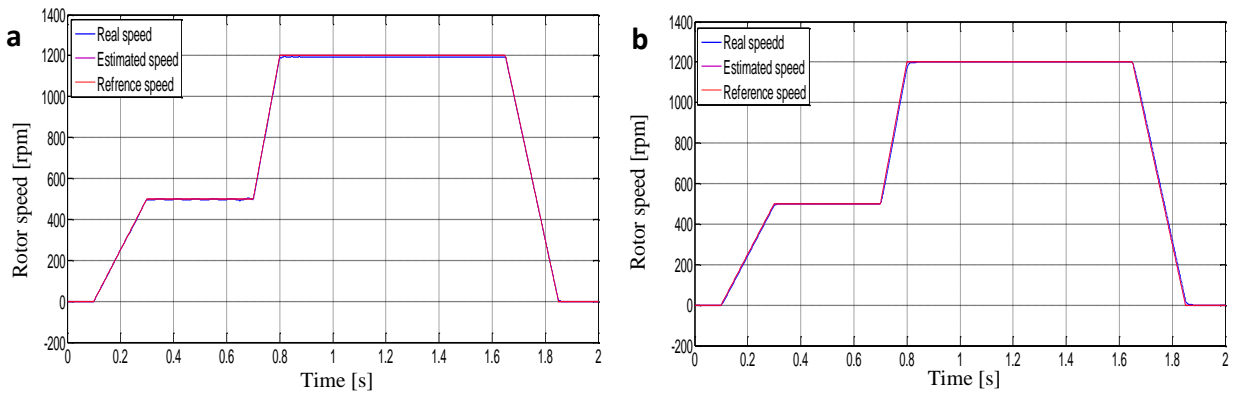


Fig.4.18 Speed estimation under industrial benchmark trajectory for different speeds.

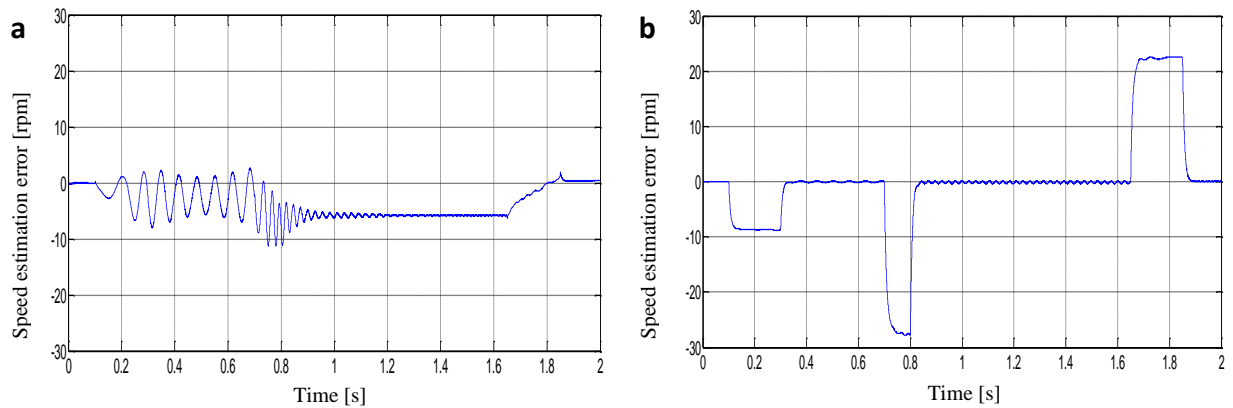


Fig.4.19 Speed estimation errors under industrial benchmark trajectory for different speeds

The zero-speed test is done in **Fig.4.16**. Firstly, we have the same remarks for both observers at the speed value of 1000 rpm . At zero speed state the SMO keeps its accuracy and minimized error level, contrary to the adaptive observer which provides a static error. **Fig.4.17** confirms that the flux estimation is always accurate and follows the control in each speed value. The last speed test is presented in **Figs.4.18-4.19**. An industrial benchmark profile is applied as a speed reference. This test can comprise all the previous tests. **Fig.4.18** shows the rotor speed estimation of both adaptive and sliding mode observers under a variable reference from zero to medium (500 rpm) until high speed values (1200 rpm). The estimation error is illustrated in **Fig.4.19**. It can be concluded that the SMO provides a considerable error only at variable states and eliminates this error in the steady state, contrary to the adaptive observer which shows some fluctuations and could not eliminate the static error.

4.7.1.4 Parameters variation test

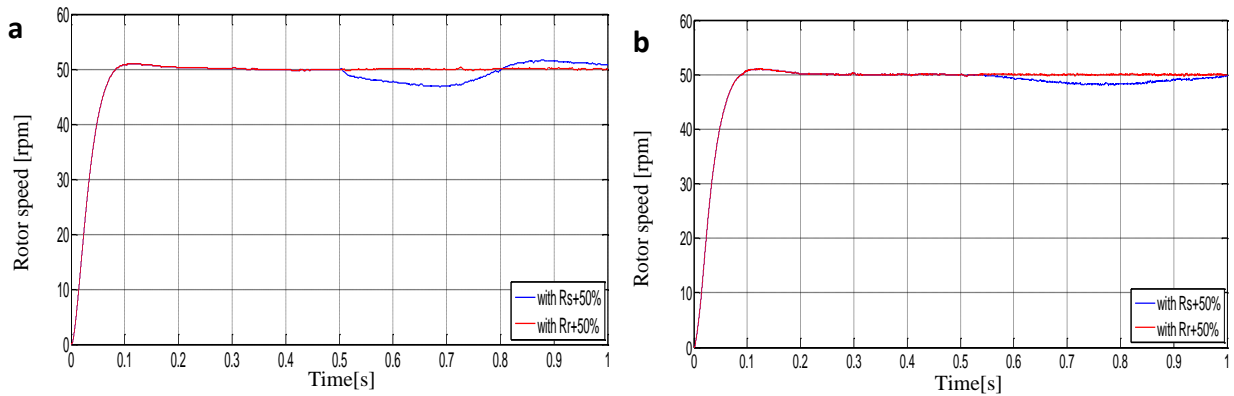


Fig.4.20 Robustness test: Low speed operation with parameters variation ($(R_s, R_r) + 50\%$).

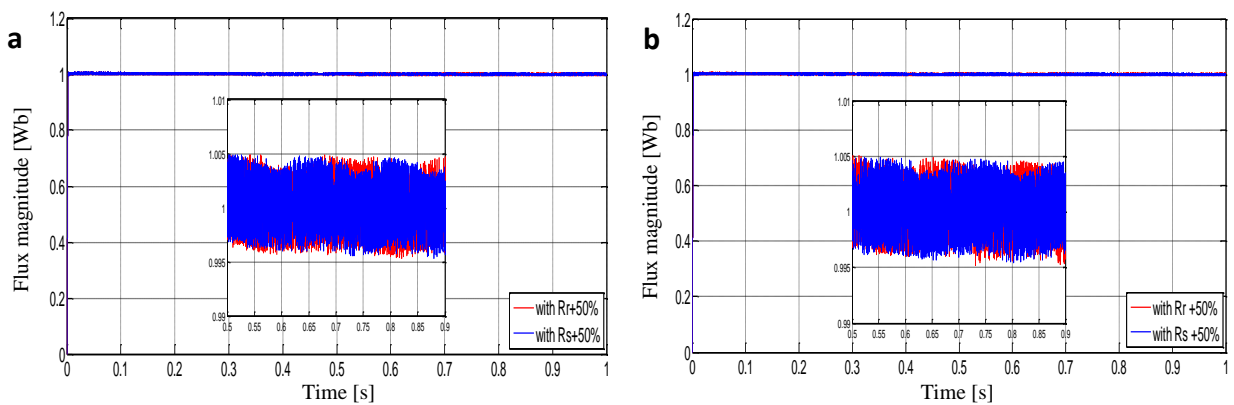


Fig.4.21 Robustness test: flux magnitude with parameters variation ($(R_s, R_r) + 50\%$).

The robustness test against parameters variation is shown in **Figs.4.20-4.21**. They show the comparison of the observed speed and flux under stator and rotor resistance variation of $+50\%$ in low speed region (50 rpm). The values of resistances increase instantaneously starting from $t=0.5\text{s}$ (as shown in the last chapter). These figures illustrate that the sensitivity of flux and speed, due to R_r variation, is not apparent. In R_s variation the affection and the error are not so considerable and have been recovered quickly especially in the case of SMO. Both observers have given similar results in this test. This point can be improved in the future work by taking the stator resistance as an adaptive quantity.

4.7.1.6 Load torque estimation

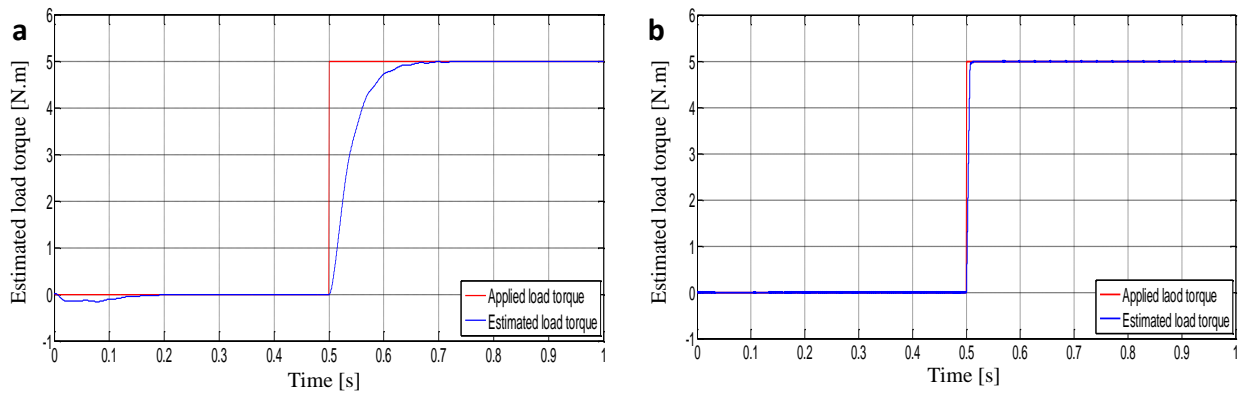


Fig.4.22. Applied and estimated load torque [N.m].

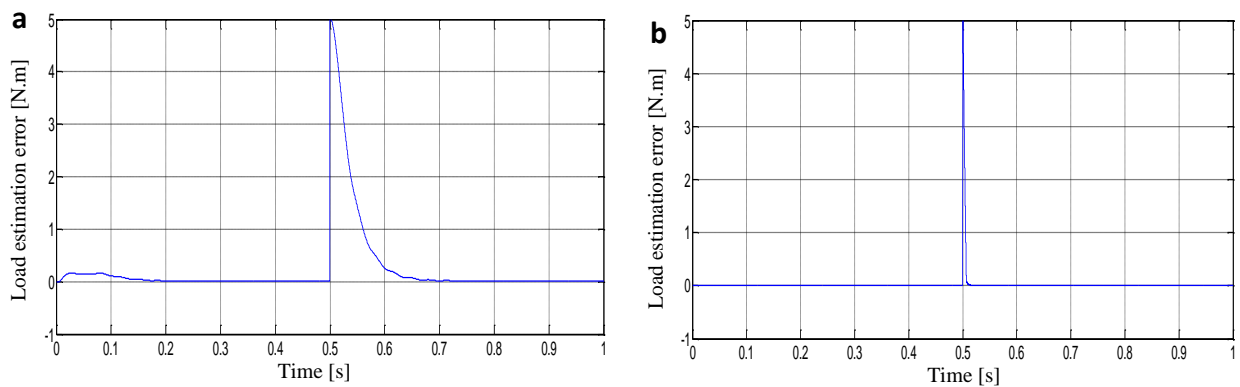


Fig.4.23 Load torque estimation error [N.m].

Figs.4.22-4.23 show the load torque estimation analysis. **Fig4.22(b)** and **4.23(b)** show that the sliding mode load torque observer has faster response and more accurate observation than the conventional Lyapunov based adaptive observer in **Fig.4.22(a)** and **4.23(a)**. At load application instant, the convergence of SMO estimation error is quicker to zero.

The simulation results prove that the SMO eliminates the static error and has more precise estimation than the adaptive observer in the steady state. The chattering effect has been reduced owing to the use of smooth switching function in sliding mode observer design. The speed estimator has an accuracy and robustness in different environments. The estimation has no influence on the inherently SMO structure. It mostly depends on the noise level and filtering operation. The low and zero speed tests show that the sensorless control scheme preserved its performance even in this region.

4.7.2 Experimental results

This section exhibits the experimental validation of the comparative analysis for the two observers design. The conducted tests are the same as those presented in the simulation section.

4.7.2.1 Starting up and steady state

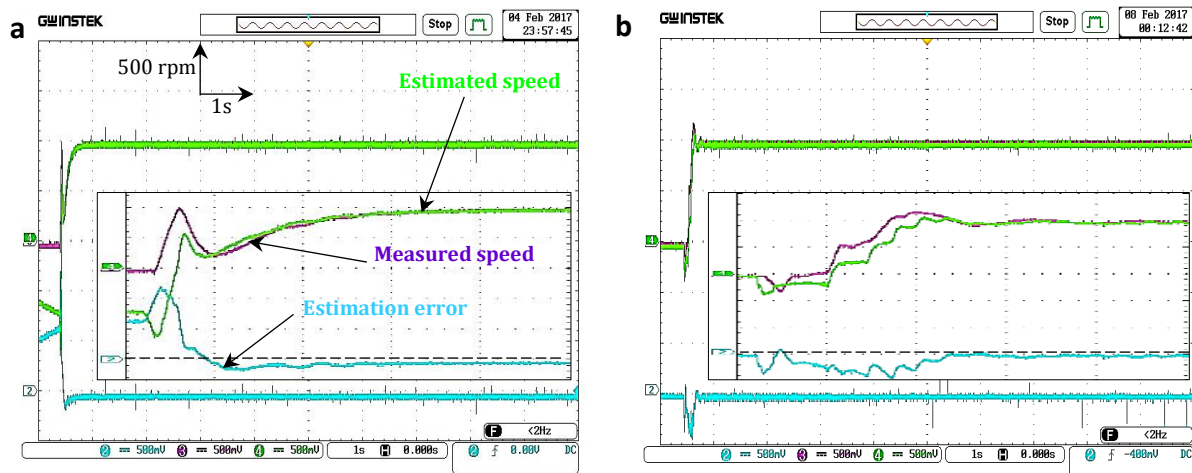


Fig. 4.24 Starting up and steady states: Estimated and real speed with estimation error.

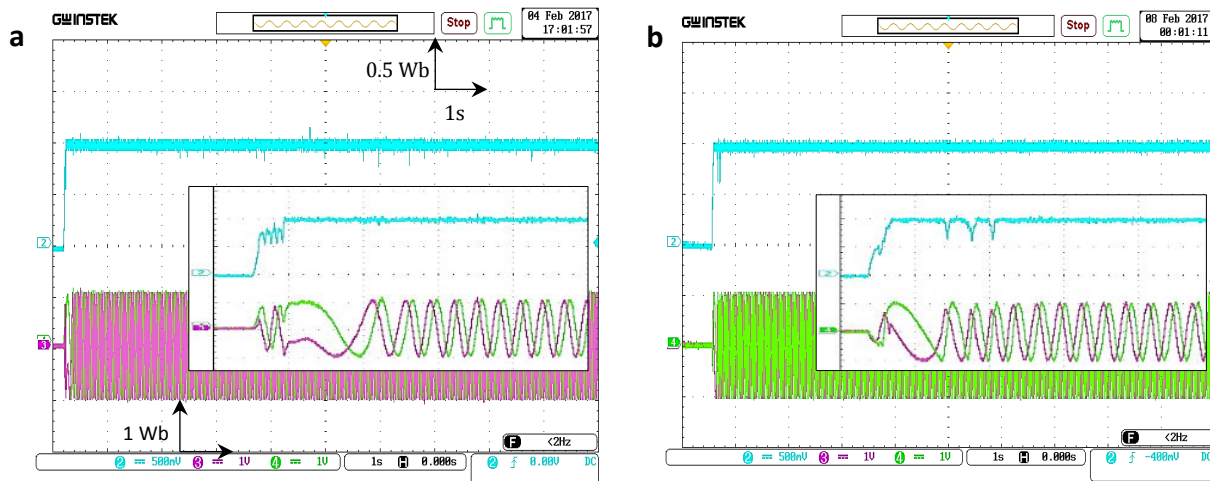


Fig. 4.25 Starting up and steady states: Estimated flux magnitude and components.

Firstly, **Fig.4.24** shows the rotor speed ($1div = 500 rpm$) at the startup state ($0-1000 rpm$) for both observers. We observe before the starting up instant (at $0 V$ alimentation), that the adaptive observer has an initial estimated speed and estimation error values. This phenomenon has not arisen in simulation results. It is caused by the noise and the offset of measurement sensors (Current and voltage) and the pure integrators in estimation algorithm. Contrariwise, SMO has avoided this problem due the separated structure of speed estimator.

The ZOOM of **Fig.4.24** shows that the measured and estimated speeds are in superposition for both observers. The SMO provides a faster response than the adaptive observer in spite of the overshoot. Moreover, the static error has been minimized. **Fig.4.25** illustrates the observed stator flux magnitude ($1div = 0.5 Wb$) and its axes components ($1div = 1 Wb$). Since there is no real measured flux value there is no estimation error. As we said before, the flux magnitude is controlled in a closed loop, that is why it provides an accurate estimation and good reference's following.

4.7.2.2 Low speed operation

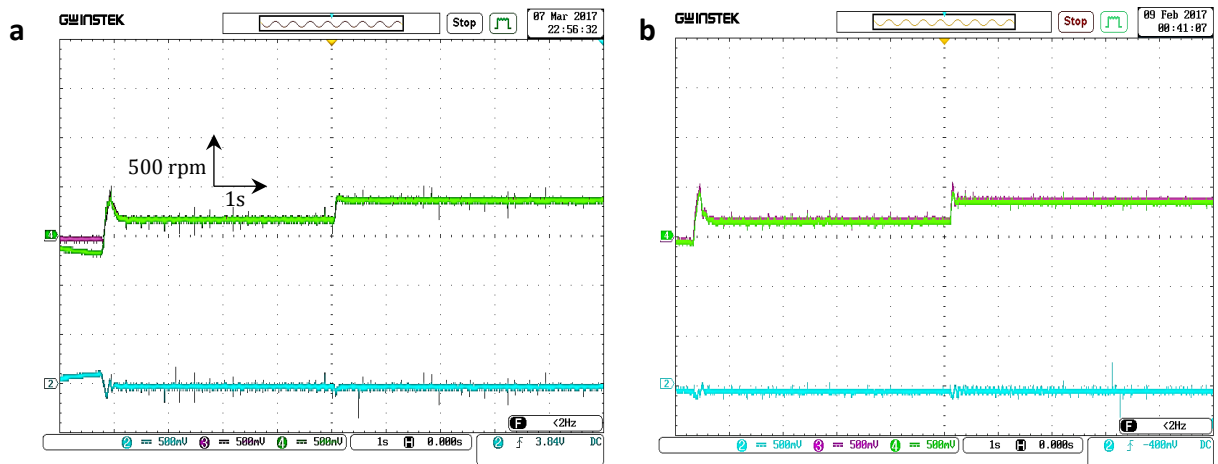


Fig.4.26 Low speed operation (200;400 rpm): Estimated and real speed with estimation error.

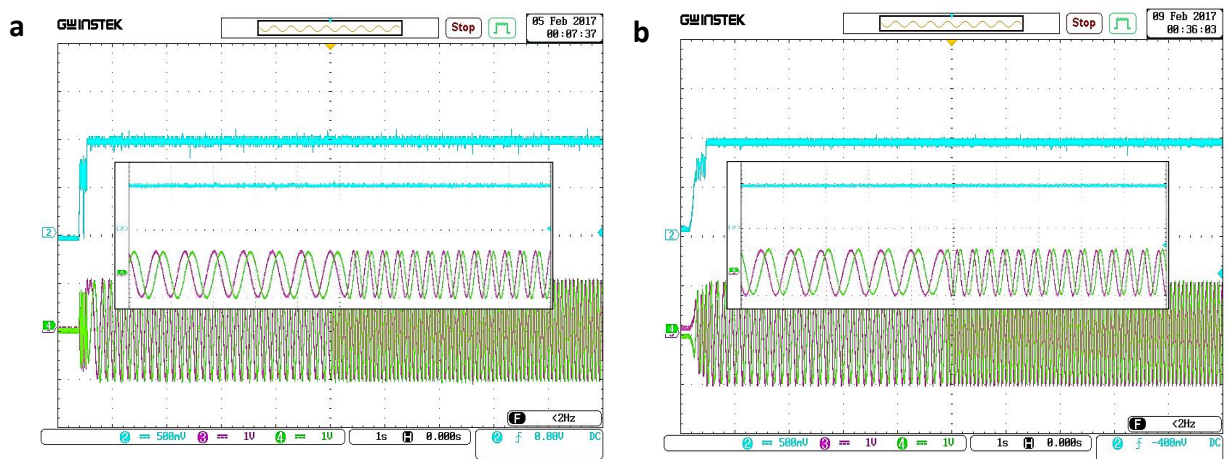


Fig.4.27 Low speed operation (200;400 rpm): Estimated flux magnitude and components.

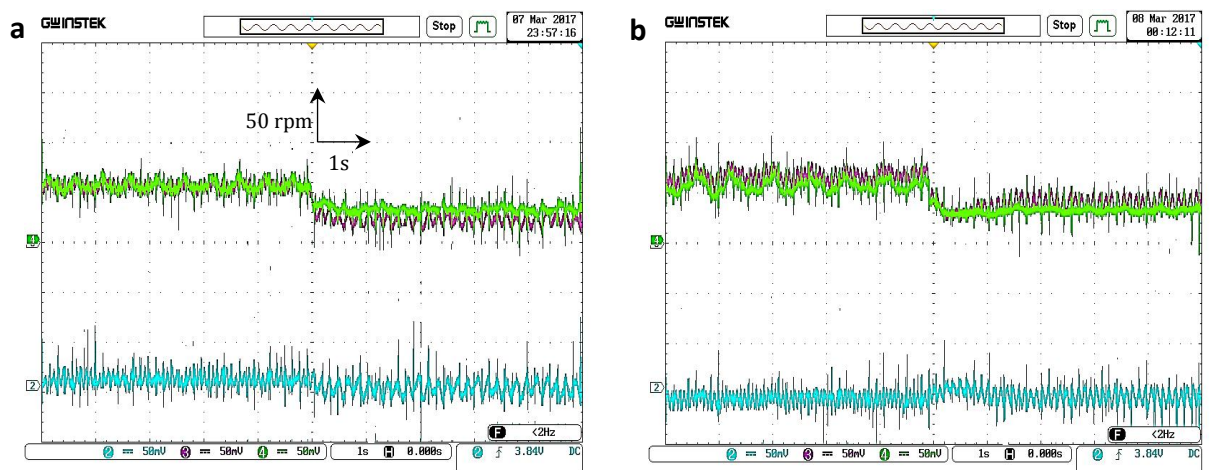


Fig.4.28 Low speed operation (50;25 rpm): Estimated and real speed and estimation error.

In **Fig.4.26**, speed variation from low to medium speed region of (200 rpm (≈ 21 rad/s) to 400 rpm) has been shown. The flux magnitude and components are depicted in **Fig.4.27**. Another speed variation test has been conducted in **Fig.4.28** for the very low speed

values (50 rpm to 25 rpm ($\approx 2.61 \text{ rad/s}$)), ($1 \text{ div}=50 \text{ rpm}$). It can be noticed that the speed and flux estimation keep the same previous performance in **Figs.4.26-4.27**. However, in **Fig.4.28**, both observers suffer from high oscillations and instability in speed. The SMO reduces a bit the static error at 25 rpm regions, but it shows high noises due to the sensitive nature of the speed estimation process.

4.7.2.3 Zero speed operation and industrial benchmark test

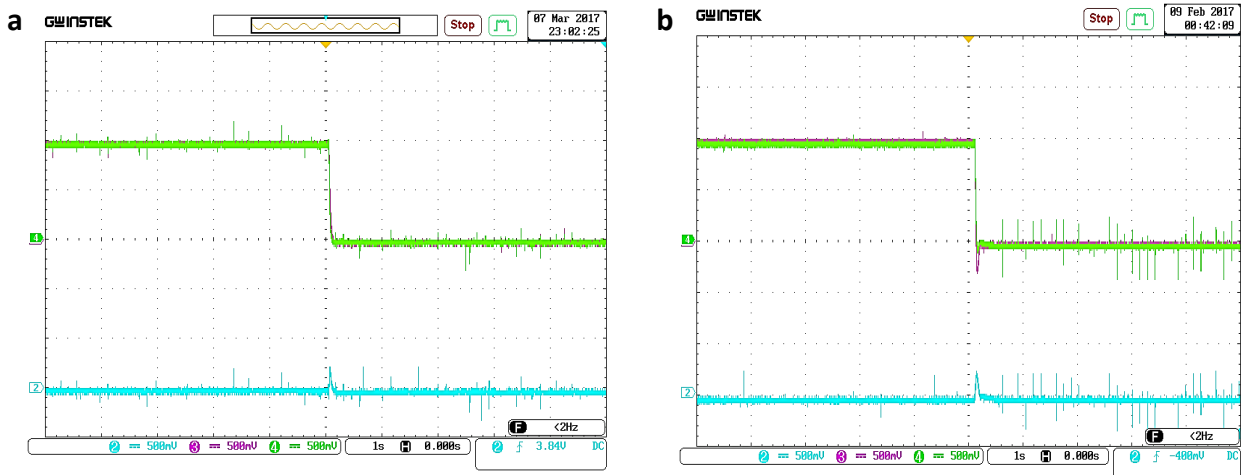


Fig.4.29 Zero speed operation: Estimated and real speed and estimation error.

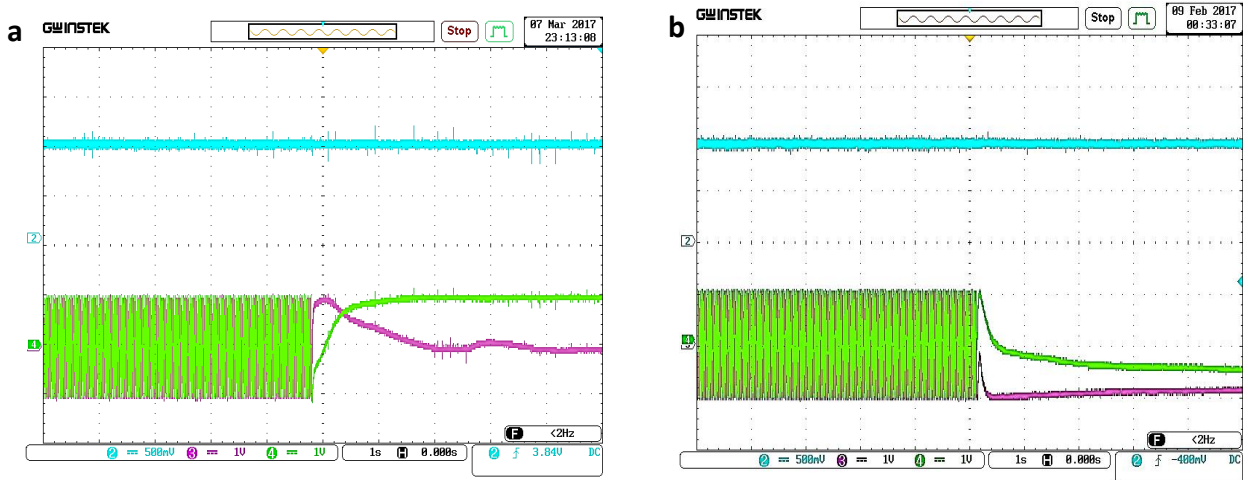


Fig.4.30 Zero speed operation: Estimated flux magnitude and its components.

The last speed tests have been done in this section, the zero-speed test is presented in **Figs.4.29-4.30**. Both observers show stable speed estimation at zero speed/frequency ($0 \text{ rpm}; 0 \text{ Hz}$). The speed value is almost correct even when the machine stops rotation. Next, the flux estimation is shown in **Fig.4.30**, the flux magnitude follows its reference. The SMO provides the better flux components waveform (**Fig.4.30(b)**). They have been deformed in case of the adaptive observer (**Fig.4.30(a)**).

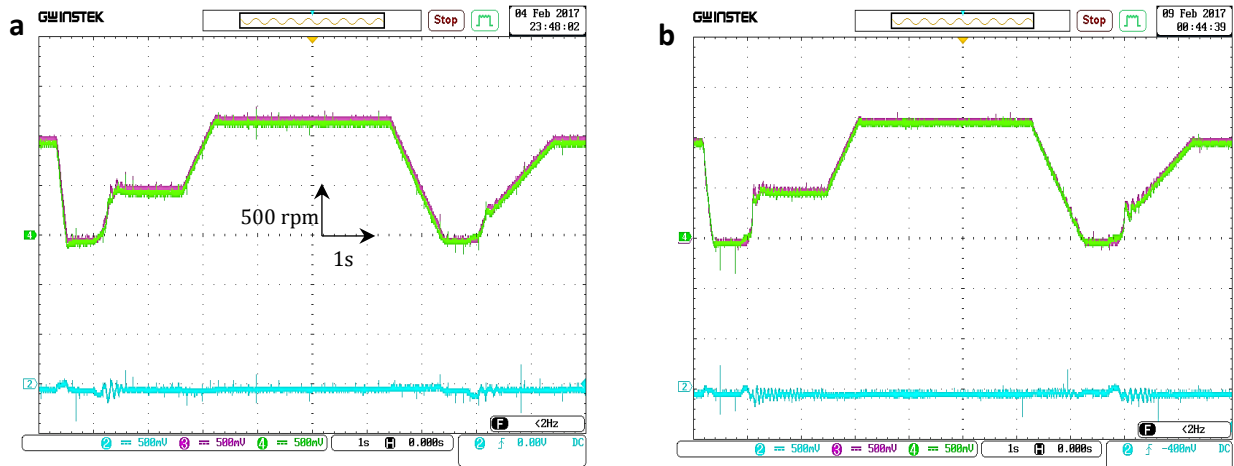


Fig.4.31 Benchmark trajectory: Estimated and real speed and estimation error.

The variable speed profile (benchmark) test is illustrated in **Fig.4.31**. This test is comprehensive to all previous speed tests. It can be seen that the obtained result of the same test in simulation section has been validated. The adaptive observer manifests a minor error during the instantaneous variation of speed but it could not minimize this error in the steady state, whilst, the SMO manifests some fluctuations and errors during the variation of speed, but it minimizes the static error in steady state.

4.7.2.4 Load torque estimation

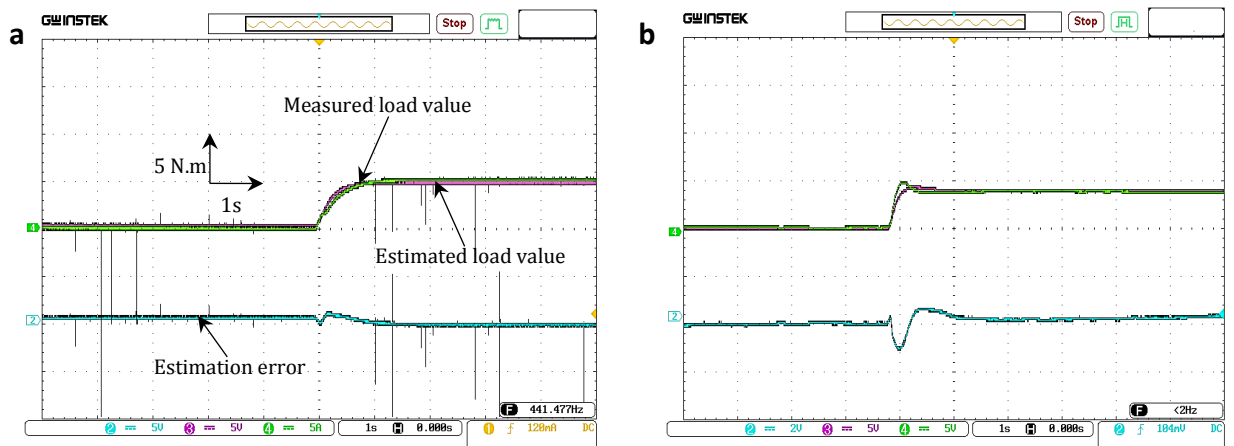


Fig.4.32 Applied and estimated load torque with estimation error.

Finally, the load torque estimation has been done in the **Fig.4.32**. The figure shows the measured applied load torque which obtained by load torque control unit and the estimated one by the super twisting observer ($I_{div}=5 N m$). In addition, it shows estimation error also. We can see a good superposition between the estimated value and the real one while the estimation error converges quickly to zero.

In view of the facts, different problems arise in the experimental implementation of the sensorless control, although we did not face these problems in the simulation due to the ideality of modeling and the absence of measurement noises or other influential factors. We

can understand that the real limits of the sensorless control appear in the real implementation. As summary, the SMO presents an accurate estimation in all tests due to its inherent structure and faster response in load estimation. Some problems appear in the experimental results in low speeds (oscillation and inaccuracy) due to high sensitivity of speed estimator to noise. A proposed solution is presented in the next section to improve the performance of the SMO.

4.8 Association of MRAS with stator flux SMO for speed estimation

The general structure of MRAS observer contains two parts: a reference model which doesn't contain the estimated quantity (rotor speed) and the adaptive model which contains the estimated quantity, in addition the adaptation mechanism. In our work, a proposed modification consists of using the sliding mode observer of section 4.5.2 as a reference model due to its performance and robustness. Then, it will be compared with an adaptive model for speed computing. The design of MRAS estimator in this case bases on a stator flux model instead of the well-known rotor flux model in order to be more suitable for DTC control algorithm.

The previous SMO model is given in (4.19) and the adaptive model (current model) is given as follows:

$$\begin{cases} \hat{\psi}_{s\alpha} = \frac{L_r}{R_r + L_r s} \left(\sigma L_s \hat{\omega} i_{s\beta} + \frac{L_s}{L_r} (R_r + \sigma L_r s) i_{s\alpha} - \hat{\omega} \hat{\psi}_{s\beta} \right) \\ \hat{\psi}_{s\beta} = \frac{L_r}{R_r + L_r s} \left(\sigma L_s \hat{\omega} i_{s\alpha} + \frac{L_s}{L_r} (R_r + \sigma L_r s) i_{s\beta} - \hat{\omega} \hat{\psi}_{s\alpha} \right) \end{cases} \quad (4.28)$$

The error between the reference and the adaptive mode can be given by:

$$\begin{cases} e_{\psi_{s\alpha}} = \psi_{smo_s\alpha} - \hat{\psi}_{s\alpha} \\ e_{\psi_{s\beta}} = \psi_{smo_s\beta} - \hat{\psi}_{s\beta} \end{cases} \quad (4.29)$$

$\psi_{smo_s\alpha}, \psi_{smo_s\beta}$ are the estimated stator flux components using SMO.

The error adaptive signal can be expressed by:

$$e_{\psi_s} = \left(\psi_{smo_s\beta} \hat{\psi}_{s\alpha} - \psi_{smo_s\alpha} \hat{\psi}_{s\beta} - \left(i_{s\alpha} e_{\psi_{s\beta}} - i_{s\beta} e_{\psi_{s\alpha}} \right) \sigma L_s \right) \quad (4.30)$$

Then a conventional PI controller is used as adaptation mechanism.

The block diagram of the association of MRAS estimator with SMO is presented in **Fig.4.33**.

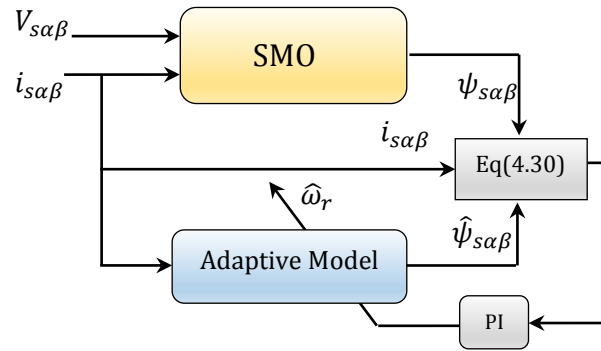


Fig.4.33 Association of Stator Flux model-MRAS speed observer with SMO.

4.8.1 Simulation results

This section presents the simulation results of sliding mode observer associated to MRAS as a speed estimator. The figures below focus on speed estimation under the operation conditions presented previously.

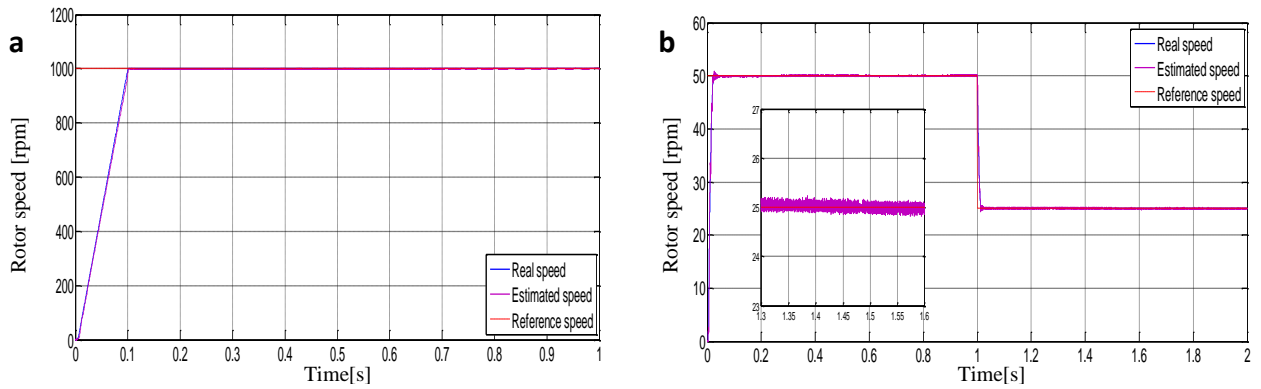


Fig.4.34 a: Starting up and steady state (1000 rpm), **b:** low speed operation (50 rpm;25 rpm).

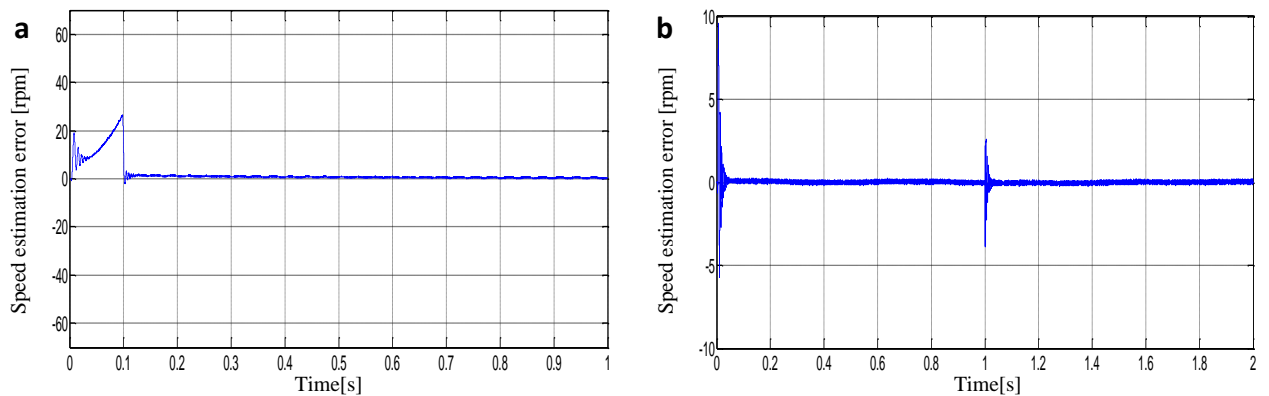


Fig.4.35 a: Speed estimation errors at 1000 rpm, **b:** Speed estimation errors at low speeds (50 rpm;25 rpm).

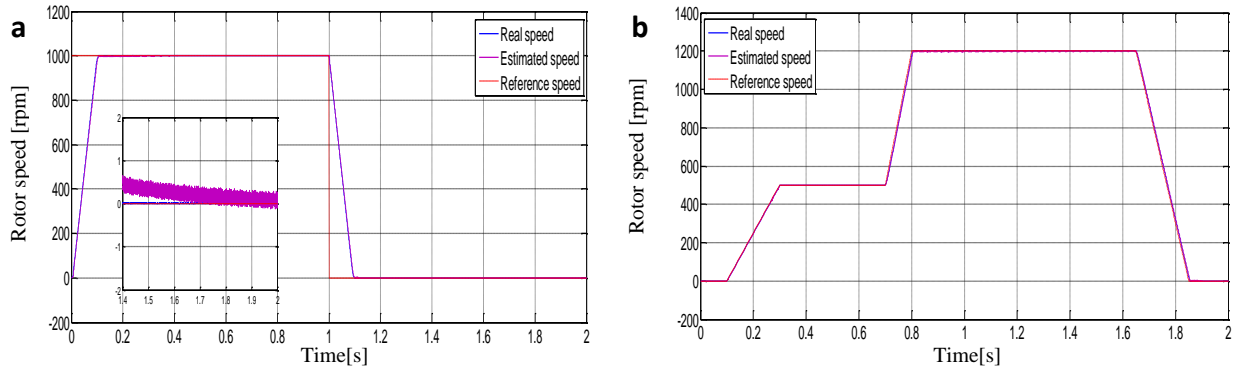


Fig. 4.36 a: Zero-speed operation, **b:** variable profile (benchmark) tests.

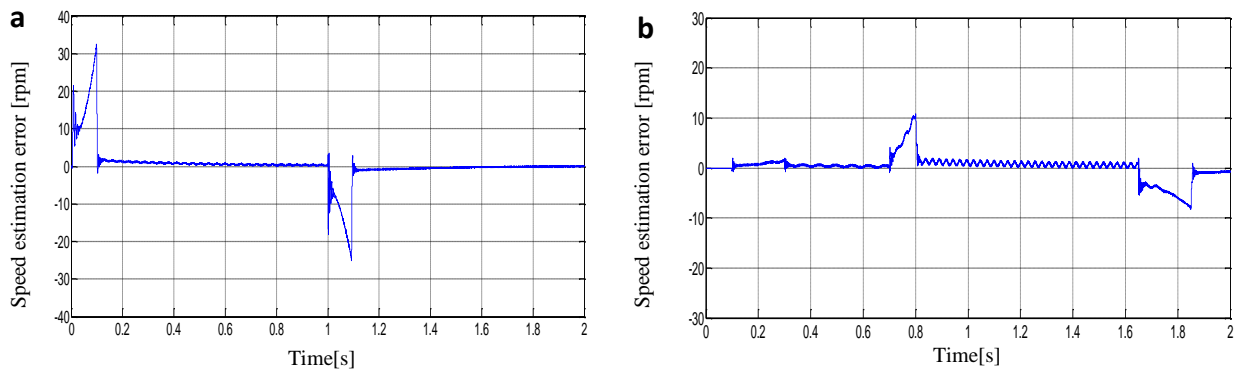


Fig.4.37 a: Speed estimation errors at zero-speed, **b:** at variable profile (benchmark) tests.

Fig.4.34(a) shows the starting up and the steady states according to step of 1000 rpm , while the low speed test of $(50\text{ rpm}-25\text{ rpm})$ is illustrated in **Fig.4.34(b)**. Then, the estimation errors are presented in **Fig.4.35**. It can be observed that the association of MRAS provides more accuracy and stability in high and low speed values. In addition, it minimizes the error in both transient and steady states. After that, **Figs.4.36-4.37** depict the zero-speed operation and benchmark trajectory tests with their estimation error. It can be seen in **Fig.4.36(a)** and **Fig.4.37(a)** that the new observer structure kept a correct estimation at zero speed/ frequency values. Moreover, in **Fig.4.36(b)** the SMO-MRAS observer provides a better superposition between speed quantities during the instantaneous variation. It can be justified in **Fig.4.37(b)** where the error has been minimized.

The following table compares the estimation accuracy between all the presented observers.

Observer	Adaptive observer	SMO	Associated MRAS-SMO
Static error (%)	$\approx 0.5\%$	$\approx 0.1\%$	$\approx 0.06\%$
Dynamic error (%)	$\approx 0.092\%$	$\approx 0.25\%$	$\approx 0.083\%$

Table.4.1 Comparative analysis between different observer structures.

4.8.2 Experimental results

The experimental validation of the proposed associated sliding mode observer with stator flux based MRAS for speed estimation is presented in **Figs.4.38-4.39**.

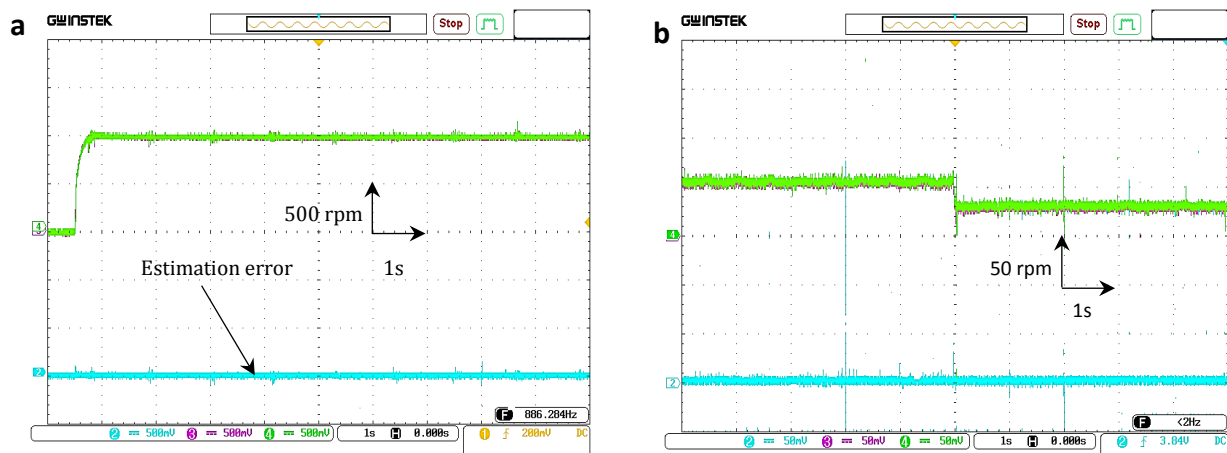


Fig.4.38 a: Starting up and steady state (1000 rpm), **b:** low speed operation (50 rpm ; 25 rpm) with estimation errors.

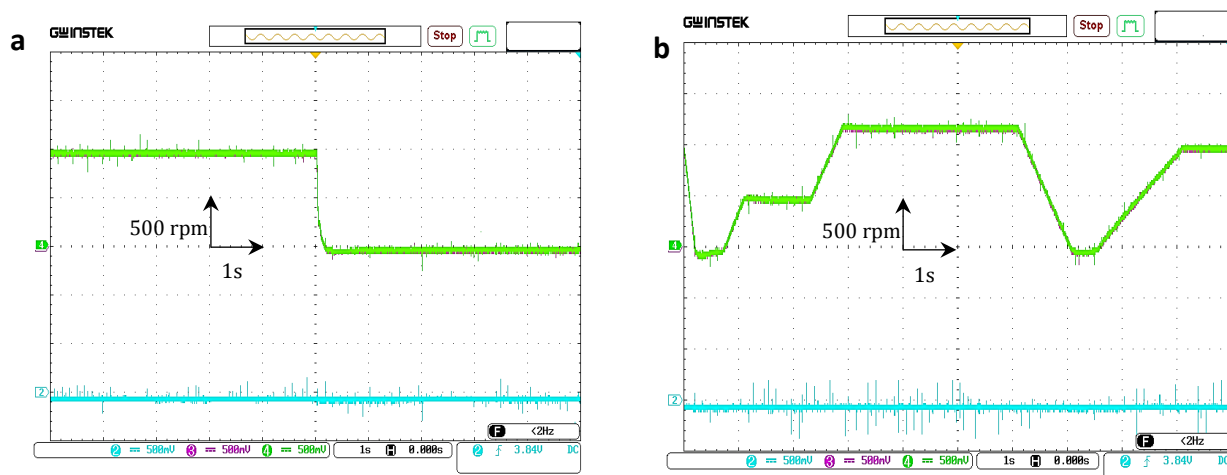


Fig.4.39 a: Zero-speed operation, **b:** variable profile tests with estimation errors.

The starting up is illustrated in **Fig.4.38(a)** ($1\text{div}=500\text{ rpm}$). By comparing the shown results to those presented in **Fig.4.24**, it can be deduced that the MRAS speed estimator provides the smoothest starting up and best accuracy in transient state compared to the adaptive and the SMO observers. The estimation error has been reduced. **Fig.4.38(b)** illustrates the low speed operation test of (50 rpm - 25 rpm) ($1\text{div}=50\text{ rpm}$). We can see that the main improvement of inserting the MRAS in SMO has appeared here, where, MRAS has solved the problem of the sensitivity to noise of the SMO in low regions. The figure shows that the estimated and the measured speed have good superposition with stability and without fluctuations.

Then, **Fig.4.39(a)** presents the zero-operation test. It can be seen that the estimation is accurate and estimation error converges always to zero. Finally, the variable speed profile

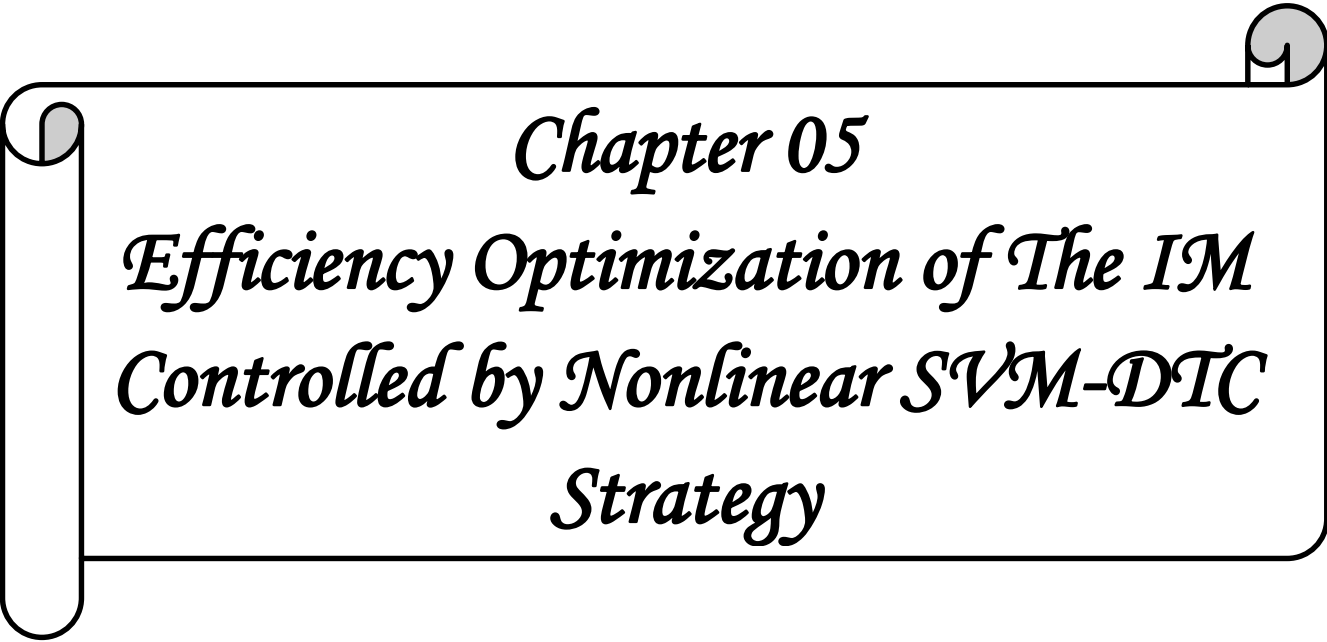
is implemented in **Fig.4.39(b)**. The speed quantities show perfect superposition and minimized error. Furthermore, the associated MRAS-SMO is more stable during the instantaneous speed variation compared to SMO in **Fig.4.31**. We conclude briefly, that the conjunction of MRAS with sliding mode observer combines the advantages of both algorithms and provides more accurate estimation.

4.9 Conclusion

This chapter has presented the estimation and the sensorless control of the induction machine which consist of association of the nonlinear SVM-DTC strategy to various observer structures. Alternative stator flux open loop estimators have been proposed firstly to solve the problems of the conventional back-emf integration. Then, we have recounted about closed loop observers and their problems in low speed.

In application part, a full order adaptive observer is compared to a non-adaptive observer based on sliding mode approach. The effectiveness and the estimation accuracy of both designs have been verified using simulation and experimental tests. Different operation conditions of the IM have been employed, such as: starting up, low and zero speeds operation, and a benchmark trajectory in different regions. The simulation and experimental results show that SMO presents good estimation accuracy in high and low speed regions and minimize the static error which has been provided by the adaptive observer. A zero frequency and industrial benchmark tests have been employed in order to check the stability and the robustness of the sensorless scheme in this operation conditions. The conjunction of MRAS with SMO for speed estimation preserves its accuracy and stability even in this condition also and improves the performance of the sensorless DTC drives.

The next chapter will present the association of the control scheme with losses minimization strategy for the purpose of the maximization of energy efficiency of the machine. This technique can be a complement to get more performance to the developed algorithm which treated various issues in one control scheme.



Chapter 05
Efficiency Optimization of The IM
Controlled by Nonlinear SVM-DTC
Strategy

5.1. Introduction

The last chapter has presented sensorless control strategy composed of nonlinear SVM-DTC with speed/flux and load torque observers. Despite of the advantages of the proposed control strategy, it can get more high performance by achieving the maximum of efficiency. Today induction motors are responsible for about 60% of the total industrial electric power consumption, and obviously, their power efficiency is a serious issue [Stu13]. The control using constant reference of flux magnitude can be non-optimal for some operations, especially, concerning the power losses and the absorbed currents. In addition, the efficiency of the IM can be reduced when the reference flux is maintained to an initial value at light loads [Bou07; Haj09]. The variable flux reference is applied in many works. This operation can be able to optimize certain quantities without significant degrading in the dynamic performances.

The control algorithms to find an optimum flux level can be divided into two categories, search controller (SC) and loss-model-based controller (LMC) [Abr98]. The principle of SC is to measure the input power and to search iteratively for the flux level (or an equivalent variables) until the minimum of input power is detected while the output power of the motor is constant. The slow convergence and the high torque ripples are important drawbacks of this method. On the contrary, LMC computes the flux level using the machine model to minimize the losses. This algorithm is faster and does not produce torque ripples [Udd08]. However, its accuracy depends on the correct modeling of machine and the knowledge of its parameters [Haj10].

The objective of this chapter is the association of an efficiency maximization strategy based on losses minimization with the robust DTC control scheme. This strategy is related to the optimum choice of the proposed flux level according to the desired load value. It is known that the high flux values increase the iron losses in magnetic circuit and drive the machine to saturation, thus, an optimal flux value should be chosen [Had07]. The model based optimization method (LMC) uses the steady-state IM model in the rotor flux field orientation coordinates frame to generate the optimal flux reference which will be tuned online and make the machine efficiency optimized. The results will be examined by simulation and experimental implementation.

5.2. Steady State Performance, Power Losses and Efficiency of The IM

5.2.1 Per phase equivalent circuit of IM

The computation of the steady state characteristic quantities of the induction machine is the first step in energy efficiency optimization. The study of electrical steady-state of induction motor is achieved by developing an equivalent circuit which can illustrate the transfer of the power from stator to rotor, thereafter, into mechanical form. The simplified per phase equivalent circuit of the induction motor is presented in **Fig.5.1**

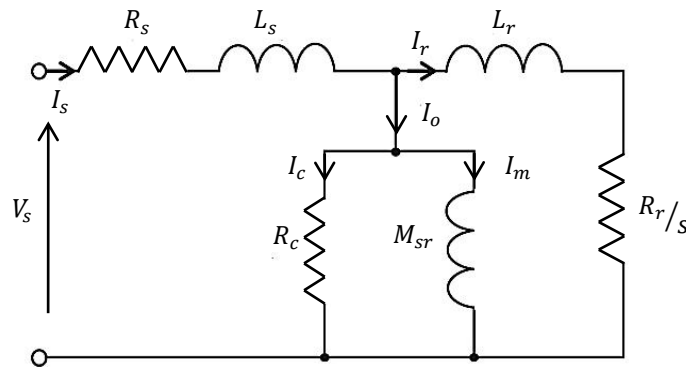


Fig. 5.1 Per-phase steady state equivalent circuit of IM.

where s is the slip, R_c is stator core loss resistance.

Referring to **Fig.5.1**, a voltage of R.M.S. value V_s is applied to the stator, then a current of R.M.S. value I_s flows in the stator windings. A part of the voltage is absorbed by the stator winding resistance and leakage inductance and the remainder is used to generate the revolving field. The current has two components, the no load (exciting) current I_o and the induced rotor current I_r . The no load current also has two components, the reactive magnetizing current I_m and the active current I_c .

5.2.2 Power Losses of IM

The losses which appear at fundamental frequency are the stator copper losses, the rotor copper losses, the core (iron) losses, the stray load losses and the mechanical losses (friction and windage). Three of this five component losses can be identified from the per-phase induction motor equivalent circuit shown in **Fig.5.1**.

5.2.2.1 Stator and rotor copper losses

The electrical windings always have resistance, however small it is, it causes ohmic power losses. They are also called Joule losses.

The stator and rotor copper losses are calculated by:

$$P_{sc} = R_s I_s^2 \quad (5.1)$$

$$P_{rc} = R_r I_r^2 \quad (5.2)$$

P_{sc} , P_{rc} are the stator and rotor copper losses respectively.

I_s , I_r are the R.M.S. values of stator and rotor phase currents respectively.

5.2.2.2 Core losses

In every cycle of operation, the flux in the core of the induction motor will be reversed causing a small losses of energy usually called hysteresis losses. Another component in iron losses, is the eddy current losses which caused by the induced current flowing in the core. In order to reduce these losses, the magnetic circuits are laminated using thin insulated sheets clamped together. However, small eddy current losses will remain. The most common way of modeling the core losses in case of sinusoidal flux distribution is to use the following Steinmetz expressions of hysteresis and eddy current losses [Abr00]:

$$P_c = P_{hs} + P_{es} = K_h f_s \psi_s^2 + K_e f_s^2 \psi_s^2 \quad (5.3)$$

where:

P_{hs} , P_{es} : stator hysteresis and eddy-current losses respectively,

K_h , K_e : hysteresis and eddy-current coefficients related to the magnetic circuit properties.

f_s : stator frequency.

The rotor core losses can be calculated by using the same expression (5.3) but with slip frequency instead of stator frequency multiplying with the ratio of the masses of rotor and stator core material.

5.2.2.3 Mechanical losses

These mechanical losses contain the friction and windage power losses. The friction losses are the result of friction between the moving parts, the windage power losses is the result of the air circulating inside the motor for cooling purposes. In general, both friction and windage losses are proportionally dependent on the motor speed. Consequently, they will drop at low speed level conditions.

5.2.2.4 Stray load losses

The copper, the core and the mechanical losses can be estimated from no load and short-circuit tests that can be performed on the induction motor. The measured losses while the presence of load are certainly greater by the amount, which called stray load losses. They consist of additional losses caused by stator slot effects and skin effect in conductors. Despite their importance, the quantification of these losses is not considering in our study.

5.2.2.5 Converters losses

There are also some additional losses when the induction motor is fed by a non-sinusoidal supply (harmonics and switching losses), such as voltage source inverter, but the use of PWM techniques can reduce these losses significantly. In addition, there is no clear relationship between harmonic losses and motor flux level. Therefore, and because these losses are not important for small size/power induction machines, they will not be included in the energy optimal control algorithm.

5.2.3 Induction motor efficiency and power factor

The efficiency of the induction motor is the ratio of output power to the input power. Mathematically, the machine efficiency can be formulated as:

$$\eta = \frac{P_{out}}{P_{in}} = \frac{P_{in} - \sum losses}{P_{in}} = \frac{P_{out}}{P_{out} + \sum losses} \quad (5.4)$$

with:

$$\sum losses = P_{sc} + P_{rc} + P_c + P_{mec} \quad (5.5)$$

where:

η is the efficiency

P_{in} , P_{out} are the input and the output power values.

P_{mec} are the mechanical losses.

The power factor of the machine is defined as the quotient of the input power to the volt-ampere quantity as expressed in the following:

$$PF = \frac{P_{in}}{V_s I_s} \quad (5.6)$$

By considering that the induction motor fed from sinusoidal balanced three phases power supply, the power factor is given as:

$$PF = \frac{V_s I_s \cos(\varphi)}{V_s I_s} = \cos(\varphi) \quad (5.7)$$

where φ is the phase angle between the phase voltage and current of the induction motor.

5.3. Efficiency Optimization Methods of IM

The operating point of IM corresponds to the point where it drives with a full load and almost it is efficient at this point. However, there are many applications where the motor needs to be driven at different load values. For FOC or DTC controlled drives the motor is always fed with rated flux. This condition can be highly undesirable with light loads. Several induction motor drive efficiency improvement methods have been reported in the literature. In general, they can be divided into power measurement based approach, known by search controllers (SCs) and the so-called loss-model based approach. It is also termed as loss model controller (LMC) [Udd08].

5.3.1 Search control (SC)

The search controller is preferred by many researchers because the controller action works on the principle of input power measurement and does not depend on machine parameters. SC adjusts iteratively the control variable (flux or d-axis current) online based on the input power measurement until the minimum power is detected for a given torque and speed. However, this strategy requires more sensors to carry out these measurements. Consequently, this process can be very expensive [Sul88]. To overcome this shortcoming, the DC link power is measured instead. It involves the use of one extra current sensor. The biggest issue with this approach is that the input power must be accurately measured to avoid the appearance of oscillatory response. Also, this kind of controllers is plagued by torque ripples [Gar94].

5.3.2. Loss model based controller (LMC)

Unlike search controller, LMC uses the machine losses modeling to find the loss minimization criteria which adjust the rotor flux level. For Direct Torque Control (DTC) drive, the stator flux linkage can be utilized for loss minimization [Had07; Wan15]. The interest advantage of using LMC approach is not exhibiting torque ripples and it is featured by fast convergence when it is compared to SC. However, considering that LMC utilizes the loss model, the performance of the controller is related to the accuracy of this model.

5.4 Application of Losses Minimization with Nonlinear DTC Control Scheme

5.4.1 Induction motor loss model in (d, q) reference frame

As a summary of the above, the machine losses can be divided into uncontrollable and controllable losses. Controllable losses are manipulable by the controlled variables (i.e. stator current) while the uncontrollable losses are only influenced by the induction machine design [Stu13].

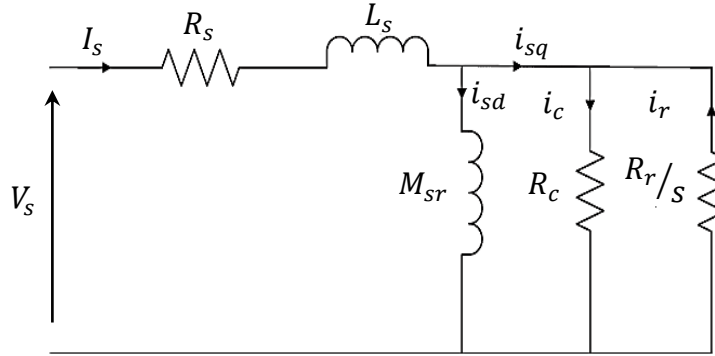


Fig.5.2 Induction motor equivalent circuit in (d, q) frame.

Fig.5.2 shows the equivalent circuit of induction motor in the (d, q) coordinates frame which rotates synchronously with an electrical angular velocity ω_s . The equivalent circuit includes the effects of the copper and iron losses. The copper losses are represented by the stator and rotor resistances R_s and R_r , whereas the iron losses are represented by the resistance R_c .

With the aid of the (d, q) model of induction motor, these losses can be computed as in terms of direct and quadratic stator current components i_{sd} and i_{sq} , as follows:

Stator copper losses:

$$P_{sc} = R_s i_s^2 = R_s (i_{sd}^2 + i_{sq}^2) \quad (5.8)$$

Rotor copper losses:

$$P_{rc} = R_r i_r^2 = R_r (i_{rd}^2 + i_{rq}^2) \quad (5.9)$$

Since the rotor currents are inaccessible, they are expressed in terms of the known stator current and rotor flux by [Bou07]:

$$i_{rd} = \frac{1}{L_r} \psi_r - \frac{M_{sr}}{L_r} i_{sd} \quad (5.10)$$

$$i_{rq} = -\frac{M_{sr}}{L_r} i_{sq} \quad (5.11)$$

Then, by substituting (5.10) and (5.11) in (5.9), the rotor copper losses can be given by:

$$P_{rc} = R_r \left[\left(\frac{\psi_r}{L_r} - \frac{M_{sr}}{L_r} i_{sd} \right)^2 + \left(-\frac{M_{sr}}{L_r} \right)^2 \right] \quad (5.12)$$

According to [Lim04], the stator core losses in (d, q) reference frame are given by:

$$P_c = (\omega_s M_{sr})^2 \frac{1}{R_c} i_{sd}^2 \quad (5.13)$$

The rotor core losses are very small compared to stator losses and they are mostly neglected.

5.4.2 Loss minimization algorithm

The loss model control (LMC) strategy based on minimizing the motor losses in steady-state by adjusting the rotor and stator flux to an optimal value to achieve the maximum of efficiency and minimize the total losses especially at light load values [Bab97]. In our work, the efficiency optimization consists of minimizing the stator and rotor copper losses in steady state. The total copper losses expression is given by the sum of stator and rotor copper losses:

$$P_{c_loss} = P_{sc} + P_{rc} \quad (5.14)$$

Based on rotor flux and electromagnetic torque expressions in (d, q) rotor field oriented frame, the current components i_{sq} and i_{sd} can be written as:

$$i_{sd} = \frac{\psi_{rd}}{M_{sr}} \quad (5.15)$$

$$i_{sq} = \frac{T_e L_r}{p M_{sr} \psi_{rd}} \quad (5.16)$$

Then, the total losses expression can be written in terms of electromagnetic torque and rotor flux:

$$P_{c_loss} = \frac{R_s}{M_{sr}^2} \psi_r^2 + \left[\frac{R_r}{p^2} + R_s \left(\frac{L_r}{p M_{sr}} \right)^2 \right] \frac{T_e^2}{\psi_r^2} \quad (5.17)$$

The optimal flux can be founded in the steady state by setting the derivative of total copper losses expression with respect to the rotor flux to zero [Bou07; Stu13]:

$$\frac{\partial P_{c_loss}}{\partial \psi_r} = 0 \quad (5.18)$$

Thus, the optimal reference value of the rotor flux $\psi_{r_opt}^*$ is a function of the electromagnetic torque and the machine parameters in field oriented (d,q) system:

$$\psi_{r_opt}^* = \lambda_{opt} \sqrt{T_e^*} \quad (5.19)$$

The coefficient λ_{opt} is given by:

$$\lambda_{opt} = \left(\frac{\lambda_2}{\lambda_1} \right)^{1/4} \quad (5.20)$$

where:

$$\lambda_1 = \frac{R_s}{M_{sr}^2}; \quad \lambda_2 = \frac{R_r}{p^2} + R_s \left(\frac{L_r}{pM_{sr}} \right)^2$$

The imposed reference value of rotor flux changes between a minimal to an optimal value according to the desired torque value [Reh11]. For the DTC controlled induction motor drive, the optimal reference value of the stator flux $\psi_{s_opt}^*$ can be deduced by [Taz15]:

$$\psi_{s_opt}^* = \frac{L_s}{M_{sr}} \sqrt{\left(\psi_{r_opt}^* \right)^2 + \left(\frac{\sigma L_r}{p} \right)^2 \left(\frac{T_e^*}{\psi_{r_opt}^*} \right)} \quad (5.21)$$

5.4.3 The optimal choice of flux level

During the application of losses minimization strategy (LMC) the machine operates with variable flux level. However, this variation should not exceed the nominal value of the flux ψ_{r_nom} to avoid saturation of the machine [Bou07]. Also, the flux level should not decrease under a minimal level to avoid degrading control performances.

Thus, the optimal flux is given by:

$$\begin{cases} \text{if } \psi_{r_opt}^* > \psi_{r_min} \text{ then } \psi_r^* = \psi_{r_opt}^* \\ \text{else } \psi_r^* = \psi_{r_min} \end{cases} \quad (5.22)$$

Therefore, the optimum flux is defined in range of flux variation limited by a minimum and maximum flux (ψ_{r_min} , ψ_{r_max}) values, this limitation is defined in [Bab97] as:

$$\psi_{r_min} < \psi_{r_opt}^* \leq \psi_{r_max} \quad (5.23)$$

and $\psi_{r_min} = 20\%(\psi_{r_nom})$ and $\psi_{r_max} = \psi_{r_nom}$

Fig.5.3 shows the global block diagram of robust SVM-DTC with efficiency optimization.

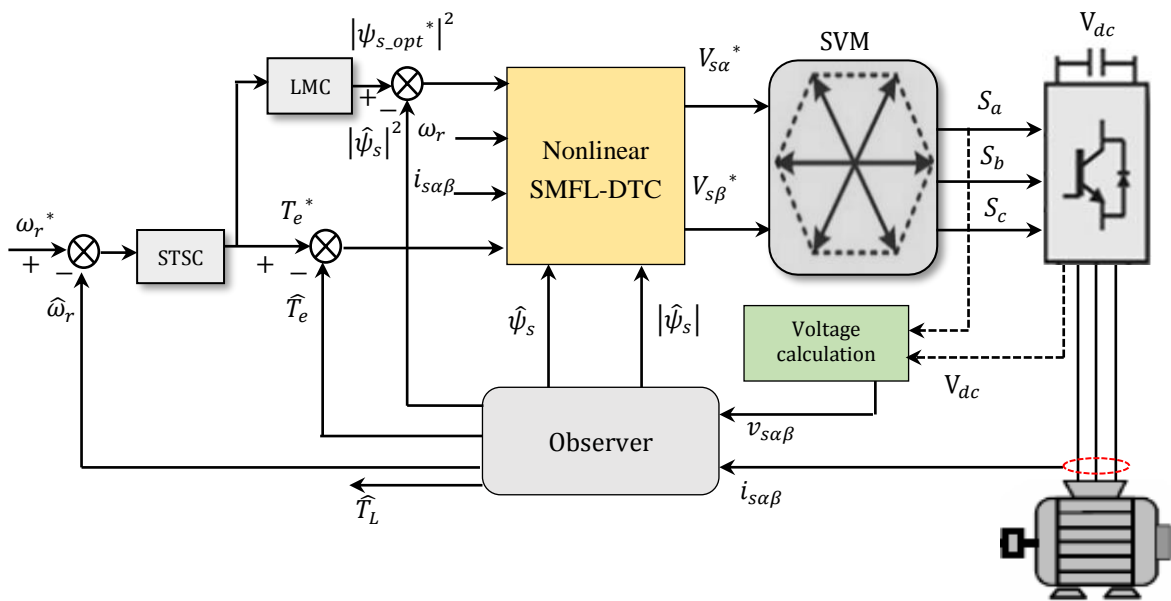


Fig.5.3 Block Diagram of SVM-DTC with efficiency optimization strategy.

5.5 Simulation Results

The simulation results exhibit the comparative study of the control scheme with constant flux reference (1Wb) and optimal flux reference which is generated by LMC strategy. The following figures (**Figs.5.4-5.9**) illustrate the transient and the study state with load introduction of 4 N.m at $t=0.5\text{ s}$. The figures are specified ((a) for the constant and (b) for optimal flux reference). The **Fig.5.10** shows the total losses and the efficiency for both cases.

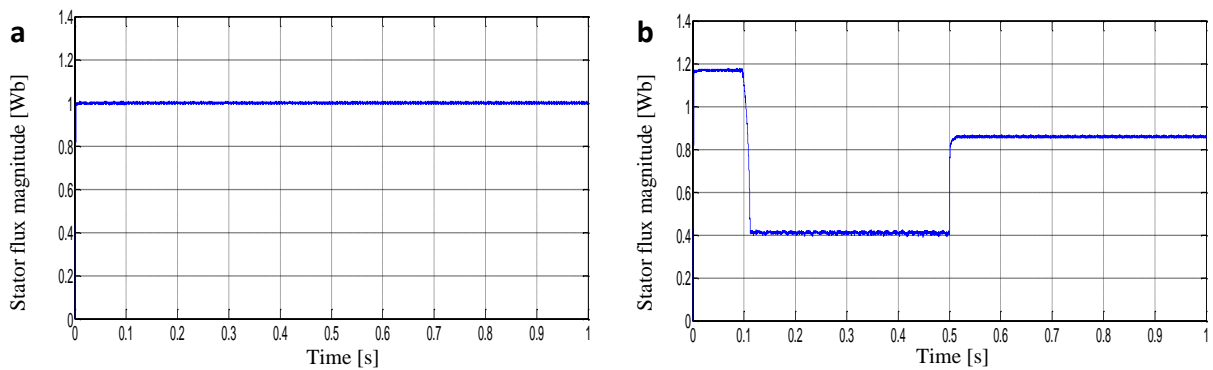


Fig.5.4 Stator flux magnitude [Wb].

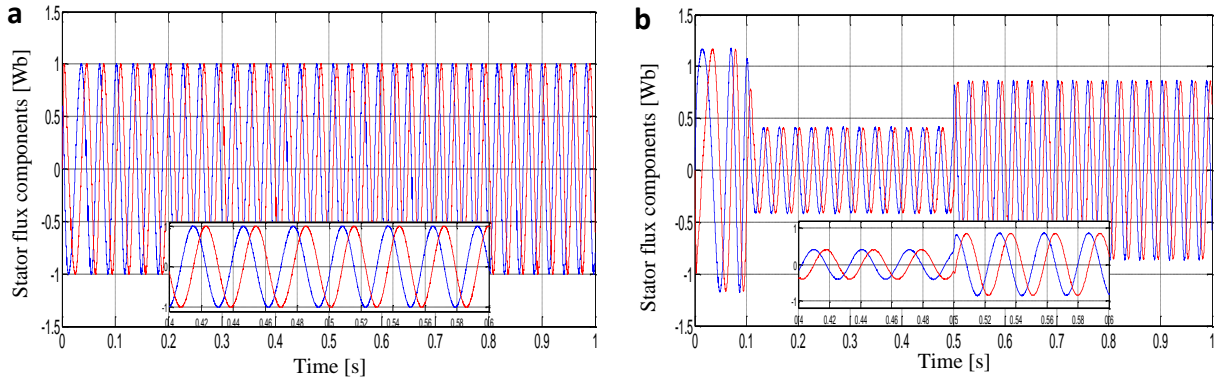


Fig.5.5 Stator flux axes components (α, β) [Wb].

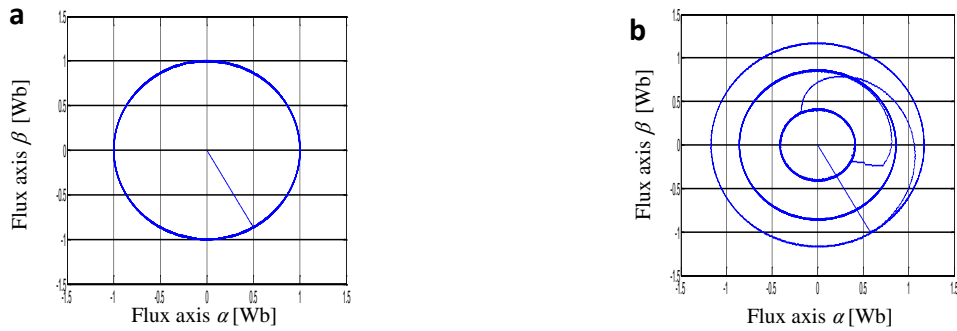


Fig.5.6 Stator flux trajectory [Wb].

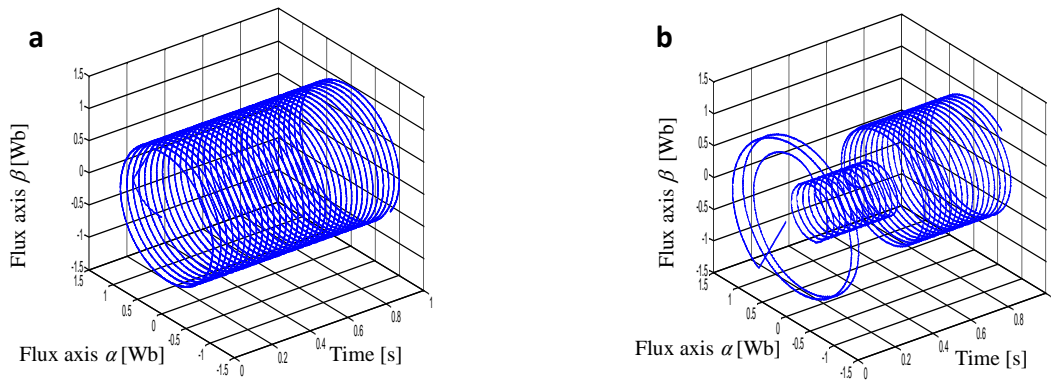


Fig.5.7 Three dimensional (3D) presentation of stator flux trajectory [Wb].

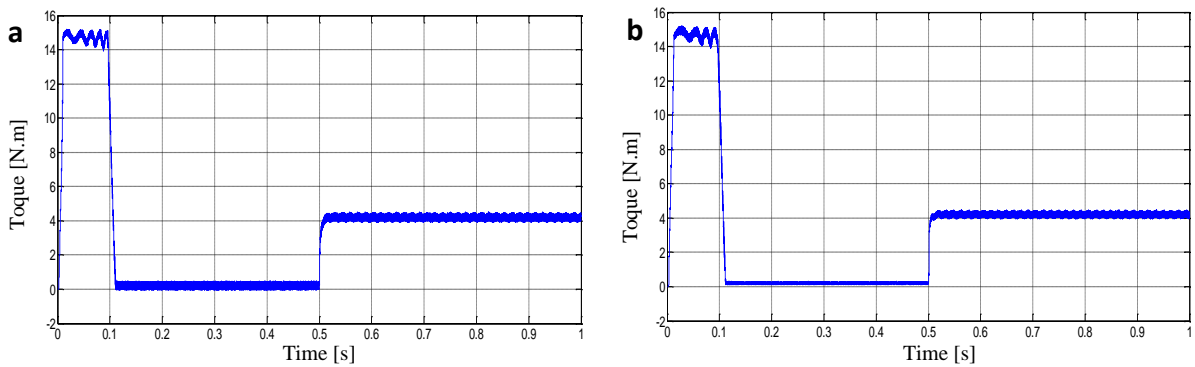


Fig.5.8 Electromagnetic torque with load application of (4N.m)

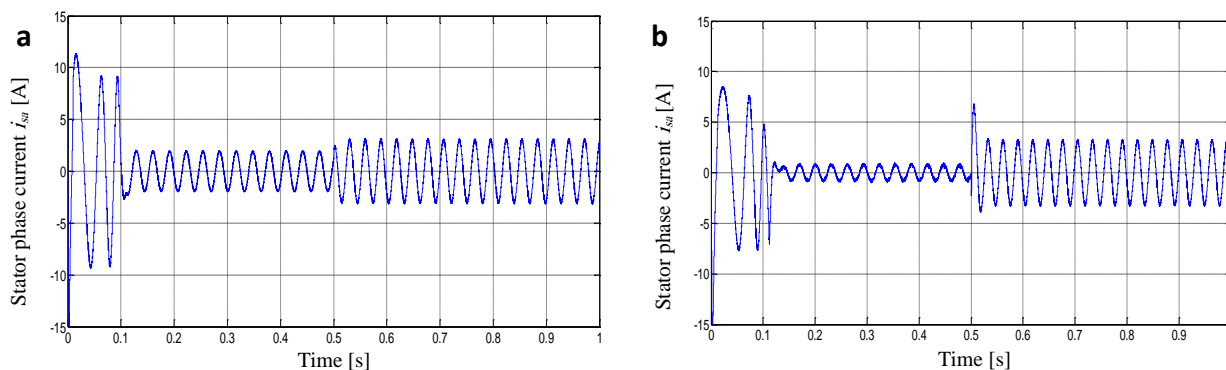


Fig.5.9 Stator phase current i_{sa} [A].

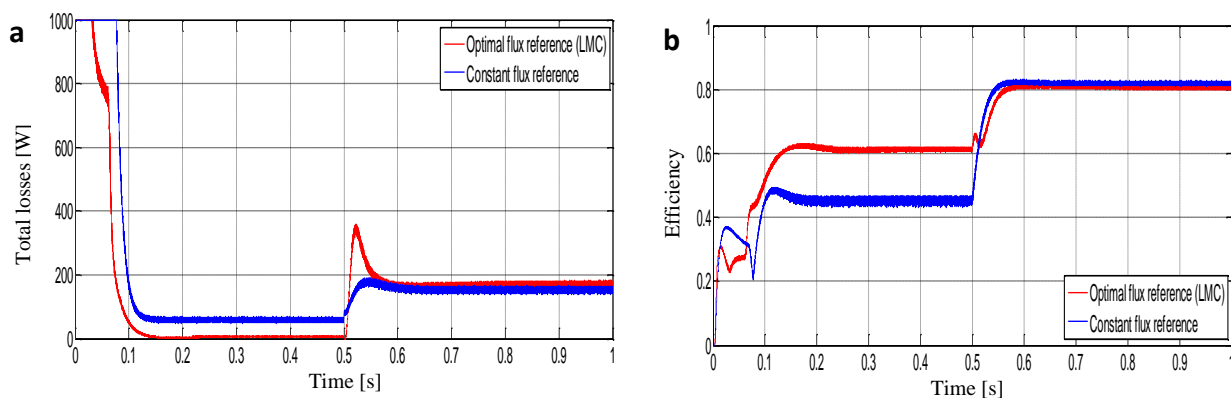


Fig.5.10 Total losses [W] and efficiency.

Firstly, **Figs.5.4-5.6** present the flux magnitude, components and circle trajectory. The proposed nonlinear SVM-DTC control strategy with LMC in **Figs.5.4(b)-5.6(b)** shows the optimal flux variation according to the load application contrary to the constant flux of ($1Wb$) in **Fig.5.4(a)-5.6(a)**. We can see that after the transient state, the flux takes an optimal value in steady state in order to minimize the losses. Consequently, the optimized technique shows its performance. **Fig.5.7** shows the evolution of flux trajectory in 3D presentation. This figure can explain clearly the optimal flux variation and conclude the main idea of optimization principle. Next, in **Fig.5.8**, the electromagnetic torque is shown. The optimized algorithm presents a reducer ripples level especially at no load state. **Fig.5.9** illustrates the stator phase current. We can notice in **Fig.5.9(b)** that the proposed technique shows an apparent reduction in current amplitude at no load operation owing to the optimal flux choice. This reduction in current can reduce considerably the copper losses in this state. Then, the **Fig.5.10** shows the total losses and efficiency of both control algorithms. We deduce that the optimized SVM-DTC with LMC has the lower losses value at no load or at light load state. As a result, it provides better efficiency than using a constant flux reference.

5.6 Experimental Results

This section presents a comparative study of nonlinear SVM-DTC with constant and optimal flux references into two phases. The figures are specified ((a) for constant flux and (b) for optimal flux references).

5.6.1 Starting up, steady state and load application

Fig.5.11-5.14 show the starting up and steady state followed by load application of 4 N.m.

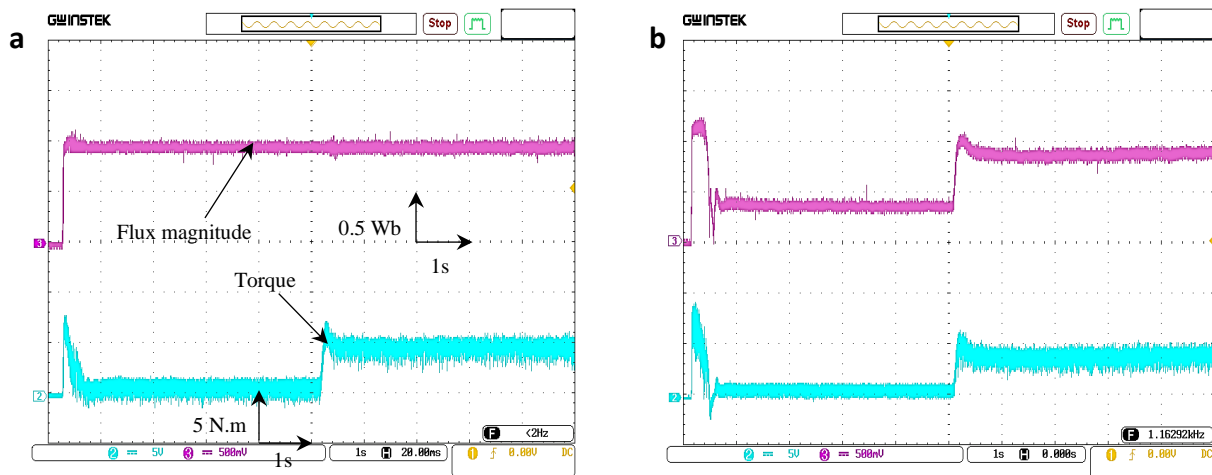


Fig.5.11 Stator flux magnitude [Wb] and electromagnetic torque [N.m].

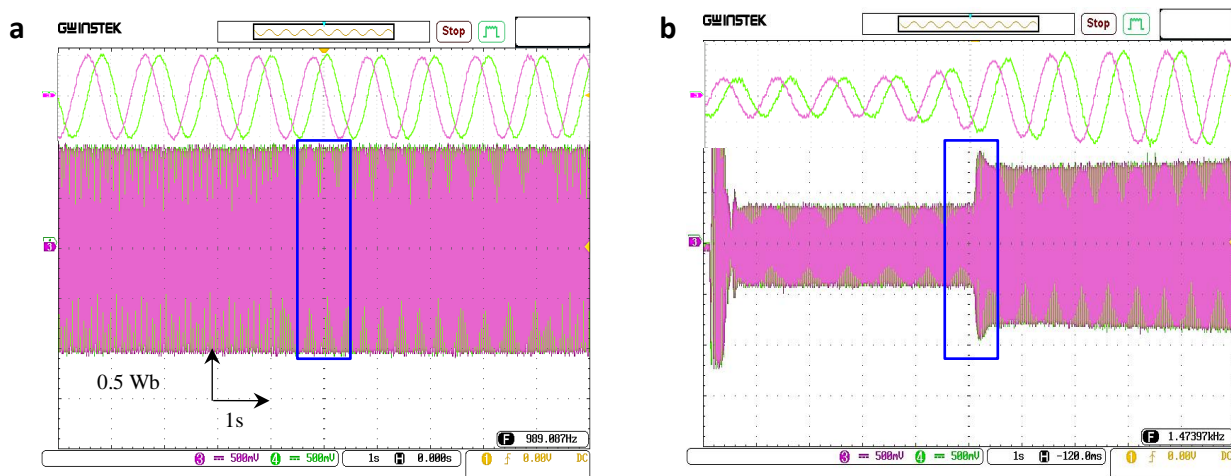


Fig.5.12 Stator flux components with zoom [Wb].

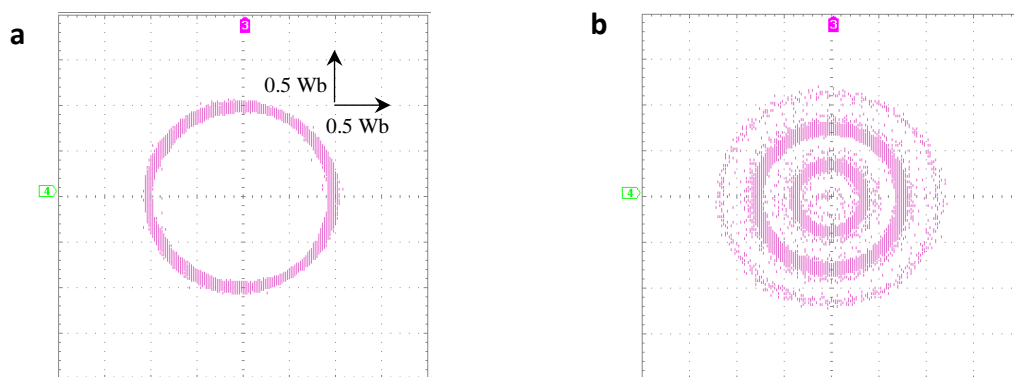


Fig.5.13 Stator flux trajectory [Wb].

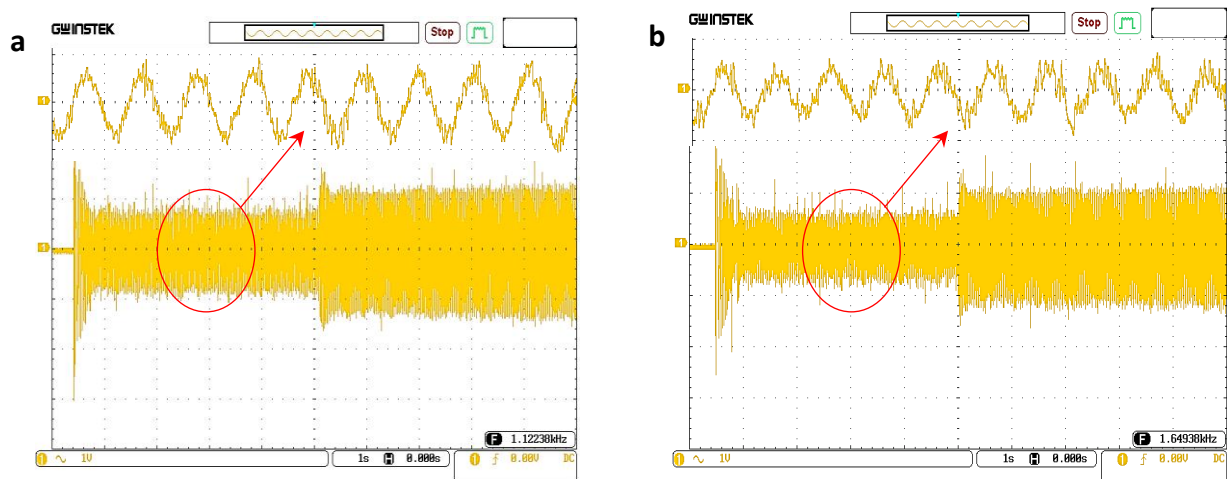


Fig.5.14 Stator phase current [A].

Figs.5.11-5.14 show the comparison between the constant and optimal flux references. The performed tests are similar to those have been conducted in simulation section. **Fig.5.11** illustrates the flux magnitude ($0.5Wb=1div$) and the electromagnetic torque ($1div=5N.m$) during the starting up, steady state, then the load application of 4 N.m. The figure shows the comparison between the constant and the optimal flux evolution according to load value. It can be observed that the optimized technique has the reducer ripples level at no load and light load values. **Figs.5.12-5.13** present the stator flux components and trajectory in both cases of constant and optimal flux reference in order to clarify more the evolution of flux due to load variation. Then, **Fig.5.14** illustrates the stator phase current, it can be seen during no load operation that the optimal control strategy provides lower current amplitude than constant reference based strategy. Hence, the copper losses can be minimized in this operation.

5.6.2 Application of different load values in steady state

This second phase presents efficiency computing and flux level estimation for both cases (i.e. constant and variable flux level) under different light load values, (*no load, 0.5 N.m, 1 N.m, 1.5 N.m and 2 N.m*).

To understand more the instantaneous variation of flux level, **Fig.5.15** presents flux evolution and torque response according to load application (0-2 N.m). **Fig.5.16** illustrates the comparison of the calculated machine efficiency at 1200 rpm of speed and 400 V as input voltage. Then, **Table 5.1** and **Fig.5.17** summarized the efficiency analysis of the IM controlled by nonlinear SVM-DTC with energy optimization.

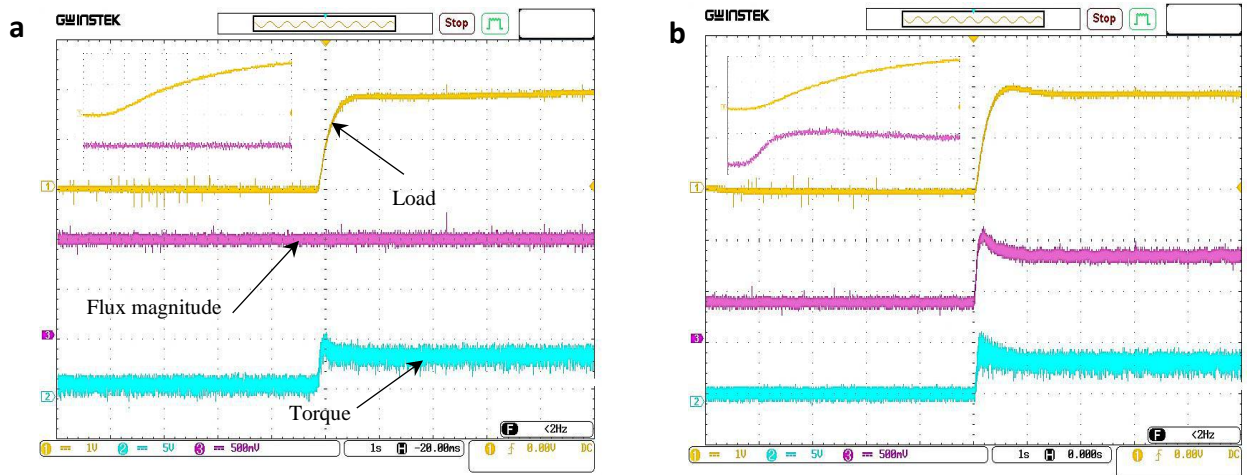


Fig.5.15 Flux and torque according to the applied load value (0-2 N.m).

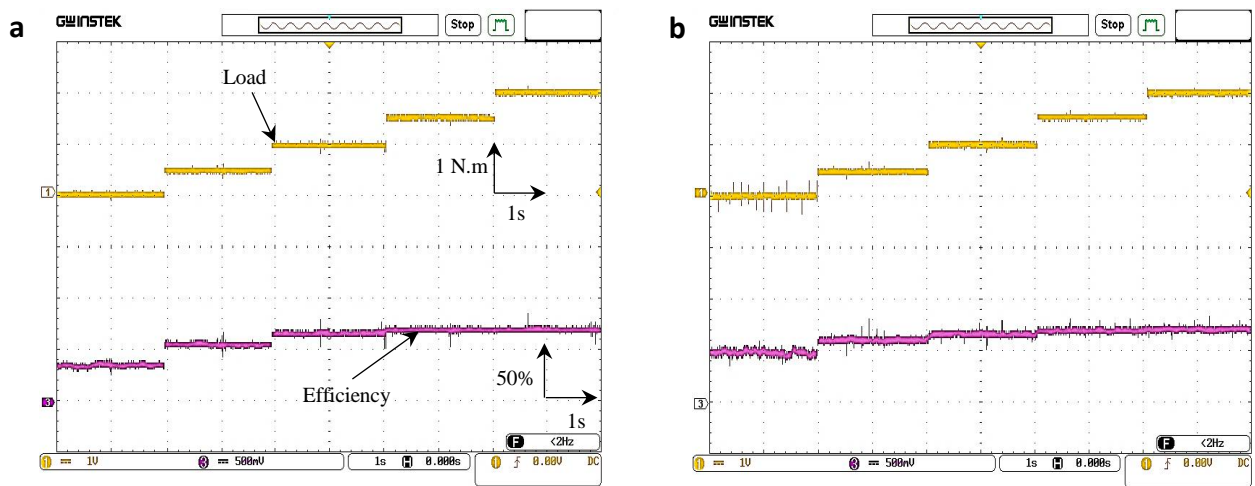


Fig.5.16 Load variation and Efficiency.

Load [N.m] [%]	Constant flux magnitude		Optimal flux magnitude	
	Flux magnitude [Wb]	Efficiency [%]	Flux magnitude [Wb]	Efficiency [%]
0 (0%)	1	42	0.4	50.5
0.5 (7%)	1	60	0.55	64.9
1 (14%)	1	71.6	0.66	72.1
1.5 (21%)	1	75	0.75	75.5
2 (28%)	1	75.5	0.9	76.4

Table.5.1 Induction motor efficiency analysis under different load values.

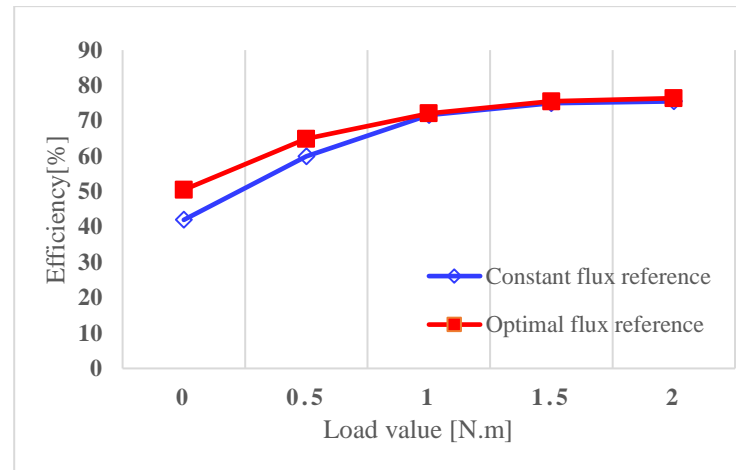


Fig.5.17 Curve of efficiency evolution according to different load values.

From **Fig. 5.16** and the curve in **Fig.5.17** and **Table.5.1** we deduce the following summary: The flux level in case of the nonlinear SVM-DTC optimized by LMC strategy increases depending on the increase of load value to achieve the necessary torque. It can be seen that the effectiveness of optimization strategy appears clearly at no or small loads, referring to the table (0 to about 0.75 N.m). Thereafter, this effectiveness decreases gradually with the increase of load value. We observed at 1 N.m load that the difference between efficiencies has begun to diminish until their values have approached at 1.5 N.m load. It can be concluded that LMC strategy can be useful for low load applications. In addition, it has the ability to adjust the flux level for each rated load value.

5.7. Conclusion

In this chapter, we have presented a simulation and real time implementation of an optimized nonlinear SVM-DTC with model based losses minimization strategy (LMC). The proposed control technique has been presented in order to optimize the IM energy. The effectiveness and performances of LMC strategy which is based on the choosing of an optimal flux reference has been verified and compared with basic technique which is based on constant flux reference. The performed tests give similar results. They show that LMC reduces losses and improves efficiency at zero and low load operations in steady state. Therefore, the coupling of robust DTC-SVM algorithms with LMC and can get higher performances and efficiency for induction motor drive.

In view of the fact, the implemented LMC optimization in this chapter is a conventional strategy. But in our view, the association with a robust control to get more high performance was an interesting proposition. This point can be improved carefully in future works by utilizing intelligent optimizers such as fuzzy logic and particle swarm optimization (PSO). Also, it can be considered for variable states using dynamic programming process.



General Conclusion

General Conclusion

Summary

This dissertation deals with the enhancement of the direct torque control for induction machine. DTC is a control method which offers a decoupled torque and flux control for the electrical drives. As an alternative to the vector control, it is featured by simple structure, fast torque dynamic and less sensitivity to the machine parameters. However, it suffers from the high flux and torque ripples and the variable switching frequency. As a result, they lead to an acoustical noise and more control difficulty in low speed regions which degrades the performance of the control algorithm.

The main objective of this thesis is the improvement of the performance of an induction motor drive controlled by DTC using various control approaches. In this context, the research work has been addressed four principal points concerning the DTC control algorithm to be treated:

1. The reduction of high ripples and harmonics level which caused by the variable switching frequency due to the use of hysteresis comparators,
2. The designing of a nonlinear control law to improve the stability and robustness of control scheme while the presence of uncertainties,
3. The insertion of a sensorless algorithms to limit the number of used sensors in purpose of increasing the reliability and reducing the cost of the controlled system,
4. The association of losses minimization strategy to maximize the energy efficiency of the machine.

Furthermore, all the aforementioned processes have been investigated by simulation and hardware experimentation using the real-time interface linked to dSpace 1104 signal card.

Related to the control algorithms of the induction motor, the first chapter has presented a state of the art about the main concepts in this field, starting by the classical methods, then passing to the nonlinear techniques and the sensorless approaches and ending with efficiency optimization strategies. The second chapter has presented a brief theoretical about the classical DTC based on switching table and the constant switching frequency DTC based on the space vector modulation. The comparative simulation and experimental results has shown the apparent effect of using SVM on the reduction of flux/torque ripples and current harmonics.

In spite of the provided improvement of the SVM-DTC scheme, due to its dependence on the PI controllers, it can expose the control system to the risk of wasting its stability and robustness. Subsequently, the third chapter has presented a proposed robust control included the injection of nonlinear control law on SVM-DTC. The nonlinear control strategy consists of combining the input-output feedback linearization with first and second order sliding mode control. The feedback linearization ensured a decoupled control without need of flux orientation or coordinates transformation. This has reduced the complexity of control scheme. The sliding mode control has been used to offer an accurate reference tracking and robust control in the presence of uncertainties or parameters variation. Moreover, the second order sliding mode controller based on super twisting algorithm has been applied in the outer speed loop instead of the conventional PI controller to enhance compressively the control stability and robustness against external load disturbance. Furthermore, it can eliminate the phenomenon of chattering which made by the first order SMC and keep its same good performance like fast dynamic and simplicity. The simulation and experimental results have illustrated also to support the proposed nonlinear DTC algorithm.

The fourth chapter has presented a design of various sensorless algorithms which linked to the nonlinear DTC control scheme to estimate speed, flux and applied load torque. Two observer structures have been presented. Firstly, an adaptive observer based on Lyapunov theory and inherently sliding mode observer which did not take the speed as adaptive quantity. The comparative results have shown that the SMO offered an accurate estimation in different operation conditions, such as speed reversal and low speed values. Due to its simple design, where the speed estimator is separated from the main observer's body, the speed estimation preserved good accuracy. After that, a conjunction between a proposed stator flux based MRAS and SMO has been presented to improve stability and estimation accuracy of senseless control in low speeds. Finally, the fifth chapter has presented a simple efficiency optimization which has been associated to the nonlinear sensorless control. LMC strategy is featured by simplicity and has the ability to minimize losses at light load operating by adjusting the level of the produced flux.

The last presented technique was a complement improvement to get more performance for the developed algorithm which has treated various issues in one control scheme, like smooth robust control, accurate estimation and optimized energy to the induction machine. Moreover, we have taken into account carefully the degree of

complexity of our algorithm due to limitation and constraints in the real system especially the calculation power of the processor.

Future prospect

For the continuity of research, the future work could be oriented to a vaster area in this field, among our perspectives:

- Passing to another sophisticated control strategy like the Model Predictive Control (MPC) which can guarantee low level of harmonics.
- Expansion in the application of the high order sliding mode approach for control and observers design.
- Improvement of the losses minimization strategies using intelligent optimizers such as the fuzzy logic and PSO, also of variables states using dynamic programming
- Development of control strategies for the induction motor under faulty system condition (Fault tolerant control).
- Development of control strategies for multiphase induction machines.
- Improve the hardware implementation ground by the use of the Field Programmable Gate Array (FPGA) instead of dSpace 1104 signal card. The new FPGA technology is featured by very high sampling frequency and it can be offered with lower cost.



Appendix

A.1 Appendix 1: Dynamic Modelling of Induction Machine

A.1.1 Description of the induction Machine

The induction machines are rugged, cheap to produce and easy to maintain. They can run at a nearly constant speed from zero to full load. The design of an induction motor is relatively simple. It consists of two main parts, a stationary stator and a rotating rotor. There are two main classes of the induction motor according to their rotors constitution. The wound induction motor and the squirrel cage induction motor.

The motor which discussed in this thesis is a three-phase squirrel cage induction motor. The rotor of a squirrel cage induction motor consists of aluminum bars which are short circuited by connecting them to two end rings so that rotor generates the induction current and magnetic field by itself. This makes the AC induction motor a robust and strong candidate for motor drive systems. **Fig.A.1** shows a Cross section of the squirrel cage induction machine.

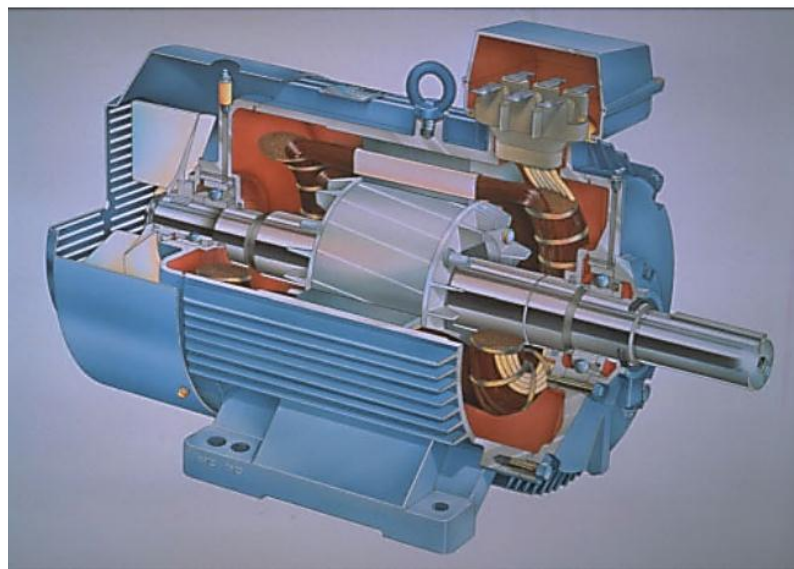


Fig.A.1 Cross section of the squirrel cage induction motor (Copyright granted, 2012, ABB)

The stator of an induction machine is composed of three windings, coupled in star or in triangle. The rotor of the machine will be considered to support a winding, similar to the one of the stator with the same number of poles.

A.1.2 Hypotheses

The modeling of the AC electrical machine generally relies on several hypotheses. These hypotheses will allow adding the fluxes to the different currents, using proper constant inductions, characterizing couplings by sinusoidal variations of the mutual inductions and representing induction flows by a spatial vector. They allow also to modeling the system with a reduced complexity which can make it easy to be implemented in practice [Rob12].

The main hypothesis consists in assuming that the magnetomotive forces created by stator and rotor phases are distributed in a sinusoidal way in the air gap, when those windings are crossed by a constant current. The machine air gap is also supposed to have a uniform thickness. The notching effects which generate space harmonic are ignored.

Another hypotheses about the physical behavior of the materials also are expressed:

- ❖ Linear magnetic characteristic (no saturation).
- ❖ The skin effect is not taken into account.
- ❖ Temperature effect, hysteresis phenomenon, and eddy currents are neglected.

A.1.3 Equivalent representation and vector formulation

The machine is represented by three-phase equivalent circuit associated to the stator and to the rotor as shown in **Fig.A.2**.

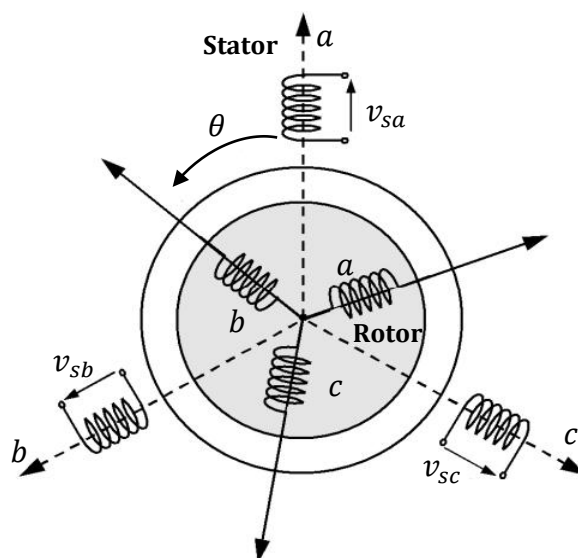


Fig.A.2 Induction motor equivalent structure.

The studied machine is described in the space by three identical windings for the stator phases whose are distant two by two of an electrical angle equal to $2\pi/3$. In addition, three rotor windings whose axes are equally distant between themselves of an electrical angle equal to $2\pi/3$ rotating at the mechanic speed ω_r . The modeling process consists of applying the electromagnetic laws to the different windings and the motion equation to the rotor carrying the load [Fou13]. The application of the electromagnetic laws yields to six voltage equations and six flux equations.

A.1.3.1 Voltage equations

$$\begin{aligned} [V_{sabc}] &= [R_s][i_{sabc}] + \frac{d}{dt}[\psi_{sabc}] \\ [V_{rabc}] &= 0 = [R_r][i_{rabc}] + \frac{d}{dt}[\psi_{rabc}] \end{aligned} \quad (\text{A.1})$$

A.1.3.2 Flux equations

$$\begin{aligned} [\psi_{sabc}] &= [L_s][i_{sabc}] + [M_{sr}][i_{rabc}] \\ [\psi_{rabc}] &= [L_r][i_{sabc}] + [M_{sr}]^T[i_{sabc}] \end{aligned} \quad (\text{A.2})$$

where:

$$\begin{aligned} [V_{sabc}] &= \begin{bmatrix} V_{sa} \\ V_{sb} \\ V_{sc} \end{bmatrix}; \quad [i_{sabc}] = \begin{bmatrix} i_{sa} \\ i_{sb} \\ i_{sc} \end{bmatrix}; \quad [\psi_{sabc}] = \begin{bmatrix} \psi_{sa} \\ \psi_{sb} \\ \psi_{sc} \end{bmatrix} \\ [V_{rabc}] &= \begin{bmatrix} V_{ra} \\ V_{rb} \\ V_{rc} \end{bmatrix}; \quad [i_{rabc}] = \begin{bmatrix} i_{ra} \\ i_{rb} \\ i_{rc} \end{bmatrix}; \quad [\psi_{rabc}] = \begin{bmatrix} \psi_{ra} \\ \psi_{rb} \\ \psi_{rc} \end{bmatrix} \end{aligned}$$

The subscripts s and r refer to the stator and the rotor, respectively, and the indices a , b , and c refer to the three phases. A direct consequence of the machine perfect symmetry is that all resistance and inductance matrices are symmetric as given below:

$$[R_s] = \begin{bmatrix} R_s & 0 & 0 \\ 0 & R_s & 0 \\ 0 & 0 & R_s \end{bmatrix}; \quad [R_r] = \begin{bmatrix} R_r & 0 & 0 \\ 0 & R_r & 0 \\ 0 & 0 & R_r \end{bmatrix} \quad (\text{A.3})$$

$$[L_s] = \begin{bmatrix} L_s & M_s & M_s \\ M_s & L_s & M_s \\ M_s & M_s & L_s \end{bmatrix}; \quad [L_r] = \begin{bmatrix} L_r & M_r & M_r \\ M_r & L_r & M_r \\ M_r & M_r & L_r \end{bmatrix} \quad (\text{A.4})$$

where:

R_s and R_r are the stator and the rotor resistances.

L_s and L_r are the self-inductances.

M_s and M_r are the mutual inductance between two stator phases and rotor phases.

Also, based on the given hypothesis above, the mutual inductances between the rotor and the stator are taken as sinusoidal functions of the rotor position θ as following:

$$[M_{sr}] = [M_{rs}]^T = M_{sr} \begin{bmatrix} \cos(\theta) & \cos(\theta + \frac{2\pi}{3}) & \cos(\theta + \frac{4\pi}{3}) \\ \cos(\theta + \frac{4\pi}{3}) & \cos(\theta) & \cos(\theta + \frac{2\pi}{3}) \\ \cos(\theta - \frac{4\pi}{3}) & \cos(\theta + \frac{2\pi}{3}) & \cos(\theta) \end{bmatrix} \quad (\text{A.5})$$

M_{sr} is the maximal mutual inductance between the stator phase and the rotor phase.

A.1.3.3 Mechanical Equations

The rotor motion can be described by the following second order differential equation:

$$J \frac{d\omega_r}{dt} = T_e - T_L - f \omega_r \quad (\text{A.6})$$

ω_r , T_e and T_L are the rotor speed, the electromagnetic torque and the load torque respectively.

J is the inertia moment and f is the friction coefficient.

A.1.4 Park transformation

This approach has been presented to simplify the study of AC machines by transforming the three phase variables (voltages, currents, and flux) from fixed reference frame (stationary) to a rotating frame (synchronous) defined by the Concordia/Clarke and Park transformations. These transformations are used to reduce the complexity of the differential equations describing the behavior of the AC machines by eliminating time-varying terms [Glu15].

The transformation from a three-phase stationary frame to a two-phase direct-quadrature (d, q, o) frame is referred by Park transformation. This transformation can be decomposed in two transformations. A first one, from a fixed three-phase system to a fixed two phase system which is known by Clarke or Concordia transformations. Then, a transformation from a fixed two-phase to a rotating two-phase frame associated to a rotating variable (mechanical position and flux, for instance). The (d, q, o) transformation can reduce three AC variables (voltages, currents, ...) to two DC variables.

A general representation of the Park transformation is given as:

$$\begin{bmatrix} x_d \\ x_q \\ x_o \end{bmatrix} = P(\theta) \begin{bmatrix} x_a \\ x_b \\ x_c \end{bmatrix} \quad (\text{A.7})$$

$$P(\theta) = n \begin{bmatrix} \cos(\theta) & \cos(\theta - \frac{2\pi}{3}) & \cos(\theta + \frac{2\pi}{3}) \\ \sin(\theta) & \sin(\theta - \frac{2\pi}{3}) & \sin(\theta + \frac{2\pi}{3}) \\ k & k & k \end{bmatrix} \quad (\text{A.8})$$

where θ is the angle between the axis- a of the three-phase frame and the axis- d of the rotating reference frame, and n is the ratio between the amplitude of the three-phase system variables (x_a, x_b, x_c) with the amplitude of the corresponding two-phase system variables (x_d, x_q, x_o).

k is a constant.

A.1.4.1 Amplitude and power preserving transformations

We define two different Park transformations, Park transformation preserving amplitude and Park transformation preserving power.

- The transformation preserving amplitude is achieved by choosing:

$$n = \frac{2}{3}; \quad k = \frac{1}{2}$$

- The transformation preserving power is achieved by choosing:

$$n = \sqrt{\frac{2}{3}}; \quad k = \frac{1}{\sqrt{2}}$$

Then, for preserving amplitude transformation

$$P(\theta) = \frac{2}{3} \begin{bmatrix} \cos(\theta) & \cos(\theta - \frac{2\pi}{3}) & \cos(\theta + \frac{2\pi}{3}) \\ \sin(\theta) & \sin(\theta - \frac{2\pi}{3}) & \sin(\theta + \frac{2\pi}{3}) \\ \frac{1}{2} & \frac{1}{2} & \frac{1}{2} \end{bmatrix} \quad (\text{A.9})$$

For preserving power transformation

$$P(\theta) = \sqrt{\frac{2}{3}} \begin{bmatrix} \cos(\theta) & \cos(\theta - \frac{2\pi}{3}) & \cos(\theta + \frac{2\pi}{3}) \\ \sin(\theta) & \sin(\theta - \frac{2\pi}{3}) & \sin(\theta + \frac{2\pi}{3}) \\ \frac{1}{\sqrt{2}} & \frac{1}{\sqrt{2}} & \frac{1}{\sqrt{2}} \end{bmatrix} \quad (\text{A.10})$$

The inverse transformations preserving amplitude and power are given respectively by:

$$P^{-1}(\theta) = \begin{bmatrix} \cos(\theta) & \sin(\theta) & 1 \\ \cos(\theta - \frac{2\pi}{3}) & \sin(\theta - \frac{2\pi}{3}) & 1 \\ \cos(\theta + \frac{2\pi}{3}) & \sin(\theta + \frac{2\pi}{3}) & 1 \end{bmatrix} \quad (\text{A.11})$$

$$P^{-1}(\theta) = \sqrt{\frac{2}{3}} \begin{bmatrix} \cos(\theta) & \sin(\theta) & \frac{1}{\sqrt{2}} \\ \cos(\theta - \frac{2\pi}{3}) & \sin(\theta - \frac{2\pi}{3}) & \frac{1}{\sqrt{2}} \\ \cos(\theta + \frac{2\pi}{3}) & \sin(\theta + \frac{2\pi}{3}) & \frac{1}{\sqrt{2}} \end{bmatrix} \quad (\text{A.12})$$

A.1.4.2 The Clarke/Concordia Transformation

By choosing $\theta = 0$, in the Park transformation (A.9) and (A.10), the resulting matrix $P(0)$ are given respectively:

$$C = \frac{2}{3} \begin{bmatrix} 1 & -\frac{1}{2} & -\frac{1}{2} \\ 0 & \frac{\sqrt{3}}{2} & -\frac{\sqrt{3}}{2} \\ \frac{1}{2} & \frac{1}{2} & \frac{1}{2} \end{bmatrix} \quad \text{and} \quad C^{-1} = \begin{bmatrix} 1 & 0 & 1 \\ -\frac{1}{2} & \frac{\sqrt{3}}{2} & 1 \\ -\frac{1}{2} & -\frac{\sqrt{3}}{2} & 1 \end{bmatrix} \quad (\text{A.13})$$

$$C_o = \sqrt{\frac{2}{3}} \begin{bmatrix} 1 & -\frac{1}{2} & -\frac{1}{2} \\ 0 & \frac{\sqrt{3}}{2} & -\frac{\sqrt{3}}{2} \\ \frac{1}{\sqrt{2}} & \frac{1}{\sqrt{2}} & \frac{1}{\sqrt{2}} \end{bmatrix} \quad \text{and} \quad C_o^{-1} = \sqrt{\frac{2}{3}} \begin{bmatrix} 1 & 0 & \frac{1}{\sqrt{2}} \\ -\frac{1}{2} & \frac{\sqrt{3}}{2} & \frac{1}{\sqrt{2}} \\ -\frac{1}{2} & -\frac{\sqrt{3}}{2} & \frac{1}{\sqrt{2}} \end{bmatrix} \quad (\text{A.14})$$

The matrix C is known as Clarke transformation and the matrix C_o is known as Concordia transformation. The Clarke transformation converts the three-phase quantities

into two-phase orthogonal quantities by keeping the amplitude of the variables and the power is not kept, contrary to Concordia transformation which preserves the power.

Park transformation can be expressed in terms of the Clark/Concordia transformation and a rotation matrix $R(\theta)$ as:

$$P(\theta) = R(\theta)C \quad (\text{A.15})$$

where:

$$R(\theta) = \begin{bmatrix} \cos(\theta) & -\sin(\theta) & 0 \\ \sin(\theta) & \cos(\theta) & 0 \\ 0 & 0 & 1 \end{bmatrix} \quad (\text{A.16})$$

Fig.A.3 represents the passage of three-phase system to the equivalent two-phase fixed system (α, β) then to the rotating frame (d, q)

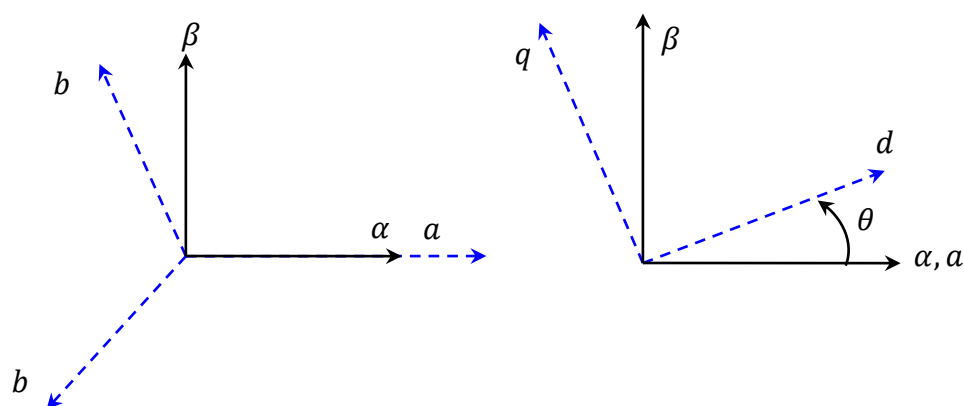


Fig.A.3 The passage of three-phase to two-phase system using Park transformation.

A.1.5 Two-phase models of induction machine

The three-phase model of the IM is simplified by applying Park transformation, where all expressed terms in the three-phase frame (a, b, c) are rewritten in terms of (d, q, o) . The perfect symmetry of the induction motor implies that the sum of the currents is null.

Depending on the choice of θ several two-coordinate frames exist, the two most common in the literature are the fixed reference frame (α, β) (i.e. stationary frame connected to the stator) and the rotating reference frame (d, q) .

The passage from the three-phase frame (a, b, c) to the fixed (α, β) frame is accomplished by setting angle $\theta=0$, in the transformation matrix (A.10), which mean the use of Clark/Concordia transformations instead of Park transformation.

The passage from the three-phase frame (a, b, c) to the rotating frame (d, q) is accomplished by setting the angle $\theta=\theta_s$, where θ_s is the stator field angle

A.1.5.1 Voltage and flux equations in (d, q) frame

By applying the transformations to the induction machine equations (A.1) and (A.2), it yields the following (d, q) equations:

$$\begin{bmatrix} v_{sd} \\ v_{sq} \end{bmatrix} = [P(\theta_s)] [v_{sabc}]; \quad \begin{bmatrix} i_{sd} \\ i_{sq} \end{bmatrix} = [P(\theta_s)] [i_{sabc}]; \quad \begin{bmatrix} \psi_{sd} \\ \psi_{sq} \end{bmatrix} = [P(\theta_s)] [\psi_{sabc}] \quad (\text{A.17})$$

$$\begin{bmatrix} v_{rd} \\ v_{rq} \end{bmatrix} = [P(\theta_s)] [v_{rabc}]; \quad \begin{bmatrix} i_{rd} \\ i_{rq} \end{bmatrix} = [P(\theta_s)] [i_{rabc}]; \quad \begin{bmatrix} \psi_{rd} \\ \psi_{rq} \end{bmatrix} = [P(\theta_s)] [\psi_{rabc}] \quad (\text{A.18})$$

Then, the voltage equations are given as:

$$\begin{cases} v_{sd} = R_s i_{sd} + \frac{d\psi_{sd}}{dt} - \omega_s \psi_{sq} \\ v_{sq} = R_s i_{sq} + \frac{d\psi_{sq}}{dt} + \omega_s \psi_{sd} \\ v_{rd} = R_r i_{rd} + \frac{d\psi_{rd}}{dt} - (\omega_s - p\omega_r) \psi_{rq} \\ v_{rq} = R_r i_{rq} + \frac{d\psi_{rq}}{dt} + (\omega_s - p\omega_r) \psi_{rd} \end{cases} \quad (\text{A.19})$$

Where:

$$\omega_s = \frac{d\theta_s}{dt}; \quad \omega_r = \frac{d\theta_r}{dt}$$

Similarly, the flux equations are given as:

$$\begin{cases} [\psi_{sdq}] = L_s [i_{sdq}] + M_{sr} [i_{rdq}] \\ [\psi_{rdq}] = L_r [i_{rdq}] + M_{sr} [i_{sdq}] \end{cases} \quad (\text{A.20})$$

A.1.5.2 Mechanical Equations

The dynamic equation of the IM is given by the following:

$$J \frac{d\omega_r}{dt} = T_e - T_L - f \omega_r \quad (\text{A.21})$$

The electromagnetic torque is calculated in (d, q) frame using the electric power and the rotor speed, then the expression of torque basing on power preserving Park transformation is given by:

$$T_e = p \frac{M_{sr}}{L_r} (\psi_{rd} i_{sq} - \psi_{rq} i_{sd}) \quad (\text{A.22})$$

The electromagnetic torque can also be expressed in the following term:

$$T_e = p (\psi_{sd} i_{sq} - \psi_{sq} i_{sd}) \quad (\text{A.23})$$

The model of the induction machine expressed in the rotating frame (d, q) is often used for the field oriented control design, contrariwise, the direct torque control uses the fixed (stationary) frame (α, β).

A.1.6 IM model in state space representation

For the conception of the motor control, it is interesting to choose the stator current components as state variables. In fact, this current as well as the flux components will be controlled and they can be easily obtained. The state space representation consists of determining only the differential equations that allow to express these variables by integration with intermediary mathematical relations [Rob12].

There are various mathematical formulations of the machine state model depending on the control system need. The common model takes the stator current and the rotor flux components as state variables which used to elaborate the rotor flux-oriented control. Another state model of IM which has been recommended in this thesis for control and observers conception takes the stator current and stator flux components as state variables. It can be written in the stationary axes reference frame as the following:

$$\dot{X} = AX + BU \quad (\text{A.24})$$

where:

$$X = \begin{bmatrix} i_{s\alpha} & i_{s\beta} & \psi_{s\alpha} & \psi_{s\beta} \end{bmatrix}^T; \quad U = \begin{bmatrix} v_{s\alpha} & v_{s\beta} \end{bmatrix}^T \quad (\text{A.25})$$

$$A = \begin{bmatrix} -\frac{1}{\sigma} \left(\frac{1}{T_s} + \frac{1}{T_r} \right) & \omega_r & \frac{1}{\sigma L_s T_r} & \frac{\omega_r}{\sigma L_s} \\ -\omega_r & -\frac{1}{\sigma} \left(\frac{1}{T_s} + \frac{1}{T_r} \right) & -\frac{\omega_r}{\sigma L_s} & \frac{1}{\sigma L_s T_r} \\ -R_s & 0 & 0 & 0 \\ 0 & -R_s & 0 & 0 \end{bmatrix}; \quad B = \begin{bmatrix} \frac{1}{\sigma L_s} & 0 \\ 0 & \frac{1}{\sigma L_s} \\ 0 & 0 \\ 0 & 0 \end{bmatrix} \quad (\text{A.26})$$

$$T_s = \frac{L_s}{R_s}; \quad T_r = \frac{L_r}{R_r}; \quad \sigma = 1 - \frac{M_{sr}^2}{L_s L_r}.$$

A.2 Appendix 2: PI controller's gains calculation

A.2.1 PI speed controller design

The used PI controller in the outer speed loop for all control schemes is the anti-windup controller. The dynamic equation and the transfer function using Laplace transform of the speed loop are given as following:

$$\frac{d\omega_r}{dt} = -\frac{f}{J} \omega_r + \frac{T_e}{J} - \frac{1}{J} T_L \quad (\text{A.27})$$

$$G_{\omega_r}(s) = \frac{\omega_r(s)}{T_e(s) - T_L(s)} = \frac{1}{Js + f} \quad (\text{A.28})$$

The transfer function (TF) of the PI controller is defined as follow:

$$PI = K_p s + \frac{K_i}{s} \quad (\text{A.29})$$

K_p and K_i are the proportional and integral gains.

s is Laplace operator

Then, **Fig.A.4.** shows the block diagram of the speed control loop.

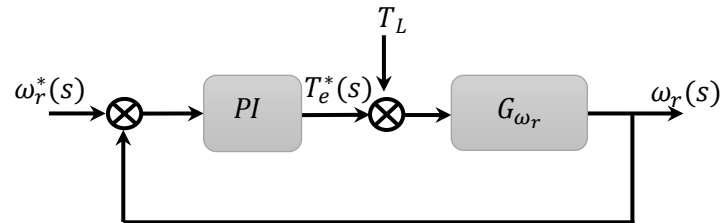


Fig.A.4 Speed control loop.

By considering the load torque T_L as a disturbance. The global transfer function of the speed control in open loop becomes:

$$G_{\omega_r}(s) = \frac{\omega_r(s)}{\omega_r^*(s)} = \frac{1}{Js + f} \left(K_p s + \frac{K_i}{s} \right) \quad (\text{A.30})$$

In closed loop, the TF becomes

$$G_{\omega_r}(s) = \frac{K_p s + K_i}{Js^2 + (K_p + f)s + K_i} \quad (\text{A.31})$$

By identification member to member, the denominator of the equations (A.31) with the canonical form of second order system given in (A.32):

$$G(s) = \frac{1}{s^2 + 2\xi\omega_n s + \omega_n^2} \quad (\text{A.32})$$

where ω_n is the natural frequency and ξ is the damping coefficient.

we obtain:

$$\begin{cases} \frac{J}{K_i} = \frac{1}{\omega_n^2} \\ \frac{K_p + f}{J} = 2\xi\omega_n \end{cases} \quad (\text{A.33})$$

The gains are determined for a damping coefficient $\xi = 1$.

A.2.2 PI controllers design for stator flux oriented SVM-DTC

The following equations express the stator field oriented machine model:

$$\begin{cases} v_{sd} = R_s i_{sd} + \frac{d\psi_s}{dt} \\ v_{sq} = R_s i_{sq} + \omega_s \psi_s \end{cases} \quad (\text{A.34})$$

The electromagnetic torque is given by:

$$T_e = p\psi_s i_{sq} \quad (\text{A.35})$$

Then, the rotor currents and rotor fluxes can be expressed respectively as:

$$\begin{cases} i_{rd} = \frac{1}{M_{sr}}(\psi_s - L_s i_{sd}) \\ i_{rq} = -\frac{L_s}{M_{sr}} i_{sq} \end{cases} \quad (\text{A.36})$$

$$\begin{cases} \psi_{rd} = \frac{L_r}{M_{sr}}(\psi_s - \sigma L_s i_{sd}) \\ \psi_{rq} = -\frac{\sigma L_s L_r}{M_{sr}} i_{sq} \end{cases} \quad (\text{A.37})$$

A.2.2.1 Design of PI flux controller

The relationship between the stator flux and direct voltage component V_{sd} can be expressed by using the (d, q) frame voltage model and Laplace transform as following [Seb11]:

$$\begin{cases} \psi_s(s) = \frac{\sigma T_r L_s}{1 + T_r s} \left[\left(\frac{1}{\sigma T_r} + s \right) I_{sd}(s) + I_{sq}(s) \omega_{sl}(s) \right] \\ I_{sq}(s) = \frac{\sigma T_r \omega_{sl}(s)}{1 + \sigma T_r s} \left(\frac{1}{\sigma L_s} \psi(s) - I_{ds}(s) \right) \end{cases} \quad (\text{A.38})$$

By expressing the direct current components I_{ds} according to the quadratic components I_{qs} and the stator flux, the stator voltages become:

$$\begin{cases} V_{sd}(s) = \frac{\psi_s(s)}{G_{\psi_s}(s)} + E_d(s) \\ V_{sq}(s) \approx \omega_s(s) \psi_s(s) \end{cases} \quad (\text{A.39})$$

where:

$$\begin{cases} G_{\psi_s}(s) = \frac{T_s(1 + \sigma T_r s)}{1 + (T_r + T_s)s + \sigma T_r T_s} \\ E_d(s) = -\frac{\sigma R_s T_r}{1 + T_r s} I_{sq}(s) \omega_{sl} \end{cases} \quad (\text{A.40})$$

The stator flux control loop is presented in **Fig.A.5**.

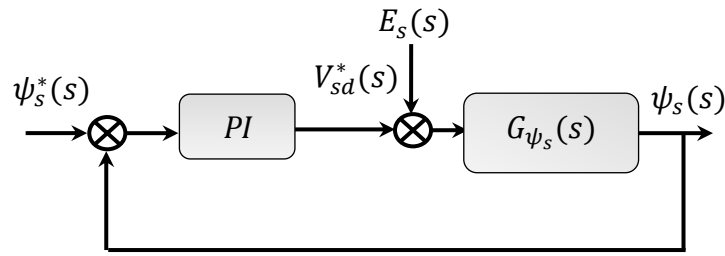


Fig.A.5 Block diagram of the stator flux control loop.

A.2.2.2 Design of PI torque controller

The relationship between the electromagnetic torque T_e and stator pulsation ω_s can be achieved as following. From Eq (A.38), the quadratic current component I_{sq} can be written as:

$$I_{sq}(s) = \frac{pK_{\sigma}\psi_s(s)\omega_{sl}(s)}{(1 + \sigma T_r s)^2 + (\sigma T_r \omega_{sl}(s))^2} \quad (\text{A.41})$$

where:

$$K_{\sigma} = (1 - \sigma)T_r / L_s$$

and the electromagnetic becomes:

$$T_e = \frac{pK_{\sigma}\psi_s^2(s)\omega_{sl}(s)}{(1 + \sigma T_r s)^2 + (\sigma T_r \omega_{sl}(s))^2} \quad (\text{A.42})$$

Basing on the principle of the direct torque control, when the stator flux is maintained constant, the electromagnetic torque becomes proportional to the slip angular speed [Bou09]. Therefore, with the small values of the slip angular speed, Eq (A.42) can be written as:

$$T_e(s) = G_{T_e}(s)(\omega_s(s) - \omega_r(s)) \quad (\text{A.43})$$

where:

$$G_{T_e}(s) = \frac{pK_{\sigma}\psi_s^2(s)}{(1 + \sigma T_r s)^2} \quad (\text{A.44})$$

Consequently, the machine torque can be regulated by controlling ω_s with taking the rotor speed ω_r as a disturbance as shown in **Fig.A.6**.

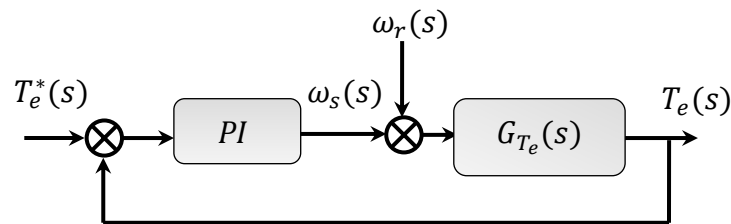


Fig.A.6 Block diagram of the torque control loop.

A.3 Appendix 3: Real Time Implementation of the Induction Motor Control

A.3.1. General description of the experimental setup:

The experimental setup of the induction motor electrical drives has been designed and constructed in order to check and validate the simulation results of the presented theory. As we mentioned in the chapter 2, the real-time control was conducted in the LGEB laboratory of Biskra which equipped by dSpace 1104 board.

The implementation ground of induction motor drive is shown in **Fig. A.7**.

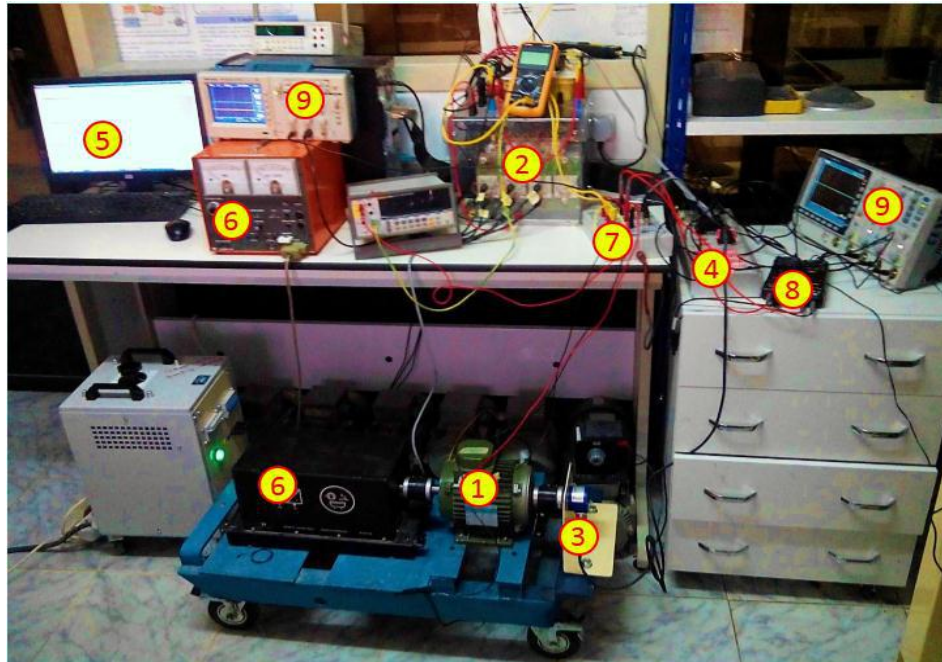


Fig.A.7 Presentation of the experimental setup.

The experimental setup is essentially composed of:

1. A squirrel cage IM of 1.1 kW.
2. Power electronics Semikron converter composed of a rectifier and an IGBT inverter.
3. Position and speed sensor (incremental encoder).
4. dSpace DS 1104 signal card.
5. Control desk/Matlab/Simulink software plugged in personnel computer.
6. Magnetic powder brake with load control unit.
7. Hall type current sensors.
8. Voltage DC-link sensor. To reduce the cost of the control system, the phase voltages will be estimated from DC-bus voltage and inverter switching states (S_a , S_b , S_c) instead of the using three voltage sensors.
9. Numerical oscilloscopes.

A.2.2 Induction motor characteristics

The parameters of the used three-phase induction motor in simulation and real time implementation have obtained through an experimental identification using conventional methods [Fat10]. The nameplate of the machine is shown in **Fig.A.8** and the parameters are shown in SI units in the **Table.A.1**

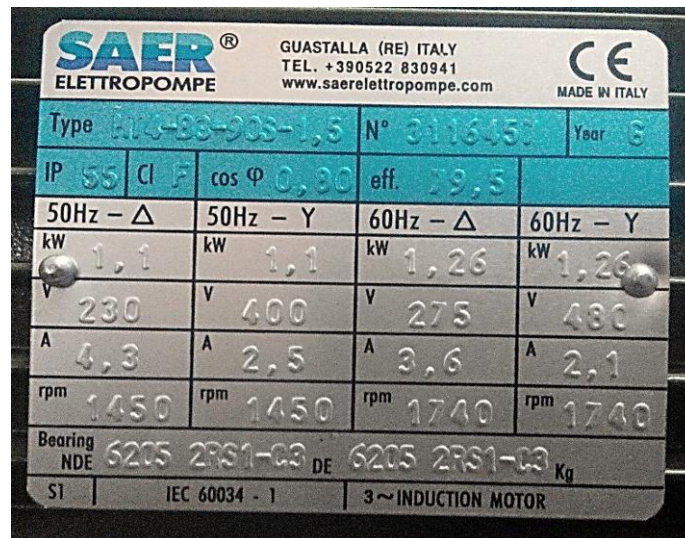


Fig.A.8 Induction machine's nameplate

Machine's Power	1.1 kW
Stator resistance	$R_s = 6.75 \Omega$
Rotor resistance	$R_r = 6.21 \Omega$
Stator inductance	$L_s = 0.5192H$
Rotor inductance	$L_r = 0.5192H$
Mutual inductance	$M_{sr} = 0.4957 H$
Number of pole pairs	$p=2$
Friction coefficient	$f=0.002 SI$
The moment of inertia	$J = 0.01240 kg.m^2$
Rated voltage	$V_s = 220/380 V$

Table.A.1 Parameters of the induction machine.

A.3.3 Digital control implementation

A.3.3.1 DSpace 1104 controller and interface board

The dSpace 1104 board is an input-output (I/O) interface between the power electronics and the software part which is MATLAB/Simulink/ControlDesk [Dsp12]. For each sampling period, the dS1104 receives the input signals from sensors (currents, voltages from ADC ports and speed from encoder through INC ports) and generates the digital control signals. These signals are provided by MATLAB/Simulink program with real-time interface (RTI), where the I/O ports of dS1104 are accessible in Simulink's library.

The dSpace DS1104 controller board is shown in **Fig.A.9**. The main processor of DS1104 is MPC8240 with PowerPC 603e core of 250 MHz. It has a memory of 32 MByte synchronous DRAM (SDRAM) and 8 MByte boot flash for applications.



Fig.A.9 dSpace DS1104 Controller.

It is characterized by 8 analog-to-digital converters (ADCs) (4 in 16 bits, 4 in 12 bits), 8 digital-to-analog converters (DACs) with 16 bits which can deliver an analog voltage between $-10V$ and $+10V$, a serial link, 2 incremental encoders, 20 digital inputs/outputs, a slave DSP (TMS320F240) and 3 independent 32-bit timers. The architecture of DS1104 is presented in **Fig.A.10**.

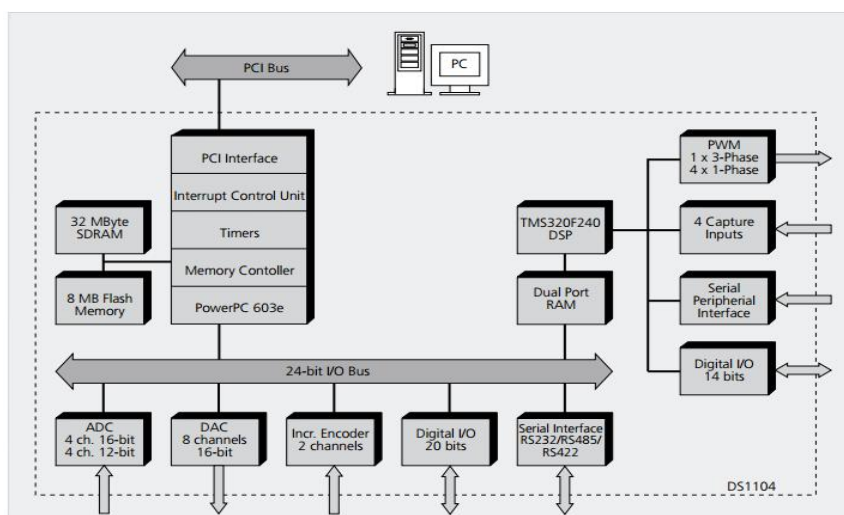


Fig.A.10 Architecture of DS1104 [Dsp12].

The real-time interface of dSpace 1104 board which linked to the power converter is shown in Fig.A.11.

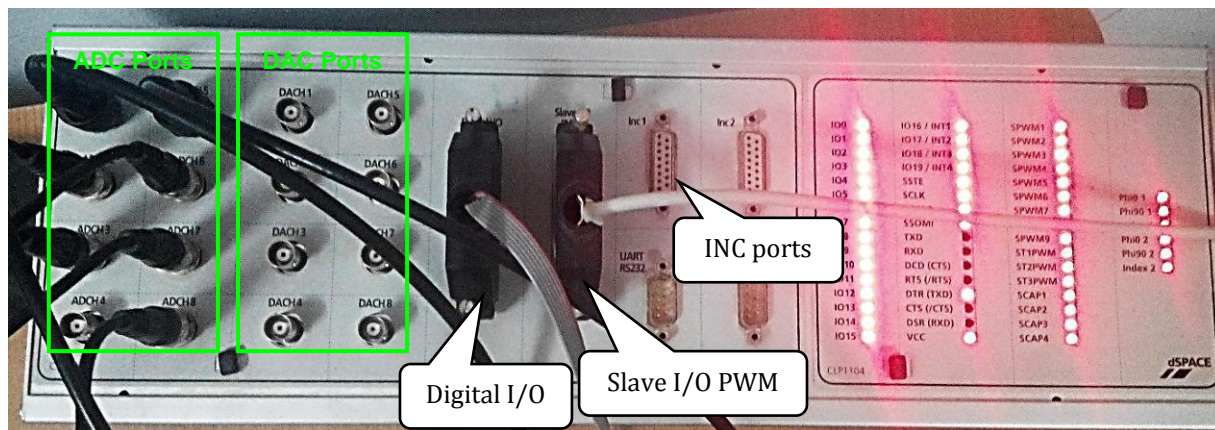


Fig.A.11 dSpace 1104 interface board.

The execution of the program inside the DSP of dS1104 board converts it into a real-time system on the hardware (dSpace 1104 RTI) after it was in the software (Simulink) [Ngu13; Dsp12]. In addition, it gives us the access to adjust all Simulink variables in real time in order to obtain a satisfied control behavior [Mun11]. The sampling frequency of dSpace 1104 can reach to 20 kHz. The suitable choice of sampling frequency has an apparent influence on quality of signals, especially the phase current and the produced electromagnetic torque.

Fig.A.12 shows a descriptive diagram of experimental setup and software/hardware linkage.

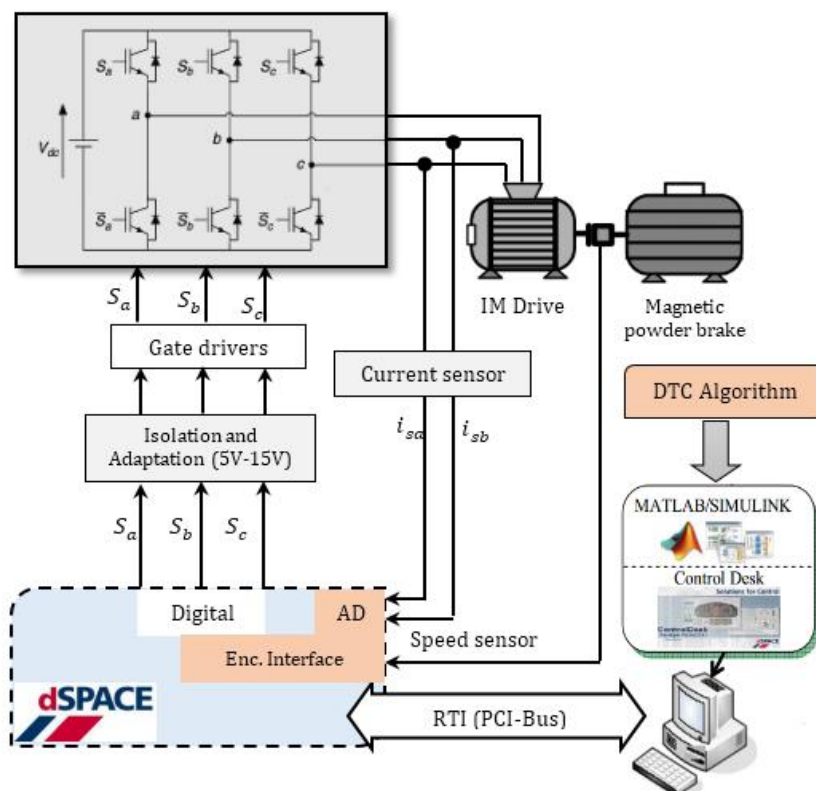


Fig.A.12 Descriptive block diagram of the dSpace based experimental setup.

A2.3.2 Controldesk window

The Controldesk software has the ability to create instrument panels to control, display and plotting possibilities. In addition, by connecting the Simulink variables (i.e. Reference signals, parameters, gains of controllers...etc.) to plotters, slide bars, displayers, it gives us the access to adjust all these variables in real time in order to obtain a satisfied control behavior [Mun11]. **Fig.A.13** shows Controldesk instrumentation panel which used for our experiments.

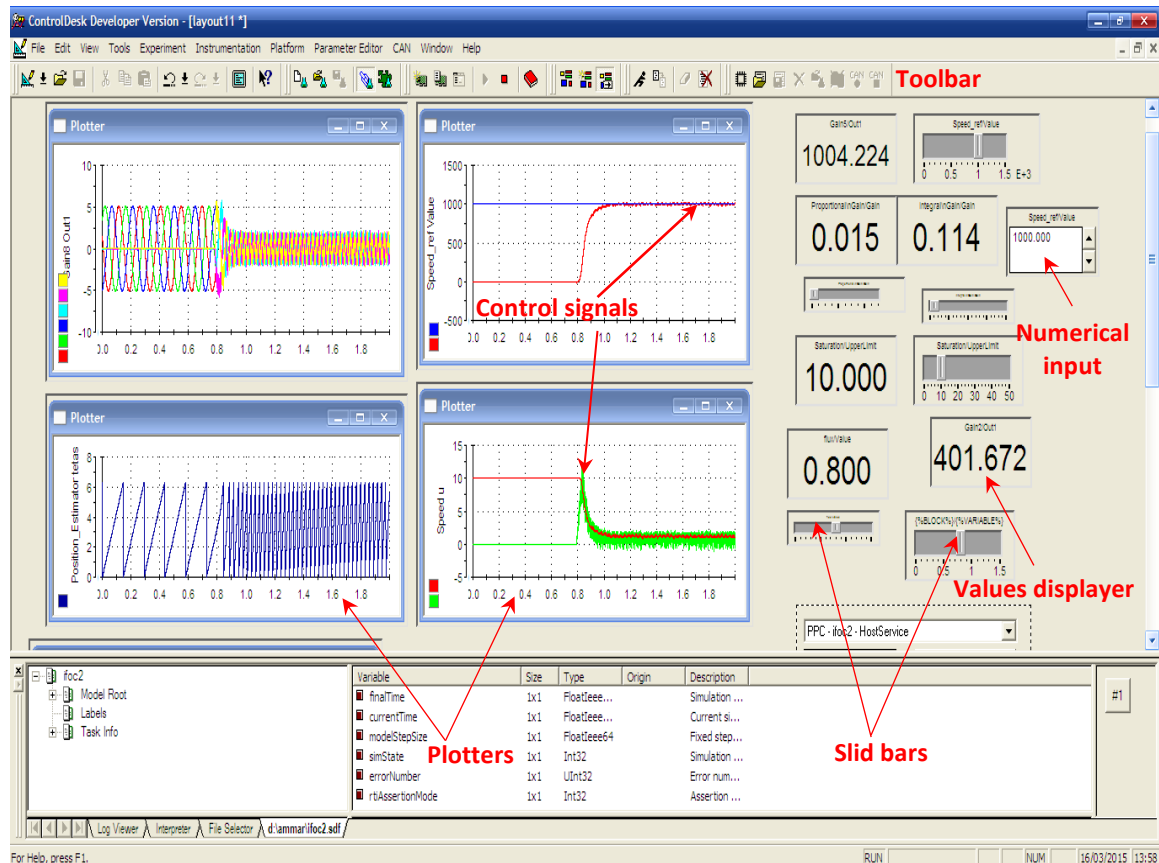


Fig.A.13 Layout of the dSpace instrumentation panel Controldesk.



References

References

- [Abr98] F. Abrahamsen, F. Blaabjerg, J. Pedersen, P. Grabowski and P. Thogersen, "On the energy optimized control of standard and high efficiency induction motors in CT and HVAC applications", *IEEE Transactions on Industry Applications*, vol. 34, no. 4, pp. 822-831, 1998.
- [Abr00] Flemming Abrahamsen "Energy Optimal Control of Induction Motor Drives" Ph.D. thesis, Aalborg University, Denmark, 2000.
- [Abr01] F. Abrahamsen, F. Blaabjerg, J. Pedersen and P. Thogersen, "Efficiency-optimized control of medium-size induction motor drives", *IEEE Transactions on Industry Applications*, vol. 37, no. 6, pp. 1761-1767, 2001.
- [Abu12] Haitham Abu-Rub, Atif Il, Jaroslaw Guzinski "High performance control of ac drives with Matlab/Simulink models" 2012 John Wiley & Sons Ltd.
- [Amr15] A. Ammar, A. Bourek and A. Benakcha, "Modified load angle Direct Torque Control for sensorless induction motor using sliding mode flux observer", in 2015 IEEE 4th International Conference on Electrical Engineering (ICEE) Proceeding, Boumerdes, Algeria, 2015.
- [Amr16] A. Ammar, A. Benakcha and A. Bourek, "Adaptive MRAC-based direct torque control with SVM for sensorless induction motor using adaptive observer", *The International Journal of Advanced Manufacturing Technology*, 2016.
- [Amr17a] A. Ammar, A. Bourek, and A. Benakcha, "Nonlinear SVM-DTC for induction motor drive using input-output feedback linearization and high order sliding mode control," *ISA Trans*, vol.67, pp. 428–442, 2017.
- [Amr17b] A. Ammar, A. Bourek and A. Benakcha, "Sensorless SVM-Direct Torque Control for Induction Motor Drive Using Sliding Mode Observers", *Journal of Control, Automation and Electrical Systems*, Vol.28(2), pp.189–202, 2017
- [Amr17c] A. Ammar, A. Bourek and A. Benakcha, "Robust SVM-direct torque control of induction motor based on sliding mode controller and sliding mode observer", *Frontiers in Energy*, 2017.
- [Asf13] I. M. Alsofyani and N. R. N. Idris, "A review on sensorless techniques for sustainable reliability and efficient variable frequency drives of induction motors," *J. Renewable and Sustainable Energy Reviews*, vol. 24, pp. 111-121, 2013.
- [Asf16] I. M. Alsofyani and N. R. N. Idris, "Simple Flux Regulation for Improving State Estimation at Very Low and Zero Speed of a Speed Sensorless Direct Torque Control of an Induction Motor," *IEEE Trans. Power Electron.*, vol. 31, no. 4, pp. 3027–3035, Apr. 2016.
- [Aur07] C. Aurora and A. Ferrara, "A sliding mode observer for sensorless induction motor speed regulation", *International Journal of Systems Science*, vol. 38, no. 11, pp. 913-929, 2007.

- [Bab97] A. Baba, E. Mendes and A. Razeq, "Losses minimisation of a field-oriented controlled induction machine by flux optimisation accounting for magnetic saturation", 1997 IEEE International Electric Machines and Drives Conference Record.
- [Bai99] J. Baillieul J.C. Willems "Mathematical Control Theory" Springer-Verlag New York, 1990.
- [Bar07] M. Barut, S. Bogosyan, and M. Gokasan, "Speed-Sensorless Estimation for Induction Motors Using Extended Kalman Filters," IEEE Trans. Ind. Electron., vol. 54, pp. 272-280, 2007.
- [Bar10] M. Barut, "Bi Input-extended Kalman filter based estimation technique for speed-sensorless control of induction motors", Energy Conversion and Management, vol. 51, no. 10, pp. 2032-2040, 2010.
- [Bar14] O. Barambones and P. Alkorta, "Position Control of the Induction Motor Using an Adaptive Sliding-Mode Controller and Observers", IEEE Trans. Ind. Electron., vol. 61, no. 12, pp. 6556- 6565, 2014.
- [Bed14] Miroslav Bednář "New Approach to Induction Motor Drive Sensorless MRAS Control" Ph.D. thesis, Czech Technical University in Prague Prague, 2014
- [Ben99a] A. Benchaib, A. Rachid and E. Audrezet, "Sliding mode input-output linearization and field orientation for real-time control of induction motors", IEEE Transactions on Power Electronics, vol. 14, no. 1, pp. 3-13, 1999.
- [Ben99b] A. Benchaib, A. Rachid, E. Audrezet and M. Tadjine, "Real-time sliding-mode observer and control of an induction motor", IEEE Transactions on Industrial Electronics, vol. 46, no. 1, pp. 128-138,1999.
- [Ben10] Samira BENAICHA "Contribution à la commande tolérante aux défauts d'un système à motorisation asynchrone "apport de l'intelligence artificielle pour l'aide à la supervision et à la décision" Ph.D. thesis, University of Batna, Algeria,2010.
- [Ben13] Hadda BENDERRADJI "Contribution à la Commande Robuste de la Machine à Induction" Ph.D. thesis, University of Batna, Algeria,2013
- [Ben15] I. Benlaloui, S. Drid, L. Chrifi-Alaoui, and M. Ouriagli, "Implementation of a New MRAS Speed Sensorless Vector Control of Induction Machine," IEEE Trans. Energy Convers., vol. 30, no. 2, pp. 588–595, Jun. 2015.
- [Ben16] BENDAAS Ismail "Contribution à la Commande Hybride par Mode Glissant Floue Appliquée à un Moteur à Induction. Apport des Techniques de L'intelligence Artificielle" Ph.D. thesis, University of Batna, Algeria,2016.
- [Bla72] F. Blaschke, "The principle of field orientation as applied to the new transvector closed-loop control system for rotating machines," *Siemens Review*, vol. 39, no. 5, pp. 217–220, 1972.
- [Bou07] Akkila boukhelifa "Les éléments d'optimisation du pilotage d'une machine asynchrone en vue d'un contrôle vectoriel" Ph.D. thesis, National Polytechnical School, Algeria 2007

- [**Bou09**] M. BOUNADJA, A. BELARBI and B. BELMADANI, "A High-Performance Space Vector Modulation - Direct Torque Controlled Induction Machine Drive based on Stator Flux Orientation Technique", *Advances in Electrical and Computer Engineering*, vol. 9, no. 2, pp. 28-33, 2009.
- [**Bra09**] Heide Brandtstädter "Sliding Mode Control of Electromechanical Systems" Ph.D. thesis, Technische Universität München, Germany, 2009.
- [**Buj04**] G. S. Buja and M. P. Kazmierkowski, "Direct torque control of PWM inverter-fed AC motors - a survey," *IEEE Trans. Ind. Electronics*, vol. 51, pp. 744-757, 2004.
- [**Cas02**] D. Casadei, F. Profumo, G. Serra, and A. Tani, "FOC and DTC: Two viable schemes for induction motors torque control," *IEEE Trans. Power Electron.*, vol. 17, no. 5, pp. 779–787, 2002.
- [**Cas05**] M. Castilla, J. Guerrero, J. Matas and J. Miret, "Sliding-mode control of quantum series-parallel resonant converters via input-output linearization", *IEEE Transactions on Industrial Electronics*, vol. 52, no. 2, pp. 566-575, 2005.
- [**Che10**] Si Zhe Chen, N. Cheung, Ka Chung Wong and Jie Wu, "Integral Sliding-Mode Direct Torque Control of Doubly-Fed Induction Generators Under Unbalanced Grid Voltage", *IEEE Transactions on Energy Conversion*, vol. 25, no. 2, pp. 356-368, 2010.
- [**Chi98**] J. Chiasson, "A new approach to dynamic feedback linearization control of an induction motor", *IEEE Transactions on Automatic Control*, vol. 43, no. 3, pp. 391-397, 1998.
- [**Cho16**] Y. Choi, H. Choi and J. Jung, "Feedback Linearization Direct Torque Control With Reduced Torque and Flux Ripples for IPMSM Drives", *IEEE Transactions on Power Electronics*, vol. 31, no. 5, pp. 3728-3737, 2016.
- [**Cla83**] Claude, D., M. Fliess. and A. Isidori, "Immersion, directe et par bouclage d'un système non linéaire dans un linéaire," *C. R. Acad. Sc. Paris*, 296,237, 1983.
- [**Com05**] Mihai Comanescu "Flux and speed estimation techniques for sensorless control of induction motors" Ph.D. thesis, The Ohio State University USA, 2005.
- [**Dep88**] M. Depenbrock, "Direct Self Control (DSC) of Inverter Fed Induction Machine", *IEEE Trans. on Power Electronics*, Vol. 3, No.4, pp.420-429, 1988.
- [**Dsp12**] "DSP based electric drives laboratory user manual" Department of Electrical and Computer Engineering University of Minnesota, 2012.
- [**Eme67**] S.V. Emelyanov, *Variable Structure Control Systems* (Nauka, Moskwa, 1967).
- [**Fat10**] Fateh MEHAZZEM "Contribution à la Commande d'un Moteur Asynchrone destiné à la Traction électrique" Ph.D. thesis, University of Constantine, 2010.
- [**Faq03**] A. Faqir, F. Betin, L. Chrifi Alaoui, B. Nahid and D. Pinchon, "Varying sliding surface control of an induction machine drive", in *IEEE Conference on Control Applications Proceedings*, 2003

- [Fra06] A. Franco, H. Bourles, E. De Pieri and H. Guillard, "Robust Nonlinear Control Associating Robust Feedback Linearization and H^∞ Control", IEEE Transactions on Automatic Control, vol. 51, no. 7, pp. 1200-1207, 2006.
- [Fou13] Fouad Giri "AC electric motors control advanced design techniques and applications" John Wiley & Sons, Ltd, 2013
- [Gad09] S. M. Gadoue, D. Giaouris, and J. W. Finch, "Sensorless Control of Induction Motor Drives at Very Low and Zero Speeds Using Neural Network Flux Observers," IEEE Transactions on Industrial Electronics, vol. 56, pp. 3029-3039, 2009
- [Gad10] S. M. Gadoue, D. Giaouris, and J. W. Finch, "MRAS Sensorless Vector Control of an Induction Motor Using New Sliding-Mode and Fuzzy-Logic Adaptation Mechanisms," IEEE Trans. Energy Convers., vol. 25, no. 2, pp. 394–402, 2010.
- [Gar03] Freddy Garces, Victor M. Becerra, Chandrasekhar Kambhampati and Kevin Warwick "Strategies for Feedback Linearization, A Dynamic Neural Network Approach" Springer-Verlag London Ltd 2003.
- [Gar94] G. Garcia, J. Luis, R. Stephan and E. Watanabe, "An efficient controller for an adjustable speed induction motor drive", IEEE Transactions on Industrial Electronics, vol. 41, no. 5, pp. 533-539, 1994.
- [Gen10] Huangfu Yi-geng "Research of Nonlinear System High Order Sliding Mode Control and its Applications for PMSM" Ph.D. thesis, University of Technology of Belfort-Montbéliard And Northwestern Polytechnical University, France 2010.
- [Glo92] D. McFarlane and K. Glover, "A loop-shaping design procedure using H^∞ synthesis", IEEE Transactions on Automatic Control, vol. 37, no. 6, pp. 759-769, 1992.
- [Glu15] Alain Glumineau • Jesús de León Morales "Sensorless AC Electric Motor Control Robust Advanced Design Techniques and Applications" Springer International Publishing Switzerland 2015
- [Hab92] T. G. Habetler, F. Profumo, M. Pastorelli, and L. M. Tolbert, "Direct torque control of induction machines using space vector modulation," Ind. Appl. IEEE Trans., vol. 28, no. 5, pp. 1045–1053, 1992.
- [Hab15] M. Habibullah and D. Lu, "A Speed-Sensorless FS-PTC of Induction Motors Using Extended Kalman Filters", IEEE Transactions on Industrial Electronics, vol. 62, no. 11, pp. 6765-6778, 2015.
- [Had07] A. Haddoun, M. Benbouzid, D. Diallo, R. Abdessemed, J. Ghouili and K. Srairi, "A Loss-Minimization DTC Scheme for EV Induction Motors", IEEE Trans. Veh. Technol., vol. 56, no. 1, pp. 81-88, 2007.
- [Haf14] M. Hafeez, M. Uddin, N. Rahim and Hew Wooi Ping, "Self-Tuned NFC and Adaptive Torque Hysteresis-Based DTC Scheme for IM Drive", IEEE Transactions on Industry Applications, vol. 50, no. 2, pp. 1410-1420, 2014.

- [Haj09] M. Hajian, G. Arab Markadeh, J. Soltani and S. Hoseinnia, "Energy optimized sliding-mode control of sensorless induction motor drives", *Energy Conversion and Management*, vol. 50, no. 9, pp. 2296-2306, 2009.
- [Haj10] M. Hajian, J. Soltani, G. Markadeh and S. Hosseinnia, "Adaptive Nonlinear Direct Torque Control of Sensorless IM Drives with Efficiency Optimization", *IEEE Transactions on Industrial Electronics*, vol. 57, no. 3, pp. 975-985, 2010.
- [Has72] K. Hasse, "Drehzahlverfahren für schnelle umkehrantriebe mit stromrichtergespeisten asynchron-kurzschlusslaufer-motoren," *Regelungstechnik*, vol. 20, pp. 60–66, 1972.
- [Hol03] J. Holtz and Juntao Quan, "Drift- and parameter-compensated flux estimator for persistent zero-stator-frequency operation of sensorless-controlled induction motors", *IEEE Transactions on Industry Applications*, vol. 39, no. 4, pp. 1052-1060, 2003.
- [Hol06] J. Holtz, "Sensorless Control of Induction Machines, With or Without Signal Injection?", *IEEE Transactions on Industrial Electronics*, vol. 53, no. 1, pp. 7-30, 2006.
- [Hu98] Jun Hu and Bin Wu, "New integration algorithms for estimating motor flux over a wide speed range", *IEEE Transactions on Power Electronics*, vol. 13, no. 5, pp. 969-977, 1998.
- [Hun93] J. Hung, W. Gao and J. Hung, "Variable structure control: a survey", *IEEE Transactions on Industrial Electronics*, vol. 40, no. 1, pp. 2-22, 1993.
- [Isi84] Isidori, A., and A. Ruberti. "On the Synthesis of Linear Input-Output Responses for Nonlinear Systems," *Sys. & Contr. Lett.*, 4, 17, 1984.
- [Isi95] Alberto Isidori "Nonlinear Control Systems" Third Edition, Springer-Verlag London 1995.
- [Kaz95] M. Kazmierkowski and D. Sobczuk, "High performance induction motor control via feedback linearization", in the *IEEE International Symposium on Industrial Electronics Proceedings*. 1995.
- [Kim94] Young-Real Kim, Seung-Ki Sul and Min-Ho Park, "Speed sensorless vector control of induction motor using extended Kalman filter", *IEEE Transactions on Industry Applications*, vol. 30, no. 5, pp. 1225-1233, 1994.
- [Kir85] D. Kirschen, D. Novotny and T. Lipo, "On-Line Efficiency Optimization of a Variable Frequency Induction Motor Drive", *IEEE Transactions on Industry Applications*, vol. -21, no. 3, pp. 610-616, 1985.
- [Ksn08] Y. Kumsuwan, S. Premrudeepreechacharn and H. Toliyat, "Modified direct torque control method for induction motor drives based on amplitude and angle control of stator flux", *Electric Power Systems Research*, vol. 78, no. 10, pp. 1712-1718, 2008.
- [Kow14a] T. Orłowska-Kowalska, G. Tarchala, M. Dybkowski "Slidingmode direct torque control and sliding-mode observer with a magnetizing reactance estimator for the field-weakening of the induction motor drive", *Math. Comput. Simul.* Vol 98, April 2014, pp 31-45.

- [Kow14b] T. Orłowska-Kowalska “Advanced and Intelligent Control in Power Electronics and Drives” Springer International Publishing Switzerland 2014.
- [Kra90] C. Kravaris and M. Soroush, "Synthesis of multivariable nonlinear controllers by input/output linearization", *AICHE Journal*, vol. 36, no. 2, pp. 249-264, 1990.
- [Kub93] H. Kubota, K. Matsuse and T. Nakano, "DSP-based speed adaptive flux observer of induction motor", *IEEE Transactions on Industry Applications*, vol. 29, no. 2, pp. 344-348, 1993.
- [Kum15] R. Kumar, P. Syam, S. Das and A. Chattopadhyay, "Review on model reference adaptive system for sensorless vector control of induction motor drives", *IET Electric Power Applications*, vol. 9, no. 7, pp. 496-511, 2015.
- [Las00] C. Lascu, I. Boldea and F. Blaabjerg, "A modified direct torque control for induction motor sensorless drive", *IEEE Transactions on Industry Applications*, vol. 36, no. 1, pp. 122-130, 2000.
- [Las04] C. Lascu, I. Boldea, F. Blaabjerg, “Variable-structure direct torque control – A class of fast and robust controllers for induction machine drives,” *IEEE Trans. Industrial Electronics*, vol. 51, no. 4, Aug. 2004, pp. 785-792
- [Las06] C. Lascu, I. Boldea, and F. Blaabjerg, “Comparative study of adaptive and inherently sensorless observers for variable-speed induction-motor drives,” *IEEE Trans. Ind. Electron.*, vol. 53, no. 1, pp. 3394–3403, Jan. 2006.
- [Las09] C. Lascu, I. Boldea, and F. Blaabjerg, “A Class of Speed-Sensorless Sliding-Mode Observers for High-Performance Induction Motor Drives” *IEEE Trans. Ind. Electron.*, vol. 56, no. 9, pp. 57–65, Sept. 2009.
- [Las14] C. Lascu and F. Blaabjerg, "Super-twisting sliding mode direct torque control of induction machine drives", in *2014 IEEE Energy Conversion Congress and Exposition (ECCE)*, Pittsburgh, PA, 2014.
- [Las17] C.Lascu, S.Jafarzadeh, M. Sami Fadali, F. Blaabjerg “Direct Torque Control With Feedback Linearization for Induction Motor Drives” *IEEE Transactions On Power Electronics*, VOL. 32, NO. 3, pp.2072-2080 March 2017.
- [Lee13] H. Lee and J. Lee, "Design of Iterative Sliding Mode Observer for Sensorless PMSM Control", *IEEE Transactions on Control Systems Technology*, vol. 21, no. 4, pp. 1394-1399, 2013.
- [Lev93] A. Levant, “Sliding order and sliding accuracy in sliding mode control”, *Int. Journal of Control*, vol. 58, no. 6, June 1993, pp. 1247-1263.
- [Lev03] A. Levant, "Higher-order sliding modes, differentiation and output-feedback control", *International Journal of Control*, vol. 76, no. 9-10, pp. 924-941, 2003.
- [Lew85] L.V. Levantovsky, *Second Order Sliding Algorithms: Their Realization, Dynamics of Heterogenous Systems* (Institute for System Studies, Moscow, 1985), pp. 32–43
- [Li05] Jingchuan Li “Adaptive sliding mode observer and loss minimization for sensorless field orientation control of induction machine” Ph.D. thesis, The Ohio State University USA, 2005.

- [Lim04] S. Lim and K. Nam, "Loss-minimising control scheme for induction motors", IEE Proceedings - Electric Power Applications, vol. 151, no. 4, p. 385, 2004.
- [Liu08] P. Liutanakul, S. Pierfederici and F. Meibody-Tabar, "Application of SMC With I/O Feedback Linearization to the Control of the Cascade Controlled-Rectifier/Inverter-Motor Drive System With Small dc-Link Capacitor", IEEE Transactions on Power Electronics, vol. 23, no. 5, pp. 2489-2499, 2008.
- [Mae00] J. Maes and J. Melkebeek, "Speed-sensorless direct torque control of induction motors using an adaptive flux observer", IEEE Transactions on Industry Applications, vol. 36, no. 3, pp. 778-785, 2000.
- [Mar01] C. Martins and A. Carvalho, "Technological trends in induction motor electrical drives", in IEEE Porto Power Tech Proceedings 2001.
- [Mun11] David Vindel Muñoz "Design, Simulation and Implementation of a PMSM Drive System" Master thesis, Chalmers University of Technology, Göteborg, Sweden 2011.
- [Ngu13] M. Ngoc Linh NGUYEN "Commande Prédicative de deux machines Synchrones alimentées en parallèle par un onduleur de tension triphasé" Ph.D. thesis, Université de Toulouse, France, 2013.
- [Obe10] A. Obeid Ahmed, M. O. Ajangnay, S. A. Mohamed and M. W. Dunnigan, "Combined Sliding Mode Control with a Feedback Linearization for Speed Control of Induction Motor", in 1st International Conference on Energy, Power and Control (EPC-IQ) Proceeding, Basrah, Iraq, 2010.
- [Otk08] Salih Baris Ozturk "direct torque control of permanent magnet synchronous motors with non-sinusoidal back-emf" Ph.D. thesis, Texas A&M University, 2008
- [Pan13] V. Panchade, R. Chile and B. Patre, "A survey on sliding mode control strategies for induction motors", Annual Reviews in Control, vol. 37, no. 2, pp. 289-307, 2013.
- [Pen94] Fang-Zheng Peng, T. Fukao and Jih-Sheng Lai, "Low-speed performance of robust speed identification using instantaneous reactive power for tacholeless vector control of induction motors", in IEEE Industry Applications Society Annual Meeting Proceedings, 1994.
- [Puj00] Antoni Arias Pujol "Improvements in direct torque control of induction motors" Ph.D. thesis, Universitat politècnica de Catalunya, Terrassa, 2000.
- [Rae09] Kyung-Rae Cho and Jul-Ki Seok, "Pure-Integration-Based Flux Acquisition with Drift and Residual Error Compensation at a Low Stator Frequency", IEEE Transactions on Industry Applications, vol. 45, no. 4, pp. 1276-1285, 2009.
- [Raf12] Muhammad Rafiq "Higher order sliding mode control based SR motor control system design" Ph.D. thesis, Faculty of Engineering, Mohammad Ali Jinnah University Islamabad, June, 2012.
- [Rao10] S. Rao, V. Utkin and M. Buss, "Design of first- and second-order sliding mode observers for induction motors using a stator-flux model", International Journal of Control, vol. 83, no. 7, pp. 1457-1464, 2010.

- [Ras05] M. Rashed, K. Goh, M. Dunnigan, P. MacConnell, A. Stronach and B. Williams, "Sensorless second-order sliding-mode speed control of a voltage-fed induction-motor drive using nonlinear state feedback", *IEE Proceedings - Electric Power Applications*, vol. 152, no. 5, p. 1127, 2005.
- [Reh02] H. Rehman, A. Derdiyok, M. Guven and Longya Xu, "A new current model flux observer for wide speed range sensorless control of an induction machine", *IEEE Transactions on Power Electronics*, vol. 17, no. 6, pp. 1041-1048, 2002.
- [Reh11] H. Rehman and L. Xu, "Alternative Energy Vehicles Drive System: Control, Flux and Torque Estimation, and Efficiency Optimization", *IEEE Trans. Veh. Technol.*, vol. 60, no. 8, pp. 3625- 3634, 2011.
- [Rob12] Benoît Robyns, Bruno Francois, Philippe Degobert, Jean Paul Hautier "Vector Control of Induction Machines, Desensitisation and Optimisation Through Fuzzy Logic" Springer-Verlag London 2012.
- [Rod04] J. Rodríguez, J. Pontt, César Silva, S. Kouro and H. Miranda "A Novel Direct Torque Control Scheme for Induction Machines with Space Vector Modulation" 35th Annual IEEE Power Electronics Specialists Conference Aachen, Germany, 2004.
- [Rod12] J. Rodríguez, Patricio Cortes "Predictive control of power converters and electrical drives" 2012, John Wiley & Sons, Ltd
- [Rum02] N. Idris and A. Yatim, "An improved stator flux estimation in steady-state operation for direct torque control of induction machines", *IEEE Transactions on Industry Applications*, vol. 38, no. 1, pp. 110-116, 2002.
- [Rum04] N. R. N. Idris and A. H. M. Yatim, "Direct torque control of induction machines with constant switching frequency and reduced torque ripple," *IEEE Trans. Ind. Electronics*, vol. 51, pp. 758-767, 2004.
- [Sab81] A. Sabanovic, D.B. Izosimov, Applications of sliding modes to induction motor control. *IEEE Trans. Ind. Appl.* 17(1), 41–49 (1981).
- [Sab89] A. Sabanovic and F. Bilalovic, "Sliding mode control of AC drives", *IEEE Transactions on Industry Applications*, vol. 25, no. 1, pp. 70-75, 1989.
- [Sab14] H. Saberi, M. Sabahi, M.B. B. Sharifian, M. Feyzi "Improved sensorless direct torque control method using adaptive flux observer" *IET Power Electronics* 2014, Vol. 7, Iss. 7, pp. 1675–1684.
- [Sag15] A. Saghafinia, H. Ping, M. Uddin and K. Gaeid, "Adaptive Fuzzy Sliding-Mode Control Into Chattering-Free IM Drive", *IEEE Transactions on Industry Applications*, vol. 51, no. 1, pp. 692-701, 2015.
- [Sch92] C. Schauder, "Adaptive speed identification for vector control of induction motors without rotational transducers," *IEEE Trans. Ind. Appl.*, vol. 28, no. 5, pp. 1054–1061, 1992.
- [Seb11] Sebti Belkacem "Contribution à la commande directe du couple de la machine asynchrone » Ph.D. thesis, Bejaia University, Algeria, 2016.

- [Sin89] S.N. Singh, Asymptotically decoupled discontinuous control of systems and nonlinear aircraft maneuver. *IEEE Trans. Aeronaut. Electron. Syst.* 25(3), 380–391, 1989.
- [Sin13] B. Singh, S. Dwivedi and S. Jain, "Torque ripple reduction technique with improved flux response for a direct torque control induction motor drive", *IET Power Electronics*, vol. 6, no. 2, pp. 326-342, 2013.
- [Slo83] J.J. Slotine, S.S. Sastry, Tracking control of nonlinear systems using sliding surfaces with application to robot manipulators. *Int. J. Control* 38(2), 465–492, 1983.
- [Slo91] J.J. Slotine, C. Canudas de Wit, Sliding observers for robot manipulators. *Automatica* 27(5), 859–864 (1991).
- [Smi16] A. Smith, S. Gadoue and J. Finch, "Improved Rotor Flux Estimation at Low Speeds for Torque MRAS-Based Sensorless Induction Motor Drives", *IEEE Transactions on Energy Conversion*, vol. 31, no. 1, pp. 270-282, 2016.
- [Sou95] G. Sousa, B. K. Bose, and J. Cleland, "Fuzzy logic based on-line efficiency optimization control of an indirect vector-controlled induction motor drive," *IEEE Trans. Ind. Electron.*, vol. 42, no. 2, pp. 192–198, Apr. 1995.
- [Sto15] D. Stojic, M. Milinkovic, S. Veinovic and I. Klasnic, "Improved Stator Flux Estimator for Speed Sensorless Induction Motor Drives", *IEEE Transactions on Power Electronics*, vol. 30, no. 4, pp. 2363-2371, 2015.
- [Stu13] J. Stumper, A. Dotlinger and R. Kennel, "Loss Minimization of Induction Machines in Dynamic Operation", *IEEE Transactions on Energy Conversion*, vol. 28, no. 3, pp. 726-735, 2013. [12] J. Stumper, A. Dotlinger and R. Kennel, "Loss Minimization of Induction Machines in Dynamic Operation", *IEEE Transactions on Energy Conversion*, vol. 28, no. 3, pp. 726-735, 2013.
- [Sul88] S. Sul and M. Park, "A novel technique for optimal efficiency control of a current-source inverter-fed induction motor", *IEEE Transactions on Power Electronics*, vol. 3, no. 2, pp. 192-199, 1988.
- [Sut13] T. Sutikno, N. Idris, A. Jidin and M. Cirstea, "An Improved FPGA Implementation of Direct Torque Control for Induction Machines", *IEEE Transactions on Industrial Informatics*, vol. 9, no. 3, pp. 1280-1290, 2013.
- [Swi05] Dariusz Świerczyński "Direct Torque Control with Space Vector Modulation (DTC-SVM) of Inverter-Fed Permanent Magnet Synchronous Motor Drive" Ph.D. thesis, Warsaw University of Technology, Warsaw, Poland, 2005.
- [Tak86] Takahashi, T. Noguchi, "A new quick-response and high-efficiency control strategy of an induction motor," *IEEE Trans. on Ind. Appl.*, Vol.22, No.5, pp.820-827, 1986.
- [Taz15] F. Tazerart, Z. Mokrani, D. Rekioua and T. Rekioua, "Direct torque control implementation with losses minimization of induction motor for electric vehicle applications with high operating life of the battery", *International Journal of Hydrogen Energy*, vol. 40, no. 39, pp. 13827-13838, 2015.

-
- [Taz16] Farid TAZERART “Étude, Commande et Optimisation des Pertes d'Énergie d'une Machine à Induction Alimentée par un Convertisseur Matriciel” Ph.D. thesis, Bejaia University, Algeria, 2016.
- [Tou07] Riad TOUFOUTI, Salima MEZIANE, Hocine BENALLA “Direct torque control strategy of induction motors” *acta electrotechnica et informatica* vol. 7, no. 1, 2007.
- [Tou08] Riad TOUFOUTI “Contribution à la commande directe du couple de la machine asynchrone » Ph.D. thesis, University of Constantine, Algeria, 2008.
- [Udd08] M. Uddin and Sang Woo Nam, "New Online Loss-Minimization Based Control of an Induction Motor Drive", *IEEE Transactions on Power Electronics*, vol. 23, no. 2, pp. 926-933, 2008.
- [Udd12] M. Uddin and M. Hafeez, "FLC-Based DTC Scheme to Improve the Dynamic Performance of an IM Drive", *IEEE Transactions on Industry Applications*, vol. 48, no. 2, pp. 823-831, 2012.
- [Utk77] V.I. Utkin, Variable structure systems with sliding modes: a survey. *IEEE Trans. Autom. Control* 22(2), 212–222,1977.
- [Utk93] V.I. Utkin, "Sliding mode control design principles and applications to electric drives", *IEEE Transactions on Industrial Electronics*, vol. 40, no. 1, pp. 23-36, 1993.
- [Utk09] Vadim Utkin, Jürgen Guldner, Jingxin Shi “Sliding Mode Control in Electro-Mechanical Systems” second edition, Taylor & Francis Group, LLC, 2009
- [Wan14] Fengxiang Wang, “Model Predictive Torque Control for Electrical Drive Systems with and without an Encoder” Ph.D. thesis, Lehrstuhl für elektrische Antriebssysteme und Leistungselektronik der Technischen Universität München, 2014.
- [Wan15] Y. Wang, T. Ito and R. Lorenz, "Loss Manipulation Capabilities of Deadbeat Direct Torque and Flux Control Induction Machine Drives", *IEEE Transactions on Industry Applications*, vol. 51, no. 6, pp. 4554-4566, 2015.
- [Wjk09] Pawel Wójcik “Direct Torque and Flux Control of Inverter–Fed Induction Motor Drive Including Field Weakening Region” Ph.D. thesis, Warsaw University of Technology, Warsaw, Poland, 2009.
- [Yan15] M. Yang, S. Tang and D. Xu, "Comments on Antiwindup Strategy for PI-Type Speed Controller", *IEEE Transactions on Industrial Electronics*, vol. 62, no. 2, pp. 1329-1332, 2015.
- [Yaz08] R. Yazdanpanah, J. Soltani and G. Arab Markadeh, "Nonlinear torque and stator flux controller for induction motor drive based on adaptive input–output feedback linearization and sliding mode control", *Energy Conversion and Management*, vol. 49, no. 4, pp. 541-550, 2008.
- [Zaa16] A. Zaafour, C. Regaya, H. Azza and A. Châari, "DSP-based adaptive backstepping using the tracking errors for high-performance sensorless speed control of induction motor drive", *ISA Transactions*, vol. 60, pp. 333-347, 2016.

-
- [Zar10] H. Abootorabi Zarchi, G. Arab Markadeh and J. Soltani, "Direct torque and flux regulation of synchronous reluctance motor drives based on input–output feedback linearization", *Energy Conversion and Management*, vol. 51, no. 1, pp. 71-80, 2010.
- [Zha05] Jun Zhang and M. Rahman, "Analysis and design of a novel direct flux control scheme for induction machine", in *IEEE International Conference on Electric Machines and Drives Proceeding*, 2005.
- [Zha10] Z. Zhang, R. Tang, B. Bai and D. Xie, "Novel Direct Torque Control Based on Space Vector Modulation with Adaptive Stator Flux Observer for Induction Motors", *IEEE Transactions on Magnetics*, vol. 46, no. 8, pp. 3133-3136, 2010.
- [Zha14] Lihang Zhao, Jin Huang, He Liu, Bingnan Li and Wubin Kong, "Second-Order Sliding-Mode Observer with Online Parameter Identification for Sensorless Induction Motor Drives", *IEEE Transactions on Industrial Electronics*, vol. 61, no. 10, pp. 5280-5289, 2014.
- [Zha15] C. Zhang, L. Jia, Y. Xiao, J. He and C. Xu, "Virtual line-shafting control for permanent magnet synchronous motor systems using sliding-mode observer", *IET Control Theory & Applications*, vol. 9, no. 3, pp. 456-464, 2015.
- [Zha16] Z. Zhang, C. Wei, W. Qiao and L. Qu, "Adaptive Saturation Controller-Based Direct Torque Control for Permanent-Magnet Synchronous Machines", *IEEE Transactions on Power Electronics*, pp. 7112-7122, 2016.
- [Zho14] Z. Yin, C. Zhao, Y. Zhong and J. Liu, "Research on Robust Performance of Speed-Sensorless Vector Control for the Induction Motor Using an Interfacing Multiple-Model Extended Kalman Filter", *IEEE Transactions on Power Electronics*, vol. 29, no. 6, pp. 3011-3019, 2014.
- [Zlk05] Marcin Żelechowski "Space Vector Modulated – Direct Torque Controlled (DTC – SVM) Inverter – Fed Induction Motor Drive" Ph.D. thesis, Warsaw University of Technology, Warsaw, Poland, 2005.